STRUCTURE AND SYNTHESIS OF BIOACTIVE POLYPHENOLS FROM *CYCLOPIA SUBTERNATA* (HONEYBUSH) AND *ASPALATHUS LINEARIS* (ROOIBOS) TEA: CONFORMATIONAL ANALYSIS OF SELECTED CHIRAL DERIVATIVES

Thesis submitted in fulfilment of the requirements for the degree

Doctor Philosophiae

in the

Department of chemistry
Faculty of Natural and Agricultural Sciences

at the
University of the Free State
Bloemfontein

by

Dirk Jacobus Brand

Supervisor: Prof. E.V. Brandt
Co-supervisor: Prof J. A. Steenkamp
Co-supervisor: Prof. B.C.B. Bezuidenhoudt

December 2007

ACKNOWLEDGEMENTS

I hereby whish to express my sincere gratitude to the following:

Professor E. V. Brandt for his professional guidance, unselfish assistance and scientifically sound advice as supervisor;

Professor J. A. Steenkamp as co-supervisor for his invaluable discussions, priceless research opportunities and international exposure initiated by him;

Professor B. C. B. Bezuidenhout as co-supervisor for his valued and kind assistance during my write-up;

Dr. B. I. Kamara for her unwavering motivation, prized advice and warm, lasting friendship;

Collogue G. Fourie, Co-students H. Howlell, E. Fourie and L. Jordaan for their friendship and unselfish assistance;

Mr. C. D. Smith for his light-hearted demeanor, friendship and helpful attitude in the workplace;

My family and friends for their encouragement and support;

Professor Yoshio Takeuchi, Professor Kuninobo Kabuto, Dr. Tomoya Fujiwara, the students, Hiromi, Seki, Krista, Inn, Saito and Murai for their friendship and kindness during my visit to Japan;

My parents Piet and Estelle for their lifetime love, moral and financial support and encouragement throughout my life and the educational background they gave me;

My grandparents for their love and encouragement;

I dedicate this thesis to my grandfather, Capt. D.J. Brand Snr. (June 2007) who so wanted to see the completion of my degree;
I thank him for his compassionate love for his grandchildren and all he encountered and the lasting example he left for me;

The N.R.F. and Dr. E. Joubert, ARC Infruitec - Nietvoorbij, for financial support;

D. J. Brand

Presently these research results have been accepted for three publications in international peer-reviewed journals:

- Kamara B. I., Brand D. J., Brandt E. V. and Joubert E., *J. Agric. Food Chem.* **2004**, *52,* (17), 5391-5395.
- Brand D. J., Steenkamp J. A., Brandt E. V., Takeuchi Y., *Tetrahedron Letters*, **2007**, *48*, 2769-2773.
- Brand D. J., Steenkamp J. A., Omata K., Kabuto K., Fujiwara T., Takeuchi Y., *Chirality*, **2008**, *20*, 351-356.

Chapter1

Isolation, Structure Elucidation and Synthesis of a metabolite from *Cyclopia subternata* (Honeybush Tea)

Introduction

The genus *Cyclopia* (Fabaceae) consists of approximately 24 species distributed only in the Western and Eastern Cape coastal regions of South Africa. *Cyclopia intermedia* and *subternata* are the two species that are primarily used to brew Honeybush tea[1], after having been subjected to high temperature oxidation ("fermentation"), necessary for the formation of the brown color and honey fragrance. The tea is caffeine free, low in tannin content and is used by people of the Eastern Cape as a medicinal beverage[2]. In the quest for new phenolic metabolites with potential health benefits our ongoing investigation into the phytochemical composition of *Cyclopia intermedia* has yielded flavonols, flavonones, isoflavones, coumestans, flavones, xanthones, cinnamic acids and pinitol, a cyclitol[3, 4].

Attempts to grow the tea commercially have had variable success, but most of the tea is harvested from the unpolluted wilderness environment. Studies of the phytochemical composition of the *Cyclopia* species should contribute to the successful commercial establishment of the Honeybush tea industry and improve the marketing potential of the tea. Our recent isolation and structural determination of compounds from *C. subternata*, revealed the presence of various flavonoids and xanthones as well as non-phenolic metabolites. Since polyphenols are reported to have significant antioxidant properties[1], these results suggest that the tentative claimed health benefits may be concomitant with the presence of these and other polyphenols in the tea.

---

[1] Du Toit, J., Joubert, E., Britz, T.J. Honeybush tea – a rediscovered indigenous South African herbal tea. *J. Sustain. Agric*. **1998**, *12*, 67-84.
[2] Watt, J.M., Breyer-Branswijk, M.G., *The Medicinal and Poisonous Plants of Southern Africa*. E & S Livingstone: Edinburg., **1932**, p.70.
[3] Ferreira D., Kamara B. I., Brandt E. V., Joubert E., *J. Agric. Food Chem.* **1998,** *46*, 3406-3410.
[4] Kamara B. I., Brandt E. V., Ferreira D., Joubert E., *J. Agric. Food Chem.* **2003**, *51*, 3874-3879.

Literature Survey

Nomenclature and occurrence of flavonoids

Flavans and proanthocyanidins

The system of nomenclature for flavans **(1)**, flavan-3-ols **(2)** and proanthocyanidins **(3)** in general employs trivial names for the basic units. All flavan-3-ols are of the (2*R*, 3*S*) configuration and those with a (2*R*, 3*R*) configuration are prefixed with 'epi', e.g. epicatechin[5]. The flavan-3-ol units with a 2*S* configuration are distinguished by the enantio (*ent*) prefix (Hemingway)[5]. The flavanoid skeleton is drawn and numbered as shown in **(1)** and **(2)**.

(1) = **(2)**

The heterocyclic C-ring of the flavan is conformationally labile and can adopt a number of possible conformations. The E and A conformers are indicated as those with the orientation of the B-ring equatorial and axial respectively. Molecular Mechanics (MM2) calculations[6] on the conformation of the C–ring show that the half-chair E-conformer is energetically preferred with various degrees of distortion[7].

[5] Porter L.J., in *The Flavonoids: Advances in Research since 1986*, (ed. J.B. Harborne), Chapman and Hall, London, **1993**, p.23. and references therein.
[6] Viswanadhan V.N., Mattice W.L., *J. Comput. Chem.,* **1986**, *7*, 711.
[7] Viswanadhan V.N., Mattice W.L., *J. Chem Soc. Perkin Trans. II,* **1987**, 739.

Flavans substituted on the heterocyclic ring (3 and 4-positions, e.g. catechin) are frequently encountered in nature, but the unsubstituted flavans are rarely found due, presumably, to their instability in solution leading to polymeric products[8]. Flavan glycosides also rarely occur in the plant kingdom.[9]

Anthocyanidins

Anthocyanins are water-soluble glycosides and acylglycosides of anthocyanidins, which are polyhydroxy and polymethoxy derivatives of 2-phenylbenzo-pyrylium (flavylium cation),[10] e.g. (**3**). They belong to the phenolic class of flavonoids with the typical A-ring benzoyl and B-ring hydroxycinnamoyl systems, with the carbon numbering system shown in **(3)**. There are at least 300 naturally occurring structures.

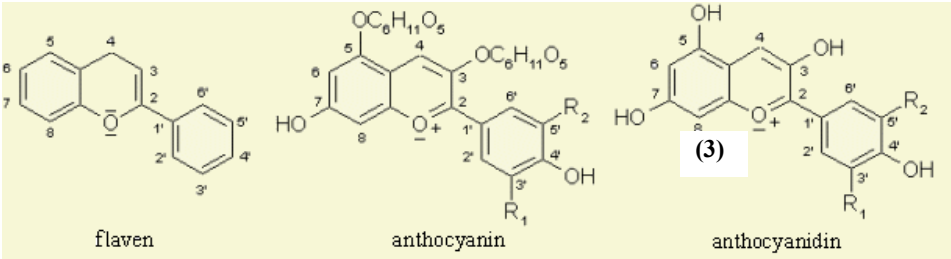

Besides the basic flavylium cation **(3)**, the 'primary structure', anthocyanidins occur in aqueous weakly acidic solution as 'secondary structures', a mixture of the quinonoidal (zwitterion) base(s), the carbinol pseudo base and the chalcone pseudo base[11]. Co-pigmentation is important as under very weakly acidic conditions, pH4-6, as is typical in cell vacuoles and in the absence of other substances, most anthocyanins exist substantially in stable colourless forms (**Scheme 1.1**).

Between pH 4 and 6, four anthocyanin structural types exist in equilibrium, namely the flavylium cation, the quinonoidal anhydrobase, the colourless carbinol bases and the pale yellow "reversed" chalcones. Equilibration between the quinonoidal and carbinol bases occurs via the flavylium cation, i.e. quinonoidal anhydrobase

[8] Kulwant S., Ghosal S., *Phytochemistry* **1984,** *23 no.11*, 2415.
[9] Kubo I., Kim M., *Tetrahedron Letters*, **1987**, *28 no. 9*, 921
[10] Strack D., Wray V. in *The Flavonoids: Advances in Research since 1986*, (ed. J.B. Harborne), Chapman and Hall, London, **1993**, p.6.
[11] Brouillard R., in *Anthocyanins as Food Colors*, ed. P. Marakakis, Academic Press, N.Y., pp 1-40.

↔ flavylium cation ↔ carbinol bases. As the pH increases above pH 6, greater amounts of the anhydrobase are formed. At neutral pH, the anionic form of the quinonoidal base (blue) is formed. In more acidic conditions the flavylium ion (red) predominates[12].

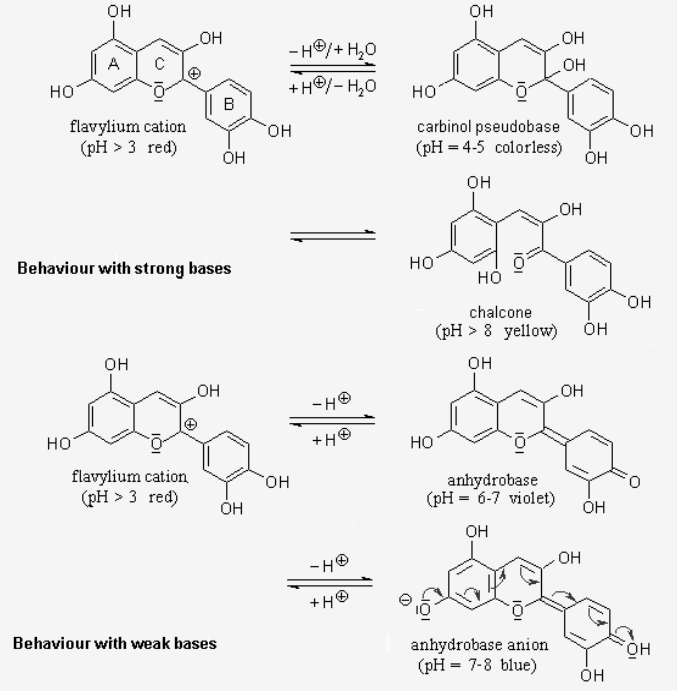

Scheme 1.1

At pH 4-6 stabilizing intermolecular co-pigmentation with the anthocyanin structure needs to be present to produce the different colors observed in plants. There are four possible stabilization mechanisms leading to 'tertiary structures', such as self-association, inter- and intramolecular co-pigmentation, and metal complex formation.[13]

With a few exceptions, e.g. the betalain, anthocyanidins are the most important group of water-soluble plant pigments visible to the human eye. They are universal plant colorants and largely responsible for the cyanic colors of flower petals and fruits[14].

[12] Gillian A.C., *Phytochemistry*, **2001**, *56*, 229-236.
[13] Strack D., V Wray in *The Flavonoids: Advances in Research since 1986*, (ed. J.B. Harborne), Chapman and Hall, London, **1993**, p.7.
[14] Strack D., Wray V. in *The Flavonoids: Advances in Research since 1986*, (ed. J.B. Harborne), Chapman and Hall, London, **1993**, p.1.

They may also occur in roots, stems, leaves and bracts, accumulating in the vacuoles[15] of epidermal or sub-epidermal cells. The anthocyanidins are usually in solution within the vacuole, although they may sometimes be located in spherical vesicles, called 'anthocyanoplasts'[16]

Flavans and Proanthocyanidins

Current knowledge of the biosynthesis and enzymology of proanthocyanidin production in plants has been described by Stafford[17]. Another article by Stafford[18] on the relationship of proanthocyanidins to lignin, found no evidence of proanthocyanidins performing a structural role in wood. He suggests a common role in defense[19]. The current picture on the biosynthesis of proanthocyanidins is summarized in **Scheme 1.2**. The route to catechin (2, 3-*trans*) is well established, while the route for the epicatechin (2, 3-*cis*) series is clouded in uncertainty. However, it is expected that the same or very similar sequence will be applicable[20]. The biosynthetic mechanism of the condensation process used by plants to produce proanthocyanidins from the flavan-3-ol and flavan-3, 4-diol units is still unresolved[21].

[15] Wagner, G.J., in *Cellular and Subcellular Localization in Plant Metabolism* (eds L.L. Creasy and G. Hrazdina), Recent Advances in *Phytochemistry*, vol 16, Plenum Press, New York, **1982**, pp. 1-45
[16] Pecket R.C., Small C.J., *Phytochemistry*, **1980**, *19*, 2571
[17] Stafford H.A., in *Chemistry and Significance of tannins*, (ed.R.W. Hemmingway and J.J. Karchesy), Plenum, New York, **1988**, 301
[18] Stafford H.A., *phytochemistry*, **1988**, 27,1
[19] K. Hahlbrock and H. Grisebach, in *The Flavonoids,* (eds. J. B. Harborne, J. B. Mabry and H. Mabry), Chapman and Hall, London, **1975,** 876
[20] Porter L.J., in *The Flavonoids: Advances in Research since 1986* (eds J. B. Harborne), Chapman and Hall, London, **1993**, 53.
[21] D. Barron and R. K. Ibrahim *Phytochemistry,* **1988,** *27,* 2362

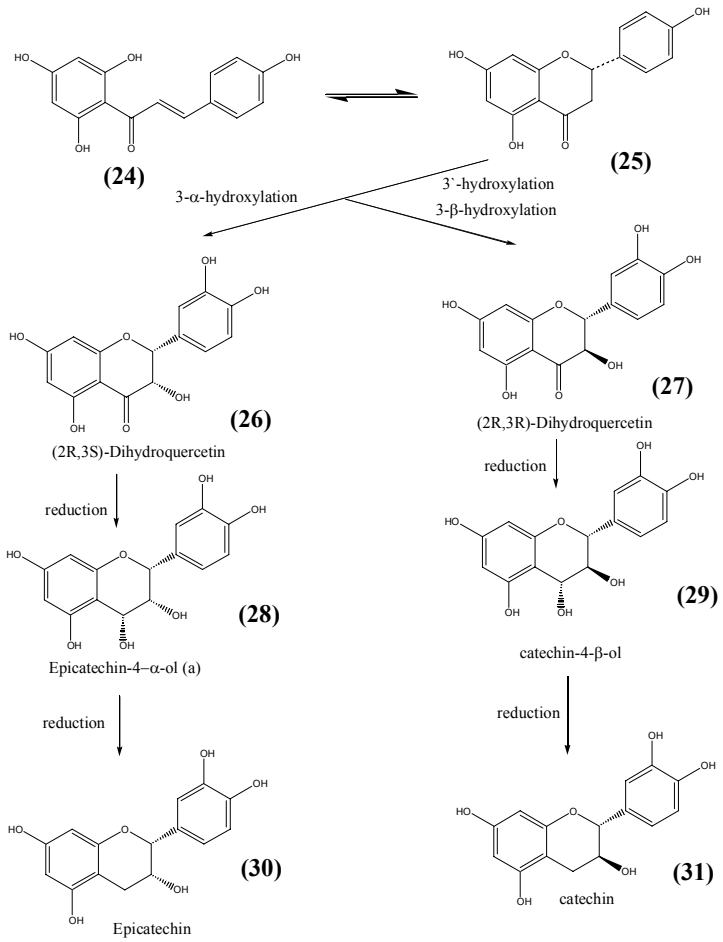

Scheme 1.2 Biosynthesis of Proanthocyanidins. The absolute stereochemistry of intermediate (a) is unconfirmed[17].

Flavones and Flavonols

Flavonols (flavon-3-ols) **(4),** only differ from flavones **(5)** with respect to the presence of a 3-hydroxy group. However, this small structural difference is of considerable biosynthetic, physiological, chemosystematic, pharmacological and analytical significance[22]. Respectively, 380 and 300 flavonols and flavones with various hydroxy and / or methoxy substitution are known. Also, more selectively (methylated or monoglycosylated) *O*-substitution exist in flavones than in

[22] Wollenheber E., in *The Flavonoids: Advances in Research since 1986,* (ed. J. B. Harborne), Chapman and Hall, London, **1993,** 259 and the references there in.

flavonols [23] . Flavones occur as anthocyanidin co-pigments to produce the characteristic purple-blue color, responsible for bee attraction and pollination, found mostly in higher plant species[24]. To increase solubility *in vivo*, polyhydroxylated flavones and flavonols occur as glycosides rather than aglycones.[22]

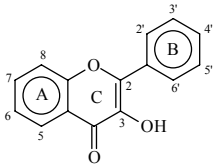

(4)

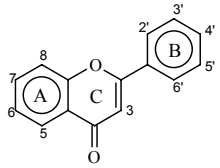

(5)

Flavanones

Flavanones are one of the minor types of flavonoids. The flavanones (2, 3-dihydroflavones) **(6)** can occur as the (2*R*) or (2*S*) configuration, although in nature almost all flavanones exist as the (2*S*) enantiomer[25]. Flavanones display a general distribution but occur most abundantly in angiosperm families such as Rosaceae, Rutaceae, Leguminosae, Ericaceae and Citrus[26,27]. Recently, microbial sources such as *streptomyces*[28] have been found to produce flavanones.

Again, flavanones are commonly associated with the presence of sugars/ methoxy groups to facilitate solubility in an aqueous biological environment of plants and animals[29].

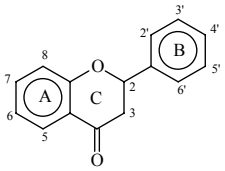

(6)

[23] Wollenheber E., in *The Flavonoids: Advances in Research since 1986,* (ed. J. B. Harborne), Chapman and Hall, London, **1993,** 260 and the references there in.
[24] Harborne J. B., C. A. Williams, Advances in flavonoid research since 1992 Review, *Phytochemistry* 55*,* **2000**, 482/3.
[25] Bohm B. A., in *The Flavonoids,* (eds. J. B. Harborne*,* T. J. Mabry, and H. Mabry), Chapman and Hall, London, **1975,** 561
[26] Albach R. F. and Redman G. H., *Phytochemistry,* **1969,** *8*, 127
[27] Nishura M., Kamiya S., Esaki S. and Ito F., *Agric, Biol, Chem*., **1971,** *35*, 1683
[28] Nakayama O., Yagi M., Tanaka M., Kiyoto S., Uchida I., Hashimoto M., Okuhara M. and Kohsaka M., *J. Antibiot*., **1990,** *43*, 1394
[29] Bohm B.A. in *The Flavonoid: Advances in Research since 1986*, (ed. J.B. Harborne), Chapman and Hall, London, **1993**, p.406-418.

Isoflavones

The isoflavonoids are biogenetically related to the flavonoids but constitute a distinctly separate class in that they contain a rearranged skeleton and may be regarded as derivatives of 3-phenylchroman (**7**).[30] The enzyme(s) responsible for this biochemical rearrangement would appear to be rather specialized, since isoflavonoids have a very limited distribution, being confined essentially to the subfamily Papilionoideae (Lotoideae) of the Leguminosae.[28] Other sources include monocotyledons (Iridaceae family), *Iris* species, two gymnosperm genera and a moss *(Bryum capillare)*. Non-plant sources include a marine coral *(Echinopora lamellosa),* and several microbial cultures, although in most cases the presence of the isoflavonoid can be traced to the food source (in microorganisms and mammals)[31]. Though isoflavonoid distribution in the plant kingdom is very limited, they have a large structural variation[32] based on various oxygenation patterns of the aromatic rings and the state of oxidation of the heterocyclic C-ring.

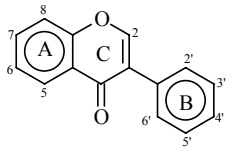

(7)

Xanthones

The term xanthone refers to dibenzo-γ-pyrone-type compounds **(8)** with a $C_6C_1C_6$ type skeleton. All xanthones have a hydroxy group at position 1 or 8 and a resorcinol or phloroglucinol nucleus as a component.

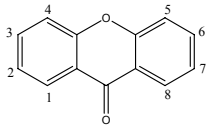

(8)

[30] Dewick P.M., in *The Flavonoids: Advances in Research* (ed. J. B. Harborne, T.J Mabry), Chapman and Hall, London, **1982,** 535
[31] Dewick P.M., in *The Flavonoids: Advances in Research since 1986* (ed. J. B. Harborne), Chapman and Hall, London, **1993,** 117
[32] Grisebach H., in *Recent Developments in the Chemistry of Natural Phenolic Compounds*, (ed. W. D. Ollis), Pergamon Press, Oxford, **1961,** 59

In addition, the majority of xanthones have a quinol or hydroxyquinol nucleus and differ markedly from all the related groups of pyrones, e.g. coumarins or flavones[31]. Although the xanthone structure is simple, a large variation of oxygenated derivatives, including methyl ethers occur in nature. While xanthones have been found in plants and in fungi (one in a lichen) they are not abundant[33]. Interestingly, the parent pyrans, the xanthenes, have not been found to occur in nature. With the exception of mangostin, which carries two isoprenoid side chains, jacareubin, which is a chromene, and sterigma tocystin, the xanthones are not complex and vary only in the number and disposition of hydroxy or methoxy substituents[34]. These rare plant metabolites have been found in higher plants such as mangiferin from the mango tree *Mangifera indica,* and mangostin, the major pigment of the mangosteen tree, *Garcinia mangostana L.* (Family *Guttiferae,)* [35] . Their presence in fungi (Ravenelin produced by *Helminthosporium ravenelli* Curtius and *H. Turcicum* Passerini)[36] are established. Lichexanthone was isolated from the Lichen, *Parnielia Fornzosana*[37].

Cyclitols

Pinitol belongs to the cyclic polyalcohols known as cyclitols. (+)-Pinitol **(9)** ("sennite or matezite") is the monomethyl ether of D-inositol **(18)**[38,35]. It is thought of as a methylated secondary plant source because of the presence of a methoxy group, which is usually produced by plants from a hydroxyl group. Inositol glycosides that are known to occur naturally include gallactinol, mannositose, and other inositol mannosides[34]. Among all the cyclitols, inositols (hexahydroxycyclohexanes), their methyl ethers are the most abundant. Nine stereoisomeric forms **(10-19)** of inositols are known to exist. Seven of the Inositols have a center of symmetry. The other two

[33] Roberts J. C., *Chem. Rev.,* **1961,** *61,* 591
[34] Dean F.M., *Naturally occurring oxygen ring compounds*, **1963,** 266.
[35] Sumb, M., Idris H. J., A. Jefferson and F. Schcinnann, *J. Chem. Soc., Perkin Trans. 1,* **1977**, 2158
[36] Raistrick H., Robinson R. and White D. E., *Biochem. J.,* **1936**, *30,* 1303.
[37] Asahina Y. and H. Nogami, *Bull. Chem. Soc. Japan,* **1942**, *17,* 202

[38] Posternak T.**,** *The Cyclitols,* Holden-Day, Inc., Publishers, U. S. A. **1965**

[35] Foxall C. D. and Morgan J. W. W.**,** *J.Chem, Soc.,* **1963,** 5573

without a center of symmetry are (+)-inositol and (-)-inositol **(17, 18),** which occur naturally.

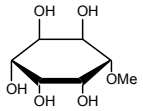

(9)

Naturally occurring cyclitols have the generic name *"*inositol*"*. Eight of these are distinguishable by the prefixes, *allo, epi, myo, muco, cis, neo, dextro* and *laevo,* the ninth being named scyllitol. *O*-methyl derivatives of the inositols are frequently encountered in plants, with D-pinitol as the most widely distributed inositol ether[34]. Berthelot's[38] first discovery of the compound in the gymnosperm family led to isolations from various species, *inter alia Picea abies, Pinus nigra, Pinus halepensis* and *Schinus molle.* Pinitol is also found among angiosperms, e.g. *Acacia mearnsii*. The wide distribution of pinitol in plants was demonstrated by the work of Plouvier[34].

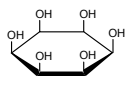

(10) Cisinositol

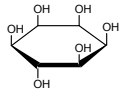

(11) Epinositol

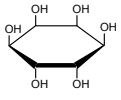

(12) Alloinositol

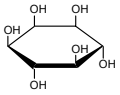

(13) Myolnositol

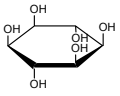

(14) Mucoinositol

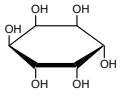

(15) Neoinositol

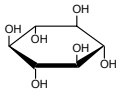

(16) Scyllitol

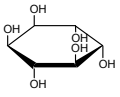

(17) (+)-Inositol

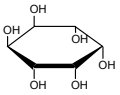

(18) (-)-Inositol

O- Glycosides

Flavonoids, which are found abundantly in plants, may play a role in reducing the risk of chronic diseases such as cardiovascular disease and cancer[39, 40, 41]. They exist in nature almost exclusively as β-glycosides. The flavonols are found mainly as the 3-*O*-

---

[39] Middleton, E. and Kandaswami, C. in *The Flavonoids: Advances in Research since 1986*, (ed. J.B. Harborne), Chapman and Hall, London, **1994,** 619.

[40] Huang M-T. and Ferraro T., in Phenolic Compounds in Foods and their Effect on Health II, (Eds. Huang M-T., Ho C. and Lee C.Y.), *American Chemical Society*, Washington, DC, **1992,** 8.

[41] Salah N., Miller N.J., Paganga G., Tijburg L., Bolwell G.P., and Rice-Evans, *C. Arch. Biochem. Biophys*. **1995,** *322*, 339-346.

glycoside, although the 7 and 4-positions may also be glycosylated, in the flavanols isolated from some plants, e.g. onions[42]. Other classes of flavonoids, such as the flavones, flavanones and isoflavones, are found mainly glycosylated in the 7-position[43]. Structural variation among the flavonoid glycosides lie both in the nature of the sugar residue (glucose, fructose, etc.) as well as the position and orientation (α,β) of attachment *via* the hydroxy groups to the aglycone. Due to the vast difference in the concentration (0.001% to 20%) of these glycosides of the plant's dry weight, the minor constituents are often overseen due to insufficient material for full identification.

Flavone and flavonol glycosides

Flavonoids occur mostly in *O*-glycosidic combinations with a number of sugars such as glucose, galactose, rhamnose, arabinose, xylose and rutinose[44]. Flavonoids carrying sugar moieties and their acylated and sulphated derivatives are all termed 'glycosides'. At least 2500 different flavone and flavonol glycosides have been reported[45] with the most common flavonols, quercetin, kaempferol and myricetin each having over seventy glycosidic combinations. Numerous derivatives of the two most common flavones, apigenin and luteolin[46] exist. Thirty-six glycosides of isoprenylated flavonols are reported[36]. Flavonol glucosides with all the hydroxy groups of the glucose unit substituted by acyl groups change the solubility properties of the flavonol glucoside, converting it into a lipophilic substance[47]. These glucosides occur in the cytoplasm or epidermal cells of the leaf and are known to have fungitoxic properties. Glycosylation and *O*-methylation of flavones and flavonols increase the hydrophilic character and polyhydroxylated flavones and flavonols occur as such glycosides rather than the aglycone[48].

---

[42] Fossen, T., Pedersen, A.T. and Anderson, O.M., *Phytochemistry* **1998,** *47*, 281.
[43] Harborne, J.B., Mabry, T.J. and Mabry, H. (1975) *The Flavonoids*, Chapman and Hall, London.
[44] U. Justesen , P. Knuthsen, T. Leth, *Journal of Chromatography A*, **1998,** 101
[45] C.A Williams, J.B Harborne, in *The Flavonoids: Advances in Research since 1986* (ed. J. B. Harborne), Chapman and Hall, London, **1993,** 337.
[46] Harborne J. B. and Williams C. A., in *The Flavonoids*, **1975,** (eds J. B. Harborne, T. J. Mabry and H. Mabry), Chapman and Hall, London, 376
[47] Romussi G., Bignardi G., Pizza C. and De Tommasi N.*, Arch. Pharm*., **1991**, *324*, 519
[48] Gottlieb O. R., in *The Flavonoids*, **1975,** (eds J. B. Harborne, T. J. Mabry and H. Mabry), Chapman and Hall, London, 297

Flavan Glycosides

Few natural flavan *O*-glycosides have been isolated and identified up to date. The general structure of natural flavan *O*-glycosides are exemplified by viscutin-1,2,3 **(21,22,23)** [49] which were found in the twigs of *Viscum tuberculatum* [50]. 7,4'-Dihydroxy-5-(xylopyranosyloxy)-flavan is isolated from the leaves of *Buckleya lanceolata*.

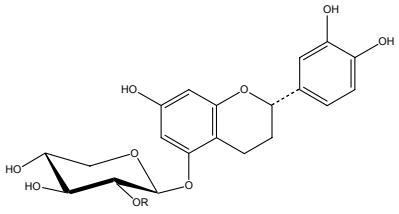

(21) R= p- Hydroxybenzoyl
(22) R= Caffeoyl
(23) R= H

In the separation and purification of glycosides, paper[50], thin layer[50] and column chromatography[50,51] are employed. Spectral methods such as UV, IR, MS and NMR play a prominent role in glycoside identification, although traditional chemical methods such as acid and enzyme hydrolysis[52], R_f values and color properties, selective methylation of phenolic hydroxy groups and periodate oxidation[23] are successfully utilized in the identification of glycosides. UV spectral analysis is of primary importance in the determination of the position of substitution of the sugars on the aglycone. When very small amounts of material are available, IR,[53,54] is also used. Techniques such as centrifugal partition chromatography (CPC) in conjunction with HPLC have been used in purification. Before spectral analysis flavonol

[49] Porter L.J., in *The Flavonoids: Advances in Research since 1986* (eds J. B. Harborne), Chapman and Hall, London, **1993**, 27.
[50] Kubo I. et.al., *Tett. Lett.*, **1987**. *28 no. 9*, 921.
[51] Johnston K. M., Stern D. J. and Waiss A. C., *J. Chromatogr.* **1968***, 33*, 539
[52] Glennie C. W. and Harborne J. B., *Phytochemistry*, **1971**, *10*, 1325
[53] Jurd L., in *The Chemistry of Flavonoid Compounds*, (ed. T. A. Geissman), Pergamon Press, Oxford, **1962**, 107-155.
[54] Wagner H., in *Methods in Polyphenol Chemistry*, (ed. J. B. Pridham), Pergamon, Oxford, **1963**, 37-48.

glycosides are often purified by gel filtration on Sephadex LH 20. Hiermann[55] claims better results if Fractogel PGM 2000 is used instead of Sephadex.

The increase in the number of reports of new glycosides, is largely due to the advances in methods of separation e.g. the excellent resolution of closely related structures by HPLC and the more prominent use of ^{1}H and ^{13}C NMR spectroscopy for glycoside identification. Mass spectrometry has played an important role and continues to be explored as a means of structural elucidation. While fast atom bombardment mass spectrometry (FAB-MS) is used by most researchers to obtain a strong molecular-ion peak which clearly indicates the number and type of sugar units present, Sakushima *et al*[56] propose desorption chemical ionisation mass spectrometry (DCI-MS) as an alternative for analyzing the sugar units as well as the presence of 1→6 linked diglycosides such as robinobiosides, gentiobiosides and rutinosides. ^{1}H NMR spectroscopy is widely used for structural analysis and is valuable for the identification of more complex derivatives[57] such as trimethyl silyl[60] and methyl ethers or acetals.

Flavone and Flavonol *O*-glycosidic units

Paper chromatography and gas chromatography of trimethylsilyl derivatives as well as ^{1}H and ^{13}C NMR spectroscopy are commonly used for the identification of the monosaccharides of flavonoid-*O*-glycosides. Oligosaccharide linkages are commonly detected with FAB-MS and ^{13}C NMR spectroscopy[58].

[55] Hiermann A., *J. Chromatogr,* **1986,** *362,* 152
[56] Sakushima A., Nishibe S. and Brandenberger H., *Biomed. Environ. Mass. Spectrom*., **1989**, *18*, 809
[57] Mabry T. J., Markham K. R. and Thomas M. B., *The Systematic Identification of Flavonoids***, 1970**, Springer-Verlag, Berlin
[58] Middleton E. and Kandaswami C., in *The Flavonoids: Advances in Research since 1986,* (ed. J. B. Harborne), Chapman and Hall, London, **1993,** 619 and the references there in

Monosaccharides

The monosaccharides are most commonly found in *O*-glycosidic combination with flavone and flavonol aglycones. The monosaccharides usually assume the pyranose form,[59] although the less stable furanose form is reported occasionally [60]. The D-sugars, glucose, galactose, glucuronic acid and xylose are usually *β*-linked to the hydroxy group of the aglycone while the L-sugars, rhamnose and arabinose are normally α-linked. However, α- and β- linked 3-arabinosides of quercetin have been reported[61, 62]. Both kaempferol 3-α- and 3-β-glycosides are present in the flowers of *Alcea nudiflora*[63]. The rarest sugar associated with flavones is apiose, a branched chain pentose, existing as 4 different isomers.

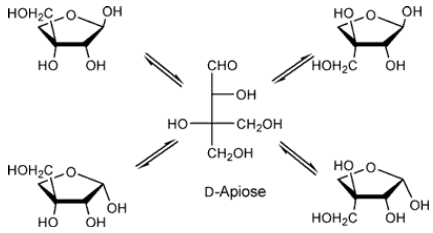

Disaccharides

Harborne *et.al* describes the combination of the disaccharide units as pentose-pentose, hexose-pentose, hexose-hexose, pentose-uroglucoronic acid and uroglucoronic acid-uroglucoronic acid. Rutinose (6-*O*-α-L-rhamnosyl-D-glucose) *e.g* quercetin-3-rutinoside[52] (Rutin), is the most common disaccharide in plants with two different sugar units. The number of known allose-containing glycosides increased in recent years with flavones bearing allosyl(1→2) glycosides fairly common in the family Labiatae. They were also found in *Teucrium, Sideritis,* and *Stachys* genus[64].

[59] El. Khadam H. and Mohammed Y. S., *J. Chem. Soc*., **1958**, 3320
[60] Pakudina Z. P. and Sadykov A. S., *Khim. Prir. Soedin*, **1970**, *6*, 27
[61] Geissman T. A., *The Chemistry of Flavanoid Compounds*, **1962,** Pergamon Press, Oxford
[62] Glyzin V. I., Bankoviskii A. I., *Khim. Prir. Soedin,* **1971,** *7*, 662
[63] Pakudina Z. P., Leontiev V. B. and Kamaev F. G., *Khim. Prir. Soedin*, **1970**, *6*, 555
[64] Harborne J.B. and Williams C. A. in *The Flavonoids: Advances in Research 1980,* (eds. J. B. Harborne), Chapman and Hall, London, **1988,** 306.

Quercetin-3-rutinoside

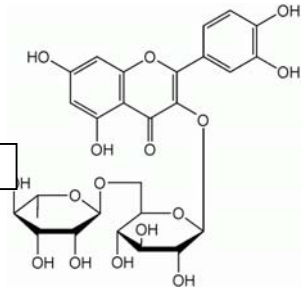

Trisaccharides

The trisaccharides of flavones and flavonols are assigned to two groups, linear and branched, mainly by FAB-MS and ^{13}C NMR spectroscopy. More linear trisaccharides are known than the branched sugars. The trisaccharide, glucosyl (1→3)-rhamnosyl-(1→6)-glucose, is found attached to the 3-position of quercetin and kaempferol in the leaves of the tea plant Teacceace (*Camellia sinensis*)[65].

Some of the novel branched trisaccharides are apiosyl-(1→2)-[rhamnosyl-(1→6)-galactose] attached to the 3-hydroxyl position of kaempferol[66,67], and glucosyl-(1→6)-[apiosyl-(1→2)-glucose] attached to the of patuletin in the same position[68]. Other glucose combinations are based on the glucose units of galactose and rhamnose [69, 70, 71].

[65] Finger A., Engelhardt U. H. and Wray V., *Phytochemistry*, **1991**, *30*, 2057
[66] De Simone F., Dini A., Pizza C., Saturnino P. and Schettino O., *Phytochemistry,* **1990,** 3690
[67] Bashir A., Hamburger M., Gupta M. P., Solis P. N. and Hostettmann K., *Phytochemistry,* **1991,** *30,* 3781
[68] Aritomi M., Komori T. and Kawasaki T., *Phytochemistry*, **1986,** *25,* 231
[69] Nawwar M. A. M., El-Mousallamy A. M. D. and Barakat H. H., *Phytochemistry*, **1989,** *28,* 1755
[70] Marco J. A., Adell J., Barbera O.. Strack D. and Wray V., *Phytochemistry*,**1989**, *28,* 1513
[71] Sekine T., Arita J., Yamaguchi A., Saito K., Okonogi S., Morisaki N., Iwasaki S. and Murakoshi I., *Phytochemistry,* **1991,** *30,* 991

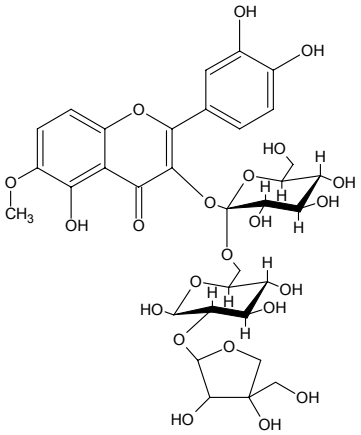

Patuletin-3-*O*-glucosyl-(1→6)
-[apiosyl-(1→2)-glucose]

Tetrasaccharides

Although no linear tetrasaccharides have been reported so far, a branched tetrasaccharide acetylated at the 6'''-position of the sophorose (2-*O*-β-D-glucopyranosyl-α-D-glucose), rhamnosyl-(1→4)-glucosyl-(1→6)sophorose, was found attached *via* the 7-hydroxy of acacetin[72]. Ultra violet and ^{1}H NMR analyses were used for structure elucidation, following acid hydrolysis to yield the free sugar moiety, and the position of the sugar linkage determined by ^{13}C NMR spectroscopy.

Acylated derivatives

Both flavone and flavonol glycosides occur in acylated form with acids such as *p*-coumaric[73], caffeic[74], sinapic[75], ferulic[76], gallic[77], benzoic[78], acetic[79] and malonic[80] acid, with the *p*-coumaric[78] and ferulic acids[81] occurring most frequently. Novel acylated derivatives (42 flavones and 99 flavonols) are reported in literature between

[72] Ahmed A.A., Saleh N. A. M., *J. Nat. Prod.,* **1987,** *50,* 256
[73] Karl C., Muller G. and Pedersen P. A., *Phytochemistry*, **1976**, *15*, 1084
[74] Gella E.V., Makarova G.V. and Borisyuk T.G., *Farmatsert. Zh. (Kiev)*, **1967**, *22,* 80
[75] Stengel B. and Geiger H., *Z. Naturforsch.,* **1976**, *31*, 622
[76] Markham K. R., Zinsmeister H. D. and Mues R., *Phytochemistry*, **1978**, *17*, 1601
[77] Collins F.W., Bohm B.A. and Wilkins C.K., *Phytochemistry*, **1975,** *14*, 1099
[78] Sconsiegel I., Egger K. and Keil M., *Z. Naturforsch.,* **1969**, *24*, 1213
[79] Radaelli C., Fotmentin L. and Santaniello E., *Phytochemistry***, 1980***, 19,* 985
[80] Woeldecke M. and Herrmann K., *Z. Naturforsch.,* **1974,** *29,* 355

1986 and 1991[2]. Most new reports view acetic acid as acylating agent of the sugar units (16 flavones and 44 new flavonol derivatives)[2]. The difficulties encountered with preparative plate (PC) and commercially obtained Thin Layer Chromatography (TLC) procedures to detect the acetic acid which is volatile and the acetyl groups which are labile by mild acid hydrolysis are overcome by the application of FAB-MS and ^{13}C NMR techniques. Hence, new acylated flavanoids such as a tri-acetate, kaempferol-3-(2''', 3''', 5'''-triacetyl)-arabinofuranosyl-(1→6)-glucoside, from flowers of *Calluna vulgaris* (Ericaceae)[81] and two tetra-acylated glycosides of kaempferol with two acetyl and two *p*-coumaroyl units on the same glucose residue have been characterized[51].

The malonate derivatives (five flavones and two flavonols) identified, include the 5-(6''-malonylglycosides) of apigenin, genkwanin (4',5-Dihydroxy-7-methoxyflavone), luteolin[82] and kaempferol-3-apiosylmalonyl glycosides[83].

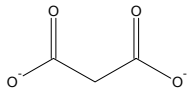

Malonyl ion structure

Biosynthesis of Flavonoids

Both flavonoid precursors (4-coumaroyl-CoA **(32)** and malonyl-CoA) are derived from carbohydrates. Malonyl-CoA is synthesized from the glycolysis intermediate, acetyl-CoA, and carbon dioxide, by acetyl-CoA carboxylase. The formation of 4-coumaroyl-CoA involves the shikimate/arogenate pathway, the main route to the aromatic amino acids phenylalanine and tyrosine in higher plants[84]. Subsequent transformation of phenylalanine to trans-cinnamate is catalyzed by phenylalanine ammonia-lyase, which provides the link between primary metabolism and the

[81] Allias D. P., Simon A., Bennini B., Chulia A. J., Kaouadji M. and Delage C., *Phytochemistry*, **1991,** *30***,** 3099
[82] Viet M., Greiger H., Czygan F.C. and Markham K.R., *Phytochemistry*, **1990**, *29,* 2555
[83] Wald B., Wray V., Galensa R. and Herrmann K., *Phytochemistry*, **1989**, *28,* 663

phenylpropanoid pathway. Aromatic hydroxylation of cinnamate by cinnamate 4-hydroxylase leads to 4-coumarate, which is further transformed to 4-coumaroyl-CoA by the action of 4-coumarate CoA ligase[85]. (**Scheme 1.3**)

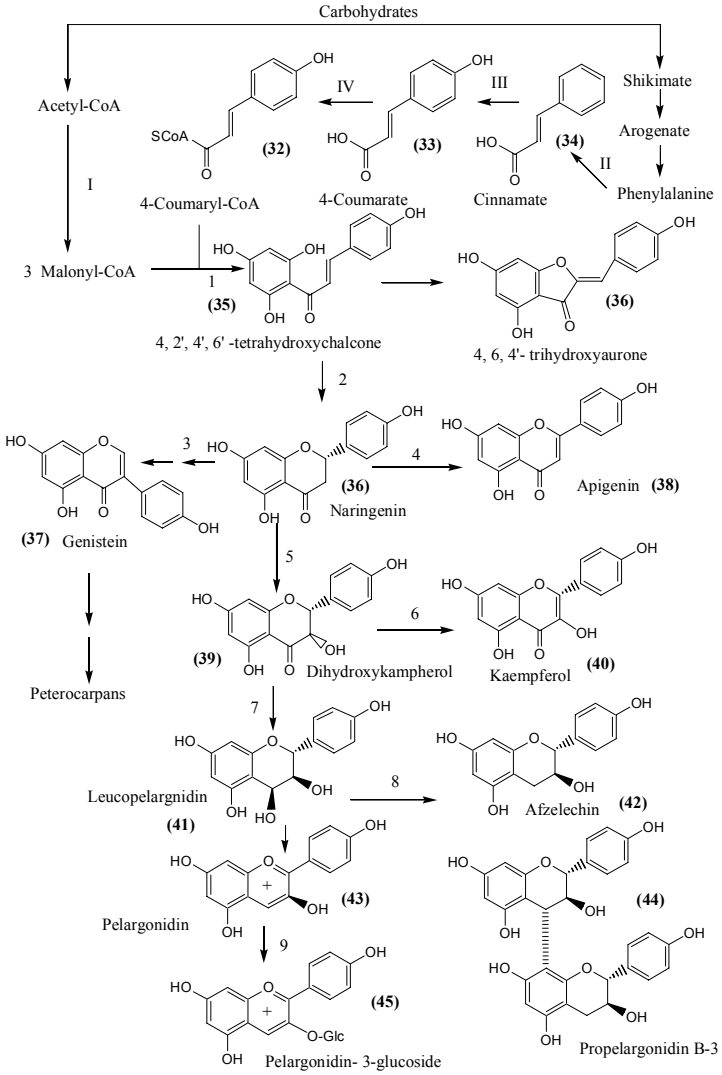

Scheme 1.3 (Biosynthesis of flavonoids)

The tetrahydroxychalcone intermediate **(35)** is formed by the condensation of three molecules of malonyl-CoA with a suitable hydroxycinnamic acid CoA ester, normally 4-coumaroyl-CoA, and is catalyzed by chalcone synthase. Flavonoids, aurones and other diphenylpropanoids are derived from the chalcone intermediate. Transformation by stereospecific action of chalcone isomerase provides the flavonoid, (2*S*)-flavanone

[85] Heller W. and Forkmann G., in *The Flavonoids: Advances in Research 1980,* (eds. J. B. Harborne), Chapman and Hall, London, **1988,** 399

(naringenin) **(37)**. Oxidative rearrangement of the flavanone, involving a 2,3-aryl shift, which is catalyzed by 'isoflavone synthase' yields an isoflavone (genistein) **(39)**. The dehydrogenation of the flavanone leads to the abundant flavones (apigenin) **(38)**, and is catalyzed by two enzymes, a dioxygenase and a mixed-function mono-oxygenase [86] . Dihydroflavonols (dihydrokaempferol) **(39)** are formed by α-hydroxylation of flavanones. This reaction is catalyzed by flavanone 3-hydroxylase. Dihydroflavonols are intermediates in the formation of flavonols, catechins, proanthocyanidins and anthocyanidins[99]. The large class of flavonoids, the flavonols (e.g. kaempferol) **(40)** are formed by the oxidation of the C-2,3 bond of dihydroflavonols and is catalyzed by flavonol synthase. Reduction of the carbonyl group of dihydroflavonols in the 4-position give rise to flavan-2,3-*trans*-3,4-*cis*-*diols* (leucopelargonidin) **(41)**. Leucoanthocyanidins, are the immediate precursors for flavan-3-ols and proanthocyanidins. These e.g. **(42)** are synthesized from leucoanthocyanidins by action of flavan 3,*4*-*cis*-*diol* reductase. Proanthocyanidins (propelargonidin B-3) **(44)** are formed by the condensation of flavan-3ols and leucoanthocyanidins. The reaction steps from leucoanthocyanidins to anthocyanidins (pelargonidin) **(43)** are still unknown. But, an obligatory reaction in the sequence is glycosylation, usually glucosylation in the 3-position of the anthocyanidin or of a suitable intermediate. This reaction leads to the first stable anthocyanin (e.g. pelargonidin 3-glucoside) **(45)**[99]. Hydroxylation, methylation of the A- and in particular the B-ring hydroxy groups, as well as glycosylation and acylation result in the great diversity of natural flavonoids. Numerous enzymes catalyzing these modifications are described, some of which can act on both intermediates (flavanone or dihydroflavonol) and end products (flavone, isoflavone, flavonol or anthocyanidin-3-glucoside), others only on the end products.

[86] Heller W. and Forkmann G., in *The Flavonoids: Advances in Research 1980,* (eds. J. B. Harborne), Chapman and Hall, London, **1988,** 401

C-Glycosylflavonoids

The *C*-glycosylflavonoids are quite common in plants and more than 300 are currently described.

Sources of flavone-*C*-glycosides are *V. lucens* (heartwood)*, Castanospermum australe* (wood)[87], and *Zelkowa serrata* (wood)[88]. Chalcone-*C*-glycosides are isolated from *Cladrastis shikokiana* (leaf), isoflavone-*C*-glucosides from *Dalbergia paniculata* (seed, bark), isoflavanone-*C*-glycosides from *Dalbergia paniculata* (flower) and flavanol-*C*-glycosides from *Cinnamomum cassia* (bark)[89].

Few xanthone *C*-glycosides are known and all are difficult to hydrolyse to the aglycones[90].

More *O*-glycosylated xanthones are known than *C*-glycosylated analogues. Two examples of naturally occurring *C*-glycosides include mangiferin and isomangiferin[91]

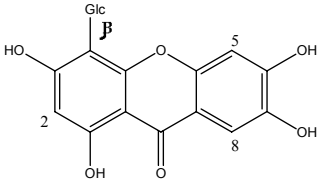

(19)

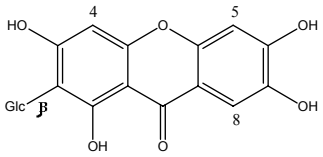

(20)

Sources of Mangiferin include *Gyrinops walla*[92] and *Mangifera indica*[93].

Synthesis of C-glycosylflavonoids

The high-yield *C*-glucosylation of 1,3,5-trimethoxy benzene with tetra-acetyl-α-D-glucosyl bromide in the synthesis of 4,5,7,-tri-*O*-methylvitexin [94] has not been repeated in the synthesis of other 4,5,7-tri-O-methyl-8-*C*-glycosylapigenins. However,

---

[87] Harborne J.B., in the *Natural Products of Woody Plants I*; (ed, J. W. Rowe), Springer-Verlag, Berlin, **1990**, 537

[88] Harborne J.B., in the *Natural Products of Woody Plants I*; (ed, J. W. Rowe), Springer-Verlag, Berlin, **1990**, 541

[89] Chopin J., Dellamonica G., in *The Flavonoids: Advances in Research since 1980* (ed. J. B. Harborne), Chapman and Hall, London, **1988,** 70-71 and references there in.

[90] Dean F.M., *Naturally occurring oxygen ring compounds*, **1963**, 268.

[91] Dean F.M., *Naturally occurring oxygen ring compounds*, **1963**, 275.

[92] Schun Y., Cordell G.A., *J. of Nat. Prod.,***1985**.*48*, 684

[93] Saleh N.A.M., El-Ansari M.A.I., *Planta Med.*, **1975**, *28*, 124

[94] Eade R.A., Pham H. P., *Aust. J. Chem.*, **1979**, *32*, 2483.

the reaction of 1,3,5-trimethoxybenzene with tetra-acetyl-α-D galactopyranosyl bromide, triacetyl-α-D-xylopyranosyl bromide, triacetyl-β-L-arabinopyranosyl bromide and triacetyl-α-L-rhamnopyranosyl bromide were successfully employed by Chari (unpublished) to synthesize the corresponding l-(2',4',6'-trimethoxyphenyl)-1,5-anhydroalditols for ^{13}C NMR spectroscopy.[95] A synthesis of 7,4'-di-*O*-methylisobayin (6-*C*-β-D-glucopyranosyl-7,4'-dimethoxyflavone) is described [96] (**Scheme 1.4**) and involves the reaction between 2,4-dimethoxyphenylmagnesium bromide **(46)** and 2,3,4,6-tetra-*O*-benzylglucopyranosyl chloride **(47)** to yield 2,3,4,6-tetra-*O*-benzyl-β-D-glucopyranosyl-2,4-dimethoxybenzene **(48)** which was converted to the tetra-acetate (**49)** after debenzylation.

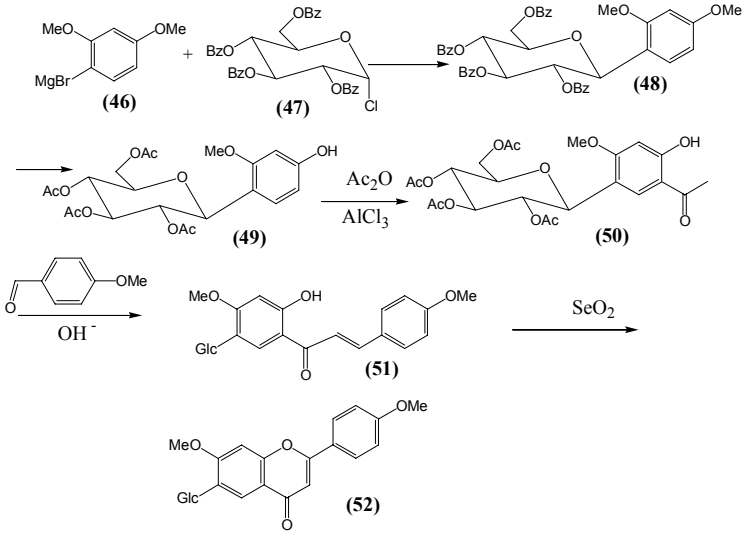

Scheme 1.4

The acylation of the tetraacetate gave 5-β-D-glucopyranosyl-2-hydroxy-4-methoxyacetophenone tetra-acetate **(50)**. Condensation of the latter with 4-methoxybenzaldehyde in alkaline medium gave 5'-β-D-glucopyranosyl-2'-hydroxy-4,4'-dimethoxychalcone **(51)** from which reacts with selenium dioxide to give 7,4', di-*O*-methylisobayin **(52)**. Many different methodologies exist for *C*-glycosylation and considerable progress was made in this regard.

[95] Markham K. R., Chari V. M., in *The Flavonoids: Advances in Research* (eds. J. B. Harborne, T. J. Mabry), Chapman and Hall, London, **1982**, 19
[96] Tschesche R., Widera W., *Liebigs. Ann. Chem.,* **1982**, 902

Identification

^{1}H and ^{13}C NMR spectroscopy are classically utilized to assign the *C*-glycosyl, *O*-glycosyl or *O*-acyl groups to the 6- or 8-position, and to indicate the configuration of the glycosidic linkage, with respect to the anomeric proton. The distinction between *C*-6 and *C*-8 linkage of the sugar moiety is made, partly on the chemical shift changes induced in aromatic protons when phenolic hydroxy groups are acetylated and finally, on the fragmentation patterns of the methylated derivative in El-MS[97].

The 5-methoxy group occurs at the most downfield position in a polymethoxylated flavone, e.g. with 6-*C*-boivinosyl-chrysoeriol (alternanthin; 6-(2,6-dideoxy-β-L-xylo-hexopyranosyl)-5,7-dihydroxy-2-(4-hydroxy-3-methoxyphenyl)-4H-1-benzopyran-4-one)[98] this signal could easily be irradiated, resulting in a highly significant n.O.e association between the methoxyl protons and anomeric proton (1"-H) when the sugar residue is attached at C-6. This is a popular method used to establish the connectivity of the glycoside unit

^{1}H and ^{13}C NMR spectra for certain 8-*C*-glycosylflavones exhibit extensive doubling of signals as in the case of 5,7,2',3',4'flavone (tricetin)-6,8-di-*C*-glycoside where two signals are noted for 2-C (164.3, 1649), 5-C (158.9, 160.2), 3-H (6.57, 6.54) and 5-OH (13.77, 13.69)[99]. This phenomenon is observed in almost all compounds containing an 8-*C*-hexosyl substituents (vitexin, vitexin-7-*O*-glucoside, tricetin-6,8-di-*C*-glucoside, lucenin-2, tricetin-6-*C*-arabinosyl-8-*C*-glucoside and stellarin-2). In contrast, no doubling of the signals are found in compounds without an 8-*C*-hexosyl residue. The spectra of vitexin-2"-*O*-rhamnoside and orientin-2"-*O*-glucoside shows only broadening of signals. These observations suggest that in flavones, interaction occur between a *C*-linked monohexose at C-8 and the B-ring. Since the 8-*C*-pentopyranosides do not exhibit this feature, the primary hydroxy group of the hexose would appear to be the functional group interacting with the B-ring. This results in restricting rotation of the B-ring and/or the hexose, giving rise to a mixture of two

[97] Jay M., in *The Flavonoids: Advances in Research since 1986* (eds J. B. Harborne), Chapman and Hall, London, **1993**, 85.
[98] Zhou B.N., Blasko G., *et al.*, *Phytochemistry,* **1988**, *27*, 3633.
[99] Markham K. R., Mues R., *et al., Z. Naturforsch*, **1987**, *42c*, 562.

rotamers, which are distinguishable by NMR[100]. An additional sugar moiety at the 2"-position complicates this situation by apparently locking the 8-*C*-hexosyl unit in a position that hinders its interaction with the B-ring. Likewise, signal doubling is not observed in the spectra of 8-*C*-hexosides in which the B-ring is moved away from possible steric interaction with the sugar moiety, as in the 8-*C*-glycosyl-isoflavones.
The existence of such rotamers are confirmed for lucenin-2 and stallarin-2 where double signals are observed at 25°C, which disappear completely at 90°C[112].

C-Glycosylflavones and ultraviolet light screening

With respect to a hypothesis regarding the potentially important evolutionary role of flavonoids as a UV light screening, a study carried out on seventeen species of the pondweed genus *Potamogeton* [101] was carried out. Several *C*-glycosylflavones was found in the floating foliage of these species which have both submerged and floating foliage. *C*-glycosylflavones would be synthesized in floating leaves because of their filtering ability. The lack of these compounds in submerged leaves would be attributable to the ability of naturally colored water to absorb UV radiation significantly. These results seem to support an earlier hypothesis suggesting the importance of flavonoid evolution in the conquest by plants of exposed terrestrial habitats[100].

Biological significance of Flavonoids

Since flavonoids are representative of the evolutionary process, it seems reasonable to assume that they perform essential physiological functions, in plants. Szent Györgyi argued that flavonoids might also be essential for man, similar to vitamins. This suggestion could not be substantiated, but the investigations of Szent Györgyi performed on vitamins at the same time initiated and promoted the use of flavonoids

[100] Jay M., in *The Flavonoid: Advances in Research since 1986*; Harborne, J. B. Ed.; Chapman and Hall: London, **1993**; p 86
[101] Les D., Sheridan D.J., *Am. J. Bot.,* **1990**, *77*, 453

as drugs. One major reason for the skepticism in accepting bioflavonoids as drugs might be their ubiquitous occurrence in the plant kingdom and their presence in vegetables, fruits and spices in our daily nutrition[117].

Thus, the question posed whether a class of compounds of which large amounts are ingested daily in food could be recognized as a drug. A second reason might be due to the polyphenolic character of many flavonoids, which means the possibility of multiple interactions with proteins on the cell surface, receptors and enzymes[118]. Such multiple interactions suggest unspecific reactions with various body functions in line with the numerous biological activities described for flavonoids.

Another characteristic property of most phenolic compounds after oral intake is their rapid oxidation/reduction, glucuronidation and sulfation which results in a very fast inactivation and elimination rate. Therefore, the amount of flavonoids ingested requires extremely high intake (grams/diet) to have them in sufficient blood concentration for their bioavailability. Nevertheless, the average daily diet of humans contain about 1g of flavonoids, which is high enough to bring the flavonoid concentration to a pharmacological significant level in tissues[119].

Antioxidant activity of flavonoids

Flavonoids act as scavengers of various oxidizing species i.e. superoxide anion (O_2^-), hydroxyl radical or peroxy radicals. They may also act as quenchers of singlet oxygen. Often an overall antioxidant effect is observed. Noteworthy is an improved method developed to compare the antioxidant activity of selected flavonoids[102] from different classes by measuring the quantum yields of sensitized photo-oxidation of individual flavonoids. This is coupled with the determination of photo-oxidation based on measuring the singlet oxygen luminescence. It was concluded that the presence of a catechol moiety in the B-ring is the main factor controlling the efficiency of O_2^- physical quenching. The presence of a C-ring 3-OH likewise

[117] Middleton E., *Pharmaceutical News*, **1994,** *1*, 6-8
[118] Spencer C.M., Cai Y., Martin R., *et al, Phytochemistry*, **1988**, *27*, 2397-2409
[119] Das D. K., *Methods Enzymol*, **1994**, *234*, 410-420
[102] Tourna ire C. and Croux S., *Journal of Photochemistry and Photobiology*, **1993,** *19*, 205.

contributes to the efficiency of their chemical reactivity with O_2^- , but the catechol moiety is generally more prominent[103].

A carbonyl group at C-4 and a double bond between C-2 and C-3 are also important features for high antioxidant activity in flavonols[104]. Butein and other 3,4-dihydroxychalcones are more active than analogous flavones because of their ability to achieve greater conjugative electron delocalization[105]. Similarly, isoflavones are often more active than flavones due to the stabilizing effects of the 4-carbonyl and 5-OH group in the former[108]. In the antioxidant action of *ortho*-dihydroxyflavonoids metal chelation becomes an important factor[106].

Antimicrobial activity of flavonoids

One of the functions of flavonoids and related polyphenols is their role in protecting plants against microbial invasion. This not only involves their presence in plants as essential agents but also their function as phytoalexins in response to microbial attack[107, 108]. Because of their widespread ability to inhibit spore germination of plant pathogens, they are proposed for use against fungal pathogens of Man. There is an ever-increasing interest in plant flavonoids for treating human diseases and especially for controlling the immunodeficiency virus, the cause of AIDS[109].

Biological activities of the isolated compounds

Hesperidin is renowned for the vitamin C like activity and anti-inflammatory, antimicrobial, and antiviral properties[110]. Hesperidin also produces analgesia and exerts mild antipyresis[111]. Indications that hesperidin reduces aggregation of blood

[103] Harborne J. B., Williams C. A., *Phytochemistry* 55*,* **2000**, 490.
[104] Das N.P., Pereira T.A*., Journal of American Oil Chemists Society*, **1990**, *67*, 255.
[105] Dziedzic S.Z., Hudson B. J. F., *Food Chemistry*, 1983**,** *11*, 161.
[106] Shahidi F., Wanasundara P., Hong C., *American Chemical Society*, **1991**, 214
[107] Grayer R.J., Harborne J.B., Kimmins E.M., Stevenson F.C., Wijayagunasekera H.N.P., *Acta Horticulturae*, **1994**, *381*, 691.
[108] Harborne J.B., *Biochemical Systematics and Ecology*, **1999**, *27*, 335.
[109] Harborne J. B. and Williams C. A., *Phytochemistry 55,* **2000**, 487.
[110] Middleton E., Kandaswami C., *The Flavonoids–Advances in Research Since 1986,* Harborne J. B., Ed., Chapman and Hall, London, **1993**, pp. 619-652.
[111] Emin J. E. D. S., Oliveira A. B., Lapa A. J., *J. Pharm. Pharmacol.* **1994,** *46*, 118-122.

cells (erythrocytes), abnormal capillary permeability and fragility, and its protection against various traumas and stress is reported[112]

Luteolin is known for its antispasmodic[113] and antioxidant properties[114]. The antioxidant[114, 115], diuretic[144], antiviral[115] antispasmodic[144] properties and cardio protective effects[116] of flavones are well established. Luteolin and its glycosides are particularly found to induce antihypertensive activity even in excess of the reference drug, papaverine[117].

Orobol have immunosuppressive and anti-inflammatory effects which are well-established[139,140].

Galloyl esters of catechins are more active as cancer preventatives than non-galloylated catechins due to their lower redox potentials[118]. They have the highest activity as antioxidants and are the most effective inhibitors of lipid peroxidation[119,120]. The antibacterial and deodorizing effects of catechins slow tooth decay and improve breath freshness[121]. Epigallocatechin gallate is capable of suppressing angiogenesis, a key process of blood vessel growth required for solid tumor development and metastasis[122,123].

Mangiferin is a common constituent of folk medicines and has potential as an antioxidant, an anti-viral agent and is used for melancholia[124]. Recently it has been reported to be a potent scavenger of free radicals[125], to be a potential cure for diabetes mellitus[126] and act as an agent for lowering body weight[127]. Generally, xanthones are

---

[112] Versantvoort C. H., Schuurhuis G. J., Pinedo H. M., Bekman C. A., Kuiper C. M., *Br. J. Cancer* **1993**, *68*, 939-946.
[113] Ratty A. K., *Biochem. Med. Metabol. Biol*. **1988**, *39*, 67-79.
[114] Rice-Evans C. A., Miller N. J., Paganga G., *Trends Plant Sci. Rev.* **1997**, *2*, 152-159.
[115] Hayashi K., Hayashi T., Arisawa M., Morita N., *Antiviral Chem. Chemother.* **1993**, *4*, 49-58.
[116] Huesken B. C. P., Dejong J., Beekman B., Onderwater R. C. A., *Cancer Chemother. Pharmacol.* **1995**, *37*, 55-62.
[117] Itoigawa M., Takeya K., Ito C., Furu Kawa H., *J. Enthnopharmacol.* **1999**, *65*, 267-272.

[118] Balentine D. A., Wiseman S. A., Bouwens L. C. M., *Crit. Rev. Food Sci. Nutr*. **1997**, *37*, 693-704.
[119] Jovanovic S. V., Steenken S., Tosic M., Marjanovic,B., Simic M. G., *J. Am. Chem. Soc.* **1994**, *116*, 4846-4851.
[120] Salah N., Miller N. J., paganga G., Tijburg L., Bolwell G. P., Rice-Evans C., *Arch. Biochem. Biophys.* **1995**, *322*, 339-346.
[121] Yasuda H., *Shokuhin Kogyo* **1992**, *35*, 28-33.
[122] Dreosti I. E., *Nutr. Rev.* **1996**, *54*, 51-58.
[123] Yang C. S., Wang Z.-Y., *J. Nat. Cancer Inst.* **1993**, *85*, 1038-1049.
[124] Bhattacharya S. K., Sanyal A. K., Ghosal S., *Naturwissenschaften* **1972**, *59*, 651.
[125] Sato T., Kawamoto A., Tamura A., Tatsumi Y., Fujii T., *Chem. Pharm. Bull*. **1992**, *40*, 721-724.
[126] Ichiki H., Miura T., Kubo M., Ishihara, E., Komatsu K., Tanigawa K., Okada M., *Biol. Pharm. Bull*. **1998**, *21*, 1389-1390.

reported to possess antitumour [128], antileukaemic, antiulcer, antimicrobial, antihepatotoxic, and CNS-depressant activity[129]. Bioactivities including cytotoxic, anti-inflammatory, and antifungal activities, enhancement of choline acetyltransferase activity and inhibition of lipid peroxidase are described[130]. Xanthones and their derivatives are shown to be effective as allergy inhibitors and bronchodilators in the treatment of asthma[131]. Structurally related 1,3,5,6-, 1,3,6,7-, 2,3,6,7- and 3,4,6,7-tetraoxygenated xanthones have been reported to possess antiplatelet effects, the mechanism of 1,3,6,7-tetraoxygenated xanthones being due to both inhibition of thromboxane formation and phosphoinositide[132, 133].

Results & Discussion

Both the acetone (M.Sc.) and the Methanol extract (Ph.D.) of *C. subternata* are discussed here to provide the reader with complete picture of the phenolic profile of the plant. Most of the compounds from the acetone extract were also isolated from the methanol extract of the plant, which warrants the discussion of compounds isolated from both extracts.

A precipitate (100 mg) from the initial acetone extract (A) (methanol extract is labeled as the B extract) was acetylated and purified by PLC in toluene–acetone (8:2) to give three bands at R_f 0.43 (10.5 mg), 0.35 (17.0 mg), and 0.30 (13.0 mg). Further purification of these bands in the same solvent yielded the *O*-acetyl derivatives (**54**), (**80**) and (**62**) of the known hesperidin (**53**) (9.0 mg), (+)-pinitol **79** (15.0 mg)[134,135] and scolymoside **61** (11.0 mg)[136], respectively.

---

[127] Yoshimi, N., Matsunaga K., Katayama M., Yamada,Y., Kuno T., Qiao Z., Hara A., Yamara J., Mori H., *Cancer Lett.* **2001**, *163*, 163-170.
[128] Kazmi S.N.-u.-H., Ahmed Z., Malik A., *Phytochemistry* **1989** *28*, 3572-3574.
[129] Peres, V., Nagem T. J., de Oliveira F. F., *Phytochemistry* **2000**, *55*, 683-710.
[130] Iinuma M., Tosa H., Tanaka T., Yonemori S., *Phytochemistry* **1994**, *35*, 527-532.
[131] Balasubramanian K., Rajagopalan K., *Phytochemistry* **1988**, *27*, 1552-1554.

[132] Lin C. N., Liou S. S., Ko F. N., Teng C. M., *J. Pharm. Sci*. **1993**, *82*, 11-16.
[133] Peres V., Nagem T. J., de Oliveira F. F., *Phytochemistry* **2000**, *55*, 683-710.
[134] Ferreira, D.; Kamara, B. I.; Brandt, E. V.; Joubert, E. Phenolic compounds from *Cyclopia intermedia* (Honeybush tea). *J. Agric. Food Chem.* **1998,** *46*, 3406-3410.
[135] Anhut S., Zinsmeister H. D., Mues R., Barz W., Mackenbrock K., Köster J., Markham K. R., *Phytochemistry* **1984**, *23,* 1073-1075.

[136] Kim N. M., Kim J., Chung H. Y., Choi J. S., *Arch Pharm Res.* **2000**, *23*, 237-239.

The acetone extract was separated on a Sephadex LH-20/EtOH column. Following TLC inspection, the collected tubes were combined to yield fractions A1-8. Fractions not reported do not contain compounds pertaining to this investigation.

Acetylation of A3 (50 mg) and PLC in toluene–acetone (8:2) afforded the peracetate derivative (**74**) of mangiferin (**73**) (R_f 0.45, 5.0 mg)[134].

Fraction A4 (50 mg) was acetylated and separated in toluene–acetone (7:3) to give one band, which on subsequent separation in the same solvent yielded the per-*O*-acetyl derivative (**76**) of 4-glucosyltyrosol (**75**) (R_f 0.21, 3.3 mg)[134].

Acetylation of A5 (50 mg) and PLC separation in toluene–acetone (8:2) afforded the peracetate derivative (**72**) of 6-*O*-glucosylkaempferol (**71**) (R_f 0.42, 5.5 mg)[134].

Fraction A6 (100 mg) was methylated and separated by PLC (toluene–acetone, 8:2) to give two bands at R_f 0.66 (13.4 mg) and 0.46 (5.5 mg). Purification of the bands in the same solvent gave the permethylated derivatives (**60**) and **(62**) of 5-deoxy luteolin (**59**) (R_f 0.66, 12.5 mg)[134] and luteolin (**61**) (R_f 0.46, 4.5 mg)[134], respectively.

Fraction A7 (100 mg) was acetylated and purified by TLC in toluene–acetone (8:2) to give two bands R_f 0.50 (9.4 mg) and 0.42 (16.0 mg). PLC purification of the R_f 0.50 band in the same solvent yielded the glucosylated flavan (**69**) as the per-*O*-acetyl derivative (**70**).

Purification of the R_f 0.42 band by PLC in toluene–acetone (8:2) afforded the peracetate derivative (**58**) of the flavanone, eriocitrin (**57**) (5.5 mg)[137].

Acetylation of fraction A8 (50 mg) and PLC in toluene–acetone (8:2) gave the peracetate derivative (**66**) of the isoflavone orobol (**65**) as a single band (R_f 0.76, 3.6 mg)[138, 139].

An aqueous suspension of the methanol extract was exhaustively extracted with ethyl acetate and separated on Sephadex LH-20/EtOH column. Following TLC inspection the collected tubes were combined to yield fractions B1-14. Fractions not reported do not contain compounds pertaining to this investigation or contained compounds already isolated from the acetone extract.

Fraction B2 (B = methanol extract) (100 mg) was acetylated and (100 mg) methylated and separated by PLC in toluene–acetone (8:2) to give two bands, which on

[137] Inoue T., Sugimoto Y. , Masuda H., Kamei C., *Biol. Pharm. Bull.* **2002**, *25*, 256-259.
[138] Mabry T. J., Kagan J., Rösler H., *Phytochemistry* **1965**, *4,* 487-493.
[139] Anhut S., Zinsmeister H. D., Mues R., Barz W., Mackenbrock K., Köster J., Markham K. R., *Phytochemistry*, **1984**, *23*, 1073-1075.

subsequent separation in the same solvent yielded the permethylated (**78**) and per-*O*-acetyl derivatives (**82**) of *p*-coumaric acid (**77**) (R_f 0.62, 4.6 mg)[139] and (±)-shikimic acid (**81**) (R_f 0.66, 32.6 mg)[140], respectively.

Fraction B3 (50 mg) was acetylated and purified by PLC in toluene–acetone (8:2) to give the peracetate derivative (**56**) of the known flavanone narirutin (**55**) (R_f 0.33, 8.0 mg)[137].

Acetylation of fraction B4 (100 mg) and subsequent PLC in toluene–acetone (8:2) yielded the peracetate derivative (**68**) of epigallocatechin gallate (**67**) as a single band (R_f 0.27, 33.6 mg)[140]in significant amounts.

The investigation on the derivatized fractions of the acetone extracts (M.Sc.) and methanol-ethyl acetate extract (Ph.D) of *C. subternata* revealed the presence of a varied range of phenolic and non-phenolic compounds as well as their glycosides (**Scheme 1.5**). These were successfully identified as flavanones (**53**), (**55**), and (**57**), flavones (**59**), (**61**), (**62**), (**63**), a flavonol (**71**), an isoflavone (**65**), epigallocatechin gallate (**67**), a flavan (**69**)**,** a xanthone (**73**), 4-glucosyl tyrosol, (**75**) *p*-coumaric acid (**77**), (+)-pinitol (**79**)**,** and (±)-shikimic acid (**81**). The highly insoluble hesperidin (**53**)[134] along with narirutin (**55**)[137] and erioctrin (**57**)[137] constituted the flavanones isolated from both extracts, and was identified as their peracetate derivatives (**54**)**,** (**56**)**,** and (**58**), respectively. Hesperidin, the major flavonoid constituent of the plant was isolated as a precipitate from an ethanolic solution of the acetone extract. The ^{1}H NMR of the peracetate derivatives of (**54**)**,** (**56**) and (**58**) show resonances at ~δ 2.75 and 3.0 (2 x H-3) and ~δ 5.5 (H-2), diagnostic of the flavanone nucleus. In addition, each of the three flavanones display two *meta* coupled doublets integrating for one proton each in the aromatic region between δ6.0-6.8, indicative of a phloroglucinol A-ring. The AA'BB' system exhibited by the peracetate (**56**) indicate a *para*-substituted B-ring, between δ7.0-7.5, which is confirmed by association of 2-H(C) with 2′,6′-H(B) in the NOESY spectrum. Similar association of 2′- and 6′-H(B) with 2-H(C) confirms an ABX system for the B-rings of *O*-acetyl derivatives (**54**) and (**58**).

[140] Yun J., Lee C.-K., Chang I.-M., Takatsu K., Hirano T., Min K.R., Lee M.K., Kim Y., *Life Sci.* **2000,** *67,* 2855–2863.

Nuclear Overhauser effect (n.O.e.) indicating association of the single OMe with 5-H(B) confirms the 4'-OMe substitution in (**53**). A sugar moiety is revealed by connectivity shown by the COSY spectrum. The linkages, rhamnosyl (1‴→6″) glucosyl and C-7-O-C-1″ of the glycosyl to ring A in flavanones (**54**)**,** (**56**) and (**58**) are confirmed by n.O.e. association of H-6″ with H-1‴ and of H-6 and 8 with H-1″, respectively. The circular dichroism (CD) spectra of these derivatives exhibited the synchronous Cotton effects (negative for the π→π* transition at ca. 300 nm and positive for the n→π* transition at ca. 340 nm), which are compatible with flavanones possessing a 2*S* absolute configuration[141]. Compound (**53**) was confirmed to be hesperedin by direct comparison of ^{1}H NMR data of its *O*-acetyl derivative (**54**) with that of an authentic sample[142]. Similarly the structures of narirutin (**55**) and eriocitrin (**57**) were confirmed by comparison of the ^{1}H NMR data of their peracetates with that in literature[143].

7-*O*-Rutinosyl-flavone (scolymoside) (**63**)[136] were isolated as the amorphous peracetate derivative (**64**). The flavone luteolin (**61**)[134] and 5-Deoxy luteolin (**59**)[134] was isolated as their permethylated derivatives (**60**) and (**62**).

The ^{1}H NMR spectra of (**60**), (**62**), and (**64**) invariably display the one proton singlet between δ6.5 and 6.8 reminiscent of the H-3 resonance of the flavones[144]. The connectivities, rhamnosyl (1‴→6″) glucosyl and C-7-O-C-1″ of the glycosyl moiety to the A-ring in (**64**) were confirmed by n.O.e. associations of H-6 and 8 with H-1‴, and H-6″ with H-1‴, respectively. All the glycosidic resonances in the ^{1}H NMR spectrum were assigned from the COSY data. The sequential connectivity, chemical shift parameters and coupling constant data, approximately 8 Hz for a β-coupled anomeric proton, confirms that the rutinosyl unit was an *O*-linked glycosyl with β-configuration[144].

A single isoflavone, (**65**)**,** display a singlet at δ 8.0 in the ^{1}H NMR spectrum of the peracetate derivative (**66**) which is characteristic of the single proton at C-2 in isoflavones. The ^{1}H NMR also exhibited the AB and ABX systems corresponding to

---

[141] Gaffield W., *Tetrahedron* **1970**, *26*, 4093-4108.

[142] Kamara B. I., Ph.D. thesis, Sasol Library, University of the Free State.

[143] Inoue T. , Sugimoto Y. , Masuda H. , Kamei C. , *Biol. Pharm. Bull.* **2002**, *25*, 256-259.

[144] Snyckers F. O., Salemi G., *S. Afr. J. Chem.*, **1974**, *27,* 5-7.

the tetra-substituted A- and tri-substituted B-rings, respectively. Subsequently, compound (**65**) was confirmed as orobol[138].

Epigallocatechin gallate (**67**), a predominant flavonoid found in different types of teas,[145] was isolated and characterized as its peracetate derivative (**68**) by comparison of it's ^{1}H NMR data with an authentic sample[146]. In the ^{1}H NMR spectrum of the *O*-acetyl derivative of epigallocatechin gallate (**68**), the aliphatic protons H-2, H-3, H-4_{ax} and H-4_{eq} are typically displayed at δ 5.65 (br, m), δ 5.20 (br, s), δ 3.08 (dd, J = 5.0 and 17.5 Hz) and δ 3.0 (dd, J = 3.0 and 17.5 Hz), respectively. The B-ring connectivity was confirmed by a n.O.e association of H-2 with the 2′,6′ singlet of the ring. H-2, -3 and -4 connectivity were confirmed by correlations in the COSY spectrum. Correlation in a HMBC spectrum from the carbonyl carbon to the singlet of H-2″,6″ distinguished the gallate from the H-2′,6′ singlet of the B-ring. The two *meta* coupled doublets in the aromatic region, between δ6.6-6.8, suggest a phloroglucinol-type hydroxylation pattern on ring A.

The peracetate derivative (**69**) of the novel flavan (**70**) was isolated from the acetone extract of the plant. The structure elucidation of this compound is discussed in Chapter 2.

A *C*-6-linked glucosylated derivative of kaempferol (**71**) was isolated as a peracetate derivative (**72**). Absence of the C-ring protons in the ^{1}H NMR spectrum in the peracetate derivative (**72**) was consistent with a flavonol skeleton. The glucosyl moiety was established from the COSY data. The structure was confirmed by comparison of the ^{1}H NMR data with that in the literature[4].

Mangiferin (**73**), 1,3,6,7-tetrahydroxyxanthone-C-2-β-*D*-glucoside, was isolated as the peracetate derivative (**54**) and its structure elucidated by comparison of its ^{1}H NMR data with that in literature[3].

Other phenolics

4-Glucosyl tyrosol (**75**) and *p*-coumaric acid (**77**), the monoaryls isolated from the tea was confirmed by comparison of ^{1}H NMR data of their peracetate (**76**) and

[145] Valcic S., Muders A., Jacobsen N. E., Leibler D. C., *Chem. Res. Toxicol.* **1999**, *12*, 382-386.
[146] Marais J.P.J., M.Sc., Sasol library, University of the Free State.

permethylated (**78**) derivatives with that of literature[134]. 4-Hydroxytyrosol is a potent antioxidant [147] . The antihepatotoxic properties of *p*-coumaric acid are well-established[148].

Nonphenolics

Pinitol (**79**), a well-established expectorant[148] was identified by comparison of the ^{1}H NMR data of its *O*-acetyl derivative (**80**) with that of the commercially available reference compound. ^{1}H NMR data of (**82**), the *O*-acetyl derivative of shikimic acid (**81**) is in agreement with the data of literature[149].

This in-depth investigation on the unfermented leaves and shoots of the *Cyclopia subternata* specie, from which honeybush tea is brewed, revealed phenolic metabolites with diverse physiological properties that have potential benefits for human health. Flavonoids (especially hesperidin), mangiferin, (a xanthone) and (+)-pinitol dominate in the tea. The results from this study may in part justify some of the claimed properties such as, use of the tonic for colds and influenza, and its effectiveness in alleviating menopausal symptoms in women. Honeybush tea is thus becoming an increasingly popular health-promoting beverage with low caffeine content and antioxidative constituents.

[147] Kris-Etherton P. M., Hecker,K. D., Bonanome A., Coval S. M., Binkoski A. E., Hilpert K. F., Griel A. E., Etherton T. D., *J. Am. Med. Assoc.* **2002**, *113*, 71-78.
[148] Rowe J. W., *Natural Products of Woody Plants II*, Beecher C. W. W., Farnsworth N. R., Gyllenhall C. Ed., Timell T. E., Springer-Verlag, Berlin, Heidelberg, New York, Paris, Tokyo, Hong Kong, **1989**, pp. 1059-1164.
[149] Haslam E., *Shikimic acid. Metabolism and metabolites* John Wiley & Sons, Chichester. New York. Brisbane. Toronto. Singapore. **1993**.

Scheme 1.5 Structures of compounds isolated from *Cyclopia Subternata* and their acetate derivatives

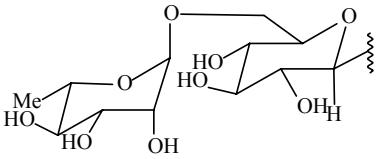

Rutinosyl moiety

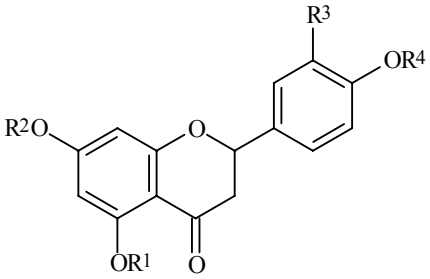

53, R^1=H; R^3=OH; R^4=Me; R^2= rutinosyl
54, R^1=Ac, R^3=OAc, R^4=Me,
R^2= hexa-*O*-acetylrutinosyl
55, R^1=R^3=R^4=H, R^2=rutinosyl
56, R^1=R^4=Ac, R^3=H,
R^2=hexa-*O*-acetylrutinosyl
57, R^1=R^4=H, R^3=OH, R^2= rutinosyl
58, R^1=R^4=Ac, R^3=OAc,
R^2= hexa-*O*-acetylrutinosyl

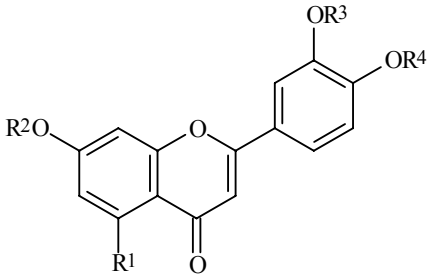

59, R^1=R^2=R^3=R^4=H
60, R^1=H, R^2=R^3=R^4=Me
61, R^1=OH, R^2=R^3=R^4=H
62, R^1=Me, R^2=R^3=R^4=Me
63, R^1=OH, R^3=R^4=Ac;
R^2= rutinosyl
64, R^1=OAc, R^3=R^4=Ac
R^2= hexa-*O*-acetylrutinosyl

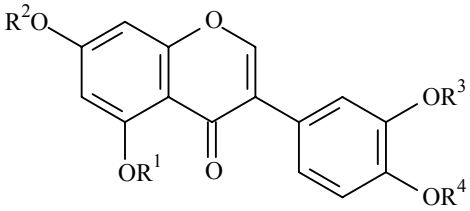

65, R^1=R^2=R^3=R^4=H
66, R^1=R^2=R^3=R^4=Ac

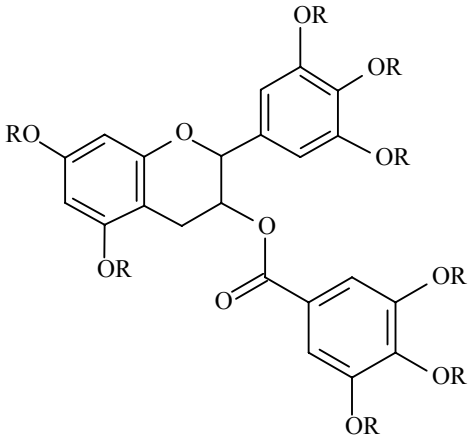

67, R=H
68, R=Ac

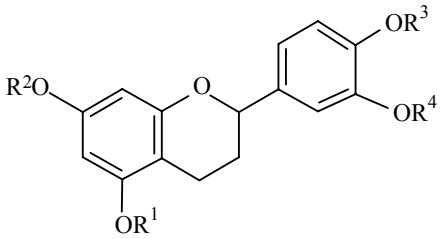

69, $R^2=R^3=R^4=H$,
R^1=2-β-*D*-glucopyranosyl
70, $R^2=R^3=R^4=OAc$
R^1=tetra -*O*-acetyl-2-β-*D*-glucopyranosyl

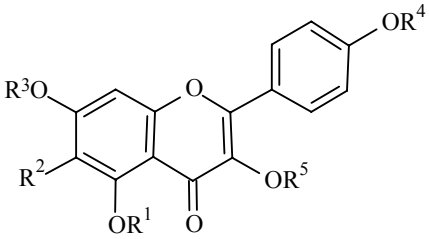

71, $R^1=R^3=R^4=R^5=H$,
R^2=2-β-*D*-glucopyranosyl
72, $R^1=R^3=R^4=R^5=Ac$, R^2=tetra-*O*-acetyl-2-β-*D*-glucopyranosyl

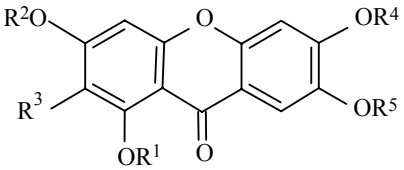

73, $R^1=R^2=R^4=R^5=H$,
R^3=2-β-*D*-glucopyranosyl
74, $R^1=R^2=R^4=R^6=Ac$,
R^3=tetra-*O*-acetyl-2-β-*D*-glucopyranosyl

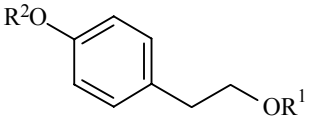

75.$R^1=H$,R^2=*O*-β-*D*- glucopyranosyl
76, $R^1=Ac$, R^2=tetra-*O*-acetyl- β-*D*-glucopyranosyl

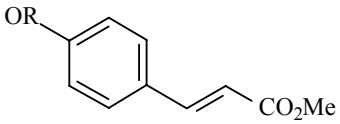

77, R=H
78, R=Me

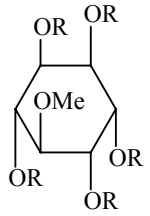

79, R=H
80, R=Ac

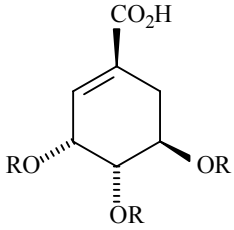

81, R=H
82, R=Ac

Experimental

Source of Plant Material.

Leaves and shoots of *C. subternata* were harvested from two experimental plantations established in the Simondium and Du Toits Kloof areas of the Western Cape region of South Africa. Drying of the plant material took place in a forced-air drying tunnel at 40 ^{o}C until moisture content of ca. 10% was reached, where after it was pulverized. A voucher specimen is kept in the Chemistry Department of the University of the Free State.

Extraction and Fractionation.

In order to remove chlorophyll, the pulverized plant material (6.0 kg) were extracted consecutively with chloroform, (2 x 6.0 L, 24 h each) to remove the chlorophyll, and acetone (2 x 5.0 L, 24 h each) at ~25 ^{o}C to yield dark green solids (155.5 and 86.8 g, respectively) on evaporation of the solvent. Ensuing extractions with methanol (4 x 5.0 L, 24 h each, ~25 ^{o}C) and subsequent ethylacetate (5 x 5.0 L, 24 h each, ~25 ^{o}C) extraction from the re-dissolved methanol (aq) extract afforded brown solids following evaporation of the solvents. These were re-dissolved in water and freeze-dried to give 495.5 and 702.5 g of extract, respectively.

Metabolites from the Acetone and Methanol Extracts.

Due to the complexity of the mixtures of the metabolites in the acetone and methanol extracts, the compounds were fractionated, purified and identified as their peracetate or methylated derivatives with acetic anhydride and diazomethane respectively. These derivatization procedures is described under the general methods section of the thesis.

This required several steps of separation, which did not allow accurate quantification of the compounds. Characterization of the glycosides by hydrolysis was not possible due to the very low masses of the compounds isolated. Identification of all

compounds is based on NMR spectroscopic methods. The acetone (49.0 g) and methanol/ethyl acetate (32.0 g) extracts were respectively fractionated by Sephadex LH-20 column chromatography (5 x 60 cm, flow rate of 1 mL/min, 32.0 mL fractions) with ethanol as the eluent. Following TLC analysis in hexane-acetone-methanol (5:4:1), the collected fractions were combined into 8 fractions for the acetone extract, A1-8: A1 (tubes 0-48, 3.23 g), A2 (tubes 49-106, 4.05 g), A3 (tubes 107-128, 4.12 g), A4 (tubes 129-204, 14.64 g), A5 (tubes 205-270, 2.56 g) A6 (tubes 271-350, 4.98 g), A7 (tubes 351-470, 4.83 g), A8 (tubes, 471-520, 3.74 g); and 5 fractions for the methanol extract, B1-5: B1 (tubes 0-30, 1.28 g), B2 (tubes 31-86, 4.21 g), B3 (tubes 87-130, 4.94 g), B4 (tubes 131-230, 4.52 g), B5 (tubes 231-290, 4.8 g). Fractions A1, A2, B1 and B5 did not contain compounds pertaining to this investigation and were not investigated further.

NMR data of compounds isolated from the methanol-ethyl acetate extract

These compounds were additional structures in the methanol-ethyl acetate extract for this degree, which was not found in the acetone extract.

1,7-*O*-methyl *p*-coumaric acid (78) [139]

^{1}H NMR ($CDCl_3$) (298K) (δ_H): 7.68 (1H, d, J = 16.0, H-α), 7.50 (2H, J = 8.0Hz, H-5, 9), 6.93 (2H, J = 8.0, H-6, 8), 6.34 (1H, J = 16.0Hz, H-β), 3.81 (3H, s, 7-OMe), 3.86 (3H, s, 1-OMe).

3',4',7,-Tri-*O*-methyl-flavone (60)

^{1}H NMR (COC_2D_6) (298K) (δ_H): 8.02 (1H, d, J = 8.0Hz, H-5'), 7.70 (1H, dd, J = 1.8Hz, 8.0Hz, H-6'), 6.98 (1H, d, J = 7.5Hz, H-2'), 7.17 (1H, d, J = 8.0Hz, H-5'), 7.05 (1H, dd, J = 1.8Hz, 8.0Hz, H-6'), 7.23 (1H, d, J = 8.0Hz, H-2'), 6.75 (1H, s, H-2), 3.92 (3H, s, OMe), 3.96 (3H, s, OMe), 3.98 (3H, s, OMe).

3',4',5,7,-Tetra-*O*-methyl-flavone (62)

^{1}H NMR ($CDCl_3$) (298K) (δ_H): 7.53 (1H, dd, J = 1.8Hz, 7.5Hz, H-6'), 7.33 (1H, d, J = 1.8Hz, H-2'), 6.98 (1H, d, J = 7.5, H-5'), 6.62 (1H, s, H-2), 6.57 (1H, d, J = 2.0Hz, H-6), 6.39 (1H, d, J = 2.0Hz, H-8), 3.95-4.02 (4 x OMe).

3',3",4',4",5,5',5",7-Octa-*O*-acetyl-epicatechin-3-*O*-gallate (68)

^{1}H NMR ($CDCl_3$) (298K) (δ_H): 7.64 (2H, s, H-2",6"), 7.25 (2H, s, H-2',6'), 6.75 (1H, d, J = 2.0Hz, H-8), 6.63 (1H, d, J = 2.0Hz, H-6), 5.65 (1H, s, H-3), 5.20 (1H, s, H-2), 3.05 (2H, m, H-4), 2.25-2.31 (H24, s, 8 x OAc).

Chapter 2

Structure conformation of novel 3',4',7-triacetoxy-5-(β-D-2'',3'',4'',6''-tetra-O-acetyl-glucopyranosyloxy) flavan.

Literature

Owing to the novelty of the flavan glucoside, 3',4',7-triacetoxy-5-(β-D-2'',3'',4'',6''-tetra-*O*-acetyl-glucopyranosyloxy) flavan (**70**), isolated from *C. subternata* and the relatively unexplored synthetic methods of flavan *O*-glycosylation, a combination of synthetic and low-energy collision induced dissociation (CID) and collision activated dissociation (CAD) mass spectra (MS) is utilized to confirm the structure of the novel aglycone of compound (**70**)[150]. Another impetus to synthesize this flavan lay in the claims that naturally occurring flavans exhibit a number of important biological activities which, if explored properly, may lead to valuable new drugs or agro-chemicals[151]. The antimicrobial activity of flavans include antibacterial action and the defensive role played by these compounds against microorganisms[152], activity against the fungus *Botrytis cinerea*[153], bactericidal activity against gram-positive bacteria[154] as well as anti-viral activity[155]. Pharmacological activity includes a mild central nervous system (CNS) depressant[156] and pronounced adaptogenic (anti-stress/anti-anxiety)[157, 158] activity.

It is known that the aglycones of (2*S*)-7,4'-dimethoxy-5-(β-D-glucopyranosyloxy) flavan, dichotosin, and 7,3',4'-trimethoxy-5-(β-D-glucopyranosyloxy) flavan, dichotosinin, is unstable in methanol and undergoes autoxidation to give a red

[150] Marcha R. E., Miaob X, Metcalfe C. D., Stobiecki M., Marczak L., *International Journal of Mass Spectrometry*, **2004**, *232*, 171–183.
[151] Kulwant S., Ghosal S., *Phytochemistry*, **1984,** 23, no.11, 2420.
[152] Takasugi M., Kumagai Y., Nagao S., Masamune T., Shirata A., Takahashi K., *Chem. Letters*, **1980**, 1459.
[153] Coxon D. T., O'Neill T. M., Mansfield J. W., Porter A. E. A., *Phytochemistry*, **1980**, *19*, 889
[154] Gnanamanickam S. S., Mansfield J. W., *Phytochemistry*, **1981**, *20*, 997
[155] Batchelor J. F., Bauer D. J., Hodson H. F., Selway J. W. T., Young D. A. B., *Eur.Pat. Appl.,* **1979**, *4*, 579.
[156] Sahai R., Agarwal S. K., Rastogi R. P., *Phytochemistry*, **1980**, *19*, 1560.
[157] Ghosal S., Saini K. S., Sinha B. N., *J. Chem. Res.,* 1983, pp. 330, 2601.
[158] Ghosal S., Saini K. S., *Abstracts, XVI Annual Scientific Conference on Indian Medicine*, Varanasi, India, pp. 1

polymeric compound in addition to other products[159]. The hydrolysis of the sugar moiety required emulsin (β-glucosidase) which resulted in an unstable aglycone in methanol with workup. Finally, the reduction of a reference sample of the relevant flavanone with $NaBH_4$ in acetic acid resulted in the desired flavan[159].

Sweeny et.al. demonstrated that the reduction of 7-OAc flavanones with $NaBH_4$ results in partially reduced 4-ol product instead of the desired flavan[160]. Dick et.al. found that the formation of the flavan required catalytic hydrogenation and preliminary conversion to the 4-hydroxy flavan, produced the by reduction with $NaBH_4$[161]. This step was found to be useful for the synthesis of flavans in general because it eliminates problems with equilibrium reversals as well as hydrogen bonding problems for all the flavanone reductions.

4-Substituted flavans exist in *trans* (**87**) and *cis* (**88**) (**Scheme 2.3**) configurations which was originally designated β- and α-isomers before their configurations was determined, and the α-isomers are now known to be *trans* and the β-isomers as *cis*. The heterocyclic ring protons in 4-substituted flavans give rise to multiplets of ABMX or ABMY type spin systems in which J_{MX} or $J_{MY} = 0$, and the configurations are easily determined from the 4-proton signal which appears as a doublet of doublets (dd) in the *cis* isomers and as a triplet in the *trans* isomers[162]. The coupling between H-4, H-3ax and H-3eq are sufficiently close for the H-4 signal to appear as a triplet although a dd is expected in the *trans* isomers. The coupling constants for 4-substituted flavans are consistent with either the half chair or sofa conformation of the heterocyclic ring, where the 2-aryl group is equatorial. However, the energy barrier between these conformations is expected to be very small and rapid inter-conversion between them is likely, which is also consistent with the NMR data. The classic synthetic route to the $C_6C_3C_6$ flavonoid skeleton is based on an aldol type condensation, under basic conditions, of a C_6C_2 unit of the appropriate acetophenone with a C_6C_1 unit of the appropriate aldehyde resulting in the corresponding

[159] Ghosal S., Jaiswal D. K., Singh S. K., Srivastava R. S., *Phytochemistry*, **1985,** *24*, no.4, 831.
[160] Sweeny J. G., Iacobucci G. A., *Tetraedron*, **1977**, *33*, 2972-2932.
[161] Dick W. E., *J. Agric. Food Chem.*, **1981**, 29, no. 2, 305.
[162] Clark-Lewis J. W., *Aust. J. Chem*., **1968**, *21*, 2059.

intermediate chalcone, in this case, 2'-hydroxy-3,4,5',7'-tetramethoxy chalcone[163] **(83) (Scheme 2.1).**

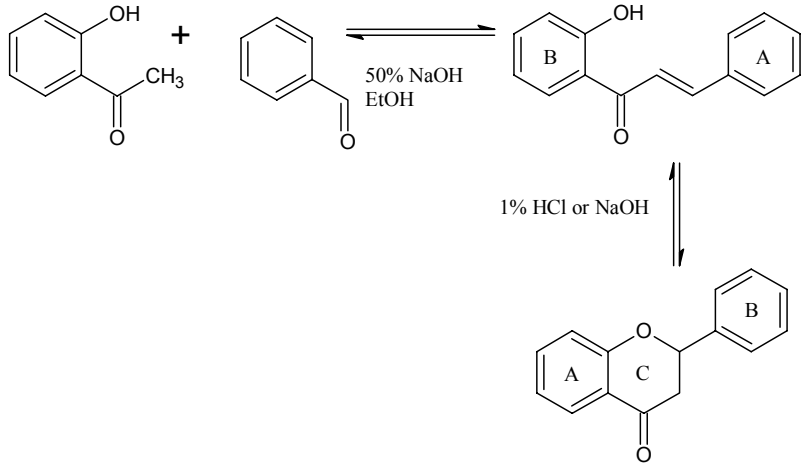

Scheme 2.1

The corresponding achiral flavanone (**32**), which is isomeric with the chalcone (**31**), is obtained from the latter by acid- or alkali catalyzed ring closure (**Scheme 2.1, 2.2**)[164, 165].

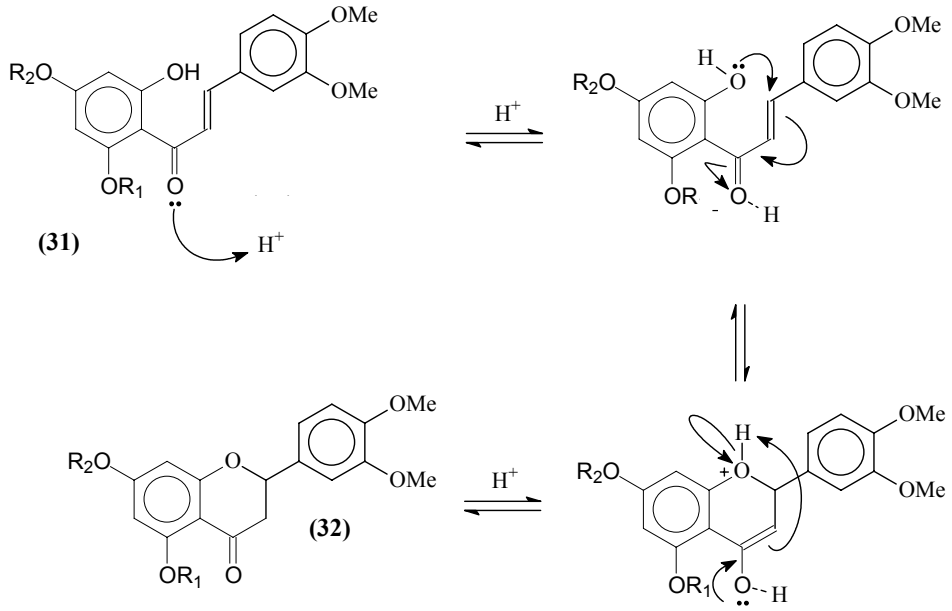

Scheme 2.2

[163] Wagner H., Farkas L., in *The Flavonoids*, (eds J. B. Harborne, T. J. Marbry and H. Mabry), Chapman and Hall, London, and references there in, **1975**, 127.
[164] Bhrara S. C., Goel R. N., Jain A. C., Seshadri T. R., *Indian J. Chem.,* **1964,** *2,* 399
[165] Kagal S. A., Nair P. M., Venkataraman K., *Tetrahedron,* **1962**, 593

Only a few natural occurring flavans have been reported. This scarcity may be attributed to the fact that they are not readily visible on chromatograms and they have relatively different spectroscopic features compared to most other flavonoid classes, regarding the high field aliphatic H-3,4 signals around 1.0-2.8 ppm.

Flavans are thought to arise from a double reduction of a flavanone carbonyl, hence many flavans co-occur with the flavanone of identical substitution pattern. The majority of naturally occurring flavanones have the C2-phenyl group in the α-orientation and is therefore designated 2*S* absolute configuration. The UV absorptions of flavanones at 270-290 nm (maximum) and 320-330 nm (inflection) have been assigned to the π→π* and n→π* acetophenone chromophore transitions, respectively. The modified octant rule defining the relationship between the chirality of α,β-unsaturated ketones and the sign of their high wavelength Cotton effect (CE), is extended to aryl ketones (acetophenones)[166]. Flavanones of 2*S* configuration and 3-hydroxyflavanones of 2*R*, 3*R* configuration, having equatorial 2-aryl substituents in the former or di-equatorial 2,3-substituents in the latter, exhibit a positive Cotton effect due to the n→π* transition (~ 330 nm) and a negative Cotton effect in their π→π* region (~280-290 nm).

Flavanone glycosides possessing chiral aglycones show Cotton effects quite similar to their optically active aglycones while flavanone glycosides having racemic aglycones show only weak Cotton effects at 250-350 mm. The π→π* Cotton effect is more suitable for determining aglycone chirality in flavanone glycosides.

In addition to the two high wavelength bands, 2-(*S*)-flavanones generally show a positive Cotton effect at 245-270 nm and a negative Cotton effect at 225-240 nm. *trans* 2*R*,3*R*-3-Hydroxy-flavanones showed two Cotton effects below 270 nm both of which were positive[167]. The large coupling constant ($J_{2,3}$) between H2 and H3(ax) of the heterocyclic ring indicates that all natural flavanones are in the thermodynamically favored conformation with the C2-aryl group equatorial. This implies that all laevorotatory flavanones possess a 2-(*S*) configuration.

[166] Snatzke G., *Tetrahedron*, **1965**, *21*, 439-448.
[167] Gaffield G., *Tetrahedron*, **1970**, *26*, 4093-4108.

The chroman chromophore is present in various naturally occurring *O*-heterocycles. The chroman derivatives belong to the benzene chromophores with a chiral second sphere. The achiral benzene A-ring chromophore is chirally perturbed by the fused chiral *O*-heterocyclic ring (second sphere) and the substituents of the heterocyclic ring (third sphere). This gives rise to the observed CE's at ca. 260–280 nm (^{1}Lb band) and ca. 200–240 nm (^{1}La band). The chirality (conformation) of the heterocyclic ring can be deduced from the CD spectrum if the relationship between the helicity (**Fig. 2.1**) of the heterocyclic ring and the sign of the ^{1}Lb band CD is known.

The absolute configuration can then be assigned from NMR spectroscopic experiments that give the relative configuration between the substituents at the chiral centers and the CD spectra.

Consequently, it follows that flavanones with 2-(*S*) configuration possessing a conformation with P-helicity (**Fig. 2.1**) of the heterocyclic ring and having a C2 equatorial aryl group will exhibit a positive CE at the n→π* transition (~330 nm) and a negative CE at the π→π* absorption band. The advantage of using the n→π* absorption band for configurational assignment is that the sign of this transition is independent of the substitution pattern of the aromatic ring system[168].

ORD and CD studies have revealed that all natural flavans have the 2*S* absolute configuration, as would be expected from the commonly found 2*S* flavanone precursor. Many of the natural flavans are listed as racemic due to an optical rotation of zero at 589 nm. The low specific rotation of flavans make this a precarious assumption. Fundamentally, the assignment of their configuration is only possible by careful scrutiny of their complete CD data. From this it is possible to infer that flavans have a half-chair conformation with the C2-phenyl group assumed to be equatorial (lowest free energy) and that they follow the P-/M-helicity rule of the *O*-heterocyclic ring (**Fig. 2.1**) in the chroman chromophore leading to negative or positive cotton effects within the ^{1}Lb band (ca. ~280nm)[170].

[168] Snatzke G., *Tetrahedron*, **1973**, *29*, 909-912.

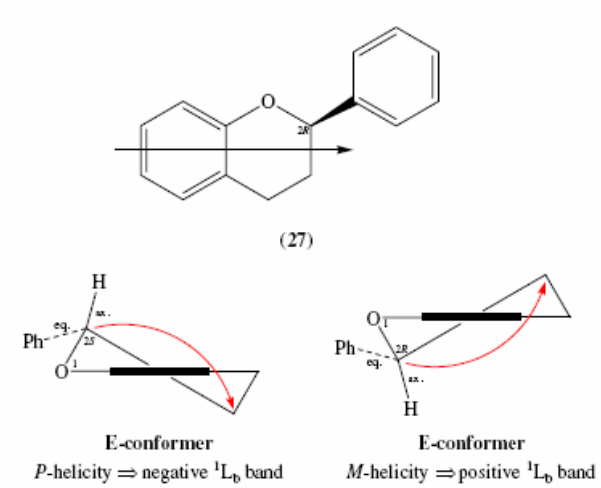

Figure 2.1. Flavan structure displaying P- and M-helicity (conformation of the heterocyclic ring)

From this it seems reasonable to deduce that a negative ^{1}Lb cotton effect (P-helicity) is the result of 2*S* absolute configuration and a positive ^{1}Lb band the result of 2*R* absolute configuration. As with other flavonoids, the presence of a chiral glucoside moiety on the fused benzene ring of the chroman moiety does have a small effect on the transition energy but the helicity, and consequently the ^{1}Lb cotton effect, of the heterocyclic ring does not change. [169,170]

Results and Discussion

The novel flavan glucoside (**70**) was isolated and purified from the acetone extract of the leaves and stems of *C. subternata*, as briefly described in the previous chapter.

The ^{1}H NMR spectrum [**Plate 7** (C_6D_6) (298K)] show two methylene multiplets [δ2.60, H-3a,b] and [δ1.65, H-4a,b] consistent with the flavan moiety. The doublet of doublets at δ4.58 (J = 3.0, 9.0Hz) defines H-2 (C) which shows n.O.e association with H-2',6'(B), and thus designates the ABX spin system of the B-ring [**Plate 7b-1** (C_6D_6) (298K)]. The n.O.e association of H-3(C) with H-2',6'(B) confirms the presence of the flavan unit **(70c)** [**Plate 7b-3** (C_6D_6) (298K)].

[169] Gaffield G., *Tetrahedron*, **1970**, *26*, 4093-4108.
[170] Slade D., Ferreira D., Marais J.P.J., *Phytochemistry*, **2005**, *66*, 2177.

The ABX spin system of the B-ring is indicated by the doublet of doublets [δ7.01, J = 2.0 and 8.0 Hz, H-6'(B)] and its associated doublets [δ7.33, J = 2.0, H-2'(B)] and [δ7.15, J= 8.0Hz, H-5'(B)]. The AB spin system of the A-ring is represented by the doublets [δ6.79, J = 2.0Hz, H-6(A)] and [δ6.87, J = 2.0Hz, H-8(A)].

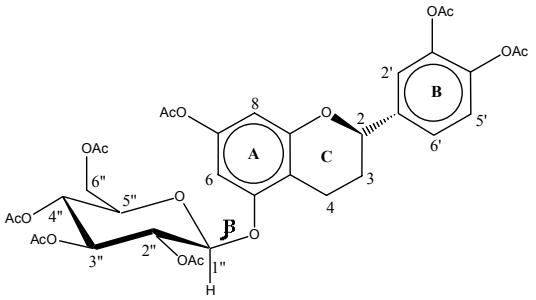

(70)

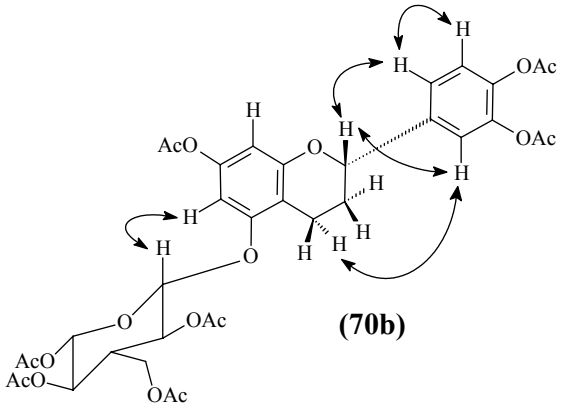

(70b)

The glycosyl protons[171] manifest as the doublet [δ4.87, J = 8.0Hz (β-coupled), H-1''], the doublet of doublets [δ5.69, J = 8.0, 10Hz, H-2''], the two triplets [δ5.50, J = 9.0Hz, H-3''], and [δ5.35, J = 9.0Hz, H-4''], the multiplet [δ3.25, H-5''] and the two methylene protons H-6" [δ4.28, J = 6.0, 12Hz, and δ4.11, J = 3.0, 12Hz], and are confirmed by a COSY experiment [**Plate 7a-1** (C_6D_6) (298K)] and n.O.e data [plate 7b-2 (C_6D_6) (298K)]. The COSY experiment [**Plate 7a-2** (C_6D_6) (298K)] also shows long range coupling between the anomeric proton (H-1'') and H-6(A), which confirms the attachment of the sugar moiety to C-5 of the aglycone. The COSY experiment [**Plate 7a-3** (C_6D_6) (298K)] furthermore confirms the spin systems of the

[171] I. Kubo, M. Kim, *Tett. Lett.,* **1987**, *28* no. 9, 921.

A and B-ring respectively. N.O.e data [**Plate 7b-1** (C_6D_6) (298K)] show strong association between H-1'' and H-6(A) and affirms the C-5 attachment to the aglycone. No n.O.e is observed between the sugar protons and 2 x H-4, which indicate little interaction between the glucoside and the heterocyclic C-ring to influence it's conformation sterically.

Characteristic n.O.e. association between the axial H-1", H-3" and H-5" glucosidic protons [**Plate 7b-2** (C_6D_6) (298K)] confirms the relative stereochemistry of the glucoside moiety.

The seven acetoxy groups resonate as singlets at δ1.89, δ1.87 x 3, δ1.86, δ1.81, δ1.76. The absence of a carbonyl functionality in this structure is concluded by a ^{13}C spectrum which indicated the absence of a signal beyond ~200ppm.[172]

The stereochemistry at C-2 have been established by CD spectra (**Fig 2.2**) and show a negative cotton effect shoulder at ~280 nm (^{1}Lb transition band) corresponding to a 2*S* absolute configuration[173]. The overpowering negative CE at 304 nm and at 335 nm may be attributed to the acetoxy groups. The instability of the aglycone under hydrolytic conditions and in methanol solution[174] prevented the hydrolysis of the acetoxy and glucoside moieties and made the recording of CD data without the acetoxy groups not viable.

Synthesis of 5,7,3',4'-Tetramethoxyflavan (89)

The relevant chalcone $C_6C_3C_6$ structure was obtained by aldol condensation of selectively protected phloroacetophenone and 3,4-dihydroxybenzaldehyde. Phloroacetophenone was selectively methylated with Me_2SO_4 in dry acetone in the presence of $CaCO_3$ to yield the desired product (85) (Scheme 2.3).

3,4-dihydroxybenzaldehyde was dissolved in methanol, cooled to 0°C and excess etheric diazomethane added slowly. The methylated product (34) was obtained in good yield after 12h at -15°C and evaporation of the solvents.

Phloroacetophenone (**85)** was dissolved in 50% (m/v) NaOH/EtOH and stirred for 30 min. before (**86)** was added. The solution was stirred for 12h to yield the characteristic

[172] S. Kulwant, S. Ghosal, *Phytochemistry* **1984,** 23 no.11, 2419.
[173] Slade D., Ferreira D., Marais J.P.J., *Phytochemistry*, **2005**, *66*, 2192.

[174] Ghosal S., Jaiswal D. K., Singh S. K., Srivastava R. S., *Phytochemistry*, **1985,** *24*, no.4, 831.

yellow chalcone (**83**). The cyclization of the chalcone was achieved in the presence of 3N HCl to yield the corresponding flavanone (**84**). The mechanism of the acid catalyzed ring closure to the β-position relative to the carbonyl proceeds by a 1,4-Michael addition, which led to the well known chalcone ↔ flavanone equilibrium[175], the direction of which is dependent on the presence of a 5-hydroxy group and the acidity of the 3-protons of the resulting flavanone **(Scheme 2.2)**.[176] The chalcone ↔ flavanone equilibrium shifts in favour of the flavanone with a stronger catalyzing acid and in favour of the chalcone with stronger base[176].

Reduction of the flavanone with excess $NaBH_4$ in the presence of THF/EtOH yields the alpha and beta 4-ol products (**87**) (2 diastereomers) (**Plate 4**), (**88**) (2 diastereomers) (**Plate 5**). Subsequent treatment of (**87**) with $H_{2(g)}$ (600 psi) in the presence of Pd/C in THF/EtOH yielded the desired flavan (**89**) (**Plate 6**) in quantitative yield.

[175] S. von Konstanecki, V. Lampe and J. Tambor, *Ber*., **1904**, *37*, 786.
[176] D. Ferreira, E. V. Brandt, F. du R. Volsteedt and D. G. Roux, *J. Chem. Soc. Perkin I*, **1975**, 1437.

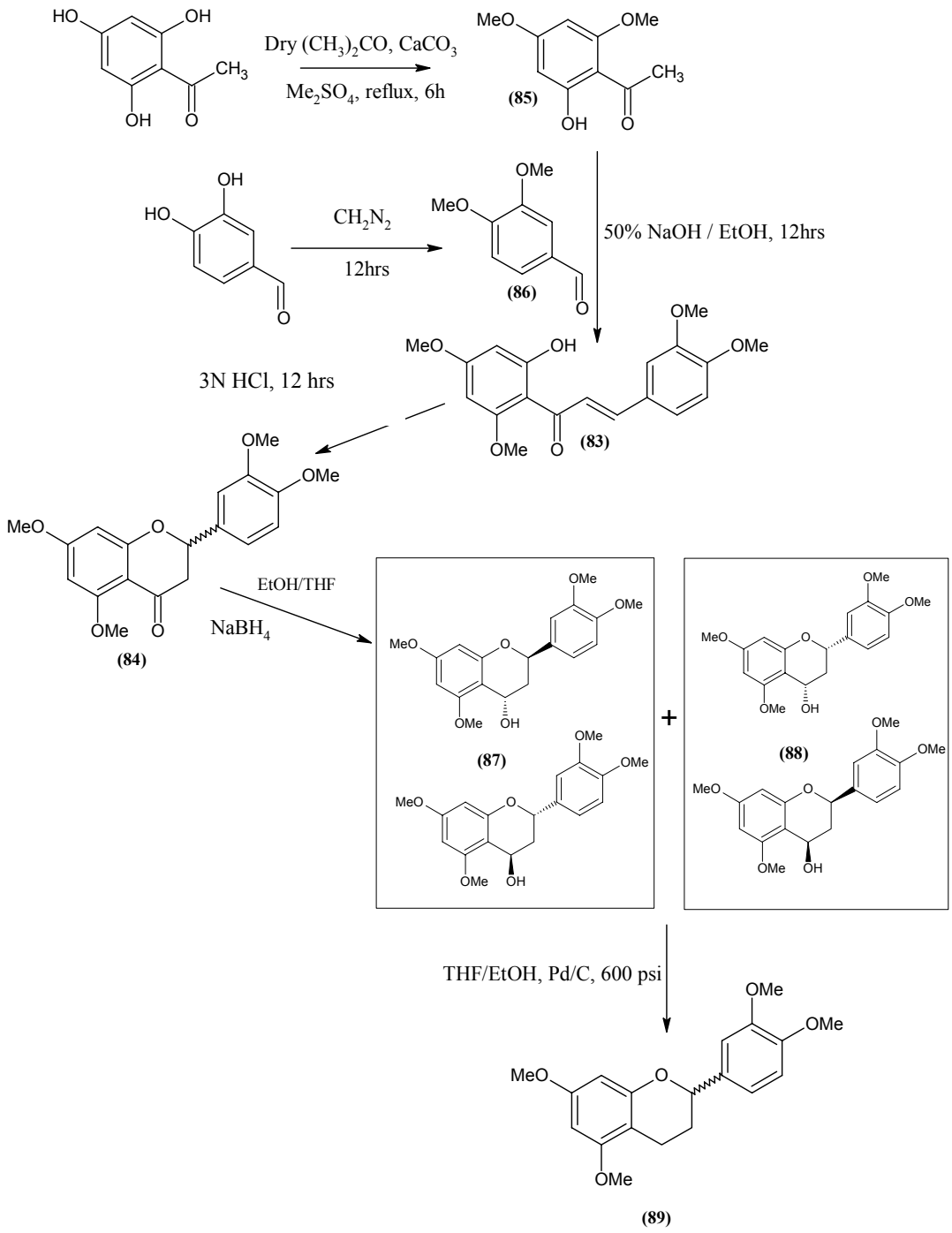

Scheme 2.3

Subsequently, the synthesized aglycone was compared directly with the MS/MS (CID) data of the natural extracted aglycone structure (**Scheme 2.4**) (**90**). Both the

natural aglycone and the synthesized flavan have a molecular ion m/z consistent with a flavan structure. The fragment ions from the respective aglycones of the synthesized (167 m/z) and natural flavan (139, 181 m/z), are characteristic ions for flavans with a unsubstituted heterocyclic ring. Fragment ion 181 m/z loses CH_2 to give the prominent 169 m/z fragment. These characteristic fragment ions from the flavan structure are formed by retro-Diels-Alder (RDA) cleavage of any flavan C-ring[47]. FAB MS spectra (**Fig 2.3**) display the molecular ion, 730 m/z, and the prominent 169 m/z ion. Collision induced dissociation spectra (MS/MS (MS^2), CID) (**Fig. 2.4**) with increasing collision energy (from the bottom to the top spectra in **Fig. 2.4**) display all the ions in **Scheme 2.4,** including the fragment ions 401 and 271 m/z representing the aglycone structure. All these ions are produced from the parent ion $[M + NH_4]^+$ = 748 m/z. An enhanced product ion scan (EPI) (**Fig. 2.4**) where the product ions of 748 m/z are trapped after collision for predetermined amount of time before being scanned out of the linear ion trap (LIT) to the detector, also confirms most of the ions in **Scheme 2.4**.

Fig. 2.5 (MS^2, CID products of 331 m/z) show the molecular ion $[M + H]^+$ = 331 m/z and the characteristic RDA product ion $[M + H]^+$ 167 m/z of the synthesized flavan.

[47] Sahai R., Agarwal S. K. and Rastogi R. P., *Phytochemistry*, **1980**, *19*, 1560.

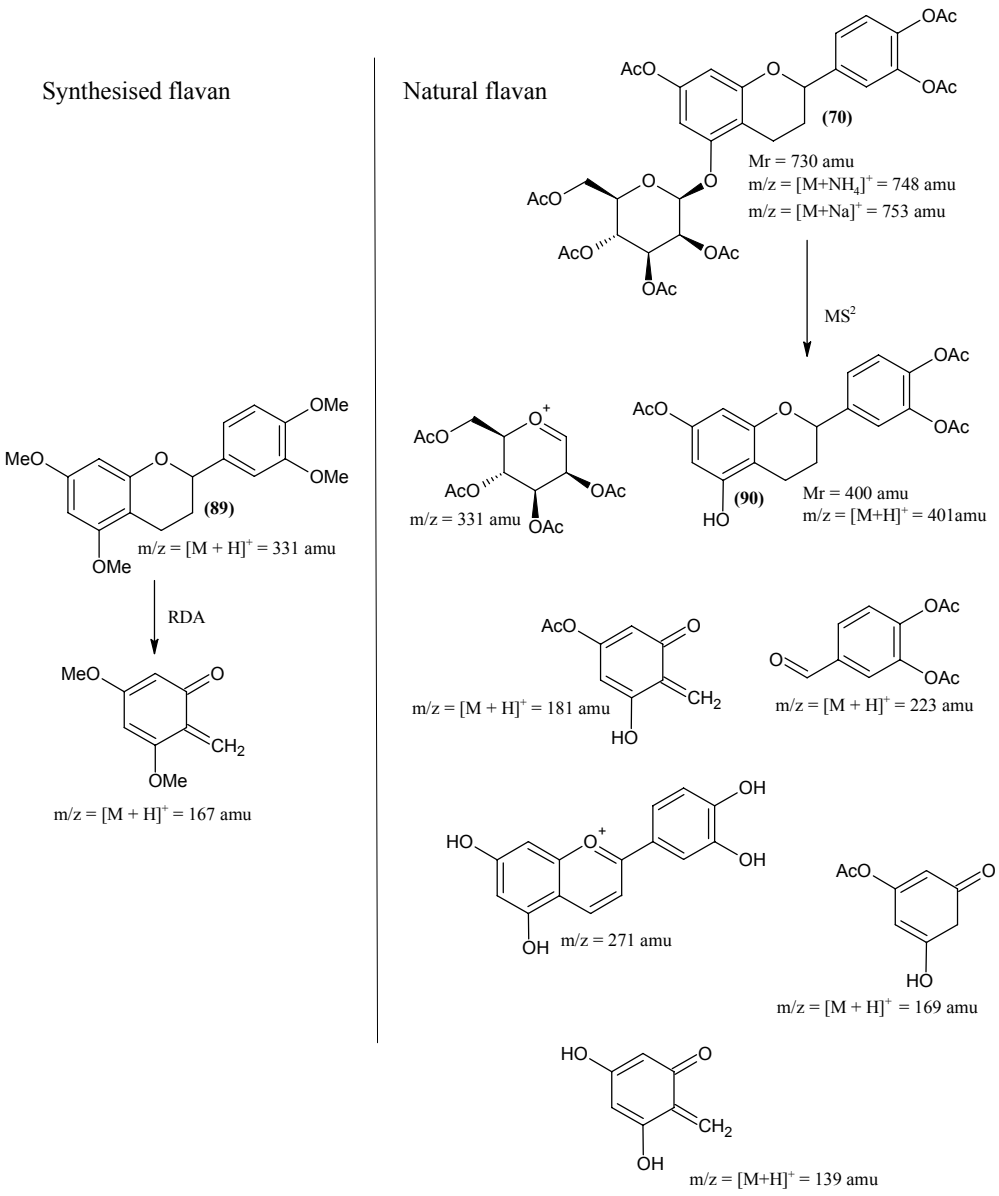

Scheme 2.4

Thus, the synthesized flavan and the natural flavan were the same by direct comparison of the synthesized and natural aglycone utilizing MS^2 spectra and confirmed the novel flavan aglycone (**90**) (**Scheme 2.4**). The hydroxylation pattern of the aglycone, the type of sugar, and the position of attachment to the flavan is confirmed by 1D ^1H NMR, 2D COSY and n.O.e experiments (**Plate 7**). The combined MS, synthetic and NMR data confirmed the novel flavan glucoside, 3',4',7-triacetoxy-5-(β-D-2'',3'',4'',6''-tetra-*O*-acetyl-glucopyranosyloxy) flavan (**70**).

Experimental

4,6-Dimetoxy-2-hydroxyacetophenone (85)

Commercial phloroacetophenone (500 mg, 2.97 mmol) was selectively methylated with dimethylsulfate to yield 4,6-dimetoxy-2-hydroxy acetophenone (204 mg, 35%) (R_f = 0.86, B:A 8:2) after FCC. ^{1}H NMR [**Plate 1** ($CDCl_3$)]: H-5(δ6.08, d, J = 2.0Hz), H-3(δ5.94, d, J = 2.0Hz), OMe(δ3.87, s), OMe(δ3.84, s), C$\underline{H}_3$(δ2.63, s).

General procedure for the preparation of chalcones.

To a solution of the appropriate acetophenone (3.0 mmol) in ethanol (20 ml / 1g acetophenone) was added 50% (m/v) *aq.* NaOH/KOH (0.4 ml /mmol acetophenone) and the mixture was stirred at room temperature for 30 min. Excess benzaldehyde (1.2 *eq*.) was added to the mixture. After exhaustion of the acetophenone (5-24h) (TLC), water was added to the solution which was then extracted with Et_2O (4 x 20ml). Drying of the extracts (Na_2SO_4) followed by evaporation of the solvent and FCC and / or crystallization from ethanol, gave the chalcone.

2'-Hydroxy-,3,4,4',6'-tetramethoxy chalcone (83)

4,6-Dimethoxy-2-hydroxy acetophenone (200mg, 1.02 mmol) and commercial 3,4-dimethoxy benzaldehyde (203mg, 1.22 mmol, 1.2 *eq*.) was condensed under basic conditions to yield 2'-hydroxy-,3,4,4',6'-tetramethoxy chalcone (91mg, 26%) after recrystalization from ethanol (Rf = 0.78, B:A 8:2). ^{1}H NMR [**Plate 2** ($CDCl_3$)]: H-α(δ7.77, d, J = 16.0Hz), H-β (δ7.83, d, J = 16.0Hz), H-6(δ7.24, dd, J = 2.0, 8.0Hz), H-2(δ7.15, d, J = 2.0Hz), H-5(δ6.92, d, H = 8.0Hz), H-5'(δ6.13, d, J = 2.0Hz), H-3'(δ5.98, d, J = 2.0Hz), OMe(δ3.97, s), OMe(δ3.96, s), OMe(δ3.95, s) and OMe(δ3.86, s).

5,7,3',4'-Tetramethoxyflavanone (84)

2'-hydroxy-,3,4,4',6'-tetramethoxychalcone (100mg, 290 mmol) in ethanol (10ml) was refluxed for 12h on a water-bath after addition of 3N HCl (5ml). After completion of the reaction (TLC) the chalcone and the isomerization product, 5,7,3',4'-tetramethoxyflavanone (15mg, 15%) was separated by chromatographic methods (FCC or PLC) (Rf = 0.38, B:A 8:2). ^{1}H NMR [**Plate 3** ($CDCl_3$)]: H-5',6'(δ7.00, m), H-2'(δ6.90, d, J = 8.5Hz), H-6(δ6.16, d, J = 2.0Hz), H-8(δ6.10, d, J = 2.0Hz), H-2 (δ5.35, dd, J = 2.5, 13Hz), OMe (δ3.93, s), 2 x OMe(δ3.90, s), OMe(δ3.83, s), H-3α (δ3.05, dd, J = 13.0, 16.5Hz), H-3β (δ2.77, dd, J = 2.5, 16.5Hz).

α, β-5,7,3',4'-Tetramethoxyflavan-4-ol (87, 88).

To a solution of 100mg (0.29 mmol) of **84** in 2ml THF/EtOH was added 10mg (0.26 mmol) $NaBH_4$. After stirring for 30 min, an additional 10mg $NaBH_4$ was added and stirring continued for another 30 min. The solution was added to cold 0.5% AcOH and extracted with $CHCl_3$. Drying (Na_2SO_4) and evaporation of the $CHCl_3$ gave a pale yellow solid. This product was purified by PLC to yield 2 pairs of diastereomers (yield: (**87**) 35.2 mg, 0.101 mmol, 35%, (**88**) 15 mg, 0.044 mmol, 15.2%). (Rf = 0.48, 0.55 Toluene: acetone 8:2). ^{1}H-NMR [**Plate 4** (**87**) ($CDCl_3$)]: H-2'(δ6.95, d, 1.9Hz), H-6'(δ7.01, dd, 1.9, 8.3Hz), H-5'(δ6.90, d, J = 8.3Hz), H-6,8 (δ6.13, s), H-4 (δ5.27, dd, J = 7.4, 9.7Hz), H-2 (δ4.97, dd, J = 1.5, 12.0Hz), H-3eq (δ2.52, ddd, J = 1.7, 7.3, 13.4 Hz), H-3ax (δ2.28, ddd, J = 9.9, 12.1, 13.4), OMe (δ3.93, s), OMe (δ3.91, s), OMe (δ3.90, s), OMe (δ3.76, s).

^{1}H-NMR [**Plate 5** (**88**) ($CDCl_3$)]: H-2'(δ7.01, d, 1.8Hz), H-6'(δ7.05, dd,, J = 1.9, 8.2Hz), H-5'(δ6.91, d, J = 8.2Hz), H-6 (δ6.17, d, J = 2.3Hz), H-8 (δ6.13, d, 2.3Hz), H-4 (δ5.12, dd, J = 1.8, 12.1Hz), H-2 (δ5.02, dd, J = 1.7, 4.3Hz), H-3eq (δ2.26, td, J = 1.9, 14.4 Hz), H-3ax (δ2.07, ddd, J = 4.1, 12.2, 14.5 Hz) OMe (δ3.93, s), OMe (δ3.91, s), OMe (δ3.90, s), OMe (δ3.76, s).

5,7,3',4'-Tetramethoxyflavan (89).

A solution of (**87**) (50mg, 0.144 mmol) in THF/EtOH (2ml) in the presence of 10% Pd/C under a $H_{2(g)}$ atmosphere (600psi) was stirred until completion of the reaction (TLC). The solution was filtered and the solvents evaporated under reduced pressure. The crude product was purified by PLC and washed off immediately to yield the desired flavan (**89**) (26.8mg, 0.081 mmol). (Rf = 0.4, Tol: EtOAc 7:3)

^{1}H-NMR [**Plate 6** (**89**) ($CDCl_3$)]: H-5' (δ6.89, d, J = 8.7 Hz), H-2',6' (δ7.99, m), H-6 (δ6.15, d, J = 2.3Hz), H-8 (δ6.10, d, J = 2.3Hz), H-2 (δ4.93, dd, J = 2.2, 10.5Hz), H-3eq (δ2.80, ddd, J = 2.7, 5.8, 16.7Hz), H-3ax (δ2.65, ddd, J = 6.3, 11.4, 16.4Hz), 2 x H-4 (δ2.10, m).

Plate 1

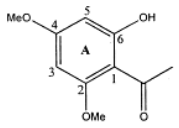
MeO
OH
A
OMe
O

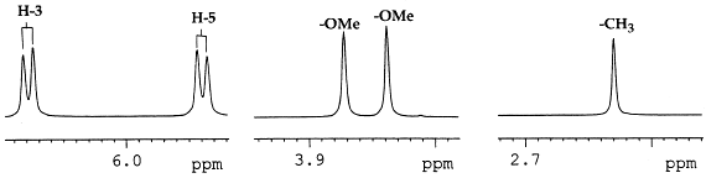
H-3
H-5
-OMe
-OMe
-CH3
6.0
ppm
3.9
ppm
2.7
ppm

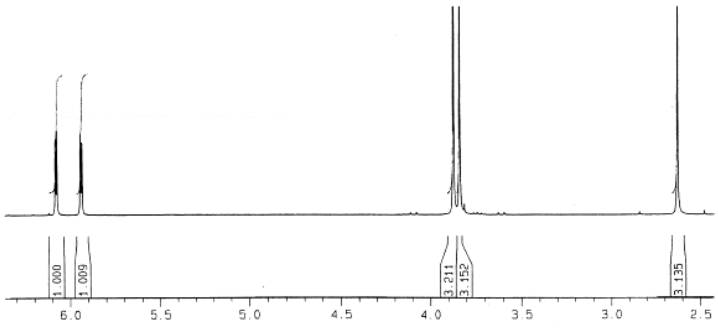
1.000
1.009
3.211
3.152
3.135
6.0
5.5
5.0
4.5
4.0
3.5
3.0
2.5

Plate 2

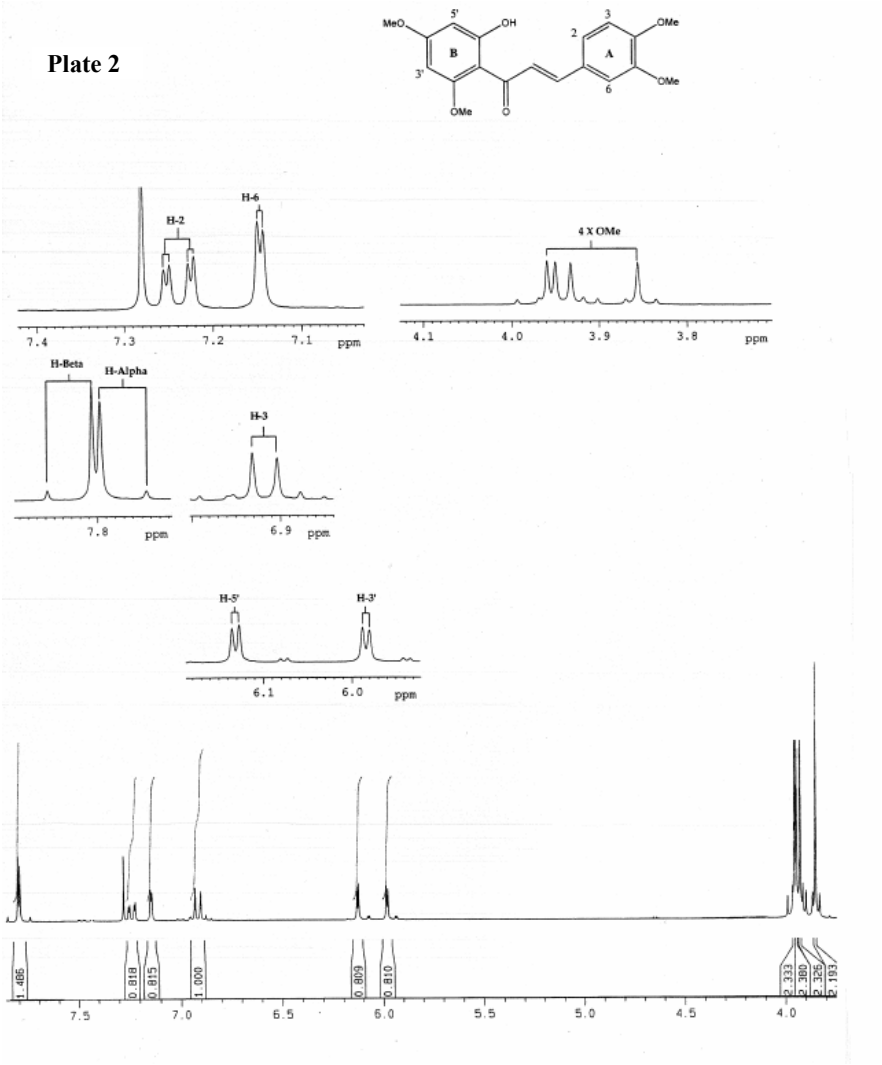
MeO
5'
OH
3
OMe
2
B
A
3'
6
OMe
OMe
O
H-6
H-2
7.4
7.3
7.2
7.1
ppm
4 X OMe
4.1
4.0
3.9
3.8
ppm
H-Beta
H-Alpha
7.8
ppm
H-3
6.9
ppm
H-5'
H-3'
6.1
6.0
ppm
1.466
0.818
0.815
1.000
0.809
0.810
2.333
2.380
2.326
2.193
7.5
7.0
6.5
6.0
5.5
5.0
4.5
4.0

Plate 3

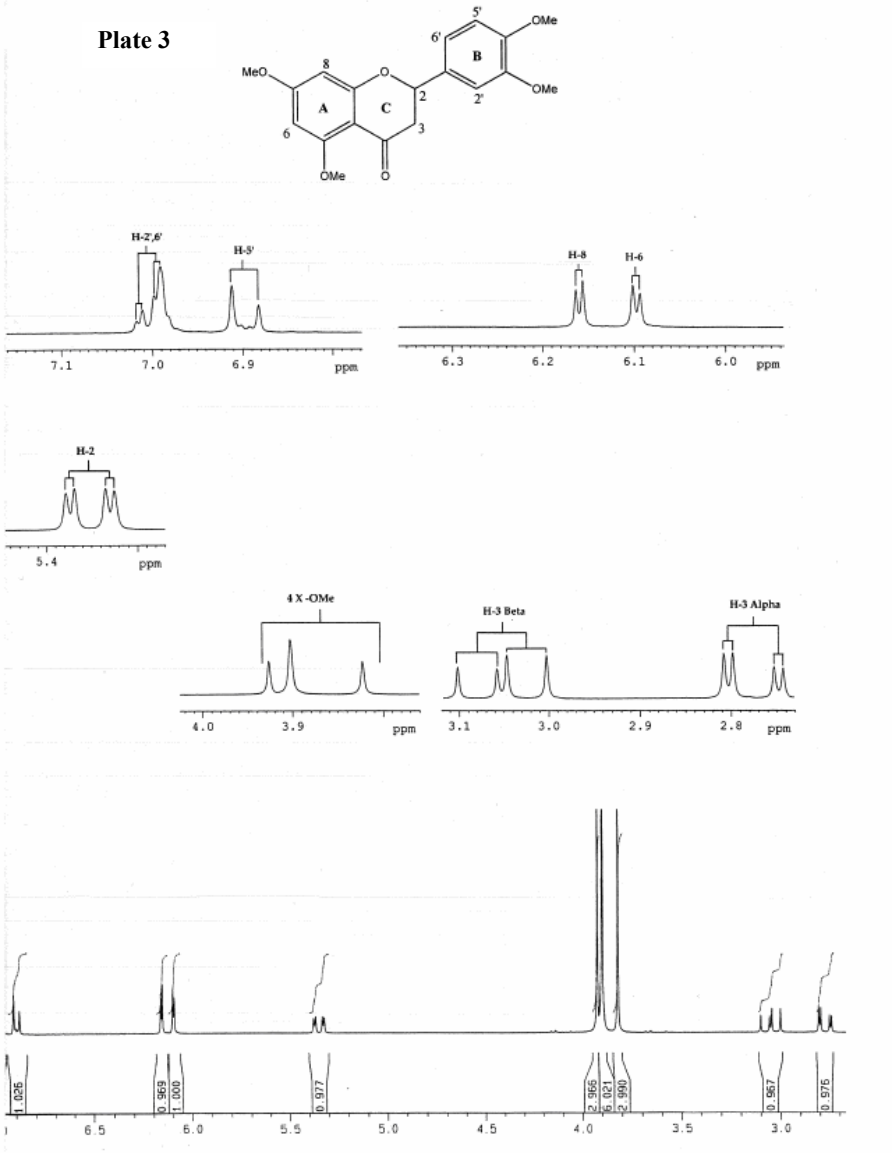
5'
OMe
6'
B
8
MeO
O
2'
OMe
A
C
2
6
3
OMe
O
H-2',6'
H-5'
H-8
H-6
7.1
7.0
6.9
ppm
6.3
6.2
6.1
6.0
ppm
H-2
5.4
ppm
4 X -OMe
H-3 Beta
H-3 Alpha
4.0
3.9
ppm
3.1
3.0
2.9
2.8
ppm
1.026
0.969
1.000
0.977
2.966
6.021
2.990
0.967
0.976
6.5
6.0
5.5
5.0
4.5
4.0
3.5
3.0

Plate 4 (87)

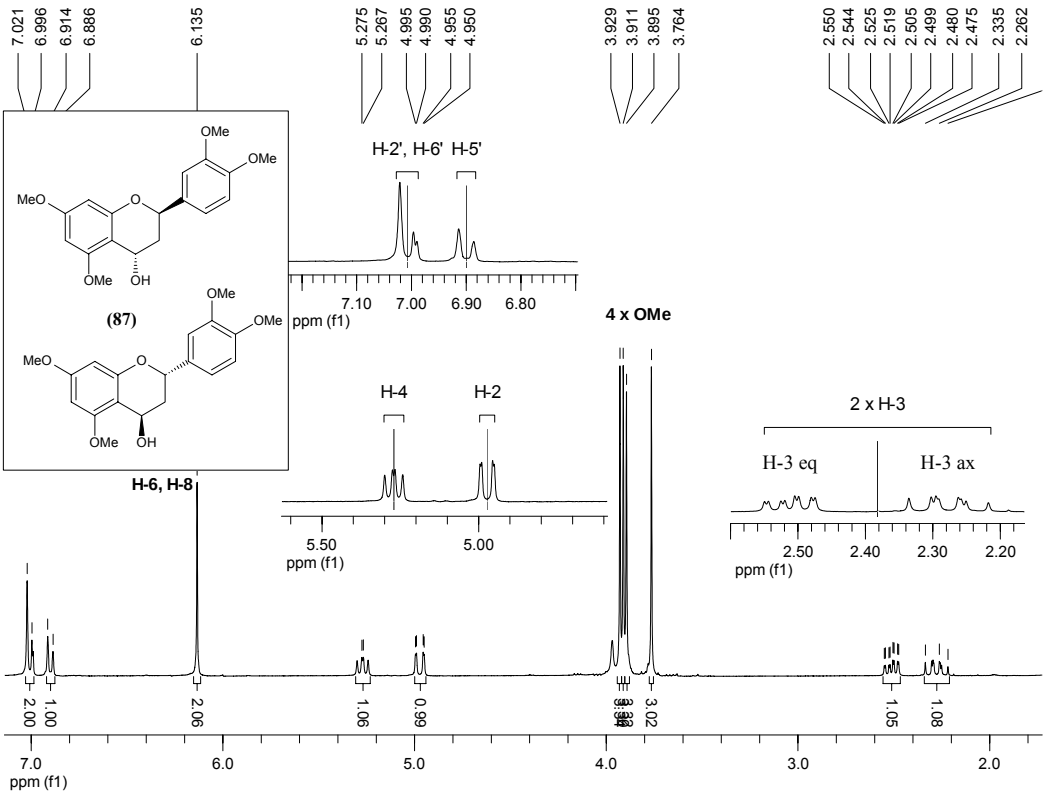
7.021
6.996
6.914
6.886
6.135
5.275
5.267
4.995
4.990
4.955
4.950
3.929
3.911
3.895
3.764
2.550
2.544
2.525
2.519
2.505
2.499
2.480
2.475
2.335
2.262
OMe
OMe
MeO
O
OMe
OH
(87)
H-2', H-6' H-5'
7.10
7.00
6.90
6.80
ppm (f1)
4 x OMe
H-4
H-2
5.50
5.00
ppm (f1)
2 x H-3
H-3 eq
H-3 ax
2.50
2.40
2.30
2.20
ppm (f1)
H-6, H-8
2.00
1.00
2.06
1.06
0.99
3.02
1.05
1.08
7.0
6.0
5.0
4.0
3.0
2.0
ppm (f1)

Plate 5 (88)

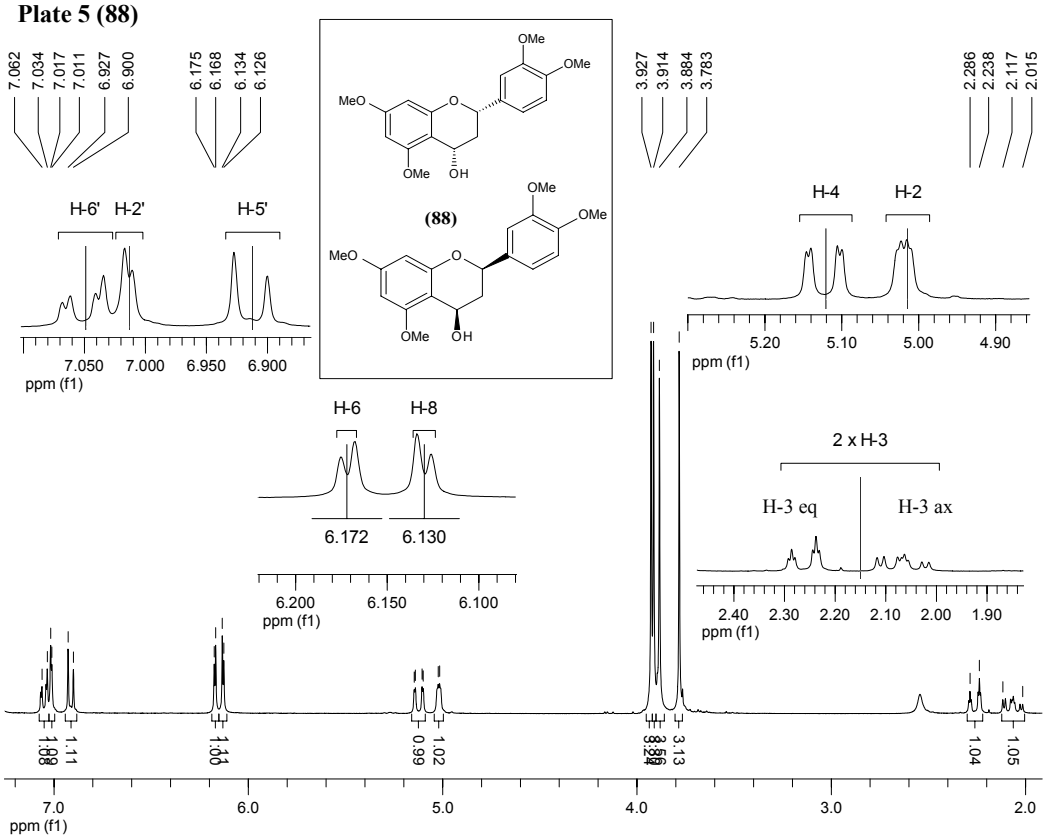
7.062
7.034
7.017
7.011
6.927
6.900
6.175
6.168
6.134
6.126
3.927
3.914
3.884
3.783
2.286
2.238
2.117
2.015
OMe
OMe
MeO
O
OMe
OH
(88)
H-6'
H-2'
H-5'
7.050
7.000
6.950
6.900
ppm (f1)
H-4
H-2
5.20
5.10
5.00
4.90
ppm (f1)
H-6
H-8
6.172
6.130
6.200
6.150
6.100
ppm (f1)
2 x H-3
H-3 eq
H-3 ax
2.40
2.30
2.20
2.10
2.00
1.90
ppm (f1)
1.08
1.11
1.00
1.01
0.99
1.02
3.13
1.04
1.05
7.0
6.0
5.0
4.0
3.0
2.0
ppm (f1)

Plate 6 (89)

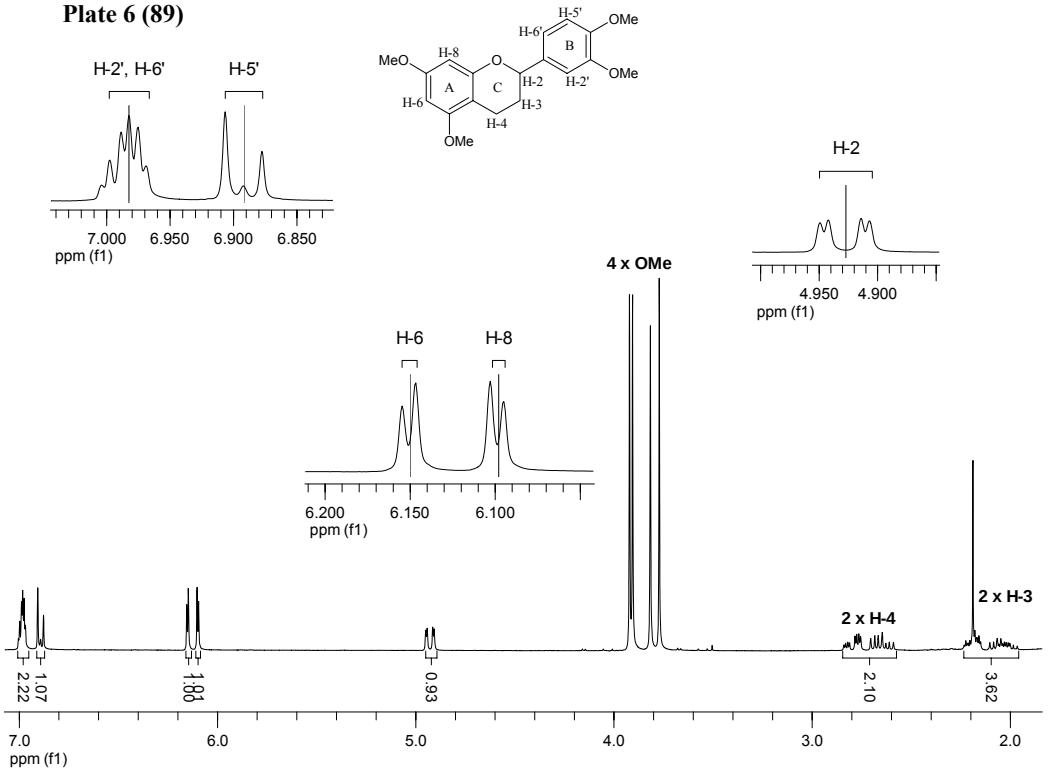
H-2', H-6'
H-5'
7.000
6.950
6.900
6.850
ppm (f1)
H-5'
OMe
H-6'
B
MeO
H-8
O
OMe
A
C
H-2
H-2'
H-6
H-3
H-4
OMe
H-2
4.950
4.900
ppm (f1)
4 x OMe
H-6
H-8
6.200
6.150
6.100
ppm (f1)
2 x H-4
2 x H-3
2.22
1.07
1.01
1.00
0.93
2.10
3.62
7.0
6.0
5.0
4.0
3.0
2.0
ppm (f1)

Plate 7 (C_6D_6) (298K)

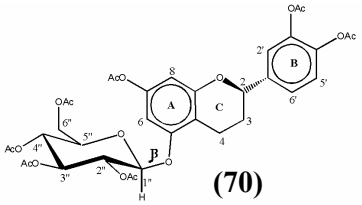

(70)

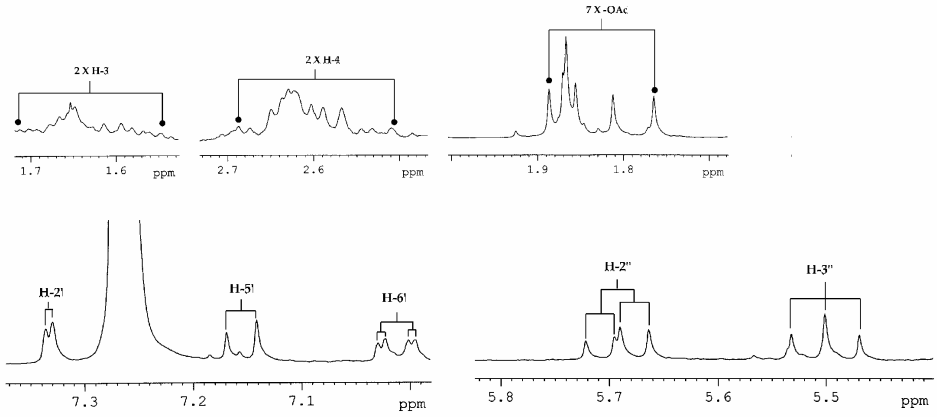

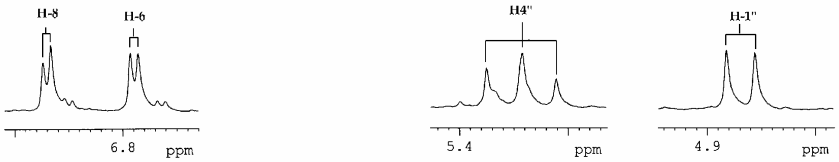

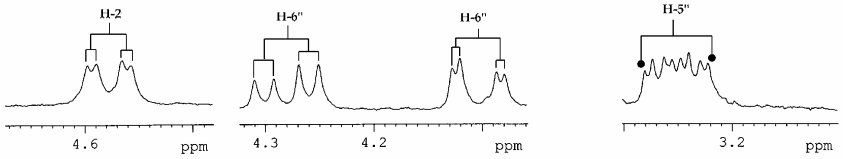

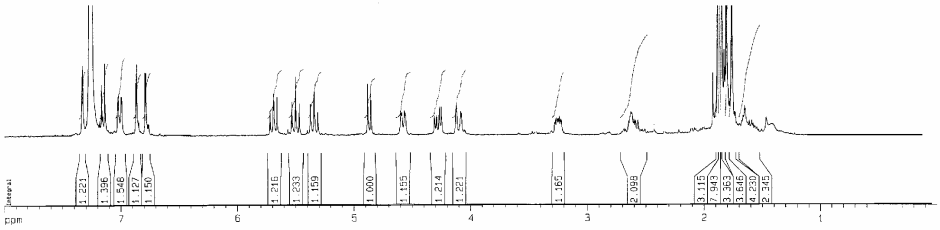

Plate 7 (C_6D_6) (298K)- COSY 7a-1

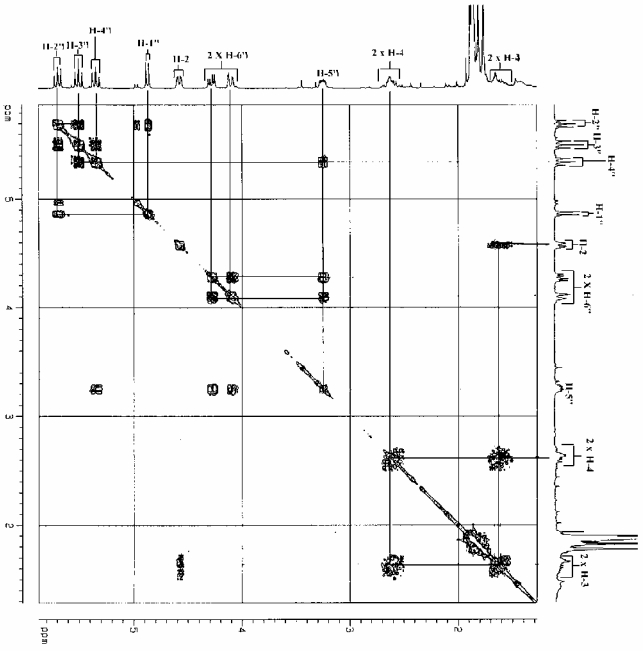

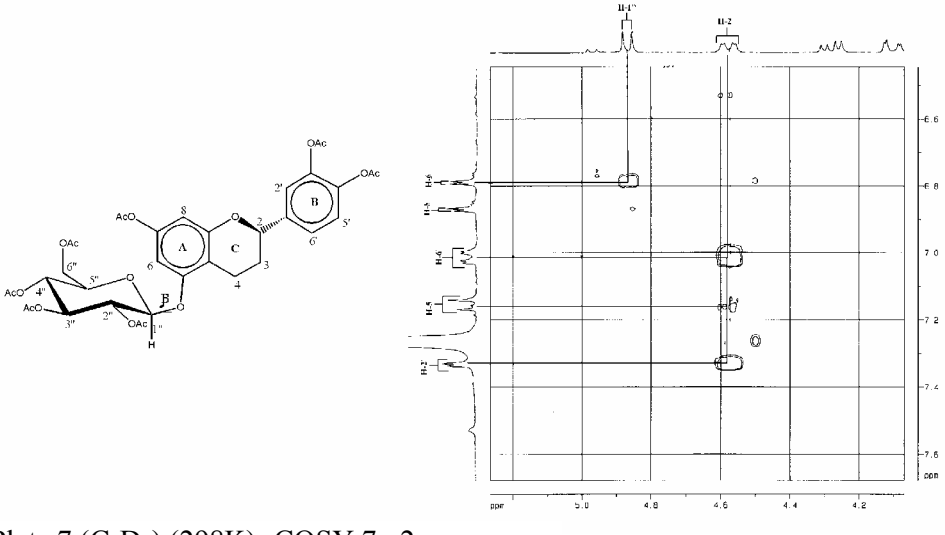

Plate 7 (C_6D_6) (298K)- COSY 7a-2

Plate 7 (C_6D_6) (298K)- COSY 7a-3

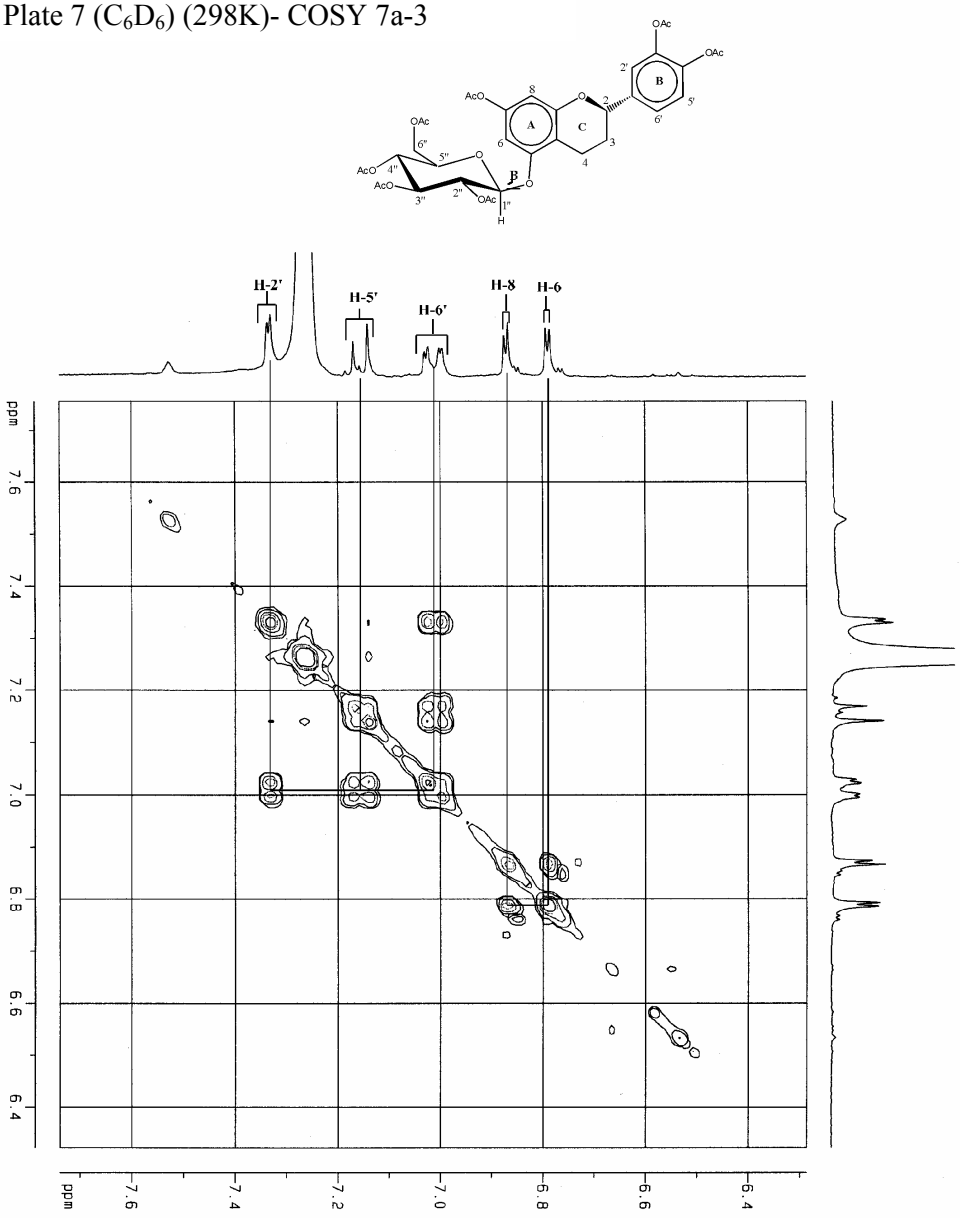

Plate 7 (C_6D_6) (298K)- NOESY 7b-1

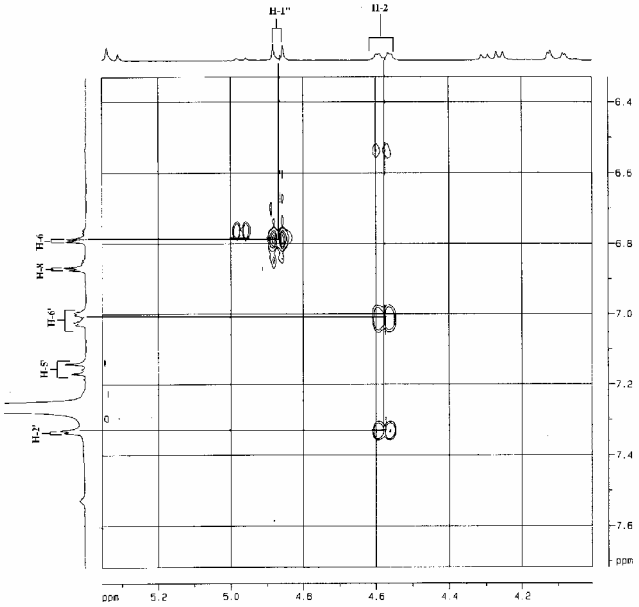

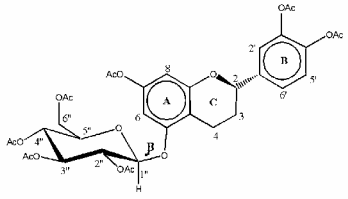

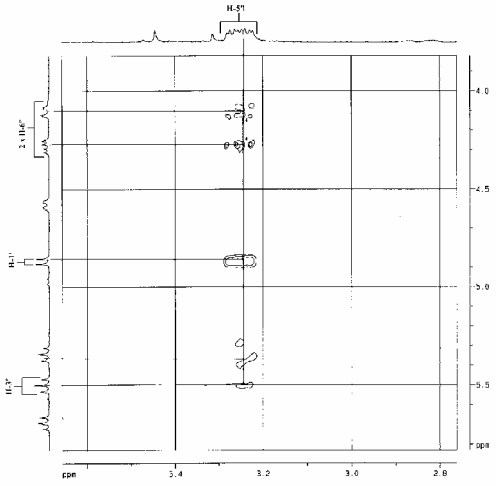

Plate 7 (C_6D_6) (298K)- NOESY 7b-2

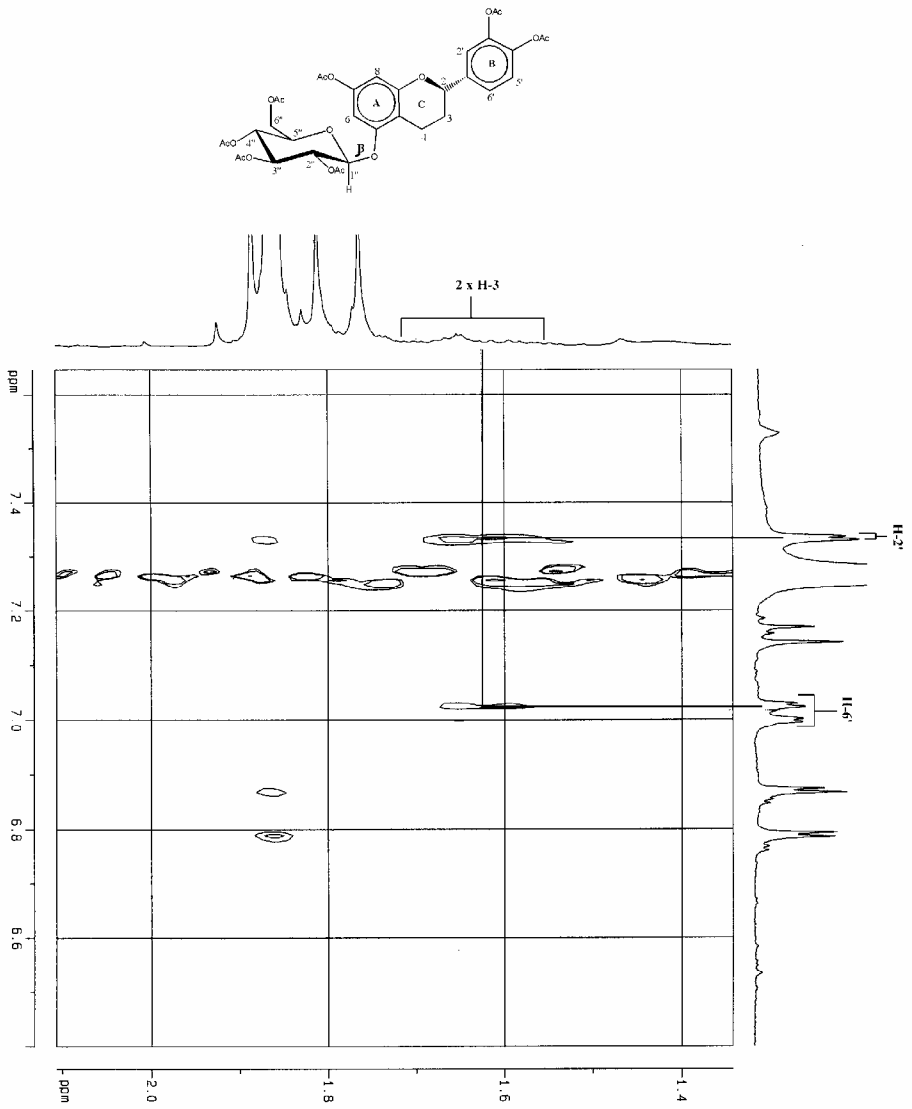
2 x H-3
H-2'
H-6'
ppm
7.4
7.2
7.0
6.8
6.6
ppm
2.0
1.8
1.6
1.4

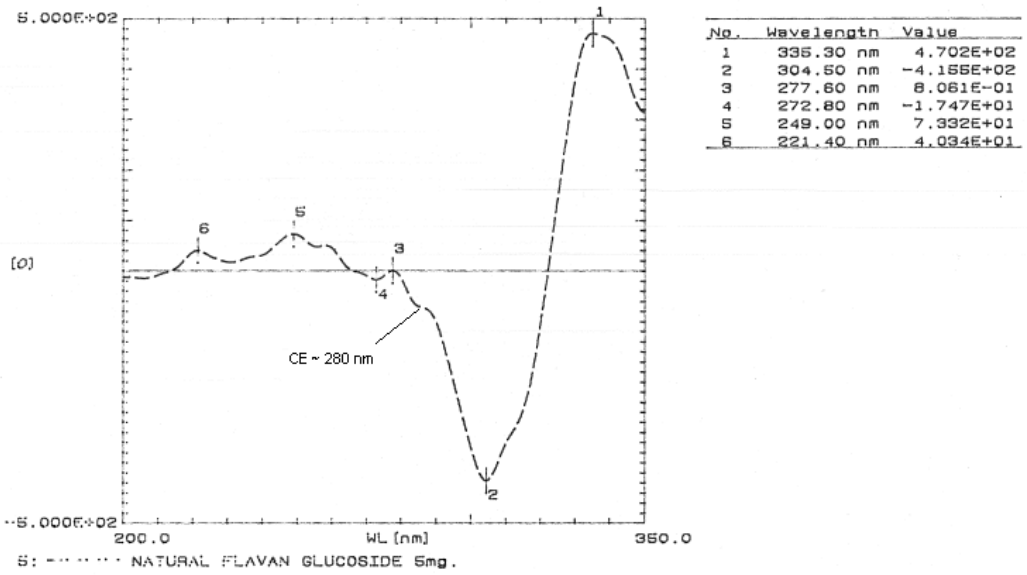

Figure 2.2 CD Spectra of (**70**) in Methanol

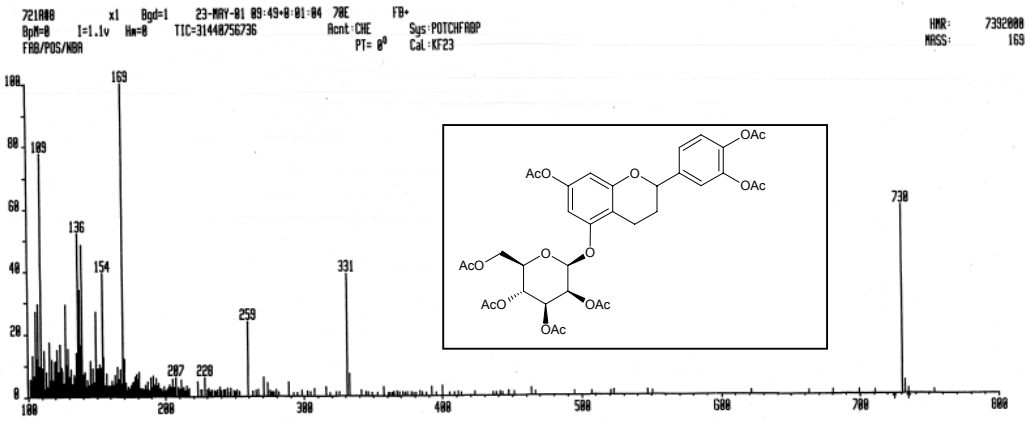

Figure 2.3 FAB-MS of (**70**)

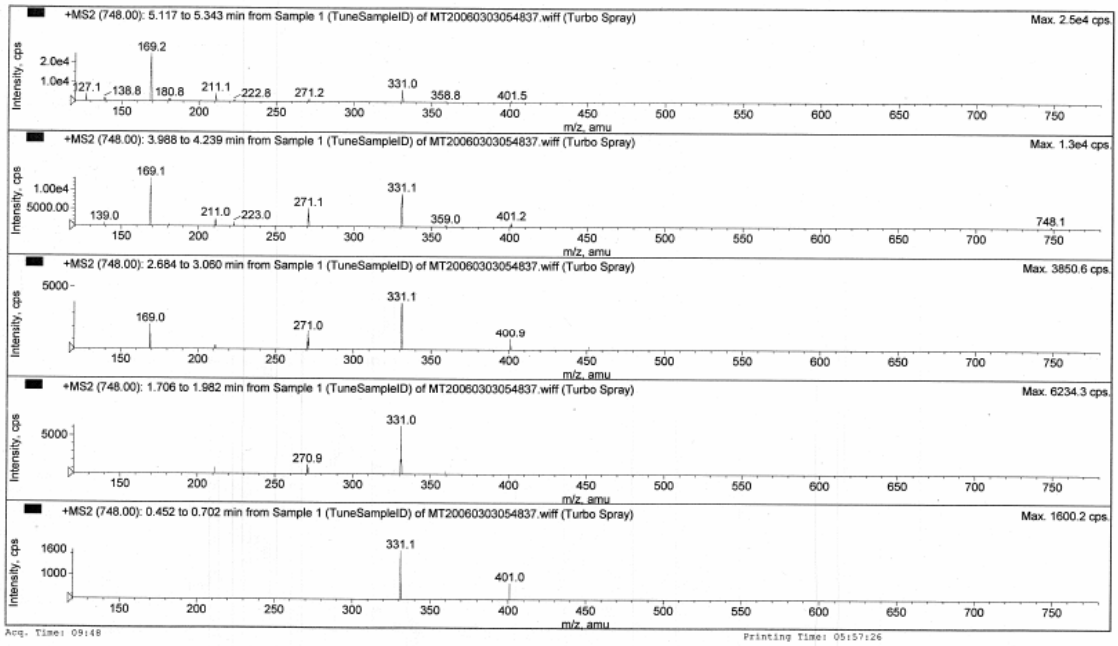

Figure 2.4. MS^2 spectra of (**70**) $[M + NH_4]^+ = 748$ m/z

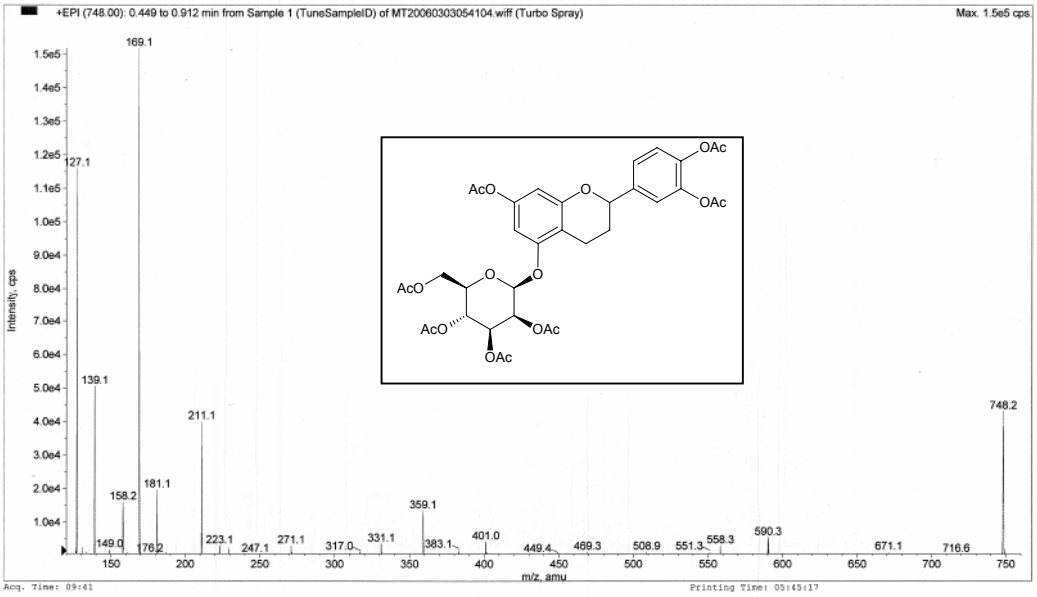

Figure 2.5. Enhanced Product ion scan of (**70**) $[M + NH_4]^+ = 748$ m/z

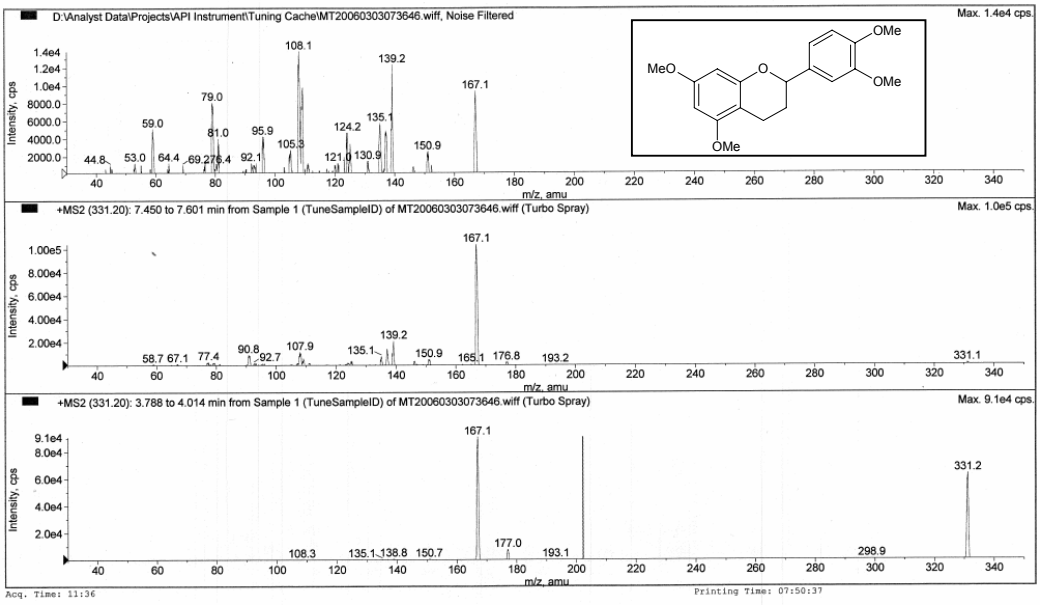

Figure 2.6. MS^2 Spectra of molecular ion $[M + H]^+ = 331.2$ m/z

Chapter 3

Synthesis of Rooibos Tea antioxidants, Aspalathin and its aglycone Phloretin

Introduction

Rooibos, a herbal tea prepared from *Aspalathus linearis*, an indigenous South African plant, is gaining in popularity on international markets, largely because it is caffeine-free and because of its proven antioxidant properties. Since emphasis was placed on the antioxidant properties of Rooibos, international sales increased from 750 t in 1993 to more than 3500 t in 2001. Extracts and powders for the ingredient market and for ready-to-drink herbal tea products are developed from Rooibos. The growth in the use of natural antioxidant preparations from plants by the food and nutraceutical market creates opportunities for the development of new products from Rooibos. Selective extraction and/or fractionation of active compounds can be employed to develop products with high potency. Knowledge of the relative potency of Rooibos extracts and its phenolic constituents could aid in the development of new antioxidant rich products. The traditional processing which entails the fermentation (oxidation) of the phenolic constituents, for the development of the red-brown color and flavor, results in major reduction of aspalathin content and antioxidant activity. The crude aspalathin ethyl acetate extracts demonstrate the most potent radical scavenging [177] and pronounced anti-tumor activity on mouse skin[178]. Techniques are developed for the selective extraction of aspalathin from the leaves of the plant[179]. The development of synthetic routes for the preparation of aspalathin is unexplored and would be useful to the cosmetic and health industries.

Phloretin, the aspalathin aglycone, is also a potent radical scavenger with similar commercial applications to aspalathin [180]. Related dihydrochalcones also show

[177] Joubert E., Winterton P., Britz T. J., Ferreira D., *Food Research International*, **2004**, *37*, 133.
[178] Marnewick J., Joubert E., Joseph S., Swanevelder S., Swart P., Gelderblom W., *Cancer Letters*, **2005**, *224*, 193.
[179] Jaganyi D., Wheeler P. J., *Food Chemistry*, **2003**, *83*, 121.
[180] Rezk B. M., Haenen G. R. M. M., van der Vijgh W. J. F., Bast A., *Biochemical and Biophysical Research Communications*, **2002**, *295*, 9.

pronounced radical scavenging abilities[181]. A one-step, environmentally friendly, unprotected synthesis of the dihydrochalcone, phloretin, is a key step in the synthesis of other dihydrochalcones and related antioxidants such as aspalathin.

Literature

A key step in the synthesis of aspalathin and numerous *C*-glycosyl flavonoids, is the formation of a *C*-aryl glycoside precursor followed by the formation of the dihydrochalcone or chalcone. *C*-Glycosylation can also be performed after the formation of the dihydrochalcone or other flavonoid aglycone

In general three basic groups of C-aryl glycoside synthesis exit, namely;

1. Lewis acids as promoters,
2. palladium as promoter and/or glycols as glycosyl donors
3. arylation

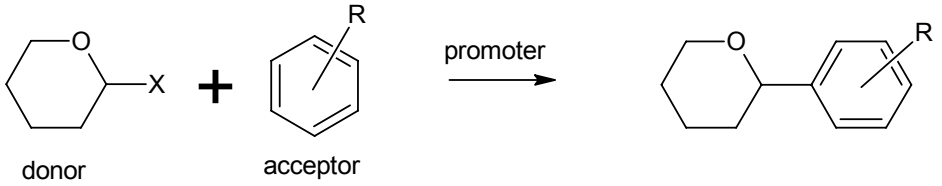

Scheme 3.1

O-glycosides are prepared by reaction of an appropriate glycosyl "donor", which is usually an electrophile activated at the anomeric position, with an alcohol as glycosyl "acceptor", which then plays the role as the nucleophile. A promoter is usually required for the coupling. The extension of this scheme to *C*-aryl glycosides represents an example of the well known Friedel-Crafts reaction (**Scheme 3.1**). The aromatic π-Lewis basic "acceptor" aryl ring is usually a weaker nucleophile than an alcohol acceptor.

The Friedel-Crafts approach was the earliest to be used with $AlCl_3$, a strong Lewis acid, as promoter[182]. The activation of the anomeric position is achieved with a variety of different electron withdrawing atoms or groups[183]. These include halides, methoxy,

[181] Nakamura Y., Watanabe S., Miyake N., Kohno H., Osawa T., *J. Agric. Food Chem.*, **2003**, *51*, 3309.
[182] Hurd C. D., Bonner W. A., *J. Am. Chem. Soc.*, **1945**, *67*, 1664.
[183] Jaramillo C., Kapp S., *Synthesis*, **1994**, 1-20.

carboxylate, trichloroacetimidate, pyridyl thioglycosides as glycoside donors; anomeric ethers and fluoride donors.

The palladium mediated arylation of olefins is an efficient method for C-C bond formation[184].

For the application to C-aryl glycosylation, glycals are used instead of the olefins[185]. A mixture of products is sometimes obtained in their reaction with aromatic nucleophiles. The final β-elimination of palladium led to the corresponding enol ether through β-hydride elimination (a), together with the rearranged glycal, arising from a β-acetoxy elimination to give product (b) (**Scheme 3.2**).

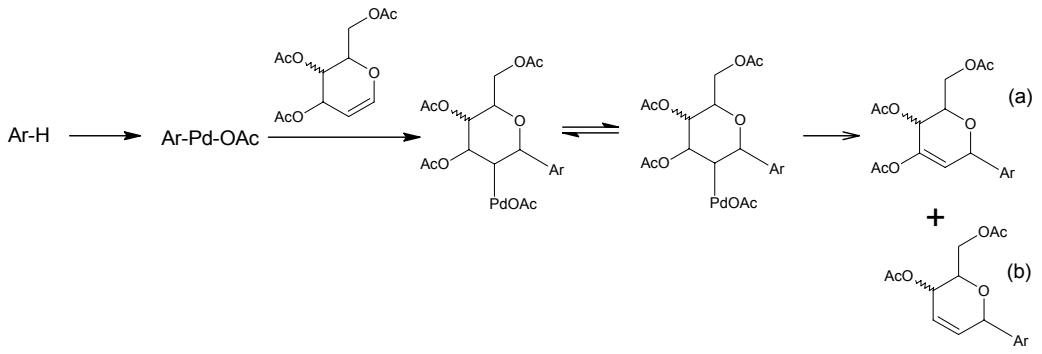

Scheme 3.2 (palladium mediated arylation)

Other examples used include palladium mediated aryl-zinc acceptors[186].

The direct displacement of an appropriate leaving group at the anomeric position in the carbohydrate by an organometallic aromatic species is the third general method for the preparation of *C*-aryl glycosides (**Scheme 3.3**)[187]. Phenyl magnesium bromide was the first arylation reaction tried. Many earlier experiments failed due to the reaction of the Grignard with the acetate protecting groups that resulted in the use of nine equivalents of Grignard reagent. Other organometallic glycosides donors like Cu, Zn, Cd and aluminium donors have also been employed[188].

[184] Ferrier R. J., *Adv. Carbohydr. Chem. Biochem*., **1969**, *24*,199.
[185] Daves G. D., *Acc. Chem. Res*., **1990**, *23*, 201.
[186] Jaramillo C., Kapp S., *Synthesis*, **1994**, *1*, 7-9.
[187] Hurd C. D., Bonner W. A., *J. Am. Chem. Soc.*, **1945**, *67*, 1972.
[188] Jaramillo C., Kapp S., *Synthesis*, **1994**, *1*, 10.

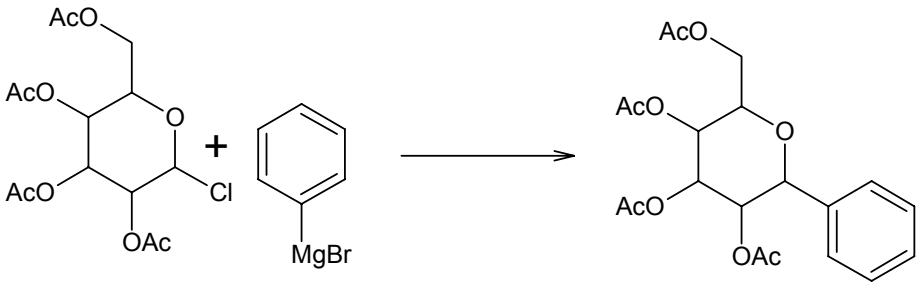

Scheme 3.3 (Arylation)

Fukazawa[189] described the synthesis of 3,4,4',6'-tetrakis-benzyloxy-3-*C*-(2",3",4",6"-tetra-*O*-benzyl-β-D-glucopyranosyl)-2'-hydroxychalcone as a precursor to the formation of the corresponding flavone. Benzylated β-D-glucopyranosylfluoride was utilized as the glycosyl donor and the selectively benzylated phloroacetophenone was the glycosyl acceptor. The *C*-glycosylation step in this synthesis was accompanied by a regio and stereoselective O→C glycosyl Fries rearrangement in the presence of borontrifluoride-diethyl etherate as the lewis acid[190]. During this rearrangement, the glycosyl moiety is transferred from a hydroxyl group to an *ortho* position of the aglycone to yield the β-coupled glycoside.

Results & Discussion

Synthesis of aspalathin utilizing benzyl protection (Scheme 3.5).

The selective benzylation of phloroacetophenone and 3,4-dihydroxybenzaldehyde was effected by the addition of benzylchloride in the presence of NaH at 0ºC in dry THF, to yield (**40**) and (**44**) respectively. C-benzylation of the aromatic ring was obtained as undesirable side products in both reactions, which decreased the overall yield significantly. The yield was 28% and 60% for (**40**) and (**44**) respectively due to the formation of these *C*-benzylated products.

After the addition of the BF_3-Et_2O in the presence of the benzylated acetophenone (**40**) and the 2,3,4,6-tetra-*O*-benzyl-D-glucopyranosyl fluoride (**41**) at -78°C under an argon atmosphere yielded the glucosylated acetophenone, 2,4, di-*O*-benzyl-6-

[189] Kumazawa T., Kimura T., Matsuba S., Sato S., Onodera J., *Carbohydrate Res*., 2001, 183-193.
[190] Kumazawa T., Akutsu Y., Matsuba S., Sato S., Onodera J., *Carbohydrate Res*., **1999**, *320*, 129.

hydroxy-(2',3',4',6'-tetra-*O*-benzyl-D-glucopyranosyl) phloroacetophenone (**42**) (58%) [191].

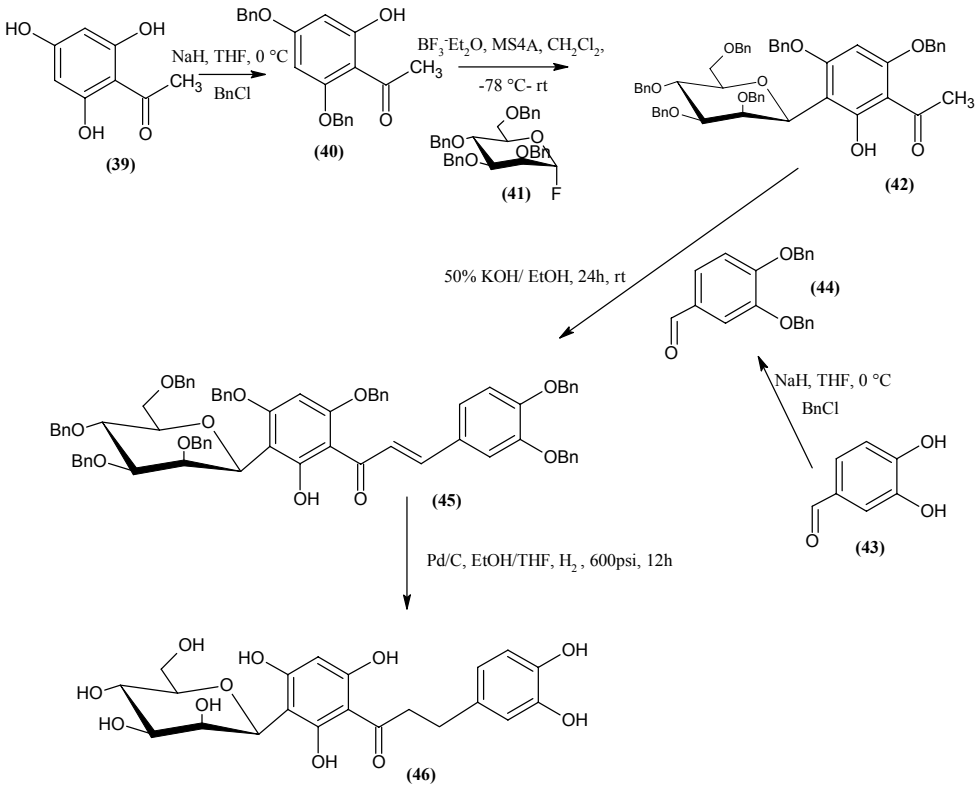

Scheme 3.5 (Synthesis of Aspalathin)

The desired chalcone (**45**) (15% yield) was effected by the normal aldol condensation conditions, reacting excess benzylated aldehyde (**44**) with the glucosylated acetophenone (**42**) in the presence of 50% KOH/EtOH.

The chalcone (**45**) was reduced overnight by Pd/C catalyst in EtOH/THF under a pressurized (600 psi) $H_{2(g)}$ atmosphere to yield the deprotected dihydrochalcone glucoside, aspalathin (**46**) (83% yield).

[191] Kumazawa T., Onda K., Okuyama H., Matsuba S., Sato S., Onodera J., *Carbohydrate Res*., **2002**, *337*, 1007.

A novel environmentally friendly selective mono-C-acylation of phloroglucinol: a commercial application towards the synthesis of Phloretin, an advanced intermediate of aspalathin.

Literature

Acylation of aromatic compounds is a well-known but still challenging topic in organic synthesis. The Friedel-Crafts acylation is one of the most popular reactions for the synthesis of aromatic ketones. While these reactions are performed by using more than a stoichiometric amount of $AlCl_3$, treatment of the aluminum residue can sometimes lead to environmental problems and drastic reaction conditions cause some severe side reactions[192]. Carboxylic acids are preferably used as acylating reagents and thus milder reaction conditions utilizing more environmentally friendly Lewis-acids are desirable. Aromatic ketones are prepared by acylation of aromatic compounds with carboxylic acids, catalyzed by various types of acids such as methanesulfonic acid[193], trifluromethanesulfonic acid[194], Nafion H[195], zeolite[196] and heteropoly salt[197]. However, these catalysts are also used in excess molar amounts. It is reported that catalytic amounts of metal triflates such as $Hf(OTf)_4$, $Sc(OTf)_3$ and $Zr(OTf)_4$ is prefered[198].

These metal triflates were also utilized successfully in conjunction with trifluoromethanesulphonic acid (TfOH) for catalyzing the Fries rearrangement[199].

TfOH which is a super acid which forms water-stable salts with non-hydrolysable metals. The use of commercial rare earth metal triflates (RET) as catalysts in organic synthesis is the topic of many publications. Triflic acid is one of the most acidic monoprotic organic acids and one may argue that mixing catalytic amounts of RET with an organic acid (carboxylic or sulfonic acids) (**Scheme 3.6**) with higher pKa than

[192] Kobayashi S., Moriwaki M., Hachiya I., *Tetrahedron Letters*, **1996**, *37* (24), 4183.
[193] Premasagar V., Palaniswamy V. A., Eisenbraum E. J., *J. Org. Chem*., **1981**, *46*, 2974-2976.
[194] Effenberger F., Epple G., *Angew. Chem., Int. Ed. Engl*., **1972**, *11*, 299-300.
[195] Yamamoto T., Hideshima, C., Prakash G. K. S., Olah G. A., *J. Org. Chem*., **1991**, *56*, 3955-3957.
[196] Chiche B., Finiels A., Gauthier C., Geneste P., Graille J., Pioch D., *J. Org. Chem*., **1991**, *51*, 2128-2130.
[197] Kaur J., Kozhevnikov I. V., *Chem. Commun*. **2002**, 2508-2509.
[198] Matsushita Y., Sugamoto K., Matsui T., *Tetrahedron Letters*, **2004**, *45*, 4723.
[199] Mouhtady O., Gaspard-Iloughmane H., Roques N., Le Roux C., *Tetrahedron Letters*, **2003**, *44*, 6379.

TfOH leads to complexation of the acid to the RET. This complexation leads to new catalytic mechanism for the Fries rearrangement. Since these rearrangements are known to be proton catalyzed, the increased Brønsted acidity of the catalyst complex might also be responsible for its catalytic activity (**Scheme 3.6**). Ligand exchange between methane sulfonic acid (MSA) and the metal triflate, generating metal sulfonate and TfOH, which is a known catalyst for the Fries rearrangement, represents another explanation for its catalytic activity. A third option would be Brønsted-Lewis acid catalysis resulting in a double activation of the ester[199].

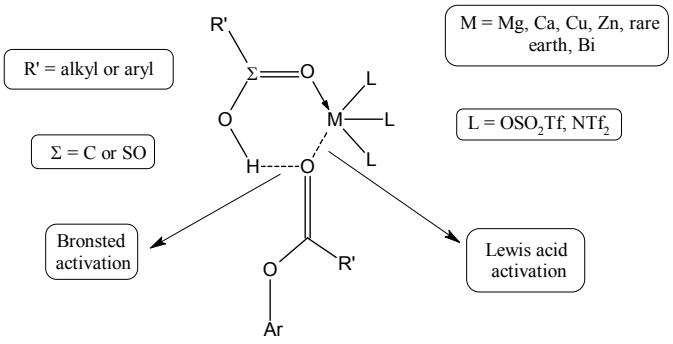

Scheme 3.6

These acylation reactions utilizing $Hf(OTf)_4$ in conjunction with lithium perchlorate-nitromethane has been described[200].

Results & Discussion

Numerous reactions, using both $Sc(OTf)_3$ and $Hf(OTf)_4$ as Lewis acid catalysts in combination with various solvent systems was performed, to attempt the unprotected acylation of phloroglucinol using cinnamic acid.

This acylation of phloroglucinol was successful with $Hf(OTf)_4$ as catalyst in a specific and critical solvent system, CH_3CN/CH_3NO_2 (6.7:1), although the yield was very low (1%) (**Scheme 3.7**)[201]. The solvent system utilized in the rare earth metal acylation play an all-important catalytic role in the acylation of phloroglucinol. Due to time constraints, the reaction was not optimized further.

[200] Hachiya I., Moriwaki M., Kobayashi S., *Tetrahedron Letters*, **1995**, *36, no. 3*, 409.
[201] Kobayashi S., Moriwaki M., Hachiya I., *Tetrahedron Letters*, **1996**, *37, no 12*, 2053.

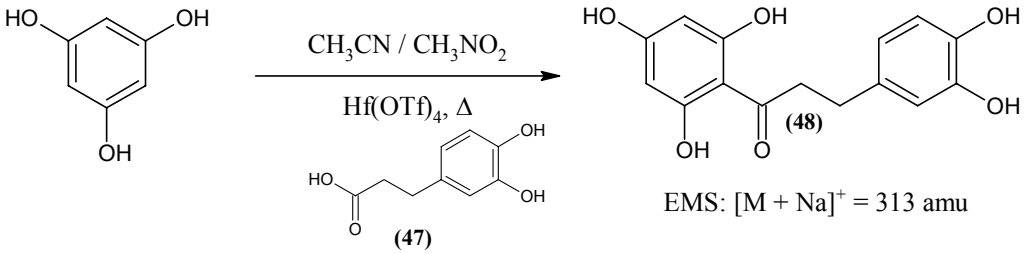

Scheme 3.7 (Synthesis of Phloretin)

The structure (**48**) was established by ^{1}H NMR in conjunction with mass spectroscopic methods. The two proton singlet chemical shift of the proton on the phloroglucinol ring was key to the confirmation of the structure and is found to be the same as in literature[202].

The structure was affirmed by ESI-MS spectroscopy which displayed the sodium adduct of the phloretin molecular ion as $[M + Na]^{+} = 313$ m/z.

[202] Ito, K., Itoigawa M., Haruna M., Murata H., Furukawa H., *Phytochemistry*, **1980**, *19*, 476.

Experimental

Protected synthesis of aspalathin

Synthesis of 4,6-di-*O*-benzyl-2-hydroxy-phloroacetophenone (40)

Phloroacetophenone (1g, 5.3 mmol) was dissolved in dry acetone and dry K_2CO_3 (3.7g, 5 eq) added over an inert atmosphere (N_2) at 0°C. Benzyl chloride (0.815g, 6.4 mmol, 1.2 eq) was added and the reaction stirred for 8hr (TLC). The reaction was quenched with water and acidified with dilute HCl and extracted with EtOAc. The organic phase was removed under reduced pressure and the crude reaction mixture purified by PLC (3 X, H:B:Tol:EtOAc 6: 3: 0.5: 0.5, Rf = 0.46) to give the title compound (0.52g, 28% yield). ^{1}H-NMR [**Plate 9** ($CDCl_3$) 293K]: 2 x Ph (δ7.4, m), H-3 (δ6.19, d, J = 2.2 Hz), H-5 (δ6.12, d, J = 2.2 Hz), 2 x CH_2 (δ5.1, s), Me (δ2.6, s).

Synthesis of 3,4-di-*O*-benzyl-benzaldehyde (44).

3,4-dihydroxy-benzaldehyde **(43)** (1g, 7.24 mmol) was added to a suspension of NaH (0.2g, 8.69 mmol, 1.2 eq) in DMF (20 ml) and the mixture was stirred for 30 min. at 0°C. Benzylchloride (1.1g, 8.69 mmol, 1.2eq) was added to the mixture and stirred at room temperature for 48hr. The reaction mixture was quenched with water, acidified with 1N HCl and extracted with EtOAc. The organic phase was washed with water and dried over $MgSO_4$. Purification by FCC afforded the title compound (**44**) as white plates (Rf = 0.38 H:Tol 8:2). (1.38g, 60% yield). ^{1}H-NMR [**Plate 8** ($CDCl_3$) 293K]: 2 x Ph, H-2, H-6 (δ7.54-7.34, m), H-5 (δ7.04, d, J = 8.24 Hz), CHO (δ9.83, s), CH_2 (δ5.28, s), CH2 (δ5.24, s).

Synthesis of 4,6-di-*O*-benzyl-2-hydroxy-3-(2',3',4',6'-tetra-*O*-benzyl-D-glucopyranosyl) phloroacetophenone.

To a stirred mixture of the acetophenone (**40**) (50mg, 0.144 mmol, 3 eq.), 2,3,4,6-tetra-*O*-benzyl-D-glucopyranosyl fluoride (**41**) (26 mg, 0.048 mmol, 1 eq.) and powdered molecular sieves in CH_2Cl_2 at -78°C, BF_3-Et_2O (16 µl, 0.096 mmol, 2 eq) was added drop wise and the mixture stirred for 30min. The temperature was then allowed to increase to -42°C and stirred for another 30 min. The temperature was then raised again to -20°C for 30 min., at 0°C and finally at room temperature for 1h. Water was added to the reaction and the mixture filtered through a Celite pad and washed with $CHCl_3$. The filtrate was extracted with $CHCl_3$ and dried over $MgSO_4$ and evaporated under reduced pressure. The resulting syrup was chromatographed on PLC using (3 X, H:B:Tol:EtOAc 6: 3: 0.5: 0.5, Rf = 0.46) (Rf = 0.35) to yield the C-glucosylated acetophenone (**42**) as a clear yellowish oil (24mg, 58%). ^{1}H-NMR [**Plate 10** (DMSO-d6) 413K]: 6 x Ph (δ7.2, m), H-5 (δ6.44, s), 2 x CH_2 (δ5.19, δ5.28, s), 4 x CH_2, H-1'-6' (δ5.00- 3.49), CH_3 (δ2.55, s).

Synthesis of 3,4,4',6'-tetra-*O*-benzyl-2'-hydroxy-3-(2",3",4",6"-tetra-*O*-benzyl-D-glucopyranosyl) chalcone.

A solution of the C-glucosylated acetophenone (**42**) (50mg, 0.057 mmol) in 50% KOH/EtOH (4ml) was stirred for a period of 15 minutes. 3,4-di-*O*-benzylbensaldehyde (**44**) (27mg, 0.085 mmol, 1.5eq.) was added and the solution stirred for 24hr (TLC). The reaction was quenched and neutralized with 0.1% HCl and subsequently extracted with dichloromethane. The organic layers was combined and dried over $MgSO_4$. The solvent was removed under reduced pressure and the resultant crude product was re-dissolved and purified by PLC method (3 X, H:B:Tol:EtOAc 6: 3: 0.5: 0.5, Rf = 0.35) to yield 3,4,4',6'-tetra-*O*-benzyl-2'-hydroxy-3-(2",3",4",6"-tetra-*O*-benzyl-D-glucopyranosyl) chalcone (**45**)
(5 mg, 0.08 mmol, 15% yield). ^{1}H-NMR [**Plate 11** (DMSO-d6) 293K]: 8 x Ph, H-α, H-β, H-2, H-5, H-6 (δ7.73-6.62, m), H-5' (δ6.02, ds), H-1"-5", 2 x H-6", 8 x CH_2 (δ5.28-3.55).

Synthesis of aspalathin.

The chalcone (**45**) (5mg, 0.08 mmol) was dissolved in EtOH/THF (4 ml) and a catalytic amount of Pd/C (1mg). The suspension was stirred under a hydrogen atmosphere (600 psi) for 12hr. The suspension was filtered and the solvent evaporated under reduced pressure to yield the desired dihydrochalcone glucoside, aspalathin (3mg, 0.06mmol) 83% yield. ^{1}H-NMR [**Plate 12** (CD_6CO/D_2O) 313K]: H-2, H-5 (δ6.66- 6.72, m), H-5' (δ5.97, s), H-1" (δ4.82, d, 9.8 Hz), H-2"-6" (δ3.40-3.95, m), H-β (δ2.75, t, J = 7.7Hz), H-α (δ3.25, t, J=7.7Hz). MS, $C_{21}H_{24}O_{11}$,$[M + 1]^+$ = 453.4 m/z, **Plate 12a**.

The spectra of the synthesized aspalathin was compared with a authentic sample, ^{1}H-NMR [**Plate 13** and MS: $C_{21}H_{24}O_{11}$, $[M + 1]^+$ = 453.1 m/z, **Plate 13a**.

Unprotected synthesis of phloretin

$Hf(OTf)_4$ (0.1 mmol, 20 mol %) was added to a solution of phloroglucinol (0.5 mmol, 63 mg) and cinnamic acid (**47**) (0.5 mmol, 9.1 mg) in ACN (1 ml) / nitromethane (0.15 ml) at room temperature. The reaction mixture was stirred for 6h at 100°C and cooled to ambient temperature. Water was added to quench the reaction and subsequently extracted with CH_2Cl_2 and dried over Na_2SO_4. The solvents was evaporated under reduced pressure to yield the crude product and cleaned by PLC (tol:acetone 6:4, Rf = 0.2) to yield the dihydrochalcone (**48**) (3mg, 1% yield)

^{1}H-NMR [**Plate 14** (CD_6CO/D_2O) 293K]: H-2 (δ6.78, d, J = 1.9Hz), H-5 (δ6.72, d, J = 8.1Hz), H-6 (δ6.59, dd, J = 2.0, 7.9Hz), H-3', H-5' (δ5.94, s), H-β (δ3.33, t, J = 7.5Hz), H-α(δ2.83, t, J = 7.5Hz), MS: $C_{15}H_{14}O_6$, $[M + Na]^+$.= 313.3 m/z., **Plate 14a**.

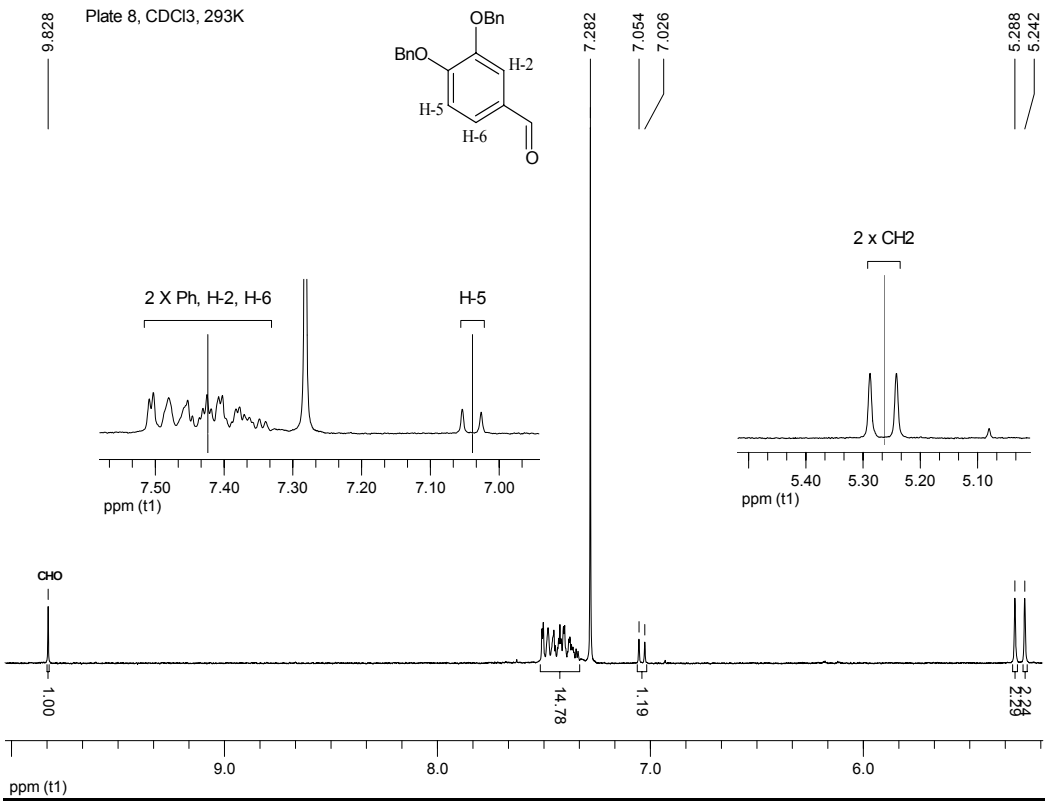
Plate 8, CDCl3, 293K
9.828
OBn
BnO
H-2
H-5
H-6
O
7.282
7.054
7.026
5.288
5.242
2 X Ph, H-2, H-6
H-5
7.50
7.40
7.30
7.20
7.10
7.00
ppm (t1)
2 x CH2
5.40
5.30
5.20
5.10
ppm (t1)
CHO
1.00
14.78
1.19
2.24
2.29
9.0
8.0
7.0
6.0
ppm (t1)

Plate 9, CDCl3, 293K

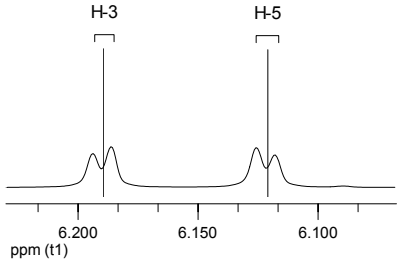

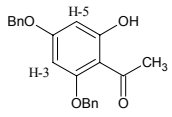

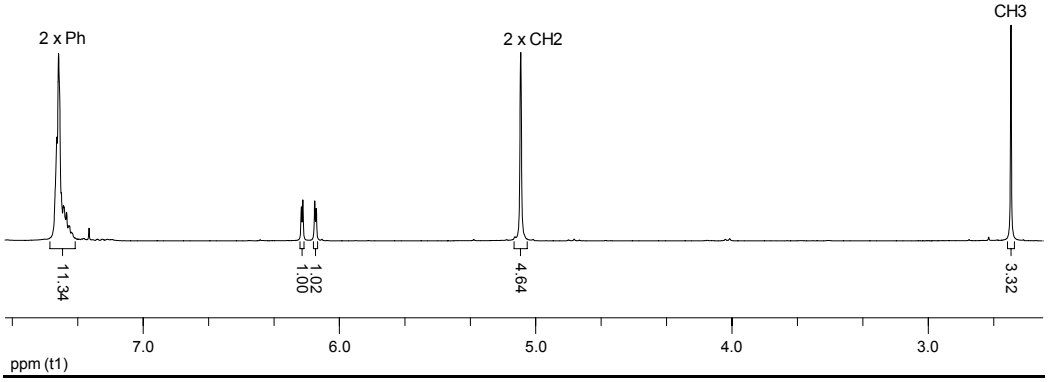

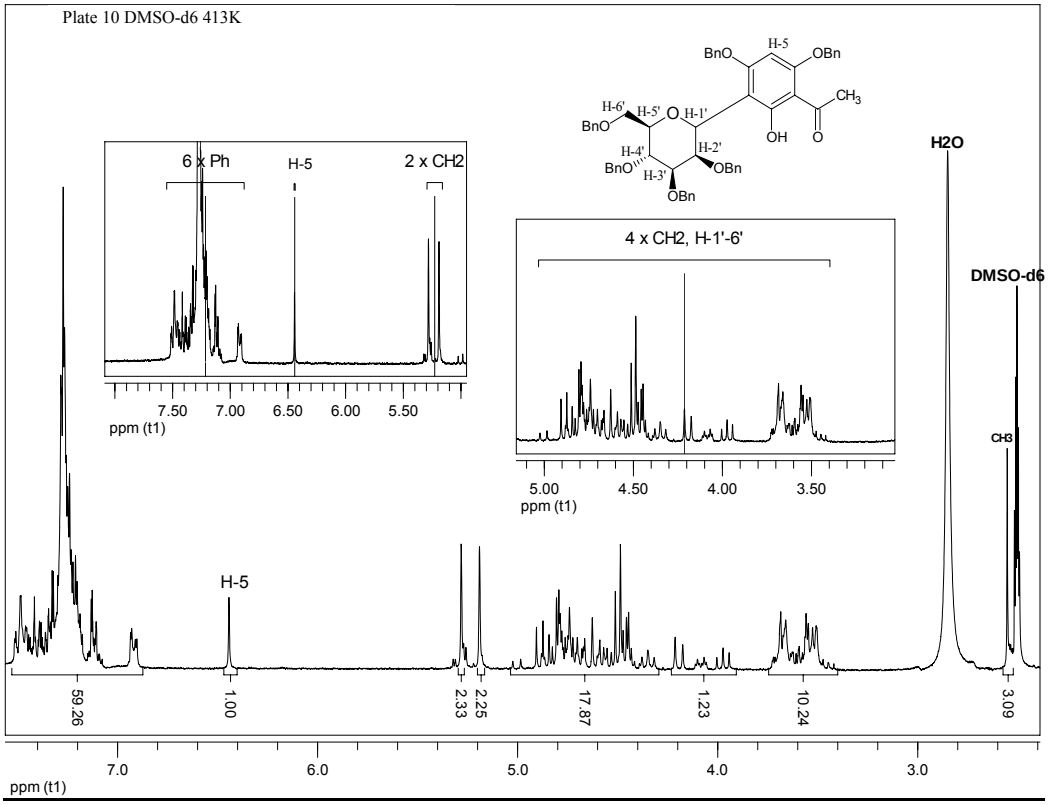

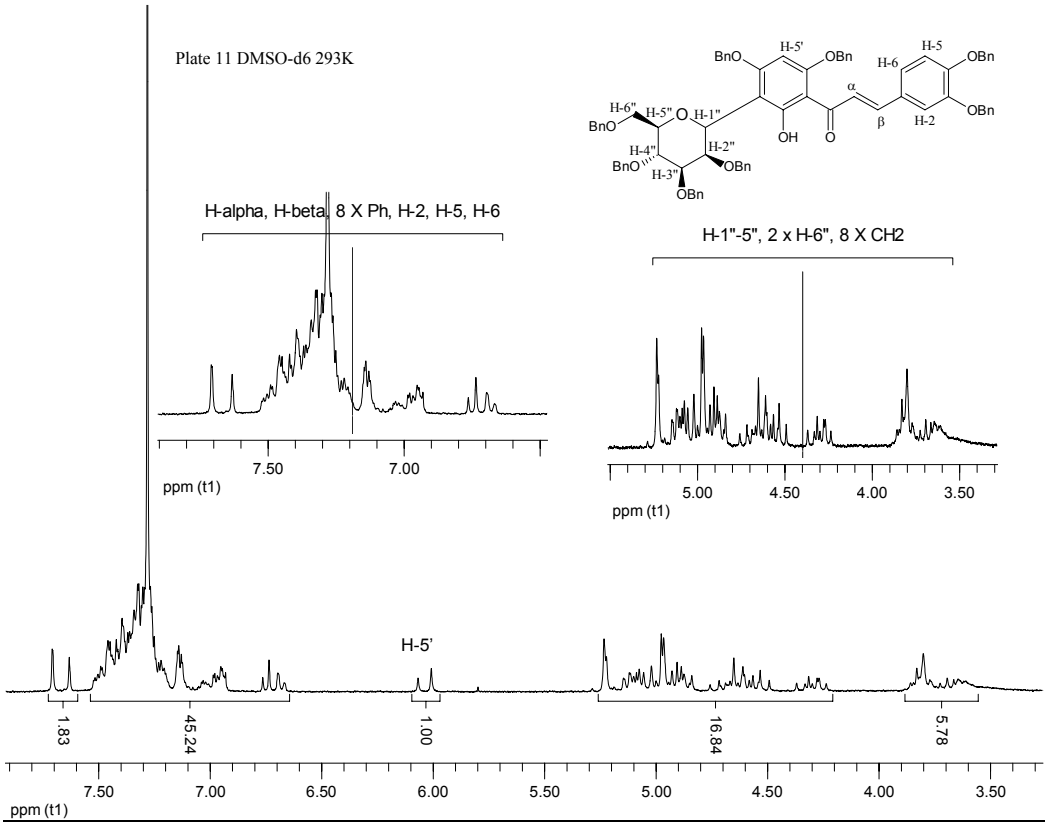
Plate 11 DMSO-d6 293K
H-alpha, H-beta, 8 X Ph, H-2, H-5, H-6
H-1"-5", 2 x H-6", 8 X CH2
H-5'
1.83
45.24
1.00
16.84
5.78
ppm (t1)

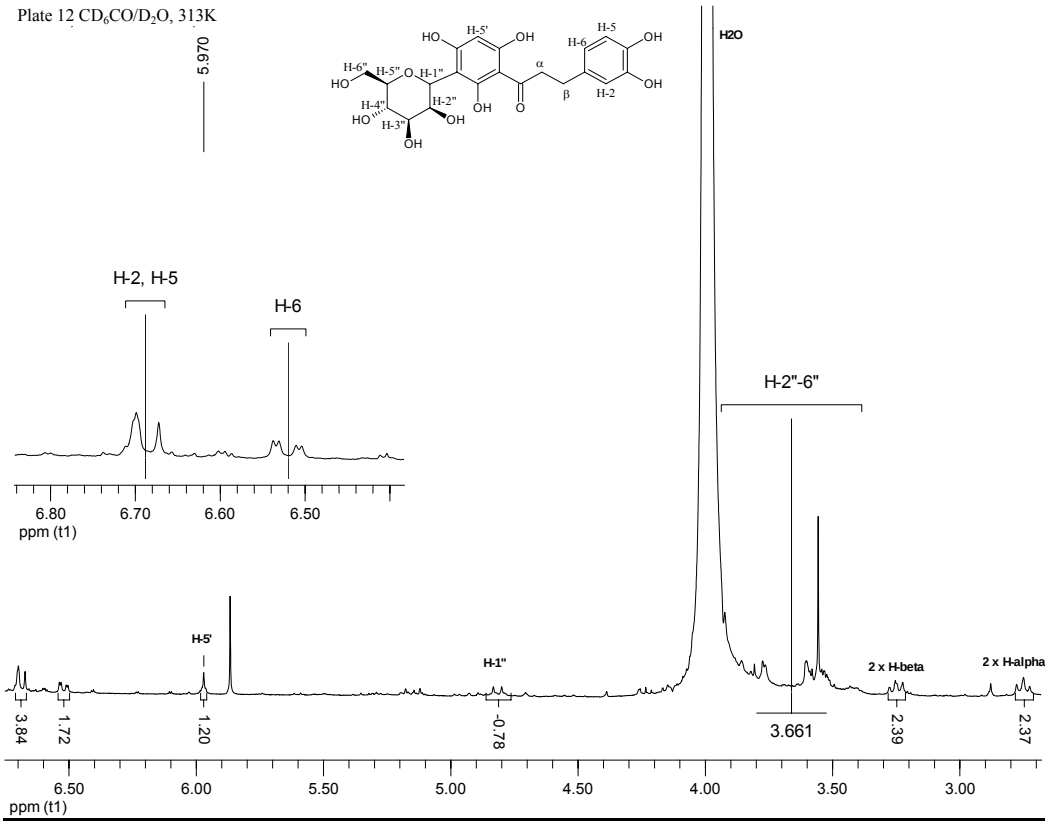
Plate 12 CD6CO/D2O, 313K
5.970
H-5'
H-5
H-6
H-6"
H-5"
H-1"
H-2"
H-4"
H-3"
H-2
α
β
H2O
H-2, H-5
H-6
H-2"-6"
6.80
6.70
6.60
6.50
ppm (t1)
H-5'
H-1"
2 x H-beta
2 x H-alpha
3.84
1.72
1.20
-0.78
3.661
2.39
2.37
6.50
6.00
5.50
5.00
4.50
4.00
3.50
3.00
ppm (t1)

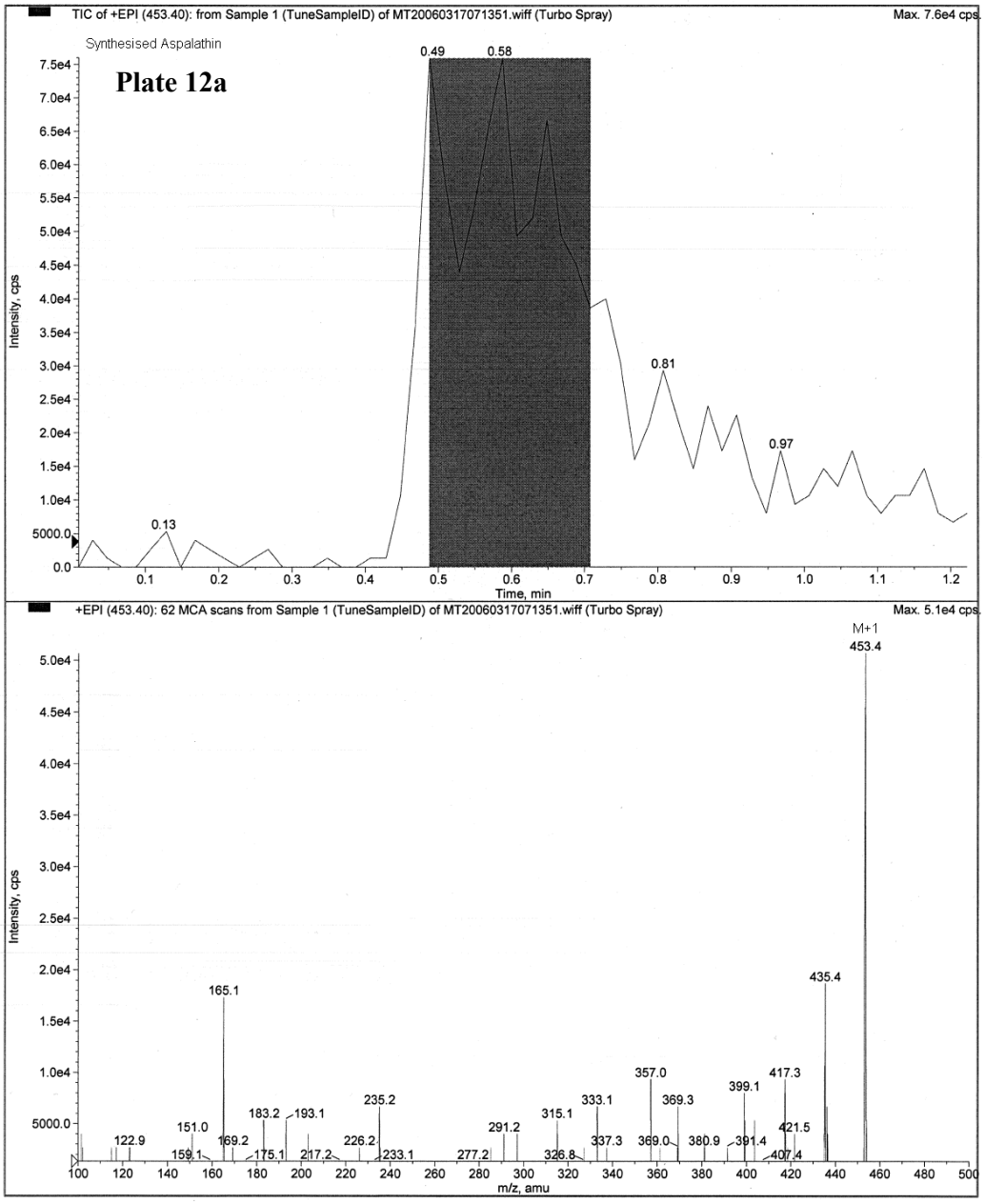
TIC of +EPI (453.40): from Sample 1 (TuneSampleID) of MT20060317071351.wiff (Turbo Spray)
Max. 7.6e4 cps.
Synthesised Aspalathin
Plate 12a
Intensity, cps
Time, min
0.13
0.49
0.58
0.81
0.97
+EPI (453.40): 62 MCA scans from Sample 1 (TuneSampleID) of MT20060317071351.wiff (Turbo Spray)
Max. 5.1e4 cps.
M+1
453.4
435.4
165.1
357.0
417.3
399.1
369.3
333.1
235.2
315.1
183.2
193.1
151.0
291.2
421.5
122.9
169.2
226.2
337.3
369.0
380.9
391.4
159.1
175.1
217.2
233.1
277.2
326.8
407.4
m/z, amu

Plate 13 CD_6CO/D_2O-d6 293K

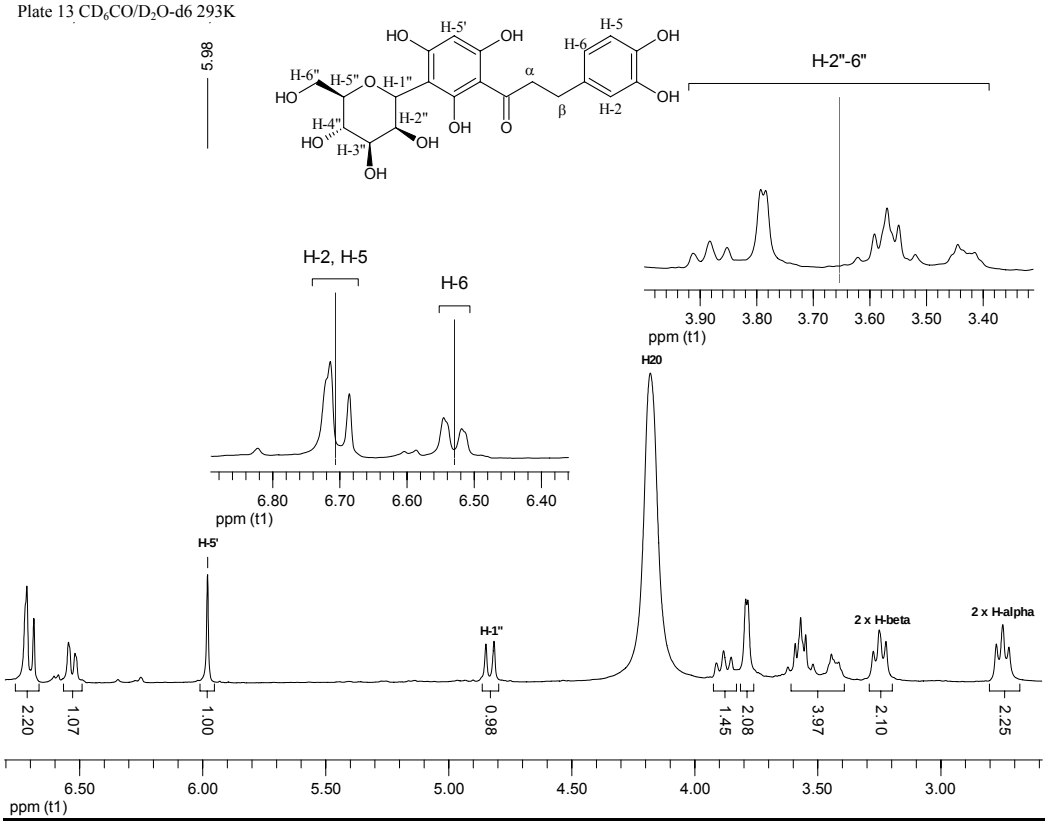

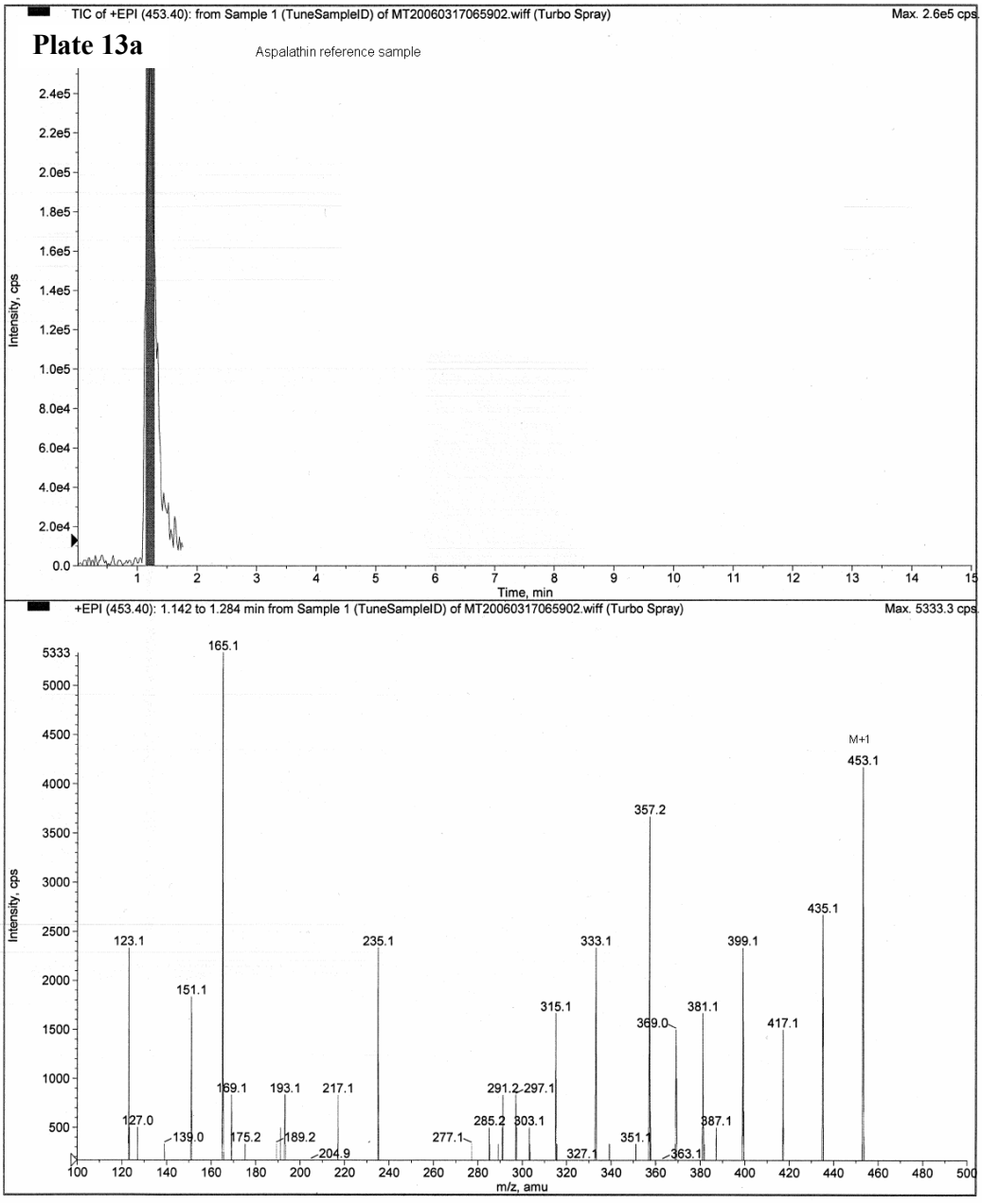
TIC of +EPI (453.40): from Sample 1 (TuneSampleID) of MT20060317065902.wiff (Turbo Spray)
Max. 2.6e5 cps.
Plate 13a
Aspalathin reference sample
Intensity, cps
Time, min
+EPI (453.40): 1.142 to 1.284 min from Sample 1 (TuneSampleID) of MT20060317065902.wiff (Turbo Spray)
Max. 5333.3 cps.
M+1
453.1
165.1
357.2
435.1
123.1
235.1
333.1
399.1
151.1
315.1
381.1
369.0
417.1
169.1
193.1
217.1
291.2
297.1
127.0
285.2
303.1
387.1
139.0
175.2
189.2
277.1
351.1
204.9
327.1
363.1
m/z, amu

Plate 14 CD_6CO/D_2O-d6 293K

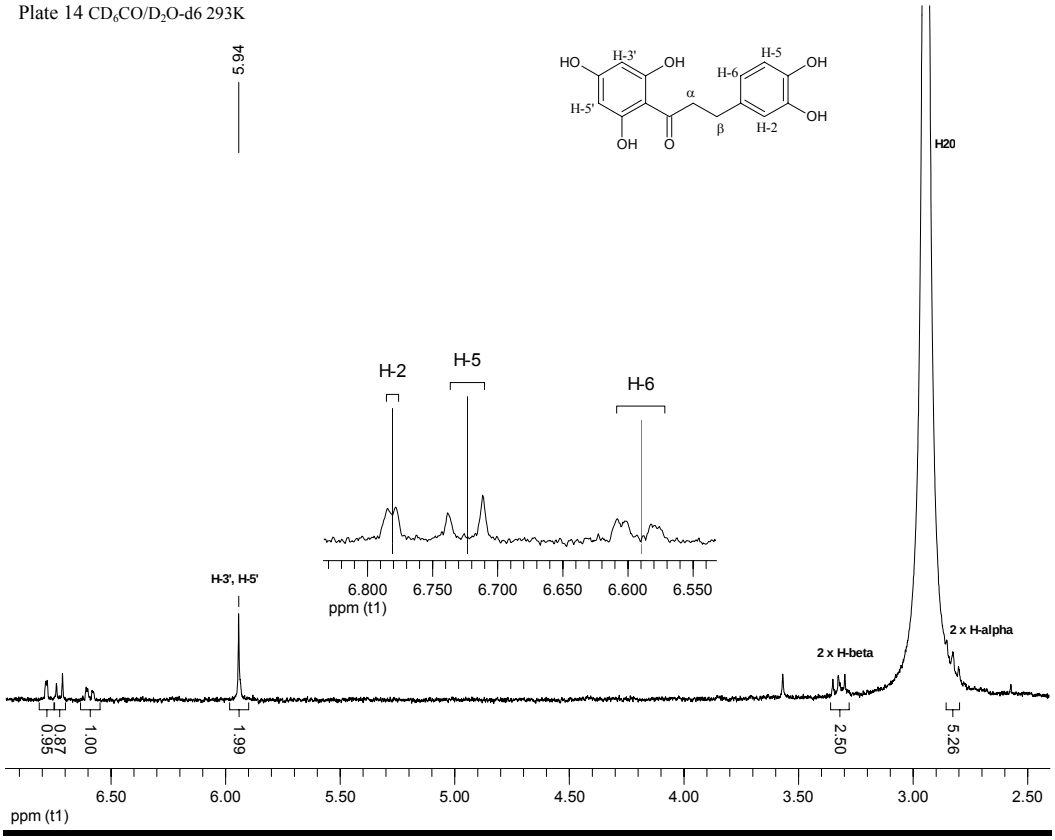

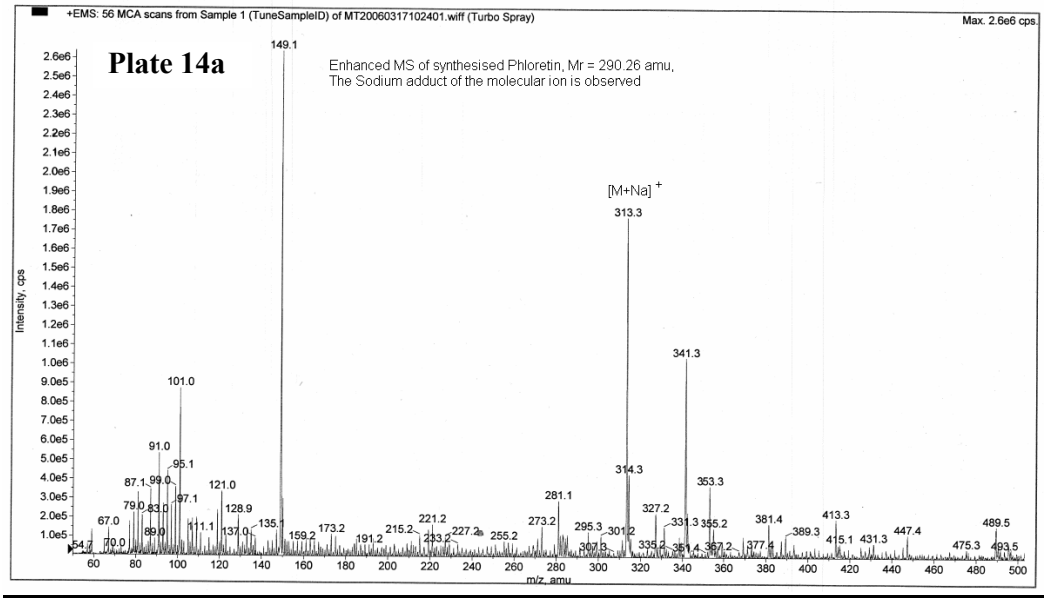

Chapter 4

Conformational and electronic interaction studies of the Mosher acid as a basis to interpret the behavior of the epicatechin Mosher ester derivatives

Introduction and Literature

Enantiopure (*R*)- or (*S*)-α-Methoxy-α-trifluoromethyl-α-phenylacetic acid (MTPA) has been the most commonly used derivatizing reagent for the determination of the absolute configuration of secondary alcohols by NMR during the last 30 years. The well documented Mosher protocol (**Scheme 4.1**)[203] works on the principal that the diamagnetic effect of the benzene ring, on a MTPA derivative of known configuration, preferentially shields protons or substituents (L_1 or L_2) on one side of the carbinol carbon atom, which makes the deduction of the absolute stereochemistry of the alcohol possible. In other words, the relative chemical shift differences of the two carbinol substituents are brought about by a time weighted average preferential shielding of these two groups by the π-electron cloud of the α-phenyl substituent on the ester. The origin of the conformational preference in these ester derivatives, which plays the key role in the assignment of the absolute configuration of the substrate has, however, hitherto not been accounted for. Investigation of the conformational dynamics of MTPA esters have been limited to Molecular Mechanics (MM) and Semi-Empirical (SE) calculations[203], which have proved to be inadequate, thus leading to erroneous conclusions.

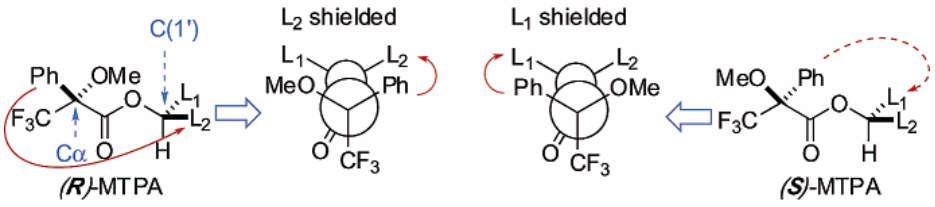

Scheme 4.1 (Preferential shielding of *R*, *S*-diastereomeric esters)

Previously, mainly three chiral derivatizing agents (CDA's), of known chirality, were utilized in this regard to afford the corresponding esters: Mandelate, *O*-Methylmadelate and Atrolactate.

---

[203] Seco J. M., Quinoa E. and Riguera R., *Chem. Rev*. **2004,** *104*, 17-117.

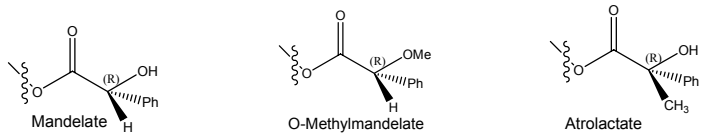

All three of these CDA's have either the α-OH or -OMe in a *syn* periplanar alignment with the carbonyl as the energetically favored rotational conformer in solution. These CDA's have greater chemical shift differences than MTPA presumably due to H-bonding between the OH and the carbonyl oxygen contributing to greater rigidity of these conformers[205]. The presence of an acidic α-hydrogen leading to the formation of a highly reactive enolate in these esters is however undesirable. The substitution of the α-hydrogen in *O*-Methylmandelate with a CF_3 group not only solves this problem but also reverses the observed shielding effects of the phenyl ring. The CF_3 group replaces the OMe group as the energetically preferred group to eclipse the carbonyl group in *O*-Methylmandelate. This implies the CF_3-carbonyl *syn* periplanar (*sp*) alignment now dominates in solution thus, highlighting the importance of this group in determining the preferred conformation. Although the MTPA ester derivatives exhibited smaller chemical shift differences between diastereomers, the reagent can be conveniently obtained in enantiomerically pure form, is configurationally stable, and reacted essentially quantitatively irrespective of the configuration of alcohol or acid[204].

Additionally, ^{19}F NMR also provided an effective method for *ee*-determinaton with the Mosher ester derivative (**Scheme 4.1a**). This widely used probe is based on the principal that one of the carbinol substituents on a diastereomer sterically hinders the preferred alignment of the ester causing the CF_3 group to be further out of plane with the diamagnetic shielding effect of the carbonyl[205]. This then creates a chemically different environment for the fluorine nuclei of the two diastereomers, from which the enantiomeric ratio is determined by the integration of the two fluorine NMR resonance peaks. The high natural abundance of ^{19}F isotope makes the application of these and other fluorinated CDA's very attractive.

[204] Dale J.A., Mosher H.S., *J. Am. Chem. Soc.*, **1968**, *90*, no. 14, 3732.

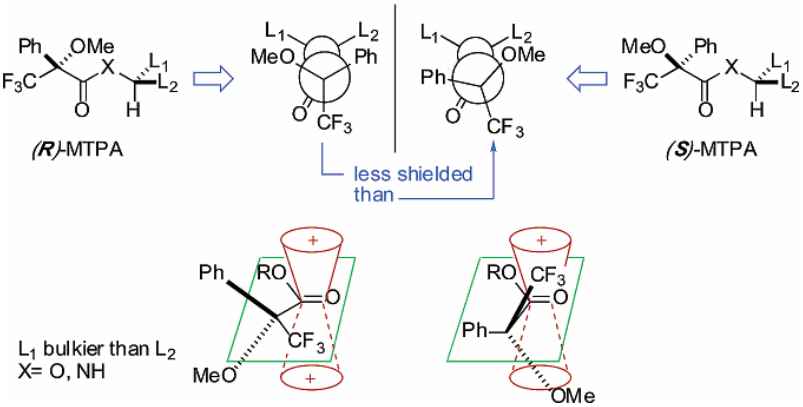

Scheme 4.1a (differential shielding of L^1, L^2 by (*R*) and (*S*)-MTPA derivatives)

As mentioned, two main conformational isomers are preferred for the free Mosher acid.[205] The more dominant of the two represents the conformation where the CF_3 group is aligned *syn* (*sp*) with the carbonyl oxygen and the other is the *anti*-periplanar (*ap*) alignment (**Fig. 4.1a, b**). An approximate ratio of 7:3 exists in solution according to the different IR carbonyl stretching frequencies of the two rotational isomers of the Mosher ester in solution[206]. Experimentally the *sp*-conformer needs to be the energetically favored conformer on the potential energy surface of the molecule to act as a chiral derivatizing agent and for the Mosher protocol to be applicable. The carbinyl H and the carbonyl also have a preferred *sp* alignment, constituting the MTPA plane (**Fig 4.2**).

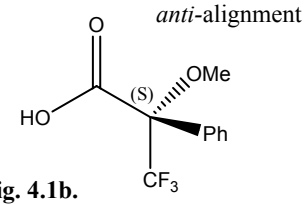

Fig. 4.1b.
α-Methoxy-α-trifluromethyl-
α-phenylacetic acid (MTPA)

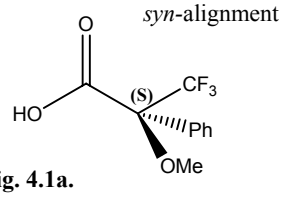

Fig. 4.1a.
α-Methoxy-α-trifluromethyl-
α-phenylacetic acid (MTPA)

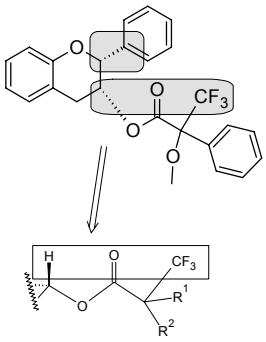

MTPA plane

Figure 4.2

[205] Dale J. A., and Mosher H. S., *J. Am. Chem. Soc.*, **1973**, 512-519.
[206] Ohtani I., Kusumi T., Kashman Y. and Kakisawa H., *J. Am. Chem. Soc.*, **1991**, *113*, 4092.

Solid state crystal structure of 3',4',5,7-Tetramethoxy-epicatechin-(3-*O*)-(*R*)-α-methoxy-α-trifluoromethyl-α-phenylacetate

The majority of flavonoids are notoriously non-crystalline, amorphic, compounds and only a handful of crystal structures exist for these compounds. Furthermore, for the crystals that exist, H-bonding usually results in monomer chains or as dimers where the dimer involves the 4-carbonyl, 3-hydroxy and other free hydroxyls in intermolecular hydrogen bonding. π-π Stacking between the phenyl rings also play an important role in the crystallization of these flavonoids,[207] especially in the planar flavonoids like flavones and isoflavones. The title compound is not only representative of an exclusive group of crystalline flavonoids, but also the first crystalline Mosher derivative of a flavonoid with known stereogenic definition.

This combined and unique features embodied in this compound, has given impetus to the current project with the aim to scientifically probe the fundamental interactions governing the dynamic conformational behavior of the ester moiety and hence a better rationalization of the widely utilized Mosher protocol which is based on highly successful empirical rules.

[207] Cantrell J. S., *Plant Flavonoids in Biology and Medicine: Biochemical, Pharmacological and Structure-Activity Relationships*, **1986**, 391-394.

Rationalizing the preferred alignment of the Mosher ester

Fluorine Negative Hyperconjugation

Introduction

The expression *"gauche* effect" has been given[208, 209, 210, 211] to the phenomenon in 1, 2-disubstituted ethanes (**4.2.1**) where the *gauche* (here also viewed as a *syn* periplanar conformation) conformer (**4.2.l a**) is populated to a larger extent than *anti* conformer (**4.2.l b**) when the substituents X and Y are both electronegative atoms such as oxygen or fluorine (**Scheme 4.2**). This preference is surprising, since both dipole repulsions between electronegative atoms and steric effects should favour the *anti* conformation.

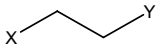

(**4.2.1**)

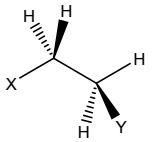

(**4.2.1**a)

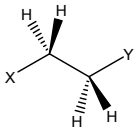

(**4.2.1**b)

Scheme 4.2

A variety of 1-substituted propanes, *e.g.* 1 (Y = CH_3, X = Cl, F, OH, CF_3), are also known to prefer a *gauche* conformation. [212, 213, 214, 215, 216]

The *gauche* effect has been attributed primarily to σ-hyperconjugation, which may be rationalized in terms of donor-acceptor atomic orbital interactions or resonance structures (**Scheme 4.3**)[217, 218, 219, 220]. More specifically, the most stable conformation

[208] Wolfe S., *Acc. Chem. Res*., **1972**, *5*, 102.
[209] Juraisti E., *J. Chem. Educ*., **1979**, *56*, 438.
[210] Nelsen S. F., *Acc. Chem. Res*., **1978**, *11*, 14.
[211] Zefirov N. S., Gurvich L. G., Shashkov A. S., Krimer M. Z. and Vorob'eva E. A., *Tetrahedron*, **1976**, *32*, 1211.
[212] Sheppard N., *Adv. Spectrosc*., **1959**, *1*, 295.
[213] Morino Y. and Kuchitsu K., *J. Chem. Phys*., **1958**, *28*, 175.
[214] Sarachman T. N., *J. Chem. Phys*., **1963**, *39*, 469.
[215] Szasz G. J., *J. Chem. Phys*., **1955**, *23*, 2449.
[216] Houk K. N., Eksterowicz J. E., Wu Y. –D., Fuglesang C. D. and Mitchell D. B., *J. Am. Chem. Soc*., **1993**, *115*, 4170.
[217] Parker D., Senanayake K., Vepsailainen J., Williams S., Batsanov A. S. and Howard J. A. K., *J. Chem. Soc. Perkin Trans. 2*, **1997**, 1445.
[218] Brunck T. K. and Weinold F., *J. Am. Chem. Soc*., **1979**, *101*, 1700.
[219] Dionne P. and St-Jacques M., *J. Am. Chem. Soc*., **1987**, *109*, 2616.

of a 1, 2-disubstituted ethane has been postulated to place the best σ-donor bond *anti* to the best σ-acceptor bond. The *syn* conformation also allows for hyperconjugative overlap, but to a lesser extent, due to reduced vicinal orbital overlap.

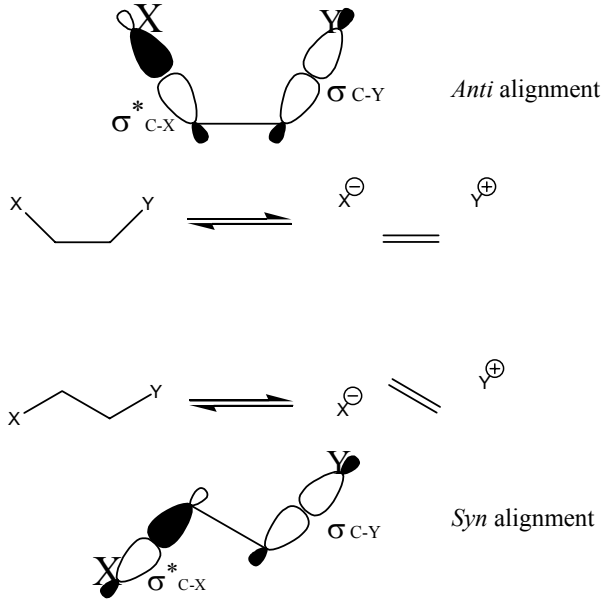

Scheme 4.3

The formula (1), $V(\theta) = V_0 + \frac{1}{2}V_1\cos(\theta) + \frac{1}{2}V_2\cos(2\theta) + \frac{1}{2}V_3\cos(3\theta)$, is used to calculate the energies (V) for the corresponding torsional angles of a molecule[221]. The V_0 term is a constant that has no conformational dependence and simply establishes the zero energy at the preferred conformation. The V_1 term has a maximum at 0° (*syn*) and a minimum at 180° (*anti*). It takes energy components of steric and electrostatic interactions into account. V_1 is positive for steric and electrostatic repulsions between the substituents on adjacent carbon atoms. Bond-bending strain of the sort described by Wiberg[222] would also presumably exhibit this periodicity, and contribute to V_1 with a negative sign, since the bending strain would be at a minimum for a dihedral angle of 0° and at a maximum for a dihedral angle of 180°. Any preference for *anti*- rather than *syn* periplanar hyperconjugation would also contribute to the V_1 term.

The V_2 term can be associated with hyperconjugation between the C-X and C-Y bonds. Hyperconjugation is at a maximum at 0° and 180°, where the C-X and C-Y

[220] For a discussion of negative hyperconjugation see: Schleyer P. v. R. and Kos A. J., *Tetraherdon*, **1983**, *39*, 1141.
[221] Allinger N. L., Hindman D., Hönig H., *J. Chem. Soc*., **1977**, 3282.
[222] Wiberg K. B., Murcko M. A., Laidig K. E., and MacDougall, J. Phys. Chem., **1990**, *94*, 6956.

bonds are periplanar, and at a minimum for 90° and 270° where these bonds are orthogonal. The sign of V_2 depends on whether the bond to the substituent, Y, at C-2 is a better or a worse hyperconjugative donor than the C-H or other bonds on this carbon. Positive values of V_2 indicate that C-Y is a weaker donor than C-H, hence conformers with 90° and 270° X-C-C-Y dihedral angles are preferred. Negative values, on the other hand, indicate that C-Y is a stronger electron donor than C-H, or the other bond on this carbon, hence conformers with 0° and 180° X-C-C-Y dihedral angles are preferred.

The V_3 term is positive, since it describes eclipsing interactions. It has its maxima at X-C-C-Y dihedral angles of 0°**,** 120° and 240° and its minima at 60°, 180° and 300°.

CF_3 and the F (X) as electronegative groups, have almost the same behavior. Apeloig Y.[223] found Molecular orbital *ab initio* calculations proving that the small changes in hydrocarbon acidities or in the rates of nucleophilic substitution reactions, which are found when a β-F is substituted by a β-CF_3 group, *do not* reflect absence of fluorine hyperconjugation, but result from the stronger inductive effect of the CF_3 group relative to F, which fully compensates for it's relatively poorer hyperconjugation.

Evidence for the importance of hyperconjugative electron donation into C-F (or C-CF_3) σ*-orbitals in neutral fluorocarbons come from a variety of calculations and experiments[224]. Therefore, if the hyperconjugative explanation of the *gauche* effect is correct, the preferred conformations of 2-substituted-1-fluoroethanes are used to establish the electron donating ability of the bond to the substituents at C-2, relative to the C-H bonds at this carbon. For example, since 1-fluoropropane is known to prefer a *gauche* conformation, the hyperconjugative explanation of the *gauche* effect implies that the C2-H σ-bonds donates more strongly than the C2-C3 σ-bond into the C1-F σ*-orbital.

The energies and geometries of a series of 2-substituted-1-fluoroethanes[225] computed at the MP2/6.311++G** (6D)//MP2/6.31+G* level of theory for both the maxima and minima of the rotation about the C-C bond. The results do not support the predictions of a hyperconjugative model, that both 1,2-difluoroethane and 1-chloro-2-fluoroethane would prefer a *gauche* conformation, and 1-fluoro-2-silylethane would strongly prefer an *anti* conformation. The existence of competing electrostatic

[223] Apeloig Y., *J. Chem. Soc. Chem. Comm*., **1981**, 396.
[224] Borden W.T., *Chem. Commun*., **1998**, 1919.

interactions between the fluorine and the substituents at C-2 was indicated by the detailed geometries of the *gauche* conformers and by the calculated sensitivity of the *gauche-anti* energy differences in the presence of a polar solvent. However, analyses of the torsional potential energies were wholly consistent with the contribution of hyperconjugative electron donation into the C-F σ*-orbital, leading to the conformational preferences of these 1-fluoroethanes. Fourier analyses also showed that hyperconjugation contributes to the small variations in C-C and C-F bond lengths and in fluorine atomic charges that were computed. The torsional potential energies, variations in geometry and atomic charge, and sensitivity to solvent are all in accord with the expected ranking of hyperconjugative electron donating ability of bonds to carbon, C-Si > C-H> C-C > C-Cl> C-F.[225]

Fughs et al.[226] have pointed out that hyperconjugation should influence bond lengths and charge densities. The better the donation of the σ-bond at C2 into the C-F σ*-orbital, the shorter the bond between C1 and C2. This implies a decrease in bond order of the C-F and the σ-bond at C2. An increase of the negative charge on the fluorine atoms should also be observed as a result of negative hyperconjugation.

Negative (Anionic) Hyperconjugation

Hyperconjugation was introduced by Mulliken to describe the "conjugation" of CH_3 with other groups containing double or triple bonds.[227] Hyperconjugation involves the interaction of orbitals of π symmetry (antisymmetric with regard to a local symmetry plane)[228] present both in unsaturated and in saturated groups. CH_3, CH_2 and CF_3, although considered σ systems, possess orbitals of π symmetry[229], which can interact with p-orbitals on adjacent atoms.

Confusion in nomenclature has arisen because organic chemists generally misuse the designations "σ" and "π" to imply single and multiple bond systems. These Greek letters should be employed in their original theoretical meaning to designate orbitals which are symmetric, σ, or antisymmetric, π, with regard to a local symmetry plane.

[225] Rablen P. R., Hoffmann R. W., Hrovat D. A. and Borden W. T., *J. Chem. Soc., Perkin Trans. 2*, **1999**, 1719.
[226] Senderowictz H., Goldender L. and Fuchs B., *Tetrahedron*, **1994**, *50*, 9707.
[227] Mulliken R. S., *J. Chem Phys*., **1933**, *1*, 492.
[228] Flemming I., *Frontier Orbitals and Organic Chemical Reactions*, Wiley NY, **1976**, 80-85.
[229] Jorgensen W. L. and Salem L., *The Organic Chemists' Book of Orbitals*, Academic Press NY, **1973**.

The term of "σ-π conjugation" is incorrect, since orbitals of different symmetry can't interact directly. "Hyperconjugation" should be used because it points to the same phenomenon, is more precise, and has historical precedence.

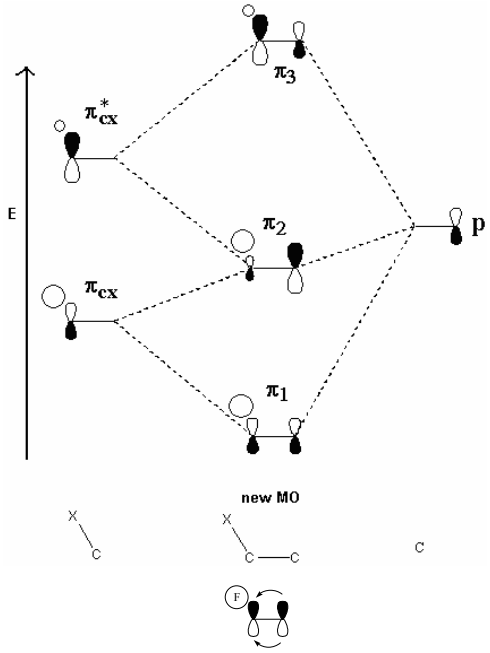

Interaction of a p-orbital (anion lone pair) with the vicinal bonding orbital (π_{cx}) and antibonding orbitals (π_{cx}^*) to form three new π molecular orbitals (center)

Scheme 4.4

Scheme 4.4 illustrates the interaction of a p-orbital with C-X bonding (π_{cx}) and antibonding orbitals (π_{cx}^*). Three new molecular orbitals (π_1, π_2 and π_3, center) are created. If the original p orbital is vacant, as in a carbocation, only π_1 will be occupied and a lowering in energy results. The concept of negative hyperconjugation, discussed in terms of "no bond resonance", was first introduced by Roberts in 1950 to help explain the electrical effects of the trifluoromethyl group.[230] Representations like **Scheme 4.3** was used then. The equivalent MO formulation (**Scheme 4.4**) involves interaction of the filled p-orbital of the anion lone pair with the filled π_{cx} and the vacant π_{cx}^* orbital. Thus, both π_1 and π_2 are now occupied, and the net effect, stabilizing or destabilizing, depends on the degree to which the π_{cx}^* orbital is involved When X is an electronegative element or group, like fluorine or a CF_3 group, this involvement is substantial and considerable stabilization is expected.[231] When X is H, the $\pi_{CH}^* \rightarrow$p interaction is weak and the destabilizing four electron $\pi_{CH} \rightarrow$p interaction may dominate. Thus, the ethyl anion is less stable than the methyl anion, but when

[230] Roberts J. D., Webb R. L. and McElhill E. A., *J. Am. Chem. Soc.*, **1950**, *72*, 408.
[231] David S., Eisenstein O., Hehre W. J., Salem L. and Hoffman R., *J. Am. Chem. Soc*., **1973**, *95*, 3806.

more electronegative atoms are involved, methyl groups can stabilize anions hyperconjugatively. [232]

Both **Scheme 4.3** and the MO representation (**Scheme 4.4**) imply a torsional angle, ω, dependence with the carbanion orbital. Hyperconjugation of the C-X bond should be at a maximum when $\omega = 0°$ or 180° and fall to zero when $\omega = 90°$ and 270°. Geminal hyperconjugation of the CH bonds, e.g. within a CH_2F group, are minor by comparison.

Negative hyperconjugation is important in neutral systems as well, like the anomeric effect. Negative (anionic) hyperconjugation and the anomeric effect are the same phenomena from a qualitative molecular orbital viewpoint. Both are well established, important, and not controversial.

Hyperconjugative stabilization is responsible for the staggered conformation of ethane[233]

Most molecules rotate internally around one or more of their bonds so that during a 360° rotation the molecule will change between stable and less stable conformations. Ethane is the age-old textbook example of a molecule exhibiting such behavior. During a full rotation of the methyl groups around the central C-C bond the molecule alternates three times between the unstable eclipsed and the stable staggered conformation. This structural preference is mostly attributed to steric effects. This is experienced when the electrons in the two C-H bonds draw closer to each other they undergo steric repulsion destabilizing the eclipsed conformation. Stabilization of the staggered structure through rotation-induced weakening of the central C-C bond and hyperconjugation is considered to be involved, but evaluation of the contribution of these effects to ethane's internal rotational barrier and conformational preference remains difficult.

Both hyperconjugation and steric repulsion are quantum mechanical effects which arise from orbital overlap. The former involves electron transfer from an occupied to an unoccupied orbital, leading to the delocalization of charge (**Fig 4.5**). The latter

[232] Chandrasekhar J., Andrade J. G. and Schleyer P. v. R., *J. Am. Chem. Soc*., **1981**, *103*, 5609.
[233] V. Pophristic, L. Goodman, *Nature*, **2001**, *411*, 565S.

involve the Pauli exclusion principal, which states that opposite spinning pairs of electrons cannot occupy the same spatial region.

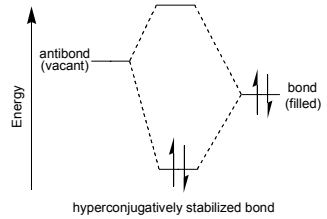

Figure 4.5

In contrast to these two orbital interactions, electrostatic or Coulomb interactions, involves classic 1/R repulsion between charges.

First electrostatic and Pauli exchange interactions are taken together as the steric factor and tested for their involvement in the conformation of ethane as they represent all-electron phenomena.

Pauli exchange interactions left out of the conformational optimization calculation of ethane proved that it played no part in the formation of the staggered conformation.

Coulomb interactions was evaluated on ethane with a rigid C-C bond rotation and where the bond is flexible. It was found that central C-C bond lengthening eliminates coulomb interactions and does not explain the staggered structural preference of this molecule.

Hyperconjugative interactions, inherently stabilizing (**Fig. 4.5**), proved to be the only factor determining the stability of the staggered conformation. Geminal hyperconjugation, within a single methyl group, was also found to have no influence on the conformational preference.

Only π-symmetric orbitals, between the two vicinal methyl groups have the necessary overlap and symmetry required for vicinal hyperconjugation. When vicinal hyperconjugative interactions were deleted from the calculation ethane remained in the eclipsed conformation. The effect of 'no vicinal hyperconjugation' was obtained by deleting the antibonds in the bonding orbital description of ethane (thus no donation into the antibonds possible), and then running the optimization with both HF/6-311G(3*df*,2*p*) and MP2/6-311G(3*df*,2*p*) methods. When it was included in the calculation, again the staggered conformation is preferred. Vicinal hyperconjugation is the only factor found to determine the staggered conformation of ethane.

Natural bond orbitals (NBO) provide the means to analyze hyperconjugative interactions in much more detail than is possible with molecular orbitals.
Molecular orbitals, are much more complex, thus making individual bond population difficult to determine.
NBO's are defined by nearly doubly occupied, localized bonding orbitals (bonds), and nearly vacant localized antibonding orbitals (antibonds). An individual hyperconjugative interaction is expressed as a charge (electron) transfer between selected bonds and antibonds, allowing specific hyperconjugative interactions that influence structural preference to be pinpointed. This can be achieved by analyzing the occupation of the selected bonds and antibonds between the different conformations.

Natural bond orbitals were not used to provide evidence for hyperconjugative preferential stabilization of the staggered conformer. Rather, their value was proved by providing insight into which charge transfer interactions are the controlling ones by partitioning the full hyperconjugative interaction into its vicinal and geminal component parts.
The important conclusion obtained from these hyperconjugation and repulsion deletion calculations is that ethane adopts the eclipsed conformation when the vicinal charge transfers are absent, and that no inversion of the staggered structure to the eclipsed occurs on removal of Coulomb and exchange interactions.
Also, that vicinal charge transfer interactions are the ones that keep ethane in the staggered conformation. The conclusion that hyperconjugation, and not steric interactions, ultimately determines ethane's conformation are expected to have an important role in analyzing such diverse molecular phenomena as polymer rheology (study of the deformation and flow of matter under the influence of an applied stress), protein folding and general chemistry at large.

Fluorine-oxygen interaction.

Perfluorinated liquids are known to dissolve significant quantities of molecular oxygen, *ca*. 30 to 60 cm^3 of gaseous oxygen per 100 cm^3 of liquid fluorocarbon at 25˚C under normal pressure. This solubility is 3-10 times as much as in the respective hydrocarbons or water respectively.

This unique property of fluorocarbons suggested application in artificial blood and liquid breathing. A ^{19}F NMR investigation into a possible mechanism for this increased solubility was undertaken.[234]

An frequency-dependance analysis of ^{19}F nuclear spin relaxation times afforded dynamic parameters for the oxygen-fluorocarbon interaction. Relaxation time was interpreted by the dipolar electron spin-nuclear spin interactions, where a short-lived solvated complex was suggested. The F-O nucleus-electron distances fall in the range of 3.6-3.9Å, which is close to the sum of the v.d Waals radii, 3.6 Å.

The same v.d Waals overlap between F and carbonyl and ester oxygen is present for MTPA in the crystal structure and in the geometry optimized esters of MTPA and CFTA. Thus, fluorine-oxygen interaction may contribute to the stability of the *syn* and *anti* isomers in these esters. This interaction may be negligible in comparison to vicinal hyperconjugative stabilization, but contributing none the less.

[234] Endo K., Yamamoto K., Kado R., *Analytical Sciences,* **1993**, *9*, 47.

Molecular Modeling

Introduction

Over the span of two decades, molecular modeling has emerged as a viable and powerful approach to chemistry. Molecular mechanics calculations coupled with computer graphics are now widely used in place of tactile models to visualize molecular shape and quantify steric demands. Quantum chemical calculations, once a mere novelty, continue to play an ever increasing role in chemical research and teaching. They offer the real promise of being able to complement experiment as a means to uncover and explore new chemistry. There are fundamental reasons behind the increased use of calculations, in particular quantum chemical calculations, among chemists. Most important, the theories underlying calculations have now evolved to a stage where a variety of important quantities, among them molecular equilibrium geometry and reaction energetics, may be obtained with sufficient accuracy to actually be of use. Closely related are the spectacular advances in computer hardware over the past decade. Taken together, this means that good theories may now be routinely applied to real systems. Also, computer software has now reached a point where it can be easily used by chemists with little if any special training. Finally, molecular modeling has become a legitimate and indispensable part of the core chemistry curriculum. Just like NMR spectroscopy several decades ago, this will facilitate if not guarantee its widespread use among future generations of chemists.

Nowadays user friendly graphical interfaces of most software packages enables one, even with limited or no theoretical background, to effectively run quite sophisticated calculations.[235,236,237] Theories underlying calculations have also presently evolved to a stage where a variety of important quantities, including molecular equilibrium geometries and reaction energies, may be calculated with sufficient accuracy and computer cost to be used with confidence to predict and support real experimental investigations.[235] The principal aim of this brief introductory to molecular modeling is to familiarize the reader with the computational concepts used and discussed in

[235] Hehre, W.J., Yu, J., Klunzinger, P.E., Lou, L., *"A Brief Guide to Molecular Mechanics and Quantum Chemical Calculations", Wavefunction, Inc.*, Irvine, California, **1998**.
[236] Jensen, F., *"Introduction to Computational Chemistry"*, John Wiley & Sons, New York, **1999**.
[237] Wilson, S., *"Chemistry by Computer"*, Plenum Press, New York, **1986**.

Chapters 4 and 5. Appendix 5.2 should also be consulted to inform the reader on the use of Natural Bond Orbital (NBO) calculations.

Theoretical Models

The most commonly used theoretical models may be divided into five distinct groups, viz. Molecular Mechanics (MM), Semi-Empirical (SE) methods, Hartree-Fock (HF) models, Møller-Plesset (MP) models and Density Functional Theory (DFT) models. For an in depth discussion of the theoretical background for all these models consult the relevant monographs by Hehre[235] and Jensen.[236]

There are significant obstacles in the way of continued progress for chemists using molecular modelling in the research laboratory. For one, the chemist is confronted with many choices to make, few guidelines on which to base these choices. The fundamental problem is, of course, that the mathematical equations which arise from the application of quantum mechanics to chemistry and which ultimately govern molecular structure and properties cannot be solved. Approximations need to be made in order to realize equations that can actually be solved. "Severe" approximations may lead to methods which can be widely applied but may not yield accurate information. Less severe approximations may lead to methods which are more accurate but which are too costly to be routinely applied. In short, no one method of calculation is likely to be ideal for all applications, and the ultimate choice of specific methods rests on a balance between accuracy and cost.

Molecular Mechanic methods describes molecules in terms of connected atoms and molecular geometry in terms of distortion from ideal bond distances, bond angles and dihedral angles. Due to no explicit consideration of electrons in MM methods, MM calculations are not suitable for accurate calculation of reaction and activation energies. Semi-Empirical, Hartree-Fock and Møller-Plesset models are all based on quantum mechanics. Semi-Empirical methods, which is not cost intensive (*i.e.* computational time) provide relatively inaccurate results, due to significant approximations, because core electrons are not taken into account. Hartree-Fock models are much more costly and accurate, but due to the overestimation of electron-electron repulsion energies for these models, estimation of total energies are usually

too high.[235,236] This phenomenon results from the fact that motions of individual electrons are treated independent from each other. Electron correlation accounts for coupling of electron motions and leads to lessening of electron-electron energy and consequently lowering of the overall total energy. Møller-Plesset models, *e.g.* MP2, which are significantly more time intensive than conventional Hartree-Fock models, accounts for electron correlation and highly accurate estimations of reaction and activation energies. For this reason, MP2 results are commonly used as reference to other theoretical models when experimental results are absent. Density Functional Theory (DFT) models provide an alternative approach to the treatment of correlation in many electron systems with significantly lower computational cost compared to MP2 and yielding results with comparable accuracy to MP2.

Gaussian Basis Sets

Basis sets for use in practical Hartree-Fock, density functional, Møller-Plesset and configuration interaction calculations make use of Gaussian-type functions. Gaussian functions are closely related to exponential functions, which are of the form of exact solutions to the one-electron hydrogen atom, and comprise a polynomial in the Cartesian coordinates (x, y, z) followed by an exponential in r^2. Several series of Gaussian basis sets now have received widespread use and are thoroughly documented. Except for STO-3G and 3-21G, any of these basis sets can be supplemented with additional polarization functions and/or with diffuse functions. It should be noted that minimal (STO-3G) and split-valence (3-21G) basis sets, which lack polarization functions, are unsuitable for use with correlated models, in particular density functional, configuration interaction and Møller-Plesset models.

Among the simplest split-valence basis sets are 3-21G and 6-31G. Each core atomic orbital in the 3-21G basis set is expanded in terms of three Gaussians, while basis functions representing inner and outer components of valence atomic orbitals are expanded in terms of two and one Gaussians, respectively. 6-31G basis sets are similarly constructed, with core orbitals represented in terms of six Gaussians and valence orbitals split into three and one Gaussian components. Additional valence-shell splitting should lead to even greater flexibility. 6-311G basis sets split the valence functions into three parts instead of two, these being written in terms of three, one and one Gaussians, respectively.

6-31G*, 6-31G, 6-311G* and 6-311G** Polarization Basis Sets**

The shortcoming of a minimal (or split-valence) basis set functions is that they are centered only on atoms and may be addressed by providing d-type functions on main-group elements where the valence orbitals are of s and p type, and optionally on p-type functions on hydrogen where the valence orbital is of s type. This allows displacement of electron distributions away from the nuclear positions. This can be thought about either in terms of hybrid orbitals, e.g., pd and sp hybrids, or alternatively in terms of a Taylor series expansion of a function (d functions are the first derivatives of p functions, p functions are the first derivatives of s functions). While the first way of thinking is quite familiar to chemists (Pauling hybrids), the second offers the advantage of knowing what steps might be taken next to effect further improvement, like adding second, third, etc. derivatives. Among the simplest polarization basis sets are 6-31G* and 6-311G*, constructed from 6-31G and 6-311G, respectively, by adding a set of d-type polarization functions written in terms of a single Gaussian for each heavy (non-hydrogen) atom. A set of six second-order Gaussians is added in the case of 6-31G* while a set of five pure d-type Gaussians is added in the case of 6-311G*. Gaussian exponents for polarization functions have been chosen to give the lowest energies for representative molecules. Polarization of the s orbitals on hydrogen atoms is necessary for an accurate description of the bonding in many systems, particularly those in which hydrogen is a bridging atom.

The 6-31G** basis set is identical to 6-31G*, except that it provides p-type polarization functions for hydrogen. Similarly, 6-311G** is identical to 6-311G* except for its description of hydrogen.

Computational Methods

Initial geometry searches and optimizations were performed using semi-empirical methods with the PM3 Hamiltonian. Selected geometries, frequencies, molecular orbital, Mulliken populations and NBO calculations were performed using density functional theory, DFT/pBP/DN**, perturbative Becke-Perdew (pBP) Density

Functional Theory model (using the DN** full polarization basis set) and three parameter hybrid method (B3) employing the correlation functional of Lee, Yang and Parr (LYP) with the standard 6.31G** basis set which requests that a set of p function for each hydrogen atom aside from the d function on the heavy ones. In selected cases, these DFT results were verified with Hartree–Fock (HF) using the 6.31G** basis set.

Software

All computational results in this study were calculated by using two PC Spartan Pro™ (Version 1.0.5) and Titan™ (Version 1.0.5) program packages as purchased from Wavefunction Inc., 18401 Von Karman Ave., Suite 370, Irvine, CA 92612. No changes were made in the default settings for the respective theoretical models. During the visit to Japan the standard Gaussian 98'™ program was used, also with default settings.

Hardware

All calculations were performed on a desktop computer, viz. a Pentium IV, 1.8 GHz, 512 MB RAM. Typical computational times for a geometry optimization, with consecutive vibrational frequency and NBO calculations, was in the order of 14 days for the largest models, while the smallest models required computational times of less than 3 days at the B3LYP/6.31G**level of theory. The Gaussian software was operated on a Silicon Graphics™ multiple (8) processor workstation with a Linux™ operating system, utilizing not more than 2 processors at a time.

Equilibrium Geometry Optimizations

Calculation of global minima equilibrium geometries for all models described in Chapters 4 and 5 involved the following procedure: (i) calculation of the lowest energy conformers, via a conformer distribution calculation at the SE/PM3 level of theory, (where necessary), followed by (ii) geometry optimization at the B3LYP/6.31G** and Unrestricted/Restricted B3LYP/6.311G (Gaussian 98') level of theory unless otherwise stated.

Main Energy conversion factors

1 unit =	hartree	kJ mol^{-1}	kcal mol^{-1}	eV	cm^{-1}
hartree	1	2625.50	627.51	27.212	2.1947×10^{5}
kJ mol^{-1}	3.8088×10^{-4}	1	0.23901	1.0364×10^{-2}	83.593
kcal mol^{-1}	1.5936×10^{-3}	4.1840	1	4.3363×10^{-2}	349.75
eV	3.6749×10^{-2}	96.485	23.061	1	8065.5
cm^{-1}	4.5563×10^{-6}	1.1963×10^{-2}	2.8591×10^{-3}	1.2398×10^{-4}	1

Results & Discussion

Conformational and electronic interaction studies of the Mosher acid as an introduction to analyze the behavior of the epicatechin Mosher ester derivatives.

This section provides a brief introductory investigation of the experimental and theoretical conformational preference of the Mosher ester.

A Semi-Empirical (SE) introductory conformer search on the (*S*)-Mosher acid was performed. **Fig. 4.3** graphs the *syn* periplanar (*sp*) alignments with a ≤ ±60° dihedral angle with the carbonyl bond and the *anti* periplanar (*ap*) alignments with a ≥ ±90° dihedral angle. A *sp* alignment is defined as the ones with a dihedral angle ≤ ±60° with the carbonyl plane where the shielding of the phenyl group is still present on the same side of this plane (**Scheme 4.1**)[205].

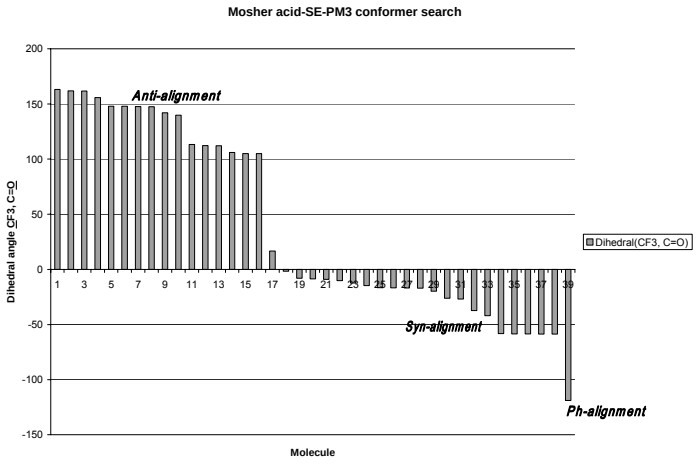

Figure 4.3. (C=O//CF_3 dihedral angle on Y-axis and molecule number on X-axis)

This calculated (SE-PM3) *syn/anti* isomer ratio of the acid is ca. 22/16 (**Fig. 4.3**). Further DFT (pBP/DN**) equilibrium geometry optimizations of the lowest energy *syn* and *anti* conformers selected from the SE conformer search show the *syn*-conformer of the acid to be 1.46 kcal/mol lower in energy than the *anti* conformer which is in line with experimental ^{1}H NMR shielding reported in literature for the Mosher phenyl ring[203]. The semi empirical PM3 optimized energy profile (**Fig. 4.4**)

shows the *anti* conformer to be the energetically preferred conformer[203], as opposed to that of the DFT (pBP/DN**) calculations, which show the *syn* conformer to be favored. In this semi empirical energy profile calculation (**Fig. 4.4**), the torsional angle of the α-C-C bond was incrementally rotated to reflect the potential energy surface of the acid with rotation around this bond.

The conformer where the Ph-group is aligned with the carbonyl oxygen plays a minor role, as is highlighted by a semi-empirical (SE-PM3) conformer search of the Mosher acid *in vacu* (**Fig. 4.3**). It is highlighted that the dihedral angle of the CF_3 group in relation to the carbonyl bond need not be exactly zero for effective preferential shielding of either of the carbinol substituents by the Ph-ring. The α-CF_3-carbonyl conformation need not be perfectly eclipsed, but can be substantially displaced from co-planarity. Hence, lowest energy conformations in which the dihedral angle varies between 60° to either side of the carbonyl plane is still sufficient for this molecule to still act as a chiral derivatizing reagent, meaning the Ph-ring stays on the same side of the vertical carbonyl plane, shielding the nearby carbinol substituents[205].

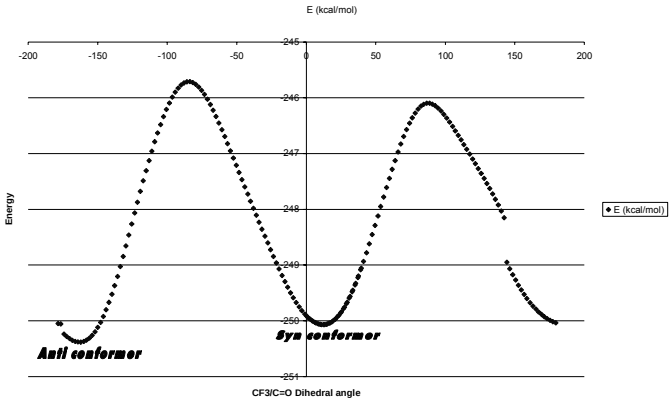

Figure 4.4 (Potential Energy surface of MTPA with rotation around αC-C bond)

SE methods are inadequate to describe the energy difference of the two rotational conformers. DFT methods, with a larger basis set, which take electron correlations into account, gives a much different picture which in turn supports the experimental IR band profile analysis and the observed NMR shielding by the Mosher phenyl ring. The SE energy profile of the acid still confirms the *syn* and *anti* conformations as the two local minima on the global energy surface of the molecule.

Thus, such IR and computational data show a predominance of the *syn*-isomer, which might be rationalized by several possible dipolar interactions stabilizing this isomer to a greater extent than the *anti*-isomer (**Fig. 4.5.1, 4.5.2**). These calculated interatomic distances are compared to the sum of their Van der Waals radii[257] in both of these major conformers, where a negative value (Δl) indicates overlap of the respective nucleic radii[238] (i.e. likely electronic interactions or contacts) (**Table 4.1, Fig. 4.6.1, 4.6.2**).

These interactions are $O^{\delta-}_{(CO)}\cdots F^{\delta-}_{(CF3)}$, $O^{\delta-}_{(CO)}\cdots C^{\delta+}_{(CF3)}$, $C^{\delta-}_{(CO)}\cdots F^{\delta-}_{(CF3)}$, $O^{\delta-}_{(OH)}\cdots C^{\delta+}_{(CH3)}$ and $O^{\delta-}_{(OH)}\cdots H^{\delta+}_{(CH3)}$ (H-bond) for the *syn*-isomer as opposed to the $O^{\delta-}_{(CO)}\cdots C^{\delta+}_{(CH3)}$, $O^{\delta-}_{(CO)}\cdots H^{\delta+}_{(CH3)}$ (H-bond), $C^{\delta+}_{(CO)}\cdots O^{\delta-}_{(OMe)}$ and $O^{\delta-}_{(OH)}\cdots C^{\delta+}_{(CF3)}$ in the *anti*-isomer.

The first three interactions (**Table 4.1**), between the carbonyl and the adjacent aligned CF_3 or OMe group, are the ones involved in the respective *sp* and *ap* conformations.

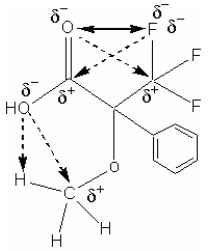

Figure 4.5.1 (*syn*)

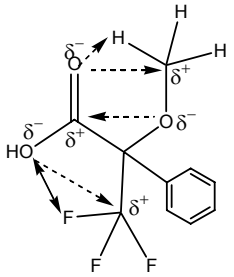

Figure 4.5.2 (*anti*)

Table 4.1

***Syn*-alignment**	Δl (Amstrong)	***Anti*-alignment**	Δl (Amstrong)
$O^{\delta-}_{(CO)}\cdots F^{\delta-}_{(CF3)}$	0.182	$O^{\delta-}_{(CO)}\cdots C^{\delta+}_{(CH3)}$	-0.215
$O^{\delta-}_{(CO)}\cdots C^{\delta+}_{(CF3)}$	-0.204	$O^{\delta-}_{(CO)}\cdots H^{\delta+}_{(CH3)}$	0.479
$C^{\delta-}_{(CO)}\cdots F^{\delta-}_{(CF3)}$	0.186	$C^{\delta+}_{(CO)}\cdots O^{\delta-}_{(OMe)}$	-0.651
$O^{\delta-}_{(OH)}\cdots C^{\delta+}_{(CH3)}$	-0.02	$O^{\delta-}_{(OH)}\cdots C^{\delta+}_{(CF3)}$	-0.275
$O^{\delta-}_{(OH)}\cdots H^{\delta+}_{(CH3)}$	-0.142	$O^{\delta-}_{(OH)}\cdots F^{\delta+}_{(CF3)}$	-0.034

[238] Olivato P. R., Hui M. L. T., Rodrigues A. Filho R. R., Rittner R., Zukerman-Schpector J., Distefano G., Colle M. D., *Journal of Molecular Structure*, **2003**, *654*, 259-271.

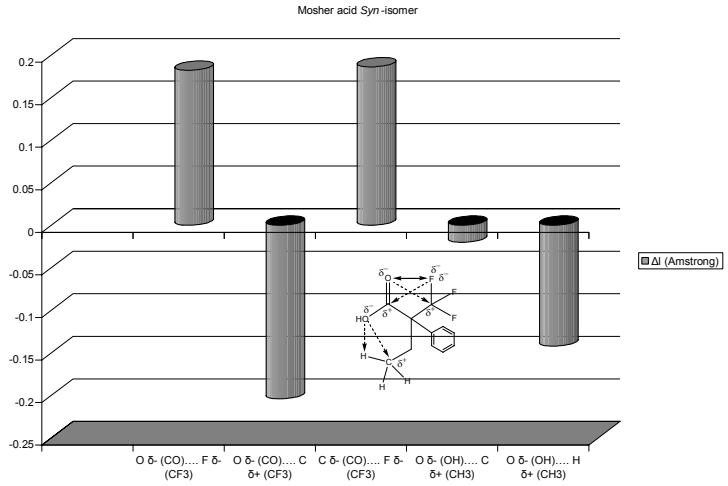

Figure 4.6.1 (Van der Waals interactions (negative values) stabilizing the *syn* conformer)

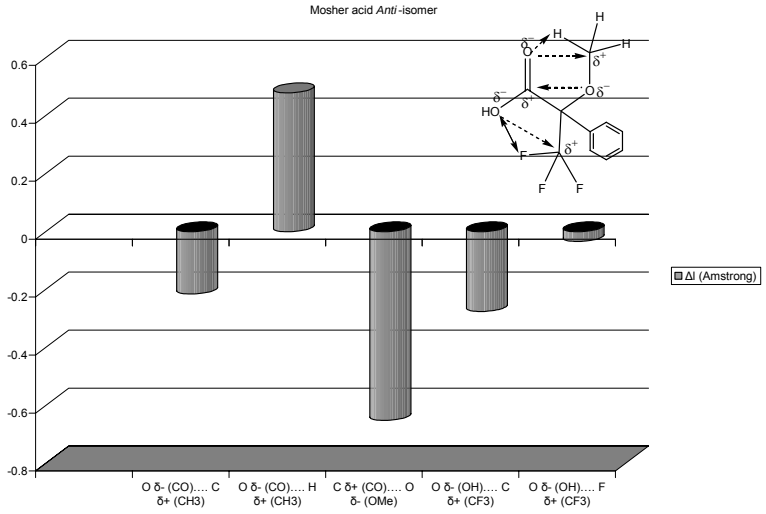

Figure 4.6.2 (Van der Waals interactions (negative values) stabilizing the *anti* conformer)

The DFT (pBP/DN**) carbonyl stretching frequencies **Fig. 4.7** of the three main alignments, obtained from the semi-empirical conformer search, of the Mosher acid are calculated. The relative lower frequency of the carbonyl group in the *sp*-conformer, indicates a lower bond order present for the C=O bond of this conformer. Band profile analysis (deconvolution) of the experimental broadened IR carbonyl stretching frequency confirms the dominant *sp* conformer (Band A, major band) to be the preferred conformer (**Fig. 4.8**). The higher IR carbonyl frequency of the *anti* conformer (Band B) normally plays a much lesser role as is well demonstrated in

literature[239] and is successfully reproduced here with the DFT calculated frequencies for the acid (**Fig 4.7**). It is reported that in some secondary alcohols the preference for the *sp* rotamer is nullified by steric hindrance due to bulky substituents on the carbinol carbon[239]. The B-ring of the flavan-3-ol structure can also have a large enough influence to render the preference for the *sp* conformation obsolete in these flavonoid structures.

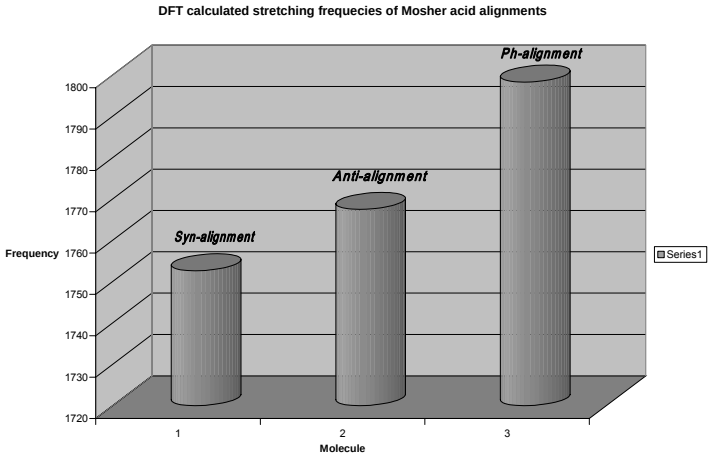

Figure 4.7 (DFT (pBP/DN**) calculated C=O stretching frequencies for MTPA)

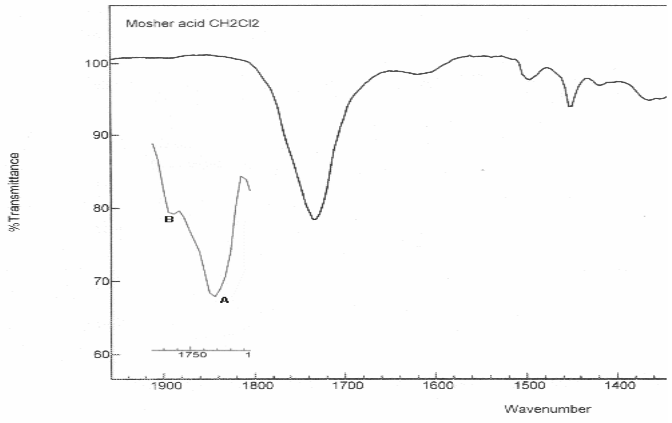

Figure 4.8 (Deconvoluted MTPA C=O band displaying the major A (*syn*) and minor B (*anti*) conformers, CH_2Cl_2)

Literature[240] cautions that although infrared spectroscopy at a single temperature with various solvents can still be an important tool for conformational analysis, it should

[239] Merckx E. M., Vanhoeck L., Lepoivre J. A., Alderwiereldt F. C., *Spectroscopy International J*., **1983**, 30-42.
[240] Freitas M.P, Tormena C.F, Rittner R., Abraham R.J, *Spectrochimica Acta A*, 2003, 59, 1783.

not be used for accurate quantification of the conformational preferences of a molecule if the molar absorbsion coefficient of each conformer is not known or amenable to experimental determination, since it might yield unreliable results. It is suggested to work at variable temperatures, where the principal use of absorbance data would be to find ΔH values from the van't Hoff equation.

Thus the IR data (**Fig 4.8**) of the Mosher acid and its derivatives is presented only as an illustration and confirmation of the preference of the *syn* isomer in solution.

The epicatechin-Mosher ester derivative

Solid state crystal structure of 3',4',5,7-Tetramethoxy-epicatechin-(3-O)-(*R*)-α-methoxy-α-trifluoromethyl-α-phenylacetate

The optically pure permethylated epicatechin was chosen as model to evaluate the Mosher behavior because its absolute stereochemistry is well established. It also represents a general flavan structure endemic to flavan-3-ol, -4-ol and 3,4-diols, including the contiguous B-ring, which could influence the behavior of the mosher ester conformational equilibrium and could render this ester unreliable as a CDA for flavan-3-ols in particular. The use of the Mosher method to establish absolute stereochemistry in the flavonoid field is rarely employed.

The title compound was synthesized and recrystallized from methanol in the orthorhombic cell symmetry and P2 (1)2(1)2(1) space group (**Fig. 4.9**).

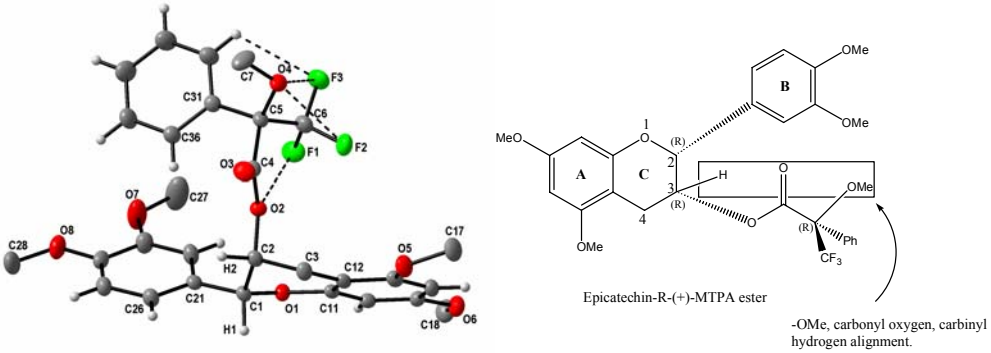

Figure 4.9: Diamond drawing of permethylated (-)-Epicatechin-(*R*)-MTPA; Ellipsoids at 20% probability, Methyl protons omitted; for phenyl rings, first digit (1-3) refers to ring number, second digit (1-6) to atom in ring. Interaction of fluorine atoms ca. 2.5-2.7 Å.

This molecule crystallized as the *in situ* non-favored *ap* alignment for the MTPA ester with the phenyl ring turned towards the epicatechin B-ring, which is certainly unexpected and gave the initial impetus to this conformational investigation. This conformation is not the energetically preferred conformation experimentally in solution, due to the experimental ^{1}H NMR preferential shielding observed[204,205,285], and is probably brought about by crystal packing, intra- and intermolecular contacts alluded to in this crystal. The short contact measured between fluorine and the ester

oxygen should be highlighted. This peculiar overlap of v.d Waals radii[257] (**Fig. 4.5.1**) of these two electronegative atoms is unexpected due to the electronegativity of both atoms. It is also found in all the subsequent geometry optimization calculations on the ester and for both *sp* and *ap* conformers. Displayed below is the intramolecular (**Fig. 4.10**), intermolecular (**Fig. 4.11**) short contacts and the cell packing viewed along one of the axes (**Fig. 4.12**).

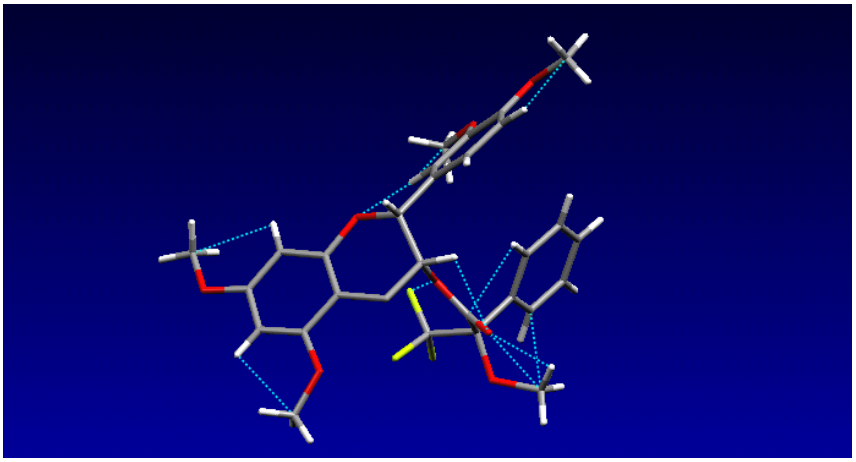

Figure. 4.10. Short intramolecular contacts defined by the software as the sum of their respective v.d. Waals radii minus 0.2Å

Relevant intramolecular contacts obtained from the x-ray data with a v.d. Waals radii overlap greater than 0.2Å, measured 2.668Å between fluorine and the ester oxygen. The distance between the carbonyl oxygen and carbinyl-H measured 2.478Å. The distance between the carbonyl oxygen and a Mosher methoxy proton 2.452Å, and Mosher methoxy carbon is 2.975Å. These atomic interactions contribute to the stabilization of the *ap* alignment of the MTPA ester in the solid state, some of which are found in the DFT/pBP/DN** optimized *ap* geometry (**Fig 4.5.2**).

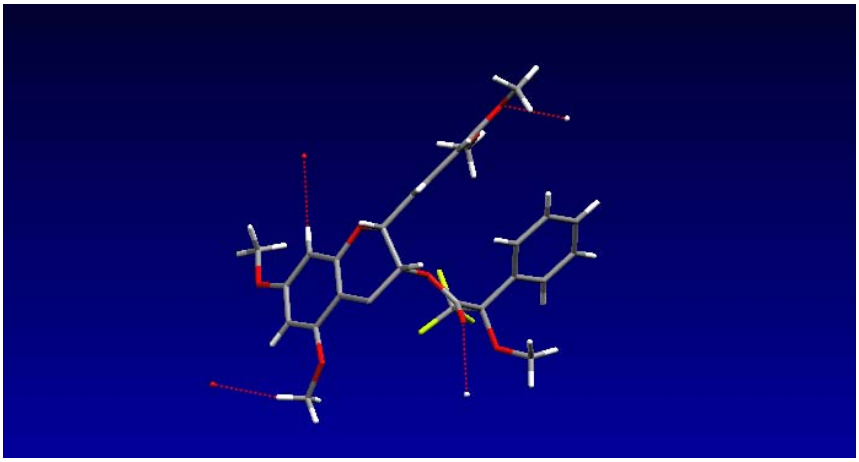

Figure 4.11. Short intermolecular contacts defined by the software as the sum of their respective v.d. Waals radii minus 0.1Å

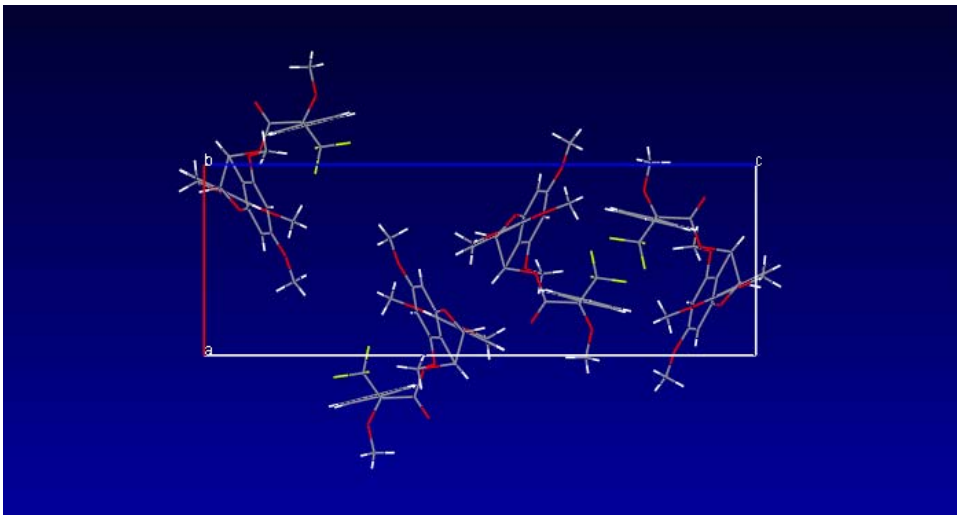

Figure 4.12. Cell packing displaying 4 molecules per cell

The crystal cell packing is illustrated in **Fig. 4.12** which depict the orientation of the four molecules occupying the cell. Among the intermolecular short contacts highlighted that can possibly play a role in the formation of the *anti* alignment in the crystal, is the one between the carbonyl oxygen and 8-H of the A-ring (**Fig.4.11, 4.13**). No apparent parallel π-π stacking is observed here, but a perpendicular (≈104.12°) CH-π interaction (2.98Å)[241] observed between the Mosher phenyl ring and the A-ring of an adjacent molecule, may be a reasonable possibility (**Fig. 4.13a**). *Ab initio* calculations show that this T-shaped (**Fig. 4.13a**) geometry is more stable than the parallel π-π stacking.[242,243,244]

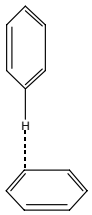

Figure. 4.13a (T-shaped π-π stacking)

[241] Nishio M. and Hirota M., *Tetrahedron*, **1989**, *45*, 7227.
[242] Pawliszyn J., Szecesniak M. M., and Schreiner S., *J. Phys. Chem*., **1984**, *88*, 1726.
[243] Jiang R., Ye W., Woo K., Du J., Che C., But P. P. and Mak T. C. W., *Journal of Molecular Structure*, **2002**, *642*, 77-84.
[244] Hunter C. A. and Sanders J. K. M., *J. Am. Chem. Soc*., **1990**, *112*, 5525-5534.

The π electrons and the C-H act as a soft base and soft acid respectively. The effect of this is observed in the slight shortening of the affected C-H bond, 0.929Å, compared to the other free C-H bonds, 0.930Å. This observed CH-π interaction distance is indeed shorter than the sum of the respective v.d. Waals radii of the atoms involved (2.792 and 2.980Å, Fig. 4.13 b: 1.2Å for H and 1.7Å for the sp^2 carbon).

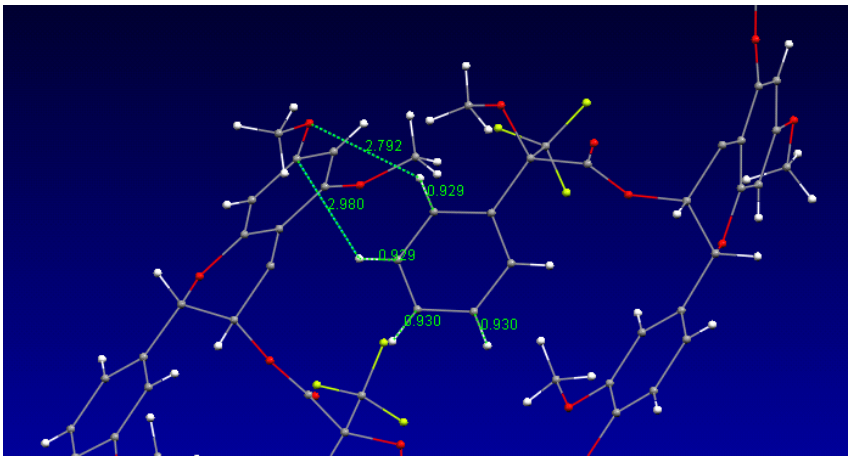

(b)

Figure 4.13 b

NMR and IR spectral aspects of the epicatechin-Mosher ester derivative

Due to the preferred *syn* periplanar (*sp*) alignment of the CF_3 and C=O group of the ester, the C-4 (substituents) or the C-2 and B-ring protons of epicatechin and entepicatechin esters are preferentially shielded as is evident from the comparison of their NMR spectra[203]. These differential and diagnostic chemical shift differences, $\Delta\delta^{SR}$, are conveniently interpreted by considering their respective Newman projections depicted in **Fig.4.14.**

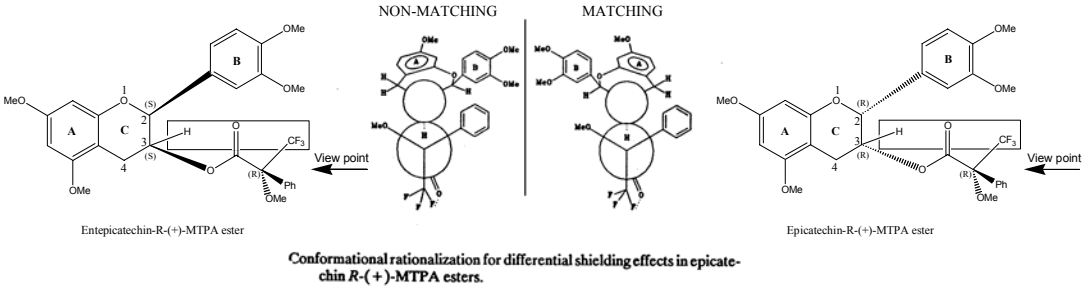

Figure 4.14.

It is evident from **Fig. 4.14** that in the non-matching[245] diastereomers, which are termed the epicatechin 3-(*S*)-esters derived from (*R*)-(+)-MTPA, the MTPA phenyl group would be quasi-eclipsed with the 2-C(C) position and its substituents, such as the B-ring. Hence, protons and substituents attached to 2-C(C) are preferentially anisotropically shielded by the MTPA phenyl group as opposed to the 4-C(C) substituents, such as the A- and (4-Aryl) D-rings. In the matching or 3-*R*-diastereomers the position is reversed since similar alignment of the MTPA moiety places the phenyl group in a quasi-eclipsed position with respect to the 4-C(C) and it's substituents, and these therefore should be preferentially anisotropically shielded as opposed to the 2-C(C) and corresponding substituents. When non-matching diastereomer shifts are subtracted from matching diastereomer shifts results in positive $\Delta\delta^{S-R}$ values for 2-C(C) protons and substituents and negative $\Delta\delta^{S-R}$ values for protons and substituents attached to 4-C(C), as is indeed found to be the case (**Fig.**

[245] Since R,R and S,S or S,R and R,S configuration of the alcohol and the acid, from which the ester is formed, give exactly the same NMR spectra a simple terminology of matching for R,R and S,S or non-matching for R,S and S,R is adopted.

4.15) (**Plate 4.1a, 4.2a**).

Experimentally then, the anisotropic shielding of the two diastereomers and the difference in shielding of protons is expressed as $\Delta\delta^{S-R}$ values. A more positive $\Delta\delta^{S-R}$ value of the protons represents greater shielding observed for the matching diastereomer (**Plate 4.1a, 4.2a**). These $\Delta\delta^{S-R}$ values are similar to the values obtained in literature for the Mosher ester derivatives[266]. The positive and negative values defines the resultant MTPA shielding plane (**Fig. 4.15**), which make the deduction of the absolute stereochemistry of the alcohol possible, because the absolute configuration of the Mosher moiety is known.

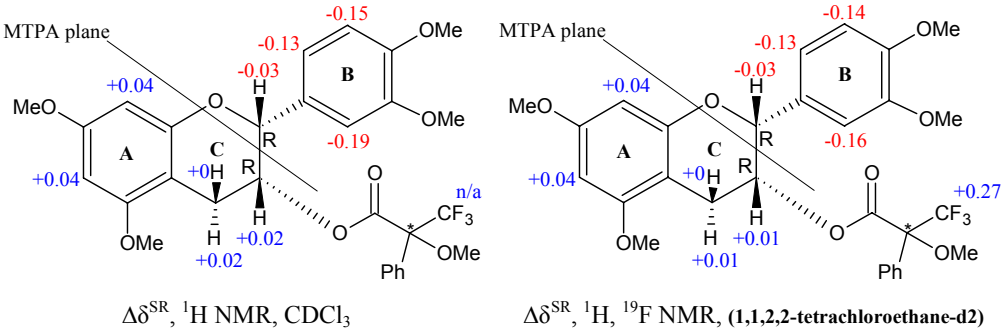

$\Delta\delta^{SR}$, ^{1}H NMR, $CDCl_3$ $\Delta\delta^{SR}$, ^{1}H, ^{19}F NMR, **(1,1,2,2-tetrachloroethane-d2)**

Figure 4.15 (-)-Epicatechin-MTPA $\Delta\delta^{SR}$ NMR values (**Plate 4.1a, 4.2a**)

A SE/PM3 conformer search, aimed at a rough quantification of the *sp* (*syn* periplanar) and *ap* (*anti* periplanar) conformations of (-)-epicatechin-(*R*)-MTPA was performed. On a SE level of theory, where the *sp* conformers are taken as having a dihedral angle between +60° and -60° (vertical axis), the preference of the *sp* conformer is illustrated. (**Fig.4.16**)

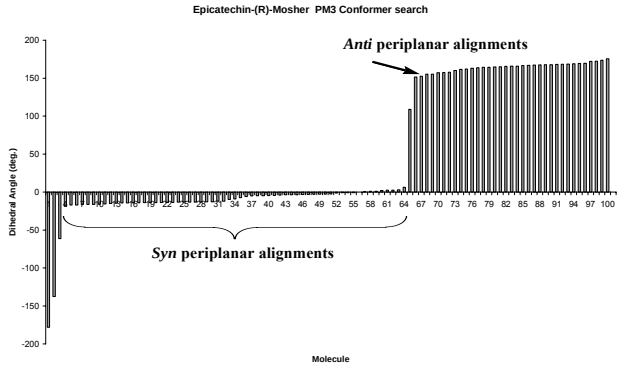

Figure 4.16

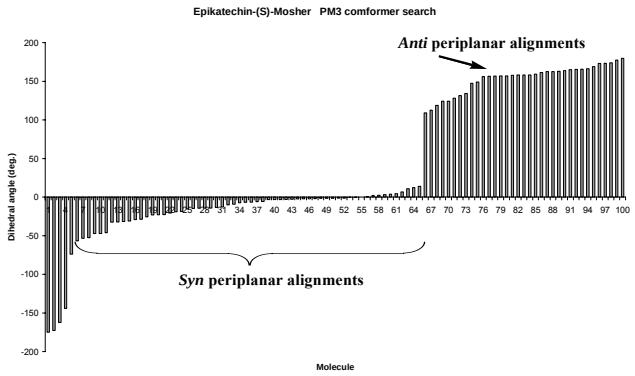

Figure 4.17

The close proximity of the B-ring of the flavonoid skeleton to the phenyl ring of the epicatechin-(*S*)-MTPA ester (**Fig. 4.17**) moiety in the preferred *sp* alignment is likely to have some influence on this crucial alignment and could be true for flavan-3-ols in general. The preferred *sp* alignment of the Mosher-(*S*)-ester (non-matching derivatives) have the aryl ring of the ester facing towards the B-ring of the flavan skeleton. This possible steric influence could render the use of the Mosher ester unreliable for flavan-3-ols. Indeed, a PM3 conformational search indicate that the B-ring have a steric influence, with more *sp* alignments (dihedral angle ≤60°) with the CF_3 skewed from planarity in the (*S*) ester, but that the *sp* alignments are still in majority (**Fig. 4.16, 4.17**). These results suggest the Mosher ester to be applicable in the flavonoid field. These conformational searches for the epicatechin-Mosher esters are extended to those of epicatechin-S-methylmandelate (**Fig 18a**), -O-methylmandelate (**Fig 18b**) and –methylmandelate (**Fig 18c**). The fluorine atoms were also replaced with chlorine (**Fig. 19a**) and bromine (**Fig. 19b**) in an experiment to estimate the role of the fluorine atom played in the preferred *sp* alignment.

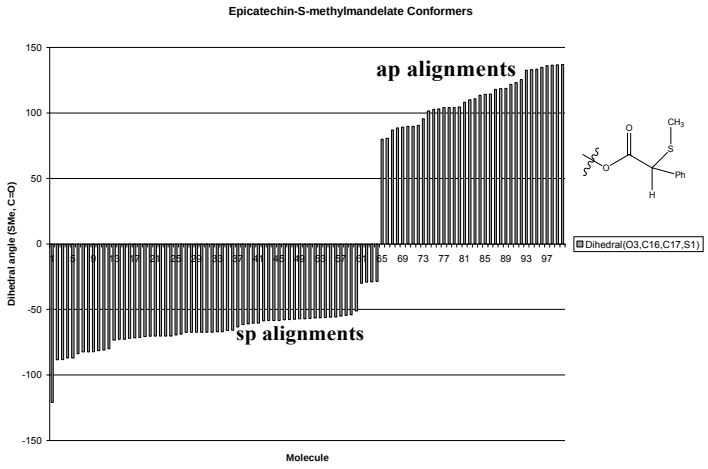

Figure 18a.

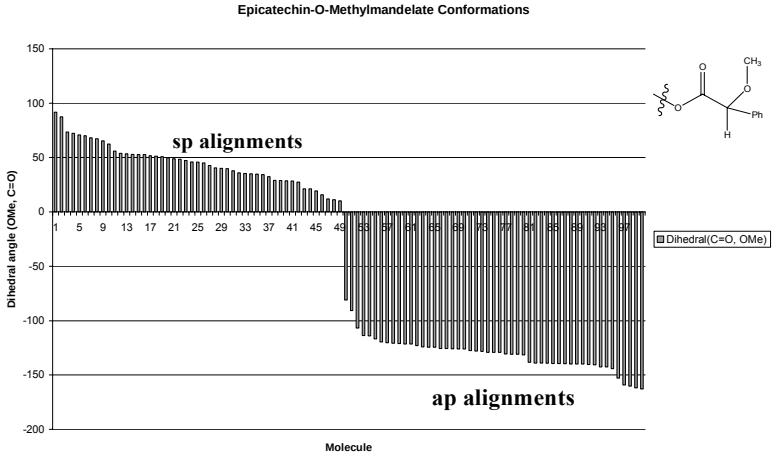

Figure 18b.

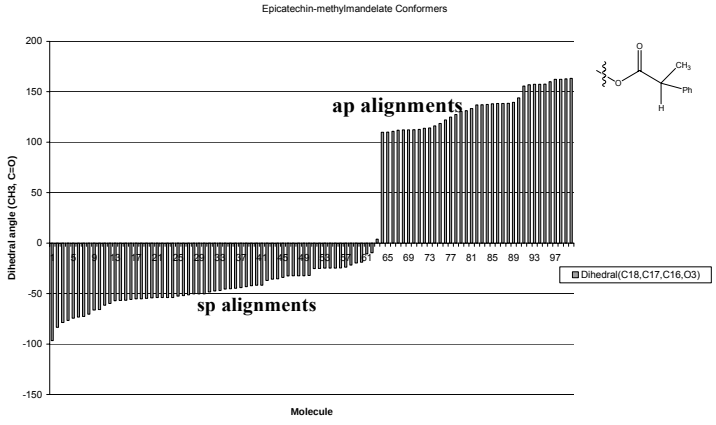

Figure 18c.

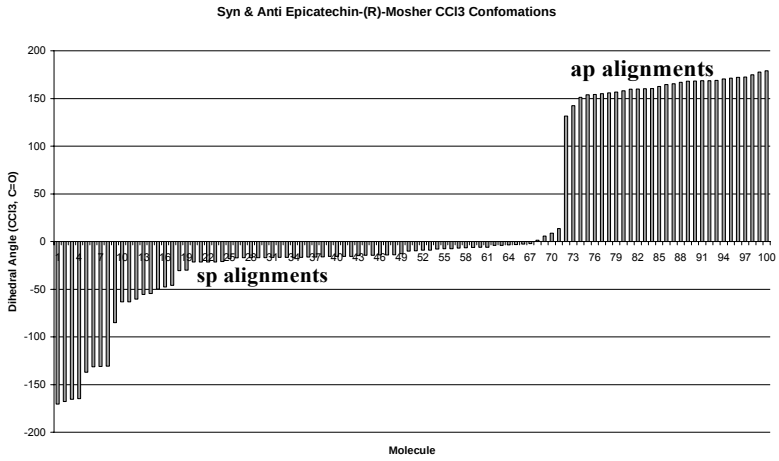

Figure 19a

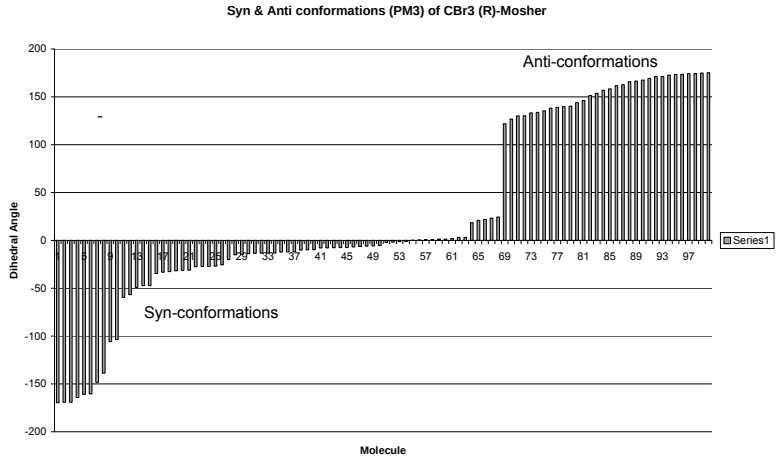

Figure 19b

In all of these examples the epicatechin Mosher ester have the most *sp* conformations with a $\leq 60°$ dihedral angle with the carbonyl bond. In addition, the CF_3 group has *sp* conformations which are complimented with smaller torsional angles with the carbonyl group.

Here again, the limitations of the semi-empirical optimization method should be noted and is not necessarily intended to be an accurate reflection of experimental behavior of the Mosher ester in solution. Although DFT, MP or DFT/HF hybrid methods would be ideal for these searches, computationally, it proves too expensive on a conventional desktop computer.

IR Data of the epicatechin-(*R*)-Mosher in solution.

As was observed for the Mosher acid, the epicatechin-(*R*)-Mosher ester also displays a lower and higher frequency component in the deconvoluted carbonyl band of the IR spectra (**Fig. 4.20**). The major lower frequency component corresponds to the *sp* conformer. This is in line with experimental NMR differential shielding observed and with DFT calculated carbonyl frequencies having the *sp* conformer with a lower energy and lower carbonyl frequency.

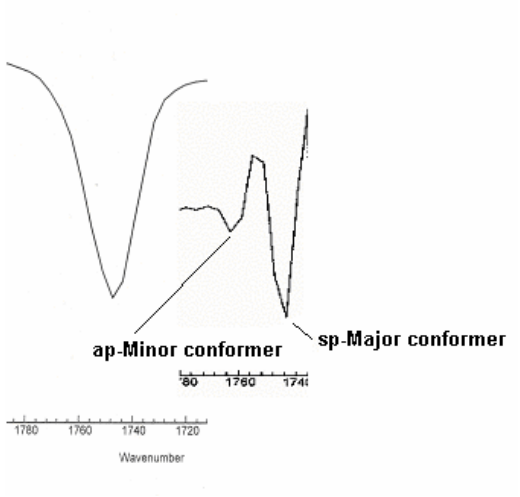

Figure 4.20 (IR deconvoluted C=O band for (-)-epicatechin-(*R*)-MTPA in chloroform)

Rationalizing the preferred alignment of the Mosher ester.

Preliminary DFT/pBP/DN** calculations

The small changes in bond lengths and electrostatic charges indicative hyperconjugative stabilization of the *sp* and *ap* epicatechin-Mosher esters were evaluated on a DFT/pBP/DN** level of theory (**Scheme 4.4**).

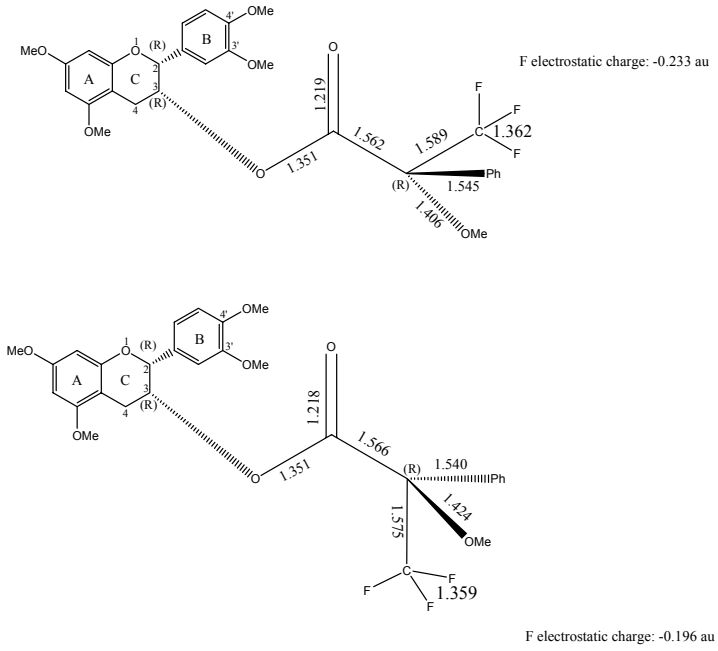

Scheme 4.4

The C=O bond of the *sp* conformer is elongated which corresponds to a decrease in bond order in the *sp* conformer and thus the lower experimental IR stretching frequency observed for this conformer. The α-C-C bond is only slightly shortened. The C-CF_3 bond is longer in the *sp* conformer which is in line with electron donation into σ*-orbital of this bond (when in the *sp* conformation). Also, the combined C-F bond lengths are elongated. According to the hyperconjugation model, the electronic charge on the fluorine atoms should increase. This is indeed observed for the *sp* conformer and is ca. -0.04 au for the three fluorine's, which is significant. The C=O-C-CF_3 dihedral angle is calculated at -37.8° and -156.2° for the *sp* and *ap* structures respectively.

Molecular Orbital calculations (B3LYP) on the Mosher-(S)-acid

In order to evaluate the possible hyperconjugation orbital overlap, the molecular orbitals in the *sp* and *ap* conformations of the acid is compared to identify small energy differences between them. The MO's with the largest energy difference displayed between the *sp* and *ap* conformations would possibly be the ones involved in the proposed hyperconjugational preferential stabilization of the *sp* conformer (**Fig 4.21**). The MO's from HOMO-10 (negative energy values) to LUMO+10 (positive energy values) of the *gauche* (*sp*) and anti (*ap*) isomers is plotted.

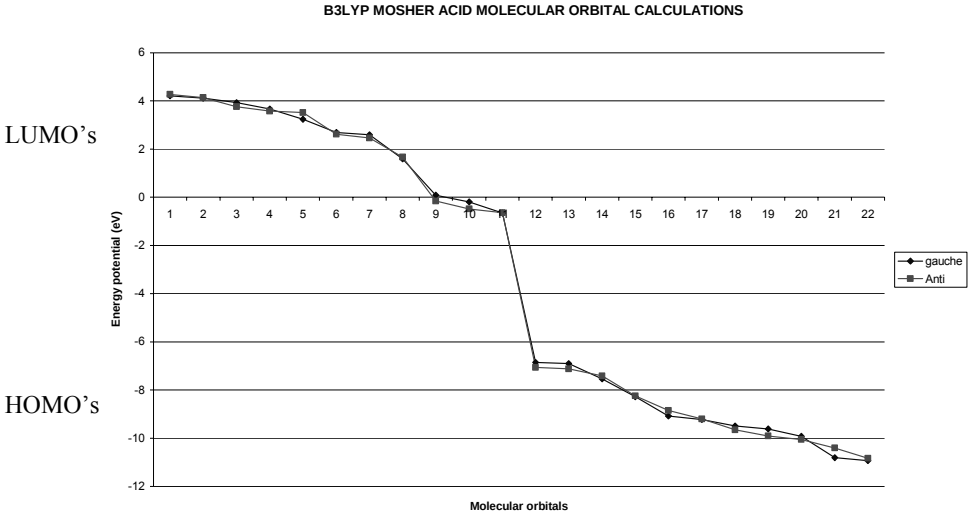

Figure 4.21. (B3LYP/6.31G** calculated MO energies (eV))

The MO's selected (**Scheme 4.5**) were the one's that show a meaningful energy difference of more than 0.2 eV between the two *sp* and *ap* conformers and thus the one's where vicinal hyperconjugational stabilization (**Fig. 4.23**) could be operative.

In LUMO+2 the double bond π*-character across the α-bond is observed. For the selected HOMO's the lone pair on the oxygen and the π-character of the carbonyl bond is prevalent as is depicted in **Scheme 4.5**.

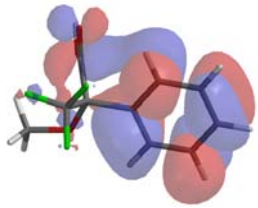

LUMO+1

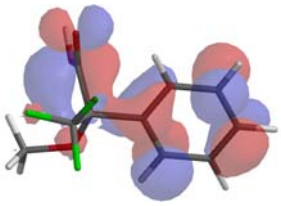

LUMO+2

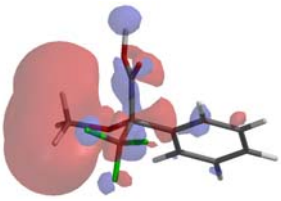

LUMO+6

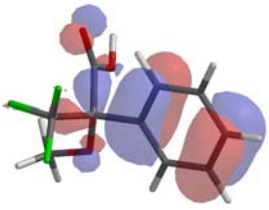

HOMO

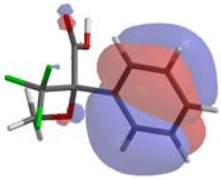

HOMO-1

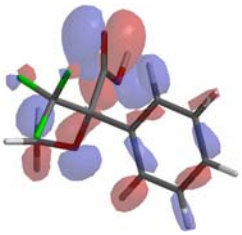

HOMO-4

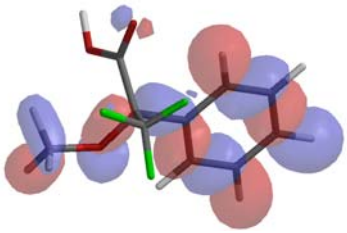

HOMO-7

Scheme 4.5.

The geometry optimization for the acid were also performed on the B3LYP/6.31G** method after the customary semi-empirical-PM3 conformational search and is summarized in **Scheme 4.6**.

The(*S*)-Mosher acid *sp* isomer is preferred by 1.48 kcal/mol for the B3LYP/6.31G++ calculation method employed. The O-CO, C=O and the C-CF_3, C-Ph bonds are longer in the *sp* conformer which are in line with the vicinal hyprerconjugative interaction model (negative fluorine hyperconjugation) across the central αC-CO bond. The lower calculated B3LYP/6.31G** carbonyl frequency for the preferred *sp* isomer is also found in experimental IR data (**Fig.4.8**) and the experimental data in literature[205]. The dihedral angle for the *sp* and *ap* isomers were measured at 30.5° and -126.7° respectively. The calculated Mulliken charges arose from the Mulliken population analysis and provide a means of estimating partial atomic charges from calculations

carried out by the linear combination of atomic orbitals molecular orbital method (LCAO)[246]. These calculated charges are indicated in **Scheme 4.6.**

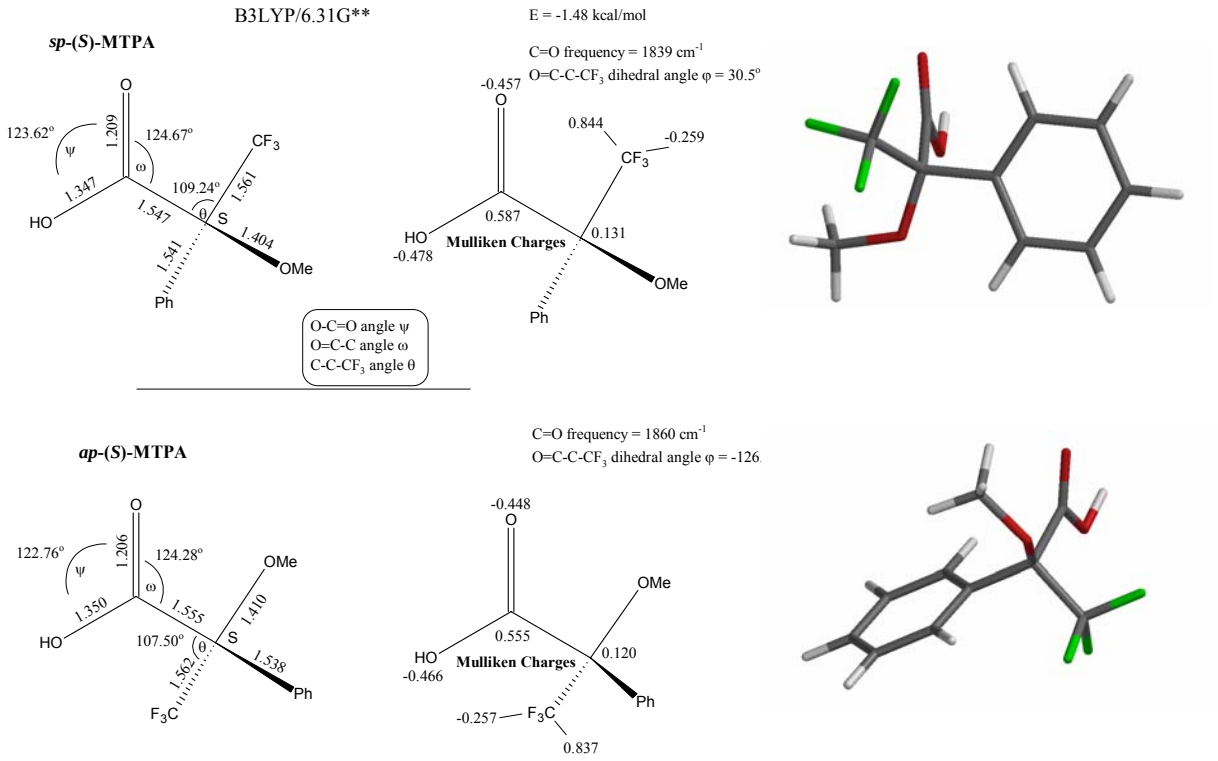

Scheme 4.6 (B3LYP/6.31G** (*S*)-MTPA geometry optimizations, bond angles, bondlengts, C=O frequencies, Mulliken charges)

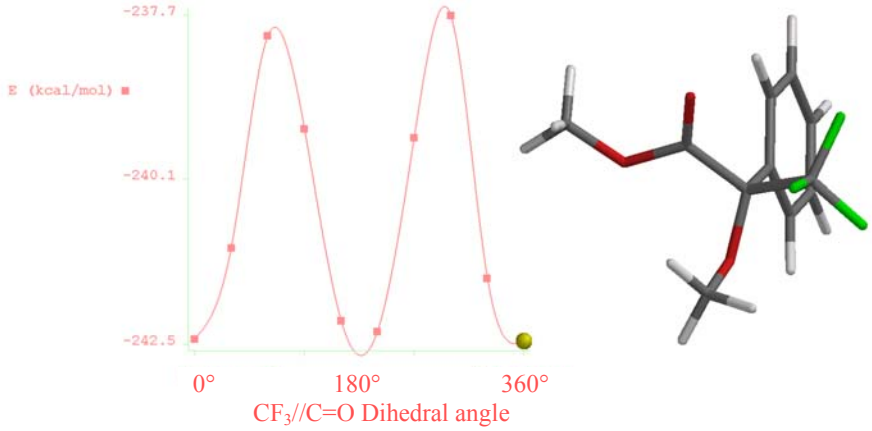

Scheme 4.7 (Me-(*S*)-MTPA SE/PM3 energy profile)

Me-(*S*)-MTPA is employed as the representative for Mosher esters in general. The energy profile (**Scheme 4.7**) of rotation about the αC-CO bond of the methyl ester of

[246] Mulliken, R. S., *Journal of Chemical Physics*, **1955**, *23*, Issue 12, 2343.

MTPA, calculated by SE/PM3 method, confirms the *sp* and *ap* conformations as low energy states with the *ap* conformer as the preferred conformer, analogous to that established earlier[203].

Higher-level re-optimizations (B3LYP/6.31G**, **Scheme 4.8**) of the Me-(*S*)-MTPA *ap*/*sp* conformations after a conformational search (SE\PM3), however, show the *sp* conformer to be favored by 1.46 kcal/mol. Subsequent frequency analyses of these optimized conformers show no imaginary frequencies reminiscent of a real energy minima obtained.

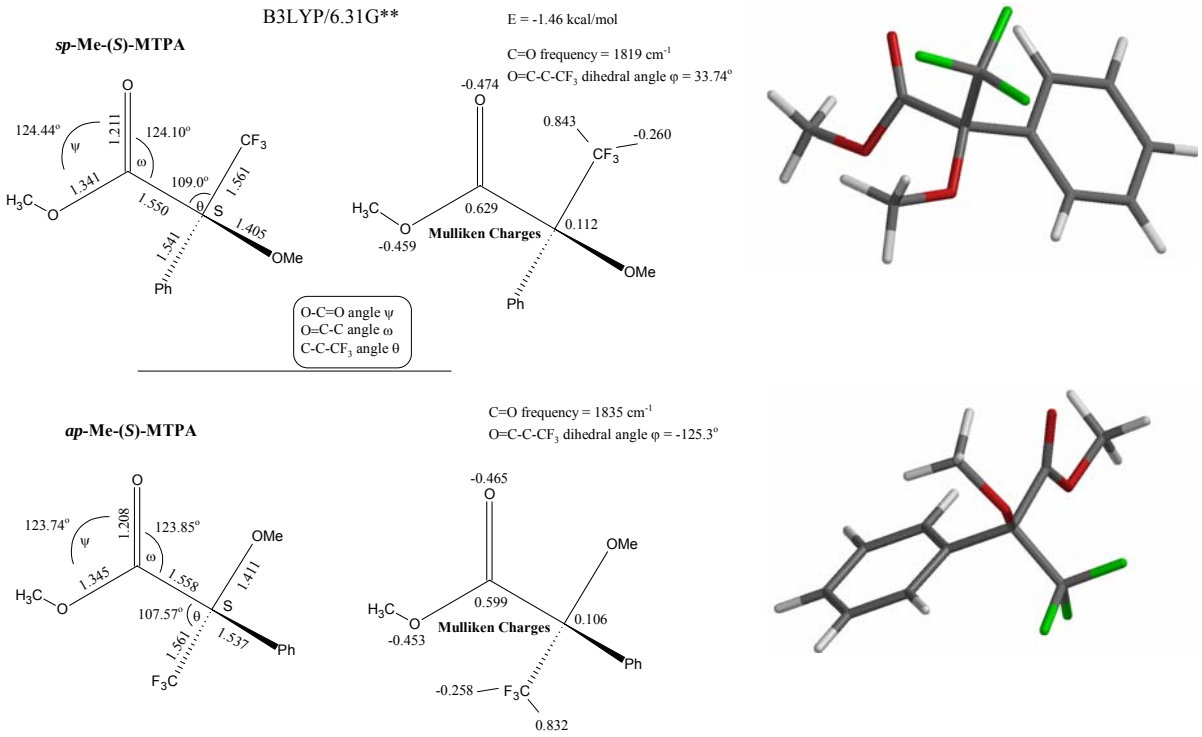

Scheme 4.8 (B3LYP/6.31G** Me-(*S*)-MTPA geometry optimizations, bond angles, bondlengts, C=O frequencies, Mulliken charges)

The calculated carbonyl IR stretching frequencies for Me-(*S*)-MTPA and (*S*)-MTPA correspond well with the experimental IR data for (*S*)-MTPA (**Fig.4.8**) in $CHCl_3$ in respect to the lower frequency component (*sp* isomer) of the deconvoluted carbonyl peak being the energetically preferred isomer in solution. The deconvoluted frequencies occur in an approximate ratio of 7:3[247] in favour of the *sp* conformer.

[247] Ohtani I., Kusumi T., Kashman Y. and Kakisawa H., *J. Am. Chem. Soc.*, **1991**, *113*, 4092.

These calculations are in line with the previously postulated predominance of *sp* conformer as the energetically preferred rotational isomer[248].

The same methodology is used on permethylated (-)-epicatechin-(*R*)-MTPA for the (B3LYP/6.31G**, **Scheme 4.9**) optimization of the *sp/ap* conformations after a semi-empirical (PM3) conformational search is performed.

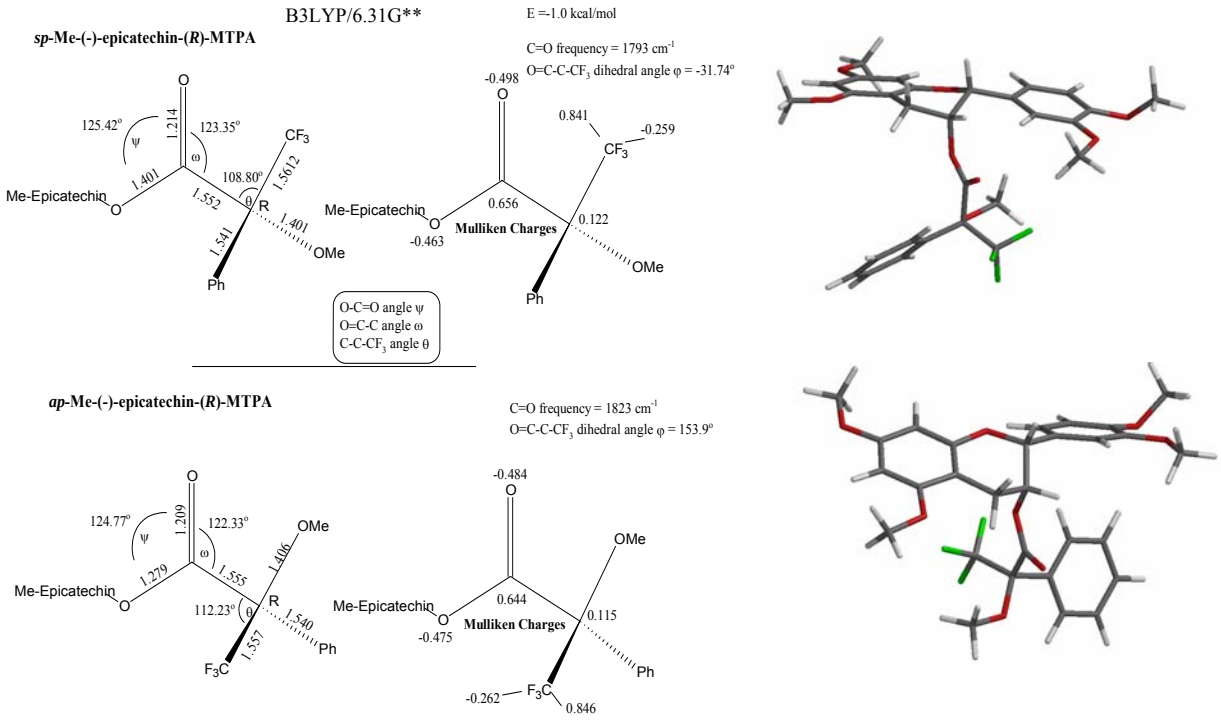

Scheme 4.9 (B3LYP/6.31G** (-)-epicatechin-(*R*)-MTPA geometry optimizations, bond angles, bondlengts, C=O frequencies, Mulliken charges)

The (B3LYP/6.31G**, **Scheme 4.9**) calculated carbonyl stretching frequency also corresponds well with the experimental values obtained after deconvolution of the carbonyl band (**Fig. 4.20**), which affirms the *sp* conformer as the preferred conformer. The calculated energy difference of 1.0 kcal/mol is obtained in favour of the *sp* conformer.

[248] Merckx E. M., Vanhoeck L., Lepoivre J. A., Alderwiereldt F. C., *Spectroscopy International J.*, **1983**, 30-42.

Mosher Hyperconjugation Calculations Summary and Discussion.

Much attention is recently focused on hyperconjugation as the major factor responsible for establishing a conformational preference in molecules[249] and to the definition of the molecular orbital(s) involved in the stabilization of these conformers. In general three types of hyperconjugation (HC) are defined, viz. sacrificial (cations)[250], isovalent (neutral)[251] and negative (anionic)[252] hyperconjugation. The MTPA-system belongs to the neutral hyperconjugation category, apparently resulting from overlap between the nearly vacant π*-(anti-bonding) orbital of the carbonyl group and the filled σ_{Ph}-(bonding) orbital on the α-carbon (**Fig. 4.22, 4.23**), and between the σ*C-CF_3 and σO-CO bonds (**Fig. 4.23**).

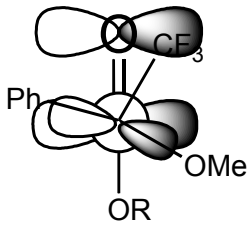

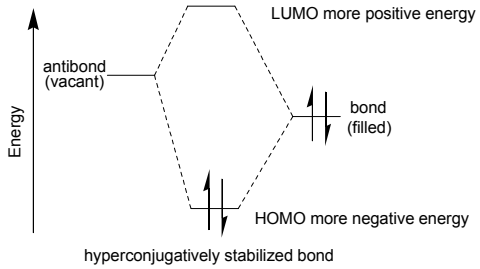

Figure 4.22 (overlap of $\pi_{C=O}$ and σ^*_{Ph}) **Figure 4.23**

In an attempt to rationalize the predominant stabilization displayed by the *sp* rotamer, a systematic comparison between the MOs of the *sp* and *ap* conformers in Me-(*S*)-MTPA, disclose a few MO's with a meaningful energy difference (approximately 0.2 eV). The MO's of MeEC-(*R*)-MTPA are too complex to make reliable deductions and pinpoint one HOMO and LUMO, because several of each seem to be involved, based on their energy criteria. Three MO's are selected on the grounds of their relative energy difference between *ap*/*sp* isomers while retaining the necessary π-orbital symmetry across the αC-CO bond, indicative of hyperconjugative orbital overlap (**Table 4.2.1, 4.2.2**).

[249] V. Pophristic, L. Goodman, *Nature*, **2001**, *411*, 565S
[250] T. Laube, Acc. *Chem. Res.*, **1995**, *28*, 399.
[251] J.B. Lambert and Robert A. Singer, *J. Am. Chem. Soc*., **1992**, *114,* 10246.
[252] I.A. Koppel, V. Pohl, I.A. Koppel, F. Anvia, *J. Am. Chem. Soc*., **1994**, *116*, 8654.

The HOMO-5 (**Fig.4.24**) with an energy decrease of 0.266 eV for the *sp* isomer clearly display π-overlap from the $\pi_{C=O}$ over the αC-CO and αC-CF_3 bonds, resulting in the slight shortening calculated for the αC-CO bond, distinctive of hyperconjugative stabilization in the *sp* isomer. HOMO-5 is also a more populated MO reflected in the more negative eigenvalue for this orbital.

LUMO+1, +2 similarly shows a high degree of π-symmetry components over the αC-CO bond together with a 0.2 eV higher relative energy in the *sp* isomer, thus participating in the hyperconjugative stabilization of this isomer (**Fig.4.25**). Hyperconjugative stabilization is then mainly prevalent in the HOMO-5 and LUMO+1, +2, which contains the stabilizing bonding and anti-bonding combination of atomic orbitals shown in **Fig. 4.22, 4.23, 4.24, 4.25**.

	MO:	Eigenvalues:	(eV):		MO:	Eigenvalues:	(eV):		*ap-sp* (eV)
		ap **MTPA-Me**				***sp*** **MTPA-Me**			
	51	-0.40748	-11.0881		51	-0.40919	-11.1347		0.04654
	52	-0.39943	-10.8691		52	-0.40371	-10.9854		0.11633
	53	-0.39598	-10.7751		53	-0.39718	-10.8078		0.03266
-10	54	-0.38326	-10.429		54	-0.38971	-10.6045		0.17546
-9	55	-0.37488	-10.2011		55	-0.37403	-10.1779		-0.02324
-8	56	-0.36285	-9.87354		56	-0.36099	-9.823		-0.05054
-7	57	-0.36068	-9.81451		57	-0.35103	-9.55192		-0.26259
-6	58	-0.35051	-9.53796		58	-0.34559	-9.40398		-0.13398
-5	59	-0.324	-8.81651		59	-0.33379	-9.08293		**0.26642**
-4	60	-0.31639	-8.60951		60	-0.31578	-8.59277		-0.01674
-3	61	-0.297	-8.0819		61	-0.30033	-8.17232		0.09042
-2	62	-0.26818	-7.29742		62	-0.27237	-7.4117		0.11428
-1	63	-0.25971	-7.06714		63	-0.25164	-6.84741		-0.21973
HOMO	64	-0.25664	-6.98348		64	-0.2492	-6.78105		-0.20243
LUMO	65	-0.02081	-0.56638		65	-0.01971	-0.53642		-0.02996
1	66	-0.01448	-0.39405		66	-0.00472	-0.12854		**-0.26551**
2	67	-0.00128	-0.03478		67	0.00609	0.16582		**-0.2006**
3	68	0.0838	2.28019		68	0.08127	2.21134		0.06885
4	69	0.09243	2.51528		69	0.09775	2.66001		-0.14473
5	70	0.10063	2.73834		70	0.09887	2.69052		0.04782
6	71	0.11906	3.23983		71	0.1206	3.28177		-0.04194
7	72	0.13164	3.58214		72	0.12541	3.41264		0.1695
8	73	0.13468	3.66496		73	0.14013	3.81316		-0.1482
9	74	0.14154	3.85146		74	0.14573	3.9655		-0.11404
10	75	0.14885	4.05054		75	0.15027	4.08907		-0.03853

Table 4.2.1

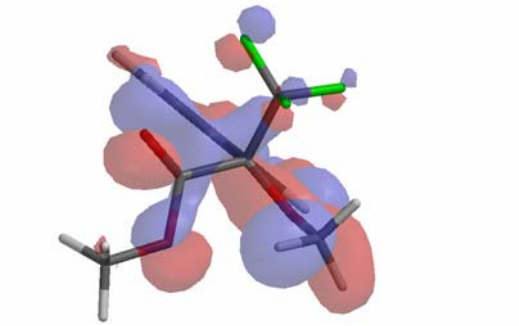

Figure 4.24 HOMO-5

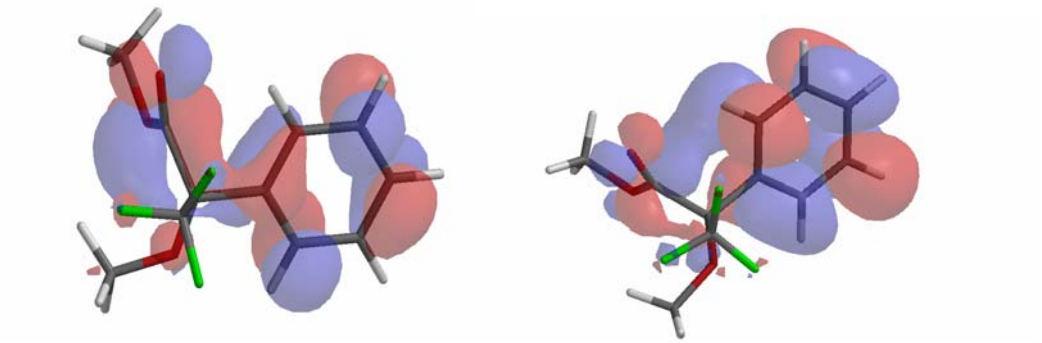

LUMO+2 **LUMO+1**

Figure 4.25

Three molecular parameters (one geometrical and two electronic) obtained via higher level re-optimizations of the relevant conformers are applied to evaluate hyperconjugative effects: (1) the four bond lengths: O=C, αC-CO, O-CO and αC-CF_3 ;(2) the Mulliken atomic populations of these atoms; (3) Natural Bond Orbital (NBO)[253] analysis. For the *sp* isomer the data (**Table 4.2**) disclosed lengthening of the C=O bond length due to the loss of π-character, the αC-CO bond is shorter due to an increase in 'π-character' and the αC-CF_3 bond is slightly longer probably due to $\sigma_{C\text{-}O}$-donation (α-ester bond) into the $\sigma^*_{\alpha C\text{-}CF3}$ orbital (**Fig. 4.26**) (located mainly on α-carbon) which is an excellent electron acceptor due to the high electronegativity of the CF_3 group[254]. These bondlength changes support the proposed HC model and is underscored by Mulliken population analysis. The latter shows the carbonyl and α-carbon to be less populated with a greater positive charge in the *sp* isomer and an increased negative charge on the fluorine atoms due to the delocalization of electron density from the carbonyl bonding orbitals to the electronegative CF_3-group on the α-carbon, reminisent of hyperconugative vicinal charge transfer. Consequently, the αC-CO bond polarization coefficient shifts to the α-carbon.

[253] F. Weinhold, in *The Ensyclopedia of Computational Chemistry (ed. Schleyer, P. v. R.)*, 1792-1811.
[254] Y. Apeloig, J. C. S. *Chem. Comm.*, **1981**, 396

Table 4.2.2 B3LYP\6.31G**	Me-(*S*)-MTPA		MeEC-(*R*)-MTPA	
	sp	***ap***	***sp***	***ap***
ΔE (kcal/mol)	-1.46	0	-1.00	0
ϕ CF_3-C-CO	-33.7°	-125.3°	-31.7°	153.8°
θ F3C-C-CO	109.0°	107.6°	108.8°	112.2°
C=O freq calc. cm^{-1}	1819	1835	1793	1823
C=O freq obs. cm^{-1}	n/a	n/a	1742	1765
Mulliken population				
C=O	-0.474	-0.465	-0.498	-0.484
C=O	0.629	0.599	0.656	0.644
α–C	0.112	0.106	0.122	0.115
C-F3	0.843	0.832	0.841	0.846
C-F3	-0.260	-0.258	-0.259	-0.257
Bond length (Å)				
C-O	1.341	1.345	1.337	1.279
C=O	1.210	1.208	1.214	1.209
α-C-CO	1.550	1.558	1.552	1.557
α-C-CF3	1.5612	1.5610	1.561	1.557
C-F3	1.347	1.345	1.348	1.350
α-C-Ph	1.541	1.537	1.541	1.540
α-C-OMe	1.405	1.411	1.401	1.406
MO with ΔE >0.2 eV (*ap*-*sp*)				
HOMO -5	0.27	0	0.18*	
LUMO +2	-0.20	0	0.15*	
LUMO +1	-0.27	0	0.01*	

*MeEC-(*R*)-MTPA is to large a molecule and MO's too complex to make reliable conclusions

NBO calculations

Natural bond orbitals (NBO's) provide a means to analyze hyperconjugative interactions with greater detail than is possible by molecular orbitals.

These orbitals are nearly doubly occupied, localized bonding orbitals (bonds) and nearly vacant localized antibonding orbitals (antibonds). A hyperconjugative interaction is expressed as a charge (electron) transfer between selected bonds and antibonds, allowing specific hyperconjugative interactions that influence structural preference, to be pinpointed (**Fig 4.23**). NBO B3LYP/6.31G** calculations (**Table 4.3**) reports a strongly delocalized structure with total core, lone pair and bond occupancy of 97.57% and a total Rydberg and antibond occupancy of 2.43% for both Me-(*S*)-MTPA isomers. The NBO calculation results of this model Me-(*S*)-MTPA structure is used to investigate the bond orbital populations of the ester because no sterric influences would be operative to influence the final optimized geometry of the ester, and it drastically shortens calculation time.

Table 4.3. B3LYP/6.31G++ NBO SUMMARY (Me-(*S*)-MTPA)

σ_{C-O}	more populated in *sp* isomer
σ^*_{C-O}	less populated in *sp* isomer
$\sigma_{C=O}$	no change in population
$\sigma^*_{C=O}$	more populated in *sp* isomer
$\pi_{C=O}$	less populated in *sp* isomer
$\pi^*_{C=O}$	more populated in *sp* isomer
$\sigma_{\alpha-C-C}$	less populated in *sp* isomer
$\sigma^*_{\alpha-C-C}$	more populated in *sp* isomer
σ_{C-CF3}	more populated in *sp* isomer
σ^*_{C-CF3}	more populated in *sp* isomer
$\sigma_{\alpha-C-Ph}$	less populated in *sp* isomer
$\sigma^*_{\alpha-C-Ph}$	less populated in *sp* isomer
$\sigma_{\alpha-C-OMe}$	more populated in *sp* isomer
$\sigma^*_{\alpha-C-OMe}$	less populated in *sp* isomer

The $\pi^*_{C=O}$ bond show a significant increase in population in the *sp* isomer which can be attributed to donation from σ-$_{C-Ph}$ with a corresponding bond population and bond length decrease. These bonds also have the π symmetry needed for such a donation (**Fig. 4.22, 4.23**). The $\pi_{C=O}$ orbital also show a significant decrease in population and the resultant bond polarization coefficient shifting to oxygen. This π-bond/antibond population changes result in a lower bond order for the carbonyl bond, which is reflected in the lower experimental and calculated IR frequencies found for the *sp* isomer.

σ^*_{C-CF3} display a big increase in population, due to overlap with the σ_{C-O} ester bond leading to the lengthening of these bonds in the *sp* isomer of EC-MTPA.

σ_{C-CF3} is more populated in the *sp* isomer but the bond polarization is shifted towards the CF_3-group, leaving the σ^*_{C-CF3} orbital concentrated on the α-carbon. The σ_{C-O} ester bond orbital overlap with the σ^*_{C-CF3} is analogous to the orbital configuration found for 1,2-difluoroethene, which is responsible for its well-known *cis* effect[255](**Fig. 4.26**). The greater overlap of CH-CF* (*anti*) relative to the *syn* configuration greatly stabilizes the *cis* conformation. This is reflected in the substantially longer calculated bond lengths of the O-CO ester and to a lesser extent, the αC-CF_3 bonds in the *sp* isomer of the MTPA derivatives. This interaction between the σ^*_{C-CF3} and σ_{C-O} orbitals is a classical example of Fluorine Negative Hyperconjugation[256] and is in line

[255] N. C. Craig and E. A. Entemann, *J. Am. Chem. Soc.*, **1961**, *83*, 3047.
[256] Schleyer P. v. R. and Kos A. J., *Tetraherdon*, **1983**, *39*, 1141.

with the NBO analysis and the slightly longer bond lengths of these interacting bonds in the *sp* isomer. Evidently, this places the $\sigma^*_{C\text{-}CF3}$ and $\sigma_{C\text{-}O}$ orbitals in an *anti* conformation necessary for greater hyperconjugative overlap. This overlap is also present in the *syn* conformation , but to a lesser extent.

This *anti* orbital overlap is further confirmed by a CO-C-CF_3 and accompanying O-C=O bonding angle (ψ and θ) increase of almost 2° in general (**Fig. 4.6 and 4.8**). This allows for increased overlap of the $\sigma^*_{C\text{-}CF3}$ and $\sigma_{C\text{-}O}$ orbitals in an *anti* conformation. This is an important indication of the vicinal, stabilizing, hyperconjugative overlap of these orbitals (**Fig 4.26**).

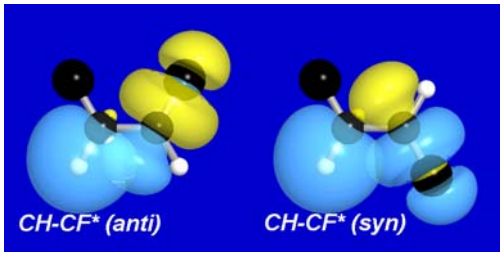

Figure 4.26

Although the αC-CO bond is only slightly shorter in the *sp* isomer, it remains in line with hyperconjugation because it is now demontstated that central C-C bond lengthening is crucial in eliminating vicinal repulsive interactions in rotational isomers[249]. It is demonstrated that the well-known staggered conformation of ethane is brought about by hyperconjugation and vicinal steric effects are nullified by central C-C bond lengthening, thus eliminating an energy increase due to steric effects. Consequently, the αC-CO bond length and the magnitude of the bond length difference is not a reliable indication of the magnitude of hyperconjugation between vicinal interacting bonds.

As discussed for the DFT (pBP/DN**) calculations for the acid, an additional factor that may play a role in stabilization of the *sp* and *ap* B3LYP\6.31G** optimized Me-MTPA conformers, may be the electrostatic interaction between the ester (*ap*) or carbonyl (*sp*) oxygen and $^{\delta+}CF_3$ group, resulting from the substantial van der Waals radii[257] overlap of 0.357 Å and 0.387 Å for the *sp* and *ap* conformations respectively.

[257] A. Bondi, *J.Phys.Chem*., **1964**, *68*, 441.

H-bonding between the OMe and the carbonyl oxygen lone pair with a v.d. Waals radii overlap ca. 0.395 Å. will contribute similarly to the stability of the *ap* conformer.

Flavonoids are notoriously non-crystalline and very few flavonoid crystal structures are known to exist[258,259]. To our knowledge permethylated Epicatechin-(*R*)-α-methoxy-α-trifluoromethyl-α-phenylacetate (MeEC-(*R*)-MTPA), is the only known flavonoid-MTPA ester derivative in a crystalline state (**Figure 4.9**). It is noteworthy that MeEC-MTPA crystallized as the *ap* conformer, which also displays a large v.d. Waals interaction between the CF_3 group and the ester oxygen, as is also indicated by the B3LYP\6.31G** calculations above. These interaction distances measures 2.721Å corresponding to a 0.499 Å v.d. Waals overlap between the ester oxygen and the CF_3 carbon and a 2.668 Å distance between this oxygen and closest fluorine on the CF_3 group. The latter corresponds to a 0.322 Å v.d. Waals overlap.

The calculations on a recently developed α-fluoroacetate chiral derivatizing agent, CFTA[260] (**Chapter 5**), with a α-fluorine atom, also show noteworthy fluorine-oxygen v.d. Waals interactions in the energetically favoured *sp* and *ap* conformations. This suggests that, in the MTPA case, the peculiar oxygen-fluorine v.d. Waals overlap in the *sp* and *ap* conformers are not necessarily only the result of the electrostatic oxygen and $^{\delta+}\underline{C}F_3$ interaction.

Conclusions

The results of this study disclose the bonding and antibonding interactions ($\pi_{C=O}/\sigma^*_{Ph}$ and $\sigma_{O\text{-}CO}/\sigma^*_{C\text{-}F}$) and the molecular orbitals involved in the hyperconjugative stabilization of the *sp* and *ap* conformer pair and the predominance of the former. The conclusions are substantiated by the calculated (B3LYP/6.31G**) bond length changes of the optimized geometries, Mulliken population and NBO analysis.

[258] Cantrell J. S., *Plant Flavonoids in Biology and Medicine: Biochemical, Pharmacological and Structure-Activity Relationships*, **1986**, 391-394.
[259] Jiang R., Ye W., Woo K., Du J., Che C., But P. P. and Mak T. C. W., *Journal of Molecular Structure*, **2002**, *642*, 77-84.
[260] Y.Takeuchi, H. Fujisawa, R. Noyori, *Org. Lett.,* **2004**, *6*, 4607.

Controrary to the (*S*)-MTPA esters investigated above, geometry optimizations of Me-(*R*)-MTPA and (*R*)-MTPA (**Scheme 4.10, 4.11**), show the *ap* conformer to be prefered by 1.41 and 1.47 kcal/mol respectively, although it is not true for the (-)-epicatechin-(*R*)-MTPA ester.

This is substantiated by literature that the *ap* conformation is prefered and two different *sp* conformations with similar energies are presented[203,261] although only SE (AM1) calculation methods are used in that instance, which is insufficient because electron correlations are not accounted for. This is indicated[261] as a major factor which renders the use of the Mosher agent unreliable in some cases. One should also be mindfull that those and my own calculations are not performed in a solvent sphere and that the presence of a solvent sphere could greatly enhance the preference of the *sp* conformer. The *sp* conformer is indeed prefered experimentally in solution according to the shielding effects observed, and the cases where it has failed are exeptions to the rule.

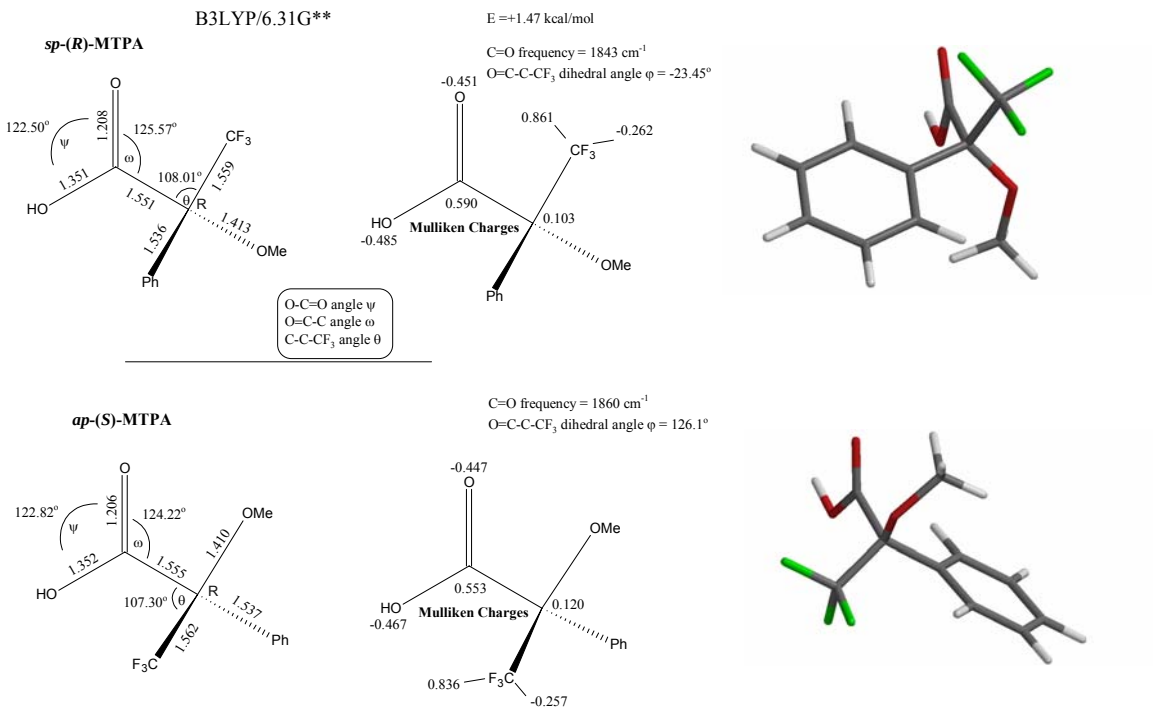

Scheme 4.10

However, the same stabilizing vicinal hyperconjugative interactions are present governing the *ap* and *sp* conformers stability. For the *sp* isomer the important

[261] Latypov, S. K., Seco J.M., Quinoa´, E., and Riguera, R., *J. Org. Chem.*, **1996,** *61,* 8569-8577.

interaction between the $\sigma^*_{C\text{-}CF3}$ and $\sigma_{C\text{-}O}$ orbitals are still operational, but to a lesser extent due to the following indicators:

- Shorter α-C-C bond
- Greater C-C-CF_3 angle to assist $\sigma^*_{C\text{-}CF3}$ and $\sigma_{C\text{-}O}$ orbital overlap
- Increased negative charge on the fluorine atoms and more positive charge on C=O due to hyperconjugative charge transfer to fluorine.

The $\pi^*_{C=O}$ and $\sigma\text{-}_{C\text{-}OMe}$ vicinal interaction (in the case of the *R*-esters) are present due to the following reasons:

- Longer C-OMe and C=O bond due to donation from $\sigma\text{-}_{C\text{-}OMe}$ into $\pi^*_{C=O}$
- The lower carbonyl frequency in the calculations and experimentally[204] as a result of donation from $\sigma\text{-}_{C\text{-}OMe}$ into $\pi^*_{C=O}$.

The $\sigma^*_{C\text{-}CF3}$ and $\sigma_{C\text{-}O}$ interaction is probably more prominent in the *ap* (*R*)-ester due to: Longer C-CF_3 and C-O bondlengts, the most important indicators, and a much greater negative charge on the α-carbon.

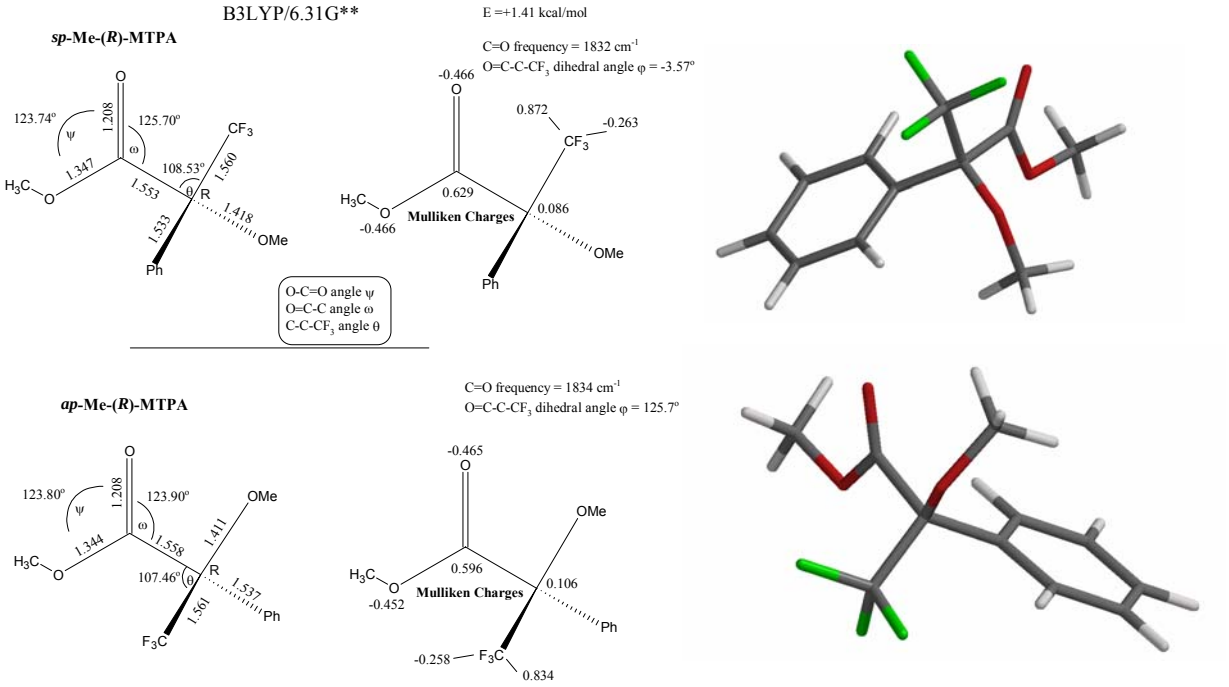

Scheme 4.11

Another property of the Mosher-(*R*)-esters that will greatly stabilize the *sp* conformer in polar solvents, compared to the *ap* conformer, is it's bigger calculated dipole moment (**Table 4.4**).

Molecule	Dipole (B3LYP/6.31G**)
sp-(*R*)-MTPA	4.224 debye
ap-(*R*)-MTPA	3.007 debye
sp-Me-(*R*)-MTPA	4.728 debye
ap-Me-(*R*)-MTPA	3.081 debye
sp-(*S*)-MTPA	2.462 debye
ap-(*S*)-MTPA	2.985 debye
sp-Me-(*S*)-MTPA	2.931 debye
ap-Me-(*S*)-MTPA	3.102 debye

Table 4.4

The (*S*)-esters all have similar dipole moments, but for the (*R*)-esters, a markedly higher dipole moment for the *sp* conformer is observed. Compounds with a higher dipole moment will be more stabilized in polar solvents. Thus, the *sp*-(*R*)-MTPA conformer will be stabilized to a greater extent in polar solvents like chloroform and methanol, which have a polarity index of 4.1 and 5.1 respectively. Solvents like dichloromethane and toluene which have polarity indexes of 3.1 and 2.4 respectively, will not favour the *sp*-(*R*)-MTPA ester, as in the more polar solvents.

A.F. Hundt[262] found that the non-matching (*S*)-MTPA (i.e. 3*R*, (*S*)-MTPA or 3*S*, (*R*)-MTPA) ester derivatives gave consistently higher shielding values compared to the (*R*)-MTPA (matching) derivatives. This was found to be true for a wide range of flavan-3-ols, 4-arylflavan-3-ols, and in the assessment of absolute configurations of C-3 of those condensed tannin structural units.

This is in line with the consistently higher B3LYP\6.31G** calculated energy found for the (*R*)-MTPA *sp* isomers compared to the (*S*)-MTPA isomers, which have a lower calculated energy for the *sp* isomer. This also confirm the greater stabilization of the (*R*)-MTPA *sp* isomer compared to the *ap* isomer in polar solvents, due to the substantially higher calculated dipole found for the (*R*)-MTPA *sp* isomer (**Table 4.4**). This makes the (*R*)-MTPA *sp* isomer the preferred isomer in polar solvents even though the *ap* isomer is energetically favored *in vacu*.

[262] Hundt A. F., *M.Sc*., **1990**, 46.

These results suggest that care should be taken when assigning the absolute stereo chemistry using the Mosher ester.

Preferably, solvents of different polarity should be used and both the (*R*), (*S*)-MTPA derivatives should be prepared and compared for reliable results.

Experimental

Synthesis of permethylated (-)-epicatechin

The title compound is selectively methylated with diazomethane using standard experimental procedure from commercially obtained (-)-epicatechin as substrate. The compound was purified by TLC using hexane: acetone 8:2 as eluent. (Rf = 0.65)
^{1}H NMR 270 MHz (**Plate 5.6**, $CDCl_3$, 293K).

Synthesis of 3', 4', 5, 8-Tetramethyl -(-)Epicatechin-(R)-MTPA

Preparation of (+)-(*S*)-α-Methoxy-α-trifluoromethylphenylacetylchloride (MTPACl):

MTPACl was freshly prepared by chlorination of the enantiomerically pure acid (Fluka GmbH) shortly before use. Enantiomerically pure (+)-(*R*)-α-Methoxy-α-trifluoromethylphenylacetic acid (MTPA) (Fluka GmbH) was chlorinated with an excess (10 ekw) of freshly distilled thionylchloride under reflux for 4 hours. The excess thionylchloride was removed by a strong stream of nitrogen at room temperature. The resultant clear, colorless, viscous liquid was weighed and without any further purification, immediately dissolved in a measured volume of carbon tetrachloride freshly distilled from P_2O_5. This solution was used immediately for esterifications.

(*R*)-MTPA Esterification

Methyl ethers of (-)-epicatechin (100 mg) were weighed and dissolved in benzene and transferred to dry round bottom 10 cm^3 flasks and the benzene removed under reduced pressure. To ensure azeotropic drying of the substrates they were re-dissolved in 3-4 cm^3 of benzene and the process repeated two more times. A measured volume of MTPACl-carbon tetrachloride solution containing 1.2-1.3 stoichiometric equivalents of MTPACl was added by glass syringe. 1-3 Drops of dry pyridine were added and the flasks fitted with reflux condensers capped with a $CaCl_2$ drying tubes.

Reaction mixtures were kept under reflux for 16-24 hours subject to monitoring by TLC. Pyridine was dried over copious amounts of sodium hydroxide pellets.
The resultant mixture was acidified with 0.1% HCl and extracted with diethyl ether. The combined organic phases were washed with 0.1% HCl followed with 10% sodium carbonate solution. The diethyl ether were evaporated under vacuum and the resultant clear yellow oil purified by preparative TLC using hexane: ethyl acetate: acetone 6:3:1. 74mg, yield 45.6% (Rf 0.57). The product became light pink after recovery from the NMR $CDCl_3$ solution.
The same procedure was followed to prepare the (*S*)-esters.

3', 4', 5, 8-Tetramethyl-(-)epicatechin-(*R*)-MTPA

^{1}H NMR 300 MHz (**Plate 4.1a**, $CDCl_3$, 293K); H-4 ax (δ3.02 dd, J = 4.2, 18.0 Hz), H-4 eq (δ3.13, dd, J = 1.8, 18.0 Hz,), OMe (δ3.77, s), OMe (δ3.78, s), OMe (δ3.80, s), OMe (δ3.93, s), H-3 (δ5.60, m), H-2 (δ5.15, s), H-6 (δ6.10, d, J = 2.1 Hz), H-8 (δ6.15, d, J = 2.1 Hz), H-5' (δ6.87, d, J = 8.4 Hz), H-6' (δ7.04, dd, J =1.8, 8.4 Hz), H-2' (δ7.09, d, J = 1.8 Hz), 5 x PhH (δ7.10-7.35, m), OMe (δ3.28, s).

3', 4', 5, 8-Tetramethyl-(-)Epicatechin-(*R*)-MTPA

^{1}H NMR 300 MHz (**Plate 4.1b**, (1,1,2,2-tetrachloroethane-d2, 293K); H-4 ax (δ3.05 dd, J = 2.7, 13.5 Hz), H-4 eq (δ3.13, dd, J = 1.2, 13.5 Hz,), OMe (δ3.78, s), OMe (δ3.80, s), OMe (δ3.82, s), OMe (δ3.92, s), H-3 (δ5.62, m), H-2 (δ5.17, s), H-6 (δ6.02, d, J = 1.2 Hz), H-8 (δ6.19, d, J = 1.2 Hz), H-5' (δ6.89, d, J = 6.0 Hz), H-6' (δ7.01, dd, J =1.0, 6.0 Hz), H-2' (δ7.05, d, J = 1.0 Hz), 5 x PhH (δ7.10-7.40, m), OMe (δ3.28, s).

3', 4', 5, 8-Tetramethyl-(-)Epicatechin-(*S*)-MTPA

^{1}H NMR 300 MHz (**Plate 4.2a**, $CDCl_3$, 293K); H-4 ax (δ3.04 dd, J = 5.4, 18.0 Hz), H-4 eq (δ3.13, dd, J = 3.0, 18.0 Hz,), OMe (δ3.69, s), OMe (δ3.80, s), OMe (δ3.81, s), OMe (δ3.90, s), H-3 (δ5.64, m), H-2 (δ5.12, s), H-6 (δ6.14, d, J = 3.0 Hz), H-8 (δ6.20,

d, J = 3.0 Hz), H-5’ (δ6.73, d, J = 8.4 Hz), H-6’, H-2’ (δ6.85, m), 5 x PhH (δ7.10-7.38, m), OMe (δ3.28, s).

3’, 4’, 5, 8-Tetramethyl-(-)Epicatechin-(*S*)-MTPA

^{1}H NMR 300 MHz (**Plate 4.2b**, (1,1,2,2-tetrachloroethane-d2, 293K); H-4 ax (δ3.05 dd, J = 2.7, 13.8 Hz), H-4 eq (δ3.13, dd, J = 1.2, 13.8 Hz,), OMe (δ3.71, s), OMe (δ3.82, s), OMe (δ3.82, s), OMe (δ3.88, s), H-3 (δ5.63, m), H-2 (δ5.15, s), H-6 (δ6.72, d, J = 1.5 Hz), H-8 (δ6.22, d, J = 1.5 Hz), H-5’ (δ6.75, d, J = 6.3 Hz), H-6’, H-2’ (δ6.88, m), 5 x PhH (δ7.16-7.40, m), Me (δ3.30, s).

NMR SPECTRA

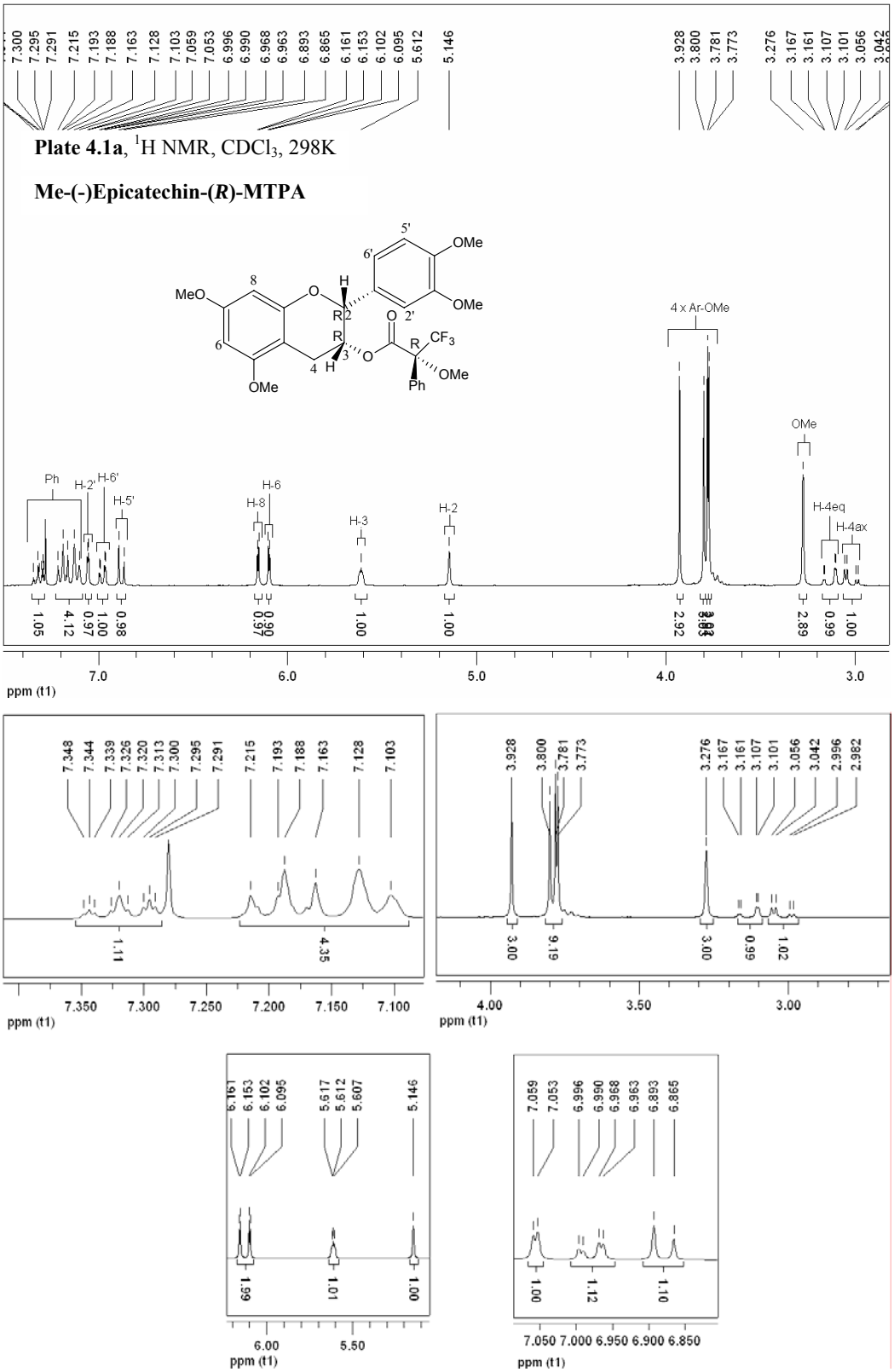

Plate 4.1a, ^{1}H NMR, $CDCl_3$, 298K

Me-(-)Epicatechin-(*R*)-MTPA

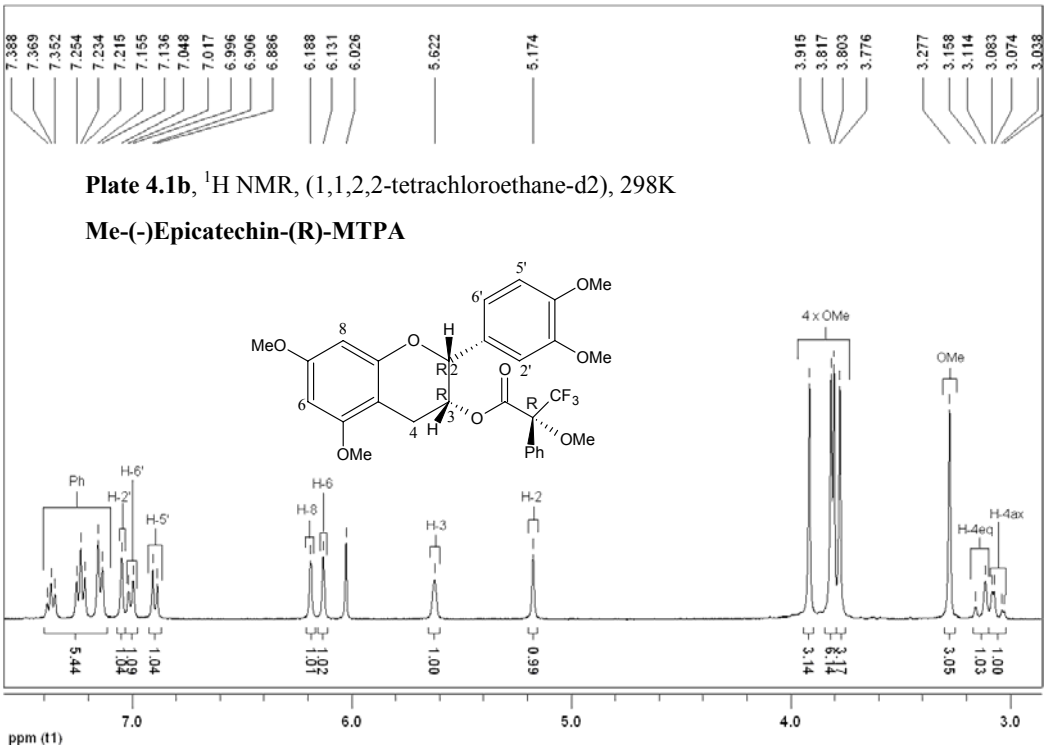

Plate 4.1b, ^{1}H NMR, (1,1,2,2-tetrachloroethane-d2), 298K

Me-(-)Epicatechin-(R)-MTPA

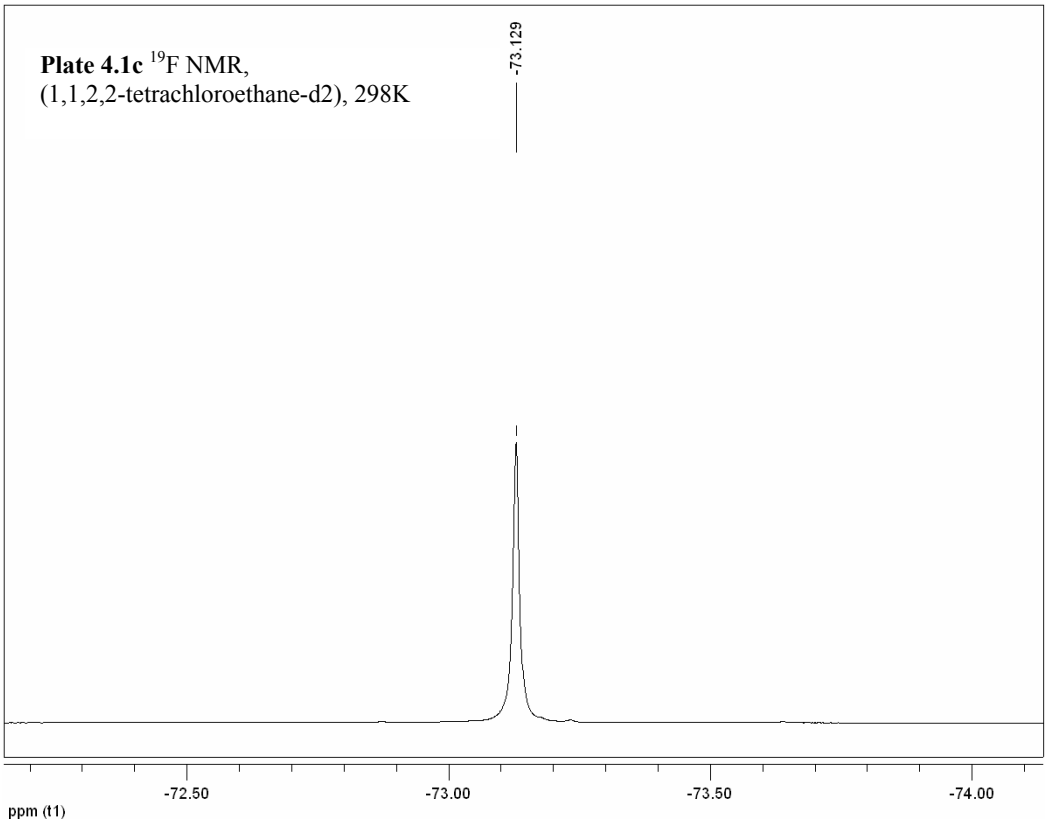

Plate 4.1c ^{19}F NMR, (1,1,2,2-tetrachloroethane-d2), 298K

Plate 4.2a, ^{1}H NMR, $CDCl_3$, 298K

Me-(-)Epicatechin-(*S*)-MTPA

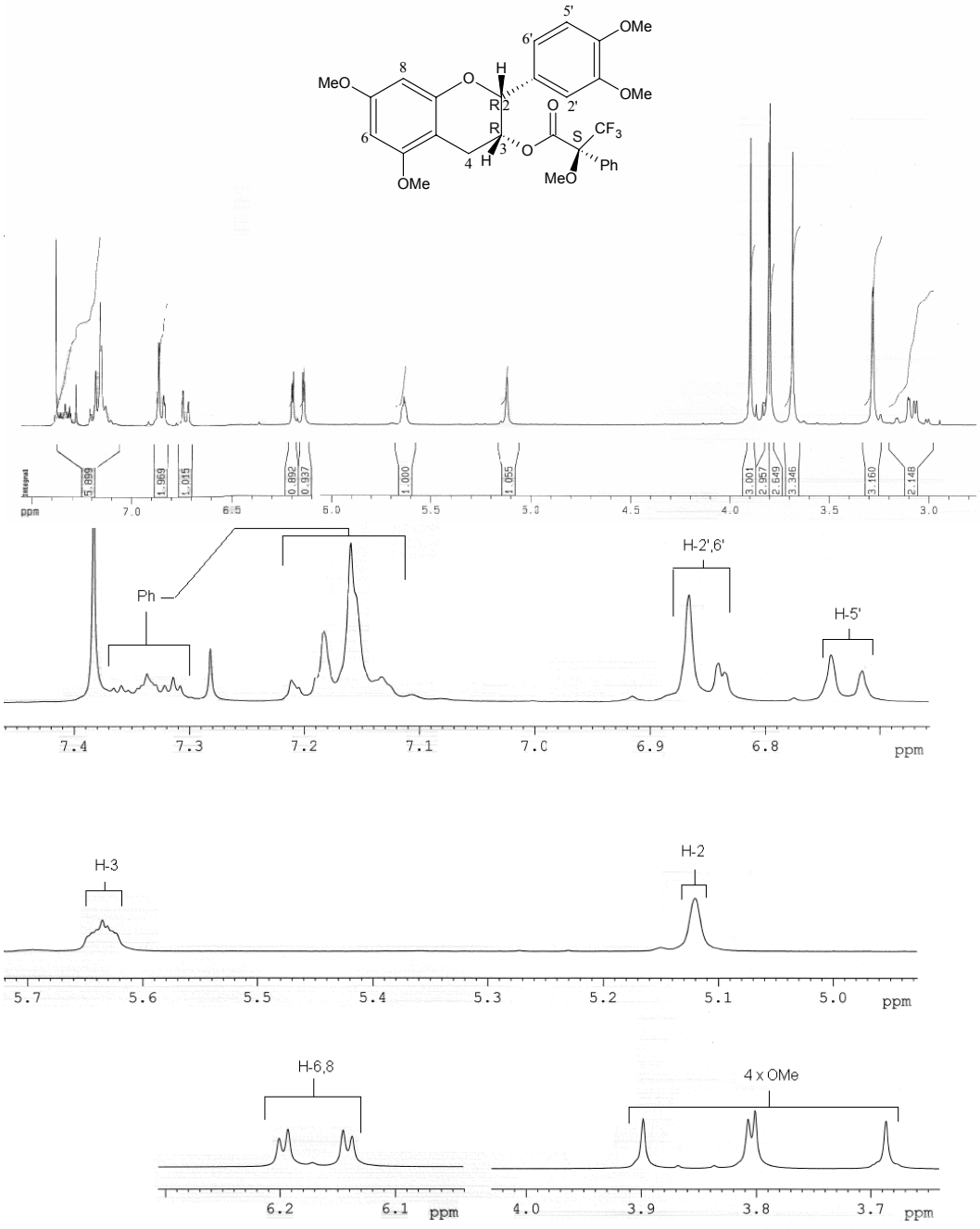

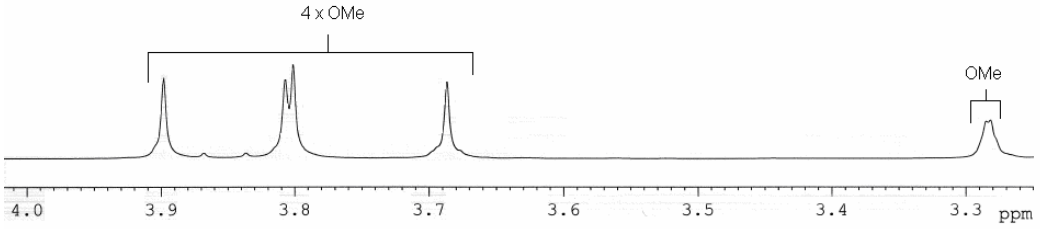

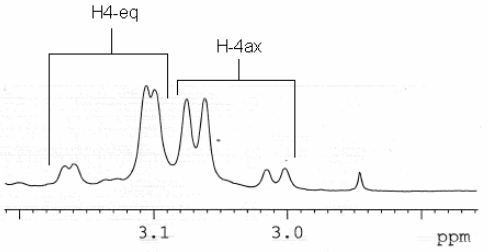

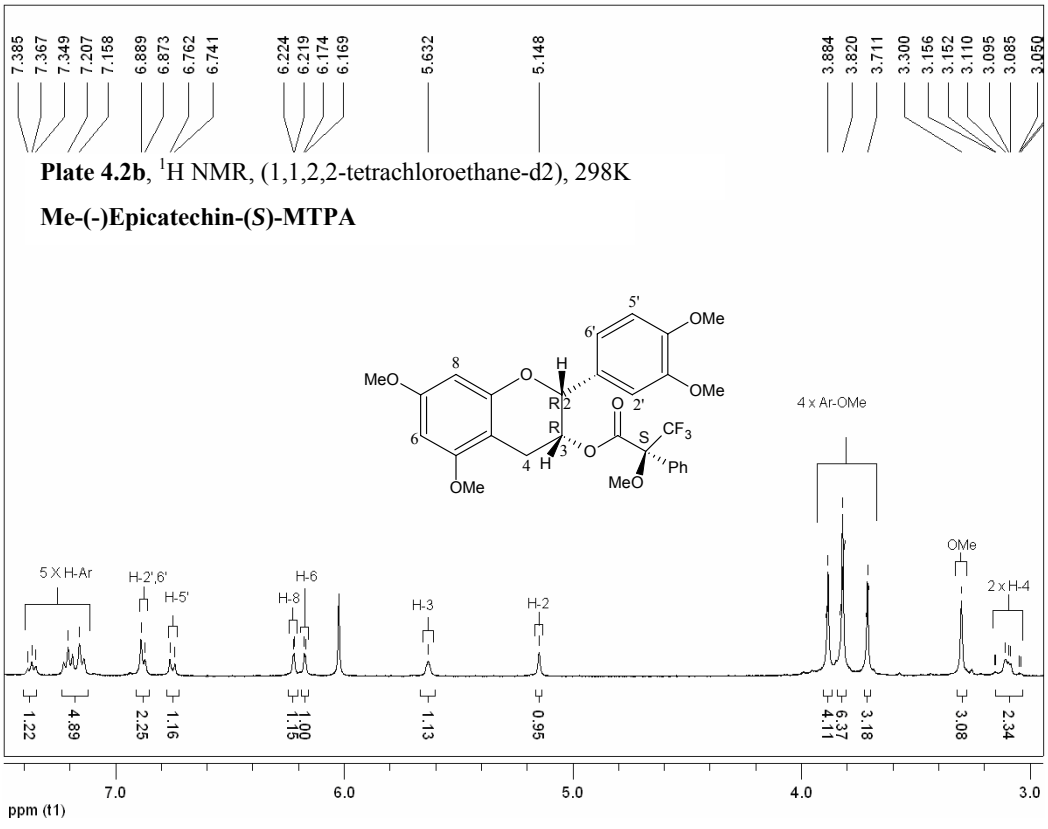

Plate 4.2b, ^{1}H NMR, (1,1,2,2-tetrachloroethane-d2), 298K

Me-(-)Epicatechin-(*S*)-MTPA

Plate 4.2c, ^{19}F NMR,
(1,1,2,2-tetrachloroethane-d2), 298K

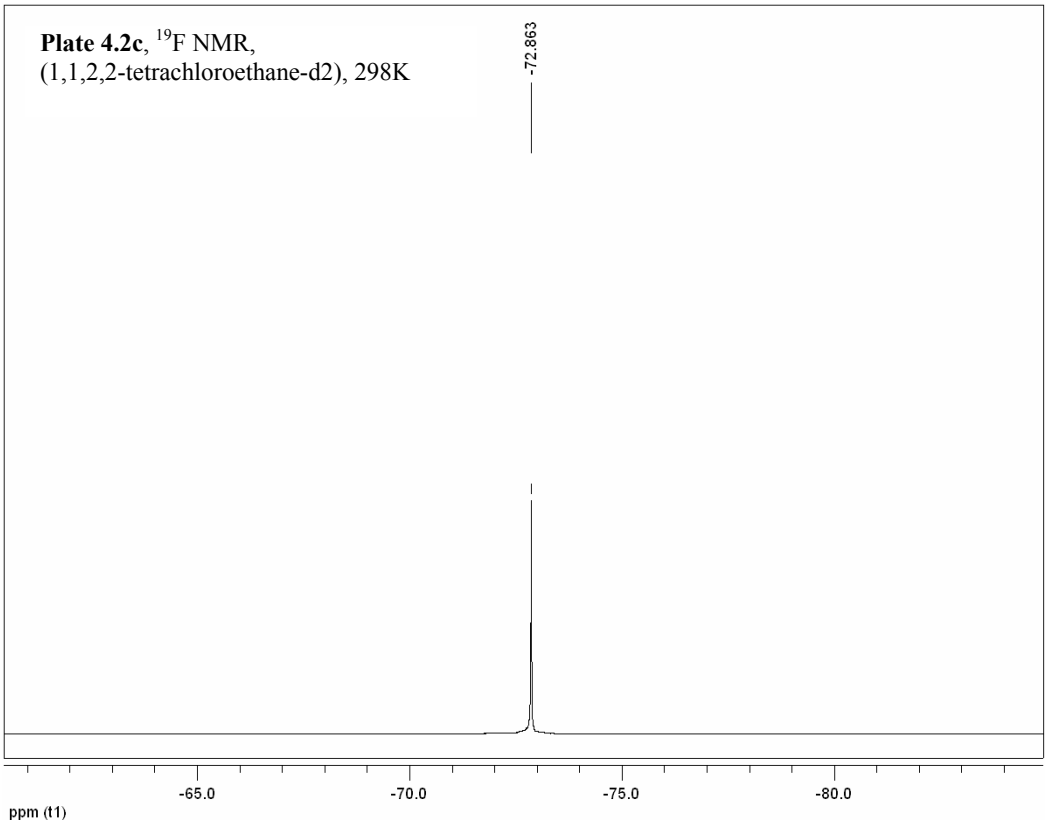

Chapter 5
CFTA

Literature

Molecular design leading to new more efficient chiral derivatizing agents.

The determination of enantiomeric excess (*ee*) of chiral molecules is one of the most important and indeed, indispensable, processes in modern organic chemistry, especially in the theoretical and practical study of asymmetric synthesis. Many methods for *ee* determination are known which involve NMR, GC, LC, and polarimetric techniques[263]. Among those, the method of derivatization of a sample of interest with a chiral derivatizing reagent and determination of optical purity through NMR spectroscopic quantization of the derived diastereomers is a very useful and practical technique. The Mosher's method, using MTPA, is currently the most widely employed for alcohols and amines because of the convenience in handling and the general availability of both ^{19}F and ^{1}H NMR probes.

However, many instances have been reported where *ee* determination by this method failed because of insufficient reactivity of MTPA chloride (MTPA-Cl) toward some secondary alcohols due to inherent steric crowding of the MTPA structure and/or because of very small ^{1}H and ^{19}F chemical shift differences between the two MTPA diastereomers[264].

In order to develop efficient *ee*-determining reagents potentially superior to MTPA, some multifunctional compounds were rationally designed by Takeuchi *et al*.[265,266] leading to the selection of α-cyano-α-fluorophenyl-acetic acid (CFPA) and α-cyano-α-fluoro-p-tolyl-acetic acid (CFTA) (**Fig. 5.1**) as CDA's.

[263] (a) Morrison J. D., *Assymetric Synthesis*, Academic Press, NY, **1983**, *vol.1*, (b) Parker D., *Chem. Rev.*, **1991**, *91*, 1441.
[264] Svatos A., Valterova I., Saman., Vrkoc J., *Collect. Czech. Chem. Commun.*, **1990**, *55*, 485.
[265] Takeuchi Y., Itoh N., Satoh T., Koizumi T., Yamaguchi K., *J. Org. Chem*., **1993**, *58*, 1812.
[266] Takahashi T., Fukuishima A., Tanaka Y., Takeuchi Y., Kabuto K. and Kabuto C., *Chem. Comm*., **2000**, 788-789.

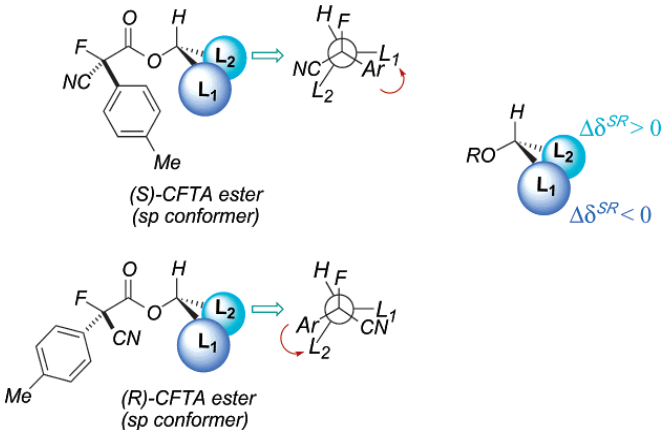

Figure 5.1.

In the design of new reagents which might exceed the capability of, but still preserve the merits of MTPA, it was found to be decisive for the molecule to have a single fluorine atom[267], as well as a phenyl group or the steric equivalent[268], directly attached to the chiral center. The third substituent on the α-carbon should have suitable steric and electronic characteristics, namely, the substituent should have no protons and an effective steric bulkiness significantly different from that of both the F and the Ph substituents, while also having a highly electronegative character[269]. They believed that this α-carbon substitution pattern would result in a molecule sufficiently reactive and it would induce, after diastereomer formation, large magnetic nonequivalence between a pair of diastereomers. It is also noted that the reagent should preferably be crystalline for convenience in handling, although CFTA and it's derivatives are oily liquids at room temperature.

From their NMR investigations of the analogous diastereomeric derivatives it was claimed that the chemical shift differences ($\Delta\delta^{SR}$ values) for each pair of diastereomers for these CFPA and CFTA ester derivatives were approximately five times greater in ^{19}F NMR spectra and two times greater in ^{1}H NMR spectra than those of MTPA esters.

[267] Takeuchi Y., Ogura H., Ishii Y., Koizumi T., *J. Chem. Soc. Perkin Trans. 1*, **1989**, 1721.
[268] Takeuchi Y., Ogura H., Ishii Y., Koizumi T., *Chem. Pharm. Bull.*, **1990**, *38*, 2404.
[269] Takeuchi Y., Itoh N., Koizumi T., *J. Chem. Soc., Chem. Commun*., **1992**, 1514.

Results & Discussion

The CFTA ester derivatives have proven to be significantly superior for *ee* determinations when compared to the corresponding MTPA derivatives, particularly in compounds having remotely disposed chiral centers.

In both CFTA and CFPA compounds the *syn* periplanar (*sp*) alignment of the fluorine and C=O group is energetically preferred to the *anti* periplanar (*ap*) conformation (**Fig. 5.2.1, 5.2.2**), which is confirmed by X-ray analysis and *ab initio* calculations[266]. The X-ray data of an aminoindanol ester crystal (**Fig 5.2.1**) display the CFTA moiety in the preferred *sp* conformation[270], with a dihedral angle of -47° between the fluorine and the carbonyl group. As mentioned in the previous chapter, the carbinyl H and the carbonyl also prefer a *syn* conformation for esters.

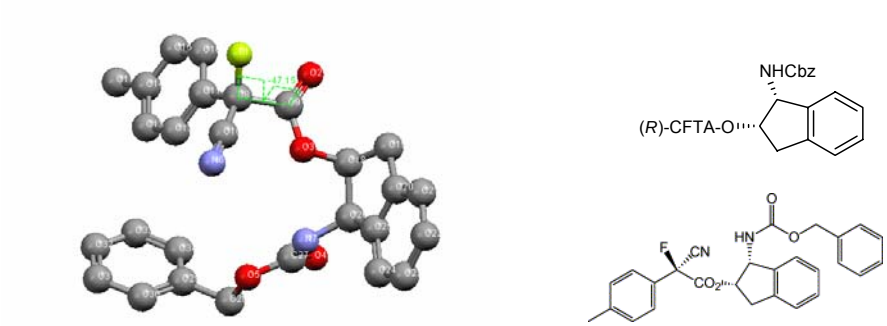

Fig 5.2.1 (1*R*,2*S*)-*N*-Carbobenzyloxy-*cis*-1-amino-2-indanyl-(*S*)-2-cyano-2-fluoro-2-*p*-tolylacetate

Research objectives

- Optimal derivitization of a natural, homochiral flavanoid by the recently developed CFTA agent, superior to (α-methoxy-α-trifluoromethyl phenylacetic acid) MTPA in reactivity and absolute stereochemistry determination of secondary alcohols and amides,[270, 271] is investigated spectroscopically and on a B3LYP/6.311G level of theory.
- The optically pure (-)-epicatechin-(*R*, *S*)-CFTA esters are prepared by known methods[272, 273] to probe the conformational behavior of the CFTA moiety with the magnetic and spatial influence of the contiguous epicatechin B-ring. The close proximity of the B-ring is intended to test and establish the proposed[272]

[270] Fujiwara T., Sasaki M., Omata K., Kabuto C., Kabuto K. and Takeuchi Y., *Tetrahedron: Asymmetry*, **2004**, *15*, 555.
[271] Takeuchi Y., Itoh N., Kawahara S., Koizumi T., *Tetrahedron*, 1993, 1861.
[272] Takeuchi Y., Fujisawa H., Noyori R., *Org. Lett*., **2004**, *6*, 4607.
[273] Takeuchi Y., Itoh N., Satoh T., Koizumi T., Yamaguchi K., *J. Org. Chem*., **1993**, *58*, 1812.

syn/anti-periplanar (*sp*/*ap*) rotational isomerism of the CFTA moiety in solution.

- The preference of the *sp* conformer over the *ap* conformer in solution is rationalized and evaluated on the flavan-3-ol skeleton.
- In addition, hyperconjugative molecular orbitals and natural bonding orbitals (NBO) are invoked to resolve the prevailing conformational isomerism of the CFTA derivatives.
- Investigate the exceptionally large $\Delta\delta^{(SR)}$ ^{19}F NMR value observed for (-)-epicatechin-(*R*),(*S*)-CFTA diastereoisomers.

^{1}H and ^{19}F NMR spectra (0.05M conc.) of the synthesized (-)-epicatechin-(*R*),(*S*)-CFTA diastereoisomers confirm the superior $\Delta\delta^{(SR)}$ values claimed[273] for CFTA compared to the identical MTPA esters (**Fig.5.2.2**). A relatively low concentration of 0.05M was selected to record the IR and NMR data as to minimize possible influence on the rotational isomerism of the CFTA esters by having a concentrated solution when obtaining these spectral data. The $\Delta\delta^{(SR)}$ ^{19}F is hitherto the largest reported for the CFTA reagent[273]. To our knowledge, this reagent has not been evaluated as a chiral derivatizing reagent (CDA) on any of the large group of biologically important flavonoid compounds. Epicatechin, as a highly regarded anti-oxidant[274, 275] and biologically active flavonoid[276], together with the A/E conformational equilibrium of the B-ring, proved to be an ideal choice to evaluate and establish CFTA as a CDA of choice for flavonoids in general. In addition, it establishes the utilization of the ^{19}F probe, as a reliable and successful tool for *ee* determinations in flavonoids in general.

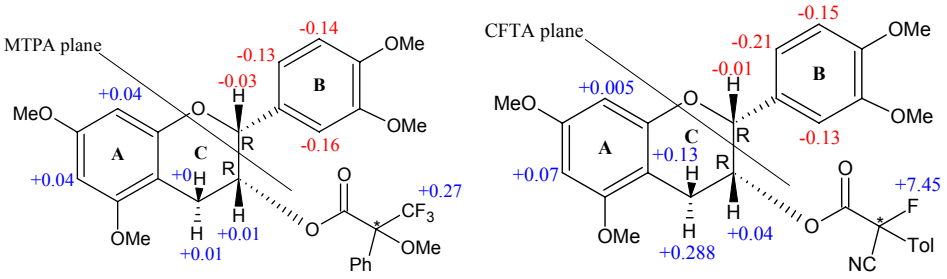

Figure 5.2.2 $\Delta\delta^{(SR)}$ ^{19}F, ^{1}H of the synthesized (-)-epicatechin-MTPA and –CFTA diastereomeric pairs.

[274] Yilmaz Y. and Toledo R.T., *J Agric Food Chem*. **2004**, *28*, 255.
[275] Sang S., Tian S., Wang H., Stark R.E., Rosen R.T. and Yang C.S., Ho C.T., *Bioorg Med Chem*., **2003**, *5*, 3371.
[276] Lambert J. D., Rice J. E., Hong J., Houand Z. and Yang C. S., *Bioorganic & Medicinal Chemistry Letters*, **2005**, *15*, 873.

A review on conformational properties of α-mono-heterosubstituted carbonyl compounds show the *syn* isomer to dominate marginally over the *gauche* (*ap*) isomer for α-fluoroacetate (FH_2COOMe)[277] which resembles the CFTA structure in terms of the α-fluoroacetate structure. Here the higher carbonyl frequency of 1777cm^{-1} was assigned to the *syn* isomer and the 1752 cm^{-1} frequency component to the *ap* isomer using chloroform as solvent.

B3LYP/6-311+G(d,p) calculations confirm the *syn/anti* as major isomers and show the *ap* isomer to be favored[278] by a very small margin (0.1 kcal/mol). The *syn* isomer is the more polar isomer and is stabilized in more polar solvents like chloroform.

A semi-empirical/PM3 energy profile of the rotation around the F-C-C=O bond ((*S*)-CFTA-Me) confirm the *sp* and the *ap* isomers as the dominant ones with a relative energy difference of 1.9 kcal/mol in favour of the *ap* isomer (**Fig. 5.3**). High level B3LYP/6.31G** re-optimizations of the selected semi-empirical/PM3 (*S*)-CFTA-Me structures show the *sp* isomer to be favored by 0.4 kcal/mol. The favoring of the *sp* isomer in the B3LYP calculations, as opposed to the SE method where the *ap* isomer is preferred, suggests a fair degree of electronic stabilization involved in CFTA esters because SE methods restrict calculations to valence electrons only (electrons associated with the core are ignored).

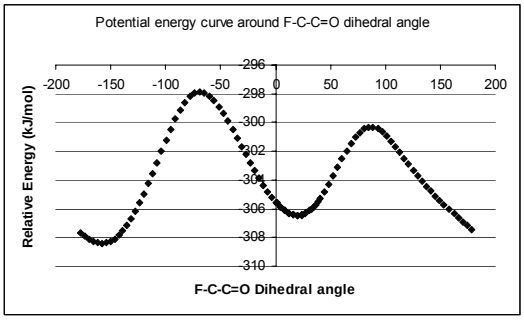

Figure 5.3 (SE/PM3 calculated energy profile of (*S*)-CFTA-Me)

The diluted (0.05M, 0.01M) IR spectra of optically pure permethylated (-)-epicatechin-(*R*)-CFTA and (-)-epicatechin-(*S*)-CFTA esters in $CHCl_3$ and CCl_4 both show the *sp* conformational isomer as the preferred higher frequency component (peak 1) of the carbonyl band (**Fig 5.4**.). Peculiarly, this is in direct contrast to the

[277] Olivato P.R., Rittner R., *Rev. Heteroatom Chem.*, **1996**, *15*, 115.
[278] Abraham R. J., Tormena C. F., Rittner R., *J. Chem. Soc. Perkin Trans.* 2, **2001**, 815

MTPA *sp* carbonyl frequency (**Fig. 4.20**) where the *sp* conformer has a lower IR frequency. IR spectra was taken for the *R* and *S* esters in $CHCl_3$ and CCl_4 in 0.05M and 0.01M concentrations over a 12hr. period at a constant room temperature. As there was insignificant difference found between the two chosen concentrations, only the 0.05M concentrations are displayed (**Appendix 5.1**).

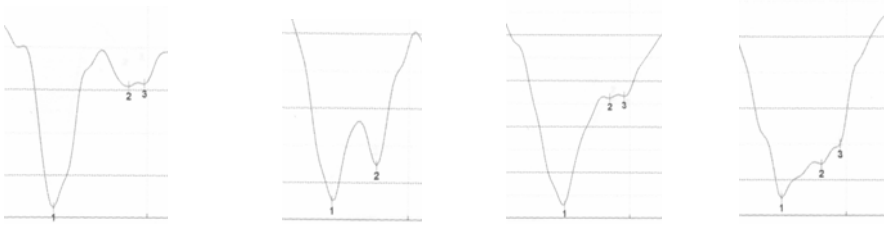

(*R*) ester CCl_4 (*S*) ester CCl_4 (*R*) ester $CHCl_3$ (*S*) ester $CHCl_3$

Figure 5.4

Comparison of the deconvoluted carbonyl band in the two diastereomers point out the influence of the B-ring on the rotational isomerism ratio of the CFTA moiety. In the *sp* conformer of the (-)-epicatechin-(*S*)-CFTA ester the tolyl group is turned towards the B-ring reducing the preference for this isomer. For the (*S*)-ester, in both solvents, the dominance of the *sp* is greatly reduced compared with the *ap* conformer (bands 2, 3). This is also reflected in the calculated comparative energy difference between the (-)-epicatechin-(*S*)-ester *ap*/*sp* conformers where the *ap* isomer is favored by 1.6 kcal/mol (**Table 5.1** *end of chapter*). This can be explained by the increased steric interaction between the tolyl-group and the B-ring in the *sp* conformation of CFTA for the epicatechin-(*S*)-ester.

The polar and non-polar solvents selected do not have a noteworthy effect on the *sp*/*ap* equilibrium of these esters. However, in $CHCl_3$ there are three carbonyl bands present, which are not always observed in CCl_4 for the (*S*) ester, illuminating the existence of another stable conformer closely related to the *ap* conformer (**Appendix 5.1**).

IR spectra of similar α-fluoro carbonyl structures also show three carbonyl bands that correspond to the *syn*, *anti* and *gauche* conformations[277]. It should be noted that the integral or intensities of the deconvoluted carbonyl frequency components representing the *sp* and *ap* conformers, although an invaluable tool, cannot be taken as

accurate ratio of the two isomers in solution, because the relative carbonyl molar absorption coefficients can be different for the two conformers[279]. Thus, firstly, the IR data confirms the calculated (RB3LYP/6.311G) carbonyl stretching frequencies (**Table 5.1, 5.2.**) with a higher frequency for *sp* isomer as the favored isomer over the *ap* isomer which has a lower frequency. Secondly, it confirms the proposed model for the CFTA agent where an F-C-C=O *syn*-periplanar conformation is presented as the only workable model to explain the observed shielding effects of the α-tolyl-group on the substrate.

To negate the influence of the B-ring on the CFTA moiety, all calculations (RB3LYP/6.311G) are also repeated for a model structure with the B-ring absent (**Fig. 5.5**). These calculations include conformational searches, geometry optimizations, NMR, molecular orbital, frequency calculations and Natural Bond Orbital analysis (NBO)[280] for the *sp/ap* (*R*) and (*S*) esters (structures **5.5-5.8**).

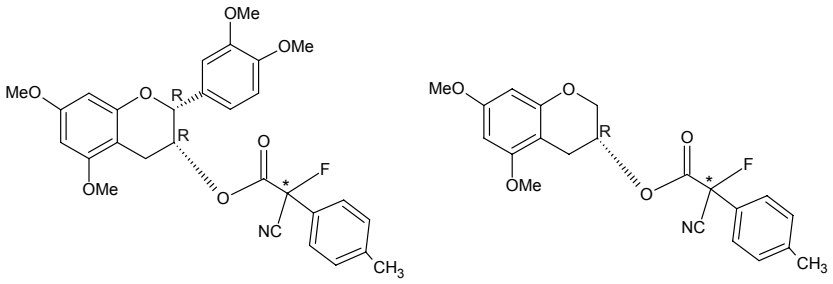

5.1 (-)-epicatechin-(*R*)-*sp*-CFTA
5.2 (-)-epicatechin-(*R*)-*ap*-CFTA
5.3 (-)-epicatechin-(S)-*sp*-CFTA
5.4 (-)-epicatechin-(S)-*ap*-CFTA

Calculation results,
See Table 5.1, Scheme 5.3

5.5 model-(*R*)-*sp*-CFTA
5.6 model-(*R*)-*ap*-CFTA
5.7 model-(S)-*sp*-CFTA
5.8 model-(S)-*ap*-CFTA

Calculation results,
See Table 5.2, Scheme 5.4

Figure 5.5 (structures 5.1-5.8)

The model compound provides a structure to evaluate the CFTA ester free from the possible steric and electronic implications of a contiguous aryl group, and consequently provides a opportunity to evaluate the influence of this B-ring present in flavan-3-ol related structures. For the *R* and *S* esters (**5.5-5.8**) of the model structure, the *sp* conformer is favored by 0.4 kcal/mol (**5.5-5.6**) and 1.2 kcal/mol respectively (**5.7-5.8**) (**Table 5.2**).

[279] Freitas M. P., Tormena C. F., Rittner R. and Abraham R. J., *Spectrochimica Acta Part A*, **2003**, *59*, 1783.
[280] F. Weinhold, in *The Ensyclopedia of Computational Chemistry (ed. Schleyer, P. v. R.)*, 1792-1811.

Recently, it was demonstrated conclusively, that vicinal hyperconjugation is the only factor controlling the conformation between vicinal groups of a central C-C bond[281]. This is conveniently rationalized by orbital overlap between a filled π like bonding or non-bonding orbital (bonds) and an empty or nearly empty anti-bonding π like orbital (anti-bonds) on the adjacent carbon atoms. Only these orbitals have the symmetry necessary for hyperconjugative orbital interaction between vicinal carbons.
Vicinal σ/σ* (sp) hybridized bonding orbitals are anti-symmetric towards a local symmetry plane and are therefore termed π like orbitals.

A systematic evaluation of the MOs of the *sp* and *ap* conformations (**5.5, 5.6, Table 5.0**) provided four orbitals with the largest energy difference (ΔE = *ap*-*sp*) for HOMO and LUMO's respectively, which can possibly play a role in the preferential stabilization of the *sp* conformer. These are, LUMO (ΔE = -0.299 eV), LUMO +6 (ΔE = -0.288 eV), HOMO -5 (ΔE = -0.0651 eV) and HOMO -6 (ΔE = -0.0870 eV).
LUMO, LUMO+6 with the highest negative ΔE values (more positive energy, **Scheme 5.1**), are in line with these molecular orbitals being part of the hyperconjugatively formed MO's in the *sp* conformer, and being virtually empty MO's. The LUMO display a high degree of π* symmetric character over the central α-C-C antibond and the LUMO+6 mainly carbonyl π* character (**Fig. 5.6**) on the CFTA moiety. Many of the lower lying LUMO's having negative eigenvalues is in line with notable antibond electron population. LUMO+6 shows a higher population and LUMO a lower population in the *sp* isomer.

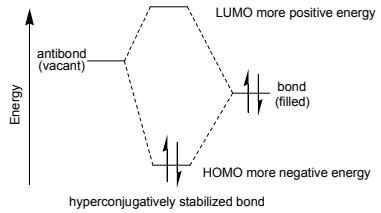

Scheme 5.1.

[281] V. Pophristic, L. Goodman, *Nature*, 2001, **411**, 565

	MO:	Eigenvalues:	E(eV):		MO:	Eigenvalues:	E(eV):		ΔE *ap-sp* (eV)
		Structure 5.5				**Structure 5.6**			
-10	91	-0.33851	-9.21146		91	-0.33821	-9.20316		-0.0083
-9	92	-0.33515	-9.11984		92	-0.33674	-9.16303		0.04319
-8	93	-0.33444	-9.10061		93	-0.33356	-9.07653		-0.02408
-7	94	-0.33146	-9.0196		94	-0.32549	-8.85706		-0.16254
-6	95	-0.31174	-8.4829		95	-0.31493	-8.56975		**0.08685**
-5	96	-0.29164	-7.936		96	-0.29403	-8.00109		**0.06509**
-4	97	-0.27401	-7.4563		97	-0.27284	-7.42443		-0.03187
-3	98	-0.26154	-7.11677		98	-0.26016	-7.07933		-0.03744
-2	99	-0.25382	-6.90676		99	-0.2506	-6.81921		-0.08755
HOMO-1	100	-0.21996	-5.98542		100	-0.21819	-5.93726		-0.04816
HOMO	101	-0.21289	-5.79291		101	-0.21141	-5.75267		-0.04024
LUMO	102	-0.04819	-1.31124		102	-0.03719	-1.01191		**-0.29933**
LUMO+1	103	-0.01737	-0.47264		103	-0.01557	-0.42371		-0.04893
2	104	-0.00264	-0.0719		104	-0.00929	-0.25288		0.18098
3	105	0.00632	0.17204		105	-0.00562	-0.15297		0.32501
4	106	0.01198	0.32594		106	0.01309	0.35621		-0.03027
5	107	0.01262	0.34351		107	0.01452	0.39499		-0.05148
6	108	0.02924	0.79566		108	0.03982	1.08343		**-0.28777**
7	109	0.07483	2.0361		109	0.07427	2.02108		0.01502
8	110	0.08647	2.35286		110	0.08561	2.32953		0.02333
9	111	0.09316	2.53514		111	0.09267	2.52161		0.01353
10	112	0.09386	2.55408		112	0.09634	2.62156		-0.06748

Table 5.0

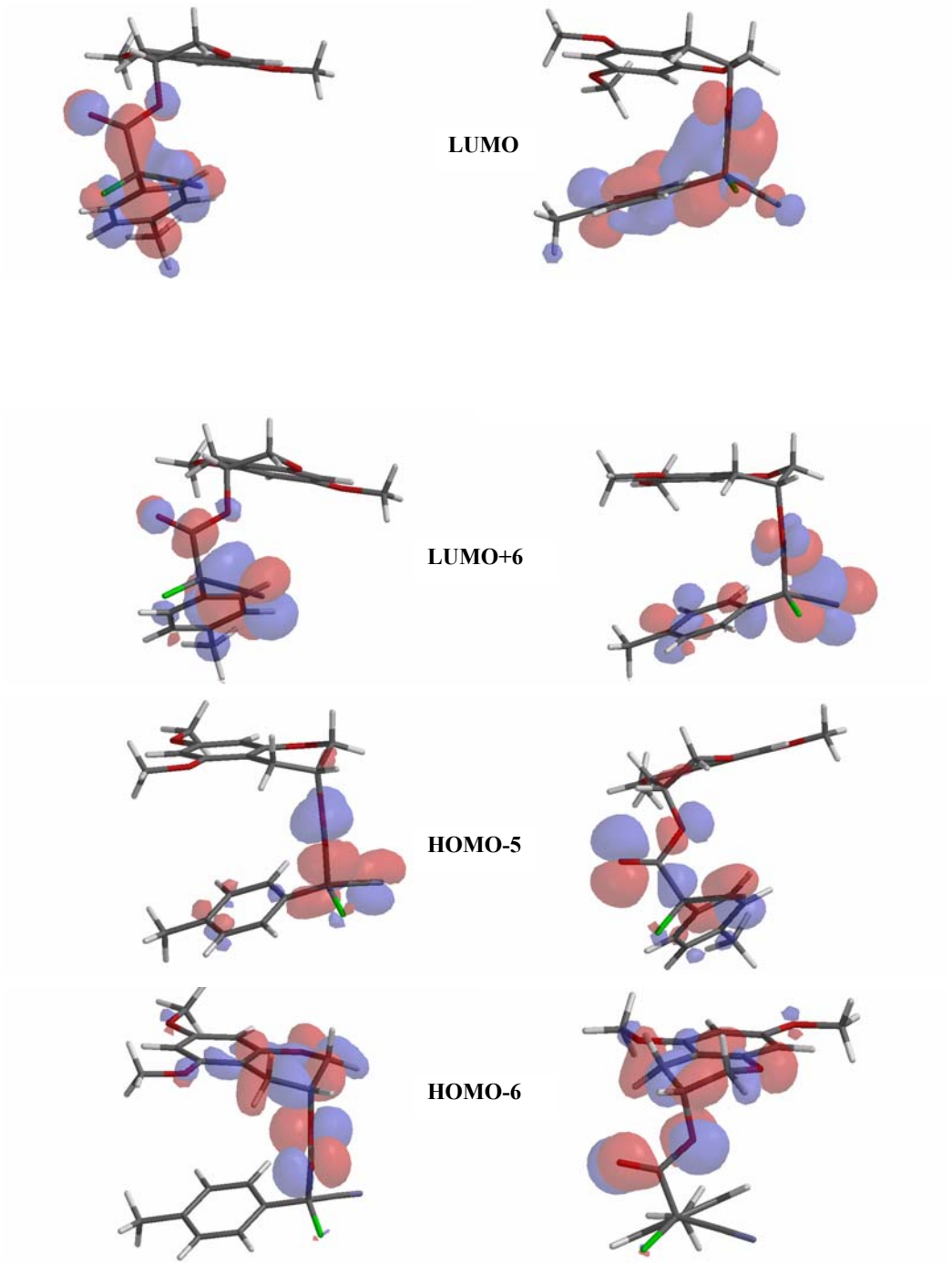

Figure 5.6.

The stabilizing HOMO-5, -6 have a lower relative energy and more negative eigenvalues and thus are more populated in the *sp* conformer (ΔE = +). These

HOMO-5, -6 contain carbonyl, ester oxygen lone pair and α-C-C bond π-components on the CFTA moiety (**Fig. 5.6**).

NBO analysis reports a strongly delocalized structure with no single Lewis structure possible. Total core, lone pair and bond occupancy of 97.94% and a total Rydberg and antibond occupancy of 2.06% for the *ap* and *sp* isomers. This antibond occupancy is in line with highly delocalized structure.

Mulliken atomic charges show the carbonyl carbon and oxygen with a more positive charge in the *sp* isomers in line with increased electron π delocalization to the α-carbon, which as a result have a more negative charge (see **Scheme 5.3, 5.4 and Table 5.1, 5.2**).

NBO analysis (**Appendix 5.2**) provides the means to analyze the hyperconjugative interactions in more detail than is possible by molecular orbitals.

An individual hyperconjugative interaction is expressed as a charge (electron) transfer between selected bonds and antibonds, allowing specific hyperconjugative interactions that influence structural preference to be pinpointed. Although it was expected to find a shorter α-C-C bond for CFTA in the *sp* isomer, if hyperconjugation is present, it was shown that central C-C bond lengthening is crucial in eliminating vicinal repulsive interactions in rotational isomers. It was conclusively demonstrated that the well-known staggered conformation of ethane is brought about by hyperconjugation and not vicinal steric factors as previously thought[281]. These steric interactions are nullified by central C-C bond lengthening, effectively eliminating any energy increase due to these steric interactions. Thus, it follows that the α-C-C bond length and the magnitude of the bond length difference is not a reliable indication of the magnitude of hyperconjugation between the vicinal groups of the two dominant CFTA isomers.

In the absence of α-C-C bond shortening to use as a reliable indication of vicinal hyperconjugation, the $\sigma^*_{\alpha\text{-C-CN}}$ and the $\sigma^*_{\alpha\text{-C(tol)}}$ NBO (**Table 5.3**) bond populations is utilized and show significant increase which is reflected in the increased positive Mulliken atomic charge found for the *sp* carbonyl carbon due to π like donation into these anti-bonds. **Appendix 5.2** explains in detail how NBO analysis is utilized to pinpoint vicinal hyperconjugative interactions.

Table 5.3. B3LYP/6.311G **NBO SUMMARY** (for structures **5.1-5.8** and (*S*)-CFTA-Me)

$\sigma_{C\text{-}O}$	less populated in *sp* isomer
$\sigma^*_{C\text{-}O}$	more populated in *sp* isomer
$\sigma_{C=O}$	no change in population
$\sigma^*_{C=O}$	less populated in *sp* isomer
$\pi_{C=O}$	more populated in *sp* isomer
$\pi^*_{C=O}$	less populated in *sp* isomer
$\sigma_{\alpha\text{–}C\text{-}C}$	less populated in *sp* isomer
$\sigma^*_{\alpha\text{–}C\text{-}C}$	more populated in *sp* isomer
$\sigma_{C\text{-}F}$	more populated in *sp* isomer
$\sigma^*_{C\text{-}F}$	less populated in *sp* isomer
$\sigma_{\alpha\text{–}C\text{-}CN}$	less populated in *sp* isomer
$\sigma^*_{\alpha\text{–}C\text{-}CN}$	more populated in *sp* isomer
$\sigma_{\alpha\text{–}C\text{-}tol}$	less populated in *sp* isomer
$\sigma^*_{\alpha\text{–}C\text{-}tol}$	more populated in *sp* isomer
$LP_{C=O}$	less populated in *sp* isomer
LP_{F}	less populated in *sp* isomer

However, this donation do not originate from the π C=O bond as it shows a higher calculated and experimental IR frequency (**Fig. 5.4**) in the *sp* conformer, where a weaker bond and lower frequency is expected. The π C=O bond also show higher NBO population in the *sp* conformer. On the other hand, there could be some π-symmetric overlap with the carbonyl oxygen lone pairs, which display a reduced negative charge in the *sp* conformer together with a notably less populated carbonyl oxygen lone pair p orbital (**Table 5.3**). As a result, the α-carbon show a more negative Mulliken atomic charge in the *sp* isomer which is in line with vicinal hyperconjugation across the α-C-C bond. This is reflected in the LUMO with large α-C-C π* components, accompanied by energy increase in the *sp* conformer (**Fig 5.6**), resulting from hyperconjugative stabilization (**Scheme 5.1**).

Vicinal C-F anti-bond and C-O bond orbital overlap is another hyperconjugative interaction operational in this moiety. The ester bond O-C=O, show a $\sigma_{C\text{-}O}$ population decrease, which leads to the substantial lengthening of this bond calculated for the *sp* conformation (**5.1-5.8, Scheme 5.3, 5.4**). The ester bond is also the bond with the largest calculated length change between the *ap* and *sp* isomers of CFTA structures.

This can be attributed to the $\sigma_{C\text{-}O}$ ester bond orbital overlap with the vicinal $\sigma^*_{C\text{-}F}$ orbital analogues to the configuration found for 1,2-difluoroethene, which is responsible for it's well-known *cis* effect (**Figure 5.7**) [282].

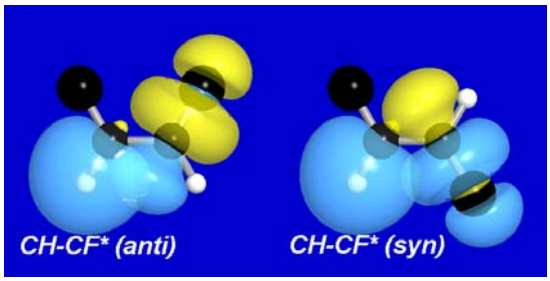

Figure 5.7

Here, the greater overlap of CH-CF* (*anti*) relative to the *syn* configuration greatly stabilizes the *cis* conformation of 1,2-difluoroethene. This interaction is also in line with the small C=O//C-F calculated dihedral angle found for all the CFTA derivatives due to such stabilizing overlap. The smaller the angle the greater amount of overlap possible. The same effect is observed for 1,2-difluoroethane (**Scheme 5.2.a**) (**Appendix 5.2**) where the best donor bond ($\sigma_{C\text{-}H}$) is placed *anti* to the best acceptor bond ($*\sigma_{C\text{-}F}$)[283].

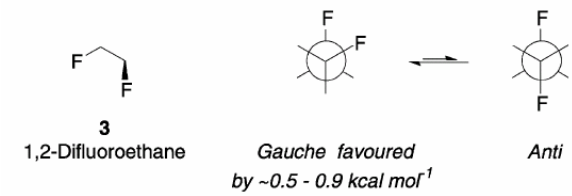

Scheme 5.2.a The gauche preference for 1,2-difluoroethane

Natural bond orbital deletion calculations (**Appendix 5.2,** textbook example) show that whereas the *gauche* preference arises from vicinal hyperconjugative interaction between *anti* C-H bonds and C-F* antibonds, the *cis* C-H/C-F* interactions are substantial (25% of the *anti* interaction). The established significantly >60° FCCF dihedral angle for the equilibrium conformer can then be rationalized in terms of the hyperconjugation model alone by taking into account both *anti* interactions that maximize near 60° and the smaller *cis* interactions that maximize at a much larger dihedral angle. This explanation does not invoke repulsive forces to rationalize the 72° equilibrium conformer angle. The relative minimum energy for the *trans* conformer is the consequence of a balance between decreasing hyperconjugative

[282] N. C. Craig and E. A. Entemann, *J. Am. Chem. Soc.*, **1961**, *83*, 3047.
[283] Goodman L., Gu H., and Pophristic V., *J. Phys. Chem. A* **2005**, *109,* 1223-1229.

stabilization and decreasing steric destabilization as the FCCF torsional angle approaches 180°. The torsional coordinate is predicted to be strongly contaminated by CCF bending, with the result that approximately half of the *trans* → *gauche* stabilization energy stems from mode coupling[283].

Another example of the role of this interaction in contributing to the greater stability of the *sp* conformer over the *ap* conformer is when CFTA is utilized in the determination the absolute conformation of α-amino esters[284] (**Scheme 5.2.b**). Here the *ap* and *sp* conformations are also the preferred conformations.

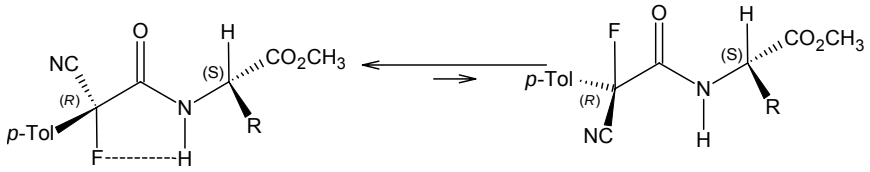

Scheme 5.2.b

In the formation of a CFTA amide diastereomer the *ap* conformation is now prefered over the *sp* conformer. Due to the F---H intereraction present in the *ap* conformer it overides the vicinal C-F anti-bond and C-N bond orbital overlap present in the the *sp* conformer. When such a F---H interaction is not possible like in the CFTA esters, the *sp* conformer is prefered again.

A better example is in the case of α-metoxy-α-phenylacetic acid (MPA)[285], where the MTPA CF_3-group is substituted by a hydrogen (**Scheme 5.2c**). Then, using the hyperconjugative model one would place the best acceptor orbital *anti* to the O-CO bond. The most electronegative group that then remains on the α-carbon, is the methoxy group and the σ*-OMe would be the best acceptor orbital and should be placed *anti* to the O-CO bond. This is indeed found to be the case for MPA where the OMe//C=O *sp* isomer is the preferred isomer by 0.6-1.0 kcal/mol.

Both of these charge transfer interactions discussed above are examples of hyperconjugation between different vicinal bonds and anti-bonds and together they contribute to the dominance of the *sp* conformer[281].

[284] Fujiwara T., Omata K., Kabuto K., Kabuto C., Takahashi T., Segawa M., Takeuchi Y., *Chem. Comm.*, **2001**, 2694.

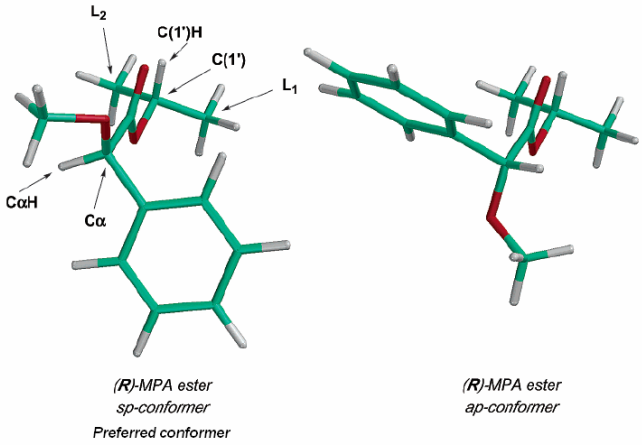

Scheme 5.2c

^{19}F NMR chemical non-equivalence has long been used as a probe for *ee* determinations with the Mosher reagent [285]. Optically pure permethylated (-)-epicatechin-(*R*)-CFTA and (-)-epicatechin-(*S*)-CFTA esters in $CDCl_3$ show a experimental ^{19}F chemical shift of -150.11 ppm and -142.67 ppm respectively, with $CFCl_3$ as internal standard. The HF/6-31+G(d) level used to calculate the fluorine chemical shift for structures **5.1-5.8** correspond the best with experimental values obtained for the epicatechin esters **(Table 5.1, 5.2)**. The RB3LYP/6.311G method is inadequate for accurate calculation of $\delta^{19}F$. For the (-)-EC-(*R*)-CFTA the experimental ^{19}F value is -150.11 ppm compared to the calculated value of -150.06 ppm where the (-)-EC-(*S*)-CFTA ester is -142.67 ppm and -133.06 ppm respectively (**Table 5.1**). Similar values are obtained for the 2*R*,3*R*-flavan-3-ol-CFTA compared to the (-)-EC-CFTA diastereomers, on the same level of theory (**Table 5.4**). The calculated $\delta^{19}F$ of the *sp* isomers are closest to the experimental values, which in turn is a time-weighted average between the *ap* and *sp* rotational isomers (**Table 5.1**). This further affirms the *sp* isomer as the energetically favored isomer in solution and show that this large $\Delta\delta^{(SR)}$ ^{19}F of the (-)-epicatechin-(*R*)-CFTA and (-)-epicatechin-(*S*)-CFTA esters can be reproduced theoretically.

Mosher suggested that the origin of the δ ^{19}F non-equivalence is due to the differential diamagnetic influence of the carbonyl group on the neighboring fluorine atom in the two diastereomers[285]. However, for these diastereomers with a $\Delta\delta^{(SR)}$ ^{19}F of 7.45 ppm, the diamagnetic influence of a carbonyl functionality is simply too small to result in

[285] Seco J. M., Quinoa E. and Riguera R., *Chem. Rev*. **2004,** *104*, 17-117.

such a large chemical shift difference. All previously prepared CFTA diastereomeric esters have a $\Delta\delta^{(SR)}{}^{19}F$ of ≤ 0.9 ppm[266].

One explanation might be the increased shielding of the F-atom by the epicatechin B-ring in the *sp* conformation of the (*R*)-CFTA moiety. However, then the epicatechin-(*S*)-CFTA *ap* isomer can experience the same shielding from the B-ring. Such an argument will not explain a $\Delta\delta^{(SR)}{}^{19}F$ of 7.45 ppm in these esters.

Further investigation into the origin of this large chemical shift difference for the epicatechin esters was conducted. The energies of second-order perturbation of Fock matrix elements, NBO $E^{(2)}$, which indicate the magnitude of interaction between the donors listed in **Table 5.5** and only the σ*(C-F) as the acceptor, was calculated. Structures (***R***)**-5.9,** (**S**)**-5.9** and **5.10** (**Fig. 5.8**) are the simplified model structures used to calculate these NBO interaction energies and their ^{19}F chemical shift. The geometry was optimized using the B3LYP/6.311G method. The nuclear magnetic shielding constants of the ^{19}F nuclei and NBO analysis was calculated using the GIAO (gauge-invariant atomic orbital, suited for NMR calculations) method at the HF/6.311G+(2d,p) level (**Table 5.4**). For structure **(*S*)-5.9** two *sp* conformations with similar calculated energies was selected and compared to the *ap* conformation.

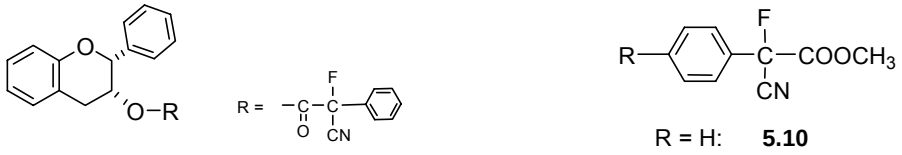

5.9 (2R,3R)--flavan-3-ol CFPA ester

These **(*S*)-5.9** *sp* conformations show an unexpected higher calculated energy compared to the *ap* conformer (**Table 5.4, Fig. 5.8**). This can be rationalized by possible interaction with the B-ring and the tolyl ring in the *sp* conformations of the (*S*)-CFTA esters. This is also evident in the experimental IR data (**Appendix 5.1**) where the epicatechin (*S*)-esters display a marked reduction in the intensity difference between the higher frequency *sp* conformer (peak 1) and the lower frequency *ap* conformers (peaks 2,3).

Table 5.4. Calculated relative energies and ^{19}F chemical shifts for **5.9** and **5.10**.

	(*R*)-5.9		**(*S*)-5.9**			**(*S*)-5.10**	
	ap	*sp*	*ap*	*sp*1	*sp*2	*ap*	*sp*
ΔE (kcal•mol^{-1})	+1.17	0	0	+0.26	+0.61	+0.48	0
δ_F^{calcd} (ppm)	–153.92	–151.41	–146.23	–145.96	–148.70	–155.62	–143.38
δ_F^{obs} (ppm)[a]	–150.12[b]		–142.67[c]			–144.43[d]	

[a] Synthesized (-)-epatechin CFTA esters (**Fig 5.2.2**), [b] (*R*), [c] (*S*), [d] CFTA-Me

It is demonstrated that electron donation to the local environment of a fluorine nucleus in alkyl fluoride systems decrease shielding and causes downfield shift instead of upfield shift which is expected from simple shift theory[286, 287, 288, 289].
Adock demonstrated the delocalization of electrons into the σ* orbital of the C-F bond (σ*C-F) as a major factor governing this 'inverse behavior'[290]. He used NBO analysis to pinpoint the electronic interactions taking place in a series of structurally similar norborn-7-yl fluorides. His work highlights the usefulness of NBO analysis in determining the origin of ^{19}F chemical shift. This decreased shielding is prevalent in the calculated δ_F of the *sp* conformers as shown in **Table 5.4**, where a more positive δ_F value is found in general compared to the *ap* conformers. This then indicate an increased donation into the σ*C-F bond of CFTA when in the *sp* conformation.

Although NBO analysis does not show a more populated σ*C-F bond (**Table 5.6**) like in MTPA for σ*C-CF_3, the calculated energies of second-order perturbation of Fock matrix elements, NBO $E^{(2)}$ (**Appendix 5.2**), which indicate the magnitude of interaction between the donors (**Table 5.5**), clearly indicate the consistent higher interaction energy between this σ*C-F bond and the σO^h-CO bond in all the *sp* conformations. It is also evident from this calculation data that the lone pair of the ester oxygen, n(O^h), have a significant interaction with the σ*C-F bond in the *sp* isomer. The *sp* isomer also have a consistently stronger interaction between σ*C-F bond and the central C^a-C^b bond. Together these interaction energies with the σ*C-F bond confirm the Negative Fluorine Hyperconjugation model[256].

[286] Adcock W., Abeywickrema AN.,*Tetrahedron Lett*., **1979**, *20*, 1809-1810.
[287] Brownlee R.T.C., Craik D.J., *Tetrahedron Lett*., **1980**, *21*, 1681-1684.
[288] Adcock W., Abeywickrema AN., *J. Org. Chem.*, **1982**, *47*, 2957-2966.
[289] Wiberg K.B., Zilm K.W., *J. Org. Chem.*, **2001**, *66*, 2809-2817.
[290] Adcock W., Lunsmann D., Peralta J.E., Contreras R.H., *Magn. Reson. Chem.*, **1999**, *37*, 167-172.

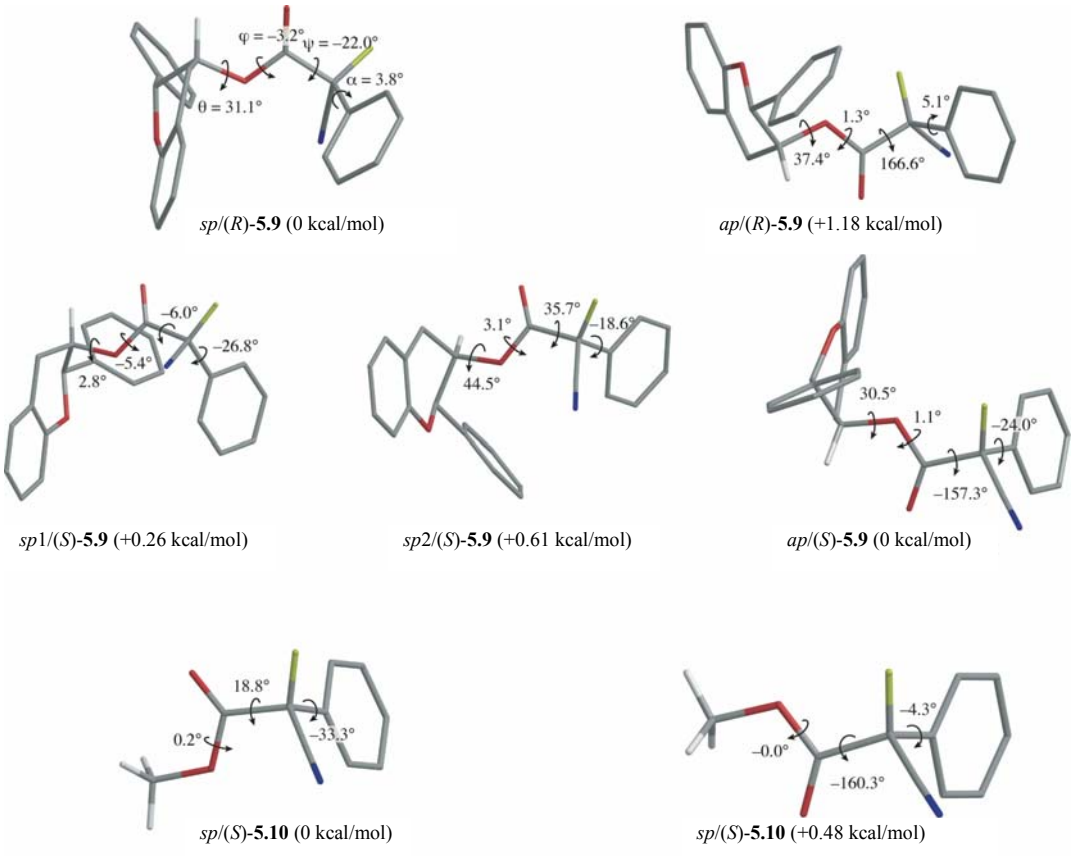

sp/(*R*)-**5.9** (0 kcal/mol)

ap/(*R*)-**5.9** (+1.18 kcal/mol)

*sp*1/(*S*)-**5.9** (+0.26 kcal/mol)

*sp*2/(*S*)-**5.9** (+0.61 kcal/mol)

ap/(*S*)-**5.9** (0 kcal/mol)

sp/(*S*)-**5.10** (0 kcal/mol)

sp/(*S*)-**5.10** (+0.48 kcal/mol)

Figure 5.8. Geometries and relative energies of CFTA ester structures **5.9** and **5.10**

Table 5.5. Selected NBO $E^{(2)}$ intraction energies (kcal/mol) with ***σC-F** in **5.9** and **5.10**.

	(*R*)-5.9		(*S*)-5.9			(*S*)-5.10	
	ap	sp	ap	sp1	sp2	ap	sp
$\sigma(C^a–C^b)$	–	0.69	–	0.80	0.69	–	0.76
$\sigma(C^b–O^h)$	–	**0.86**	–	**0.90**	**0.63**	–	**0.86**
$\sigma(C^b=O^i)$	–	–	**0.83**	–	–	**0.66**	–
$\pi(C^b=O^i)$	–	–	–	–	0.77	–	–
$\pi(C^c=N)$	6.94	6.80	7.01	6.83	7.01	7.02	6.97
$\sigma(C^d=C^e)$	0.67	0.62	0.59	0.55	0.65	0.66	–
$\pi(C^d=C^e)$	–	**0.84**	1.29	**1.82**	**0.88**	–	–
$\sigma(C^d=C^f)$	1.64	1.51	1.48	1.31	1.50	1.65	1.17
$\pi(C^d=C^f)$	–	–	–	–	–	–	**3.17**
$n(C^a)$	2.54	2.39	2.61	2.37	2.42	2.55	2.40
$n(O^h)$	–	0.64	–	0.78	–	–	0.63
$n(O^i)$	1.13	–	1.01	–	–	1.06	–
$\pi^*(C^b=O^i)$	–	–	0.99	–	–	0.69	–
$\pi^*(C^d=C^e)$	–	0.54	0.84	1.09	1.04	–	–
$\pi^*(C^d=C^f)$	–	–	–	–	0.57	–	1.38

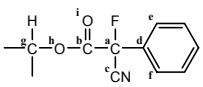

E^2 energies smaller than 0.5kcal/mol are not shown

Table 5.6. NBO occupancy number of C-F bonds, antibonds and lone pairs in **5.9** and **5.10**.

	(*R*)-5.9		(*S*)-5.9			5.10	
	ap	sp	ap	sp1	sp2	ap	sp
C–F(σ)	1.99184	1.99126 (–0.00058)	1.99136	1.99090 (–0.00046)	1.99084 (–0.00052)	1.99192	1.99100 (–0.00092)
F(CR)	1.99994	1.99994 (0.00000)	1.99994	1.99994 (0.00000)	1.99994 (0.00000)	1.99994	1.99994 (0.00000)
F(LP1)	1.99241	1.99239 –(0.00002)	1.99228	1.99228 (0.00000)	1.99242 (+0.00014)	1.99260	1.99241 (–0.00019)
F(LP2)	1.97570	1.97569 (–0.00001)	1.97655	1.97539 (–0.00116)	1.97632 (–0.00023)	1.97604	1.97636 (+0.00032)
F(LP3)	1.97098	1.97079 (–0.00019)	1.97130	1.97026 (–0.00104)	1.97134 (+0.00004)	1.97145	1.97080 (–0.00065)
C-F(σ*)	0.02740	0.02724 (–0.00016)	0.03101	0.02903 (–0.00198)	0.02834 (–0.00267)	0.02765	0.03141 (+0.00376)
F(RY1*)	0.00186	0.00218 (+0.00032)	0.00210	0.00206 (–0.00004)	0.00218 (+0.00008)	0.00229	0.00235 (+0.00006)
F(RY2*)	0.00146	0.00146 (0.00000)	0.00145	0.00149 (+0.00004)	0.00145 (0.00000)	0.00156	0.00151 (–0.00005)

The results clearly demonstrate the importance of this interaction in the *sp* conformation and in establishing the resulting fluorine chemical non-equivalence between *R* and *S* CFTA diastereomers. The largest calculated interaction energy between σ*C-F and σO-CO bond is found for *sp* conformations with the smallest dihedral angle (ψ) between C=O and the C-F bond. **(*R*)-5.9** *sp* have a ψ-angle of 22.0º with $E^{(2)}$ = 0.86, **(*S*)-5.9** *sp*1 a angle of -6.0º with $E^{(2)}$ = 0.90 and **(*S*)-5.10** *sp*2 a angle of 35.7º with $E^{(2)}$ = 0.63 kcal/mol (**Fig. 5.8**). This illustrates, the dependence of the interaction energy ($E^{(2)}$) on the dihedral angle between σ*C-F and σO-CO bond.
The difference in ψ between the most stable conformers of (*R*)- and (*S*)-CFTA derivatized diastereomers will result in a ^{19}F chemical shift difference between them.

The role of the large phenyl $\pi C^d=C^e$ interaction energy with σ*C-F in the *sp* conformations is also highlighted to play a role in the determination of ^{19}F chemical shift non-equivalence, which is dependant on the dihedral angle (α) between them (**Table 5.5 and Fig 5.8**). The largest interaction of $\pi C^d=C^e$ with σ*C-F is observed when the phenyl plane is closest to an orthogonal angle with the C-F bond, which results in a π-symmetric configuration of these bonds. The π(C=C) –σ*(C–F) interaction is then considered to be maximum at α = 90° and minimum at 0°. The order of the π^*(C=C) –σ^*(C–F) interaction energy is *sp* (*S*)-**5.10**, 3.17 kcal/mol > *sp*1 (*S*)-**5.9**, 1.82 kcal/mol > *ap* (*S*)-**5.9**, 1.29 kcal/mol > *sp*2 (*S*)-**5.9**, 0.88 kcal/mol • *sp* (R)-**5.9**: 0.84 kcal/mol and corresponds to the order of the α angle, *sp* (*S*)-**5.10**, 33° > *sp*1 (*S*)-**5.9**, 27° > *ap* (*S*)-**5.9**, 24° > *sp*2 (*S*)-**5.9**, 19° > *sp* (R)-**5.9**, 18° (**Table 5.5 and Fig 5.8**).

It is conceivable that π-π interaction between the flavanol B-ring and the CFTA tolyl ring could be responsible for a significant difference in $\pi C^{d}=C^{e}//\sigma^{*}C\text{-}F$ dihedral angle between the *S* and *R*-CFTA diastereomers, contributing to the exceptionally large $\Delta\delta^{(SR)}\,^{19}F$ observed for this diastereomer pair.

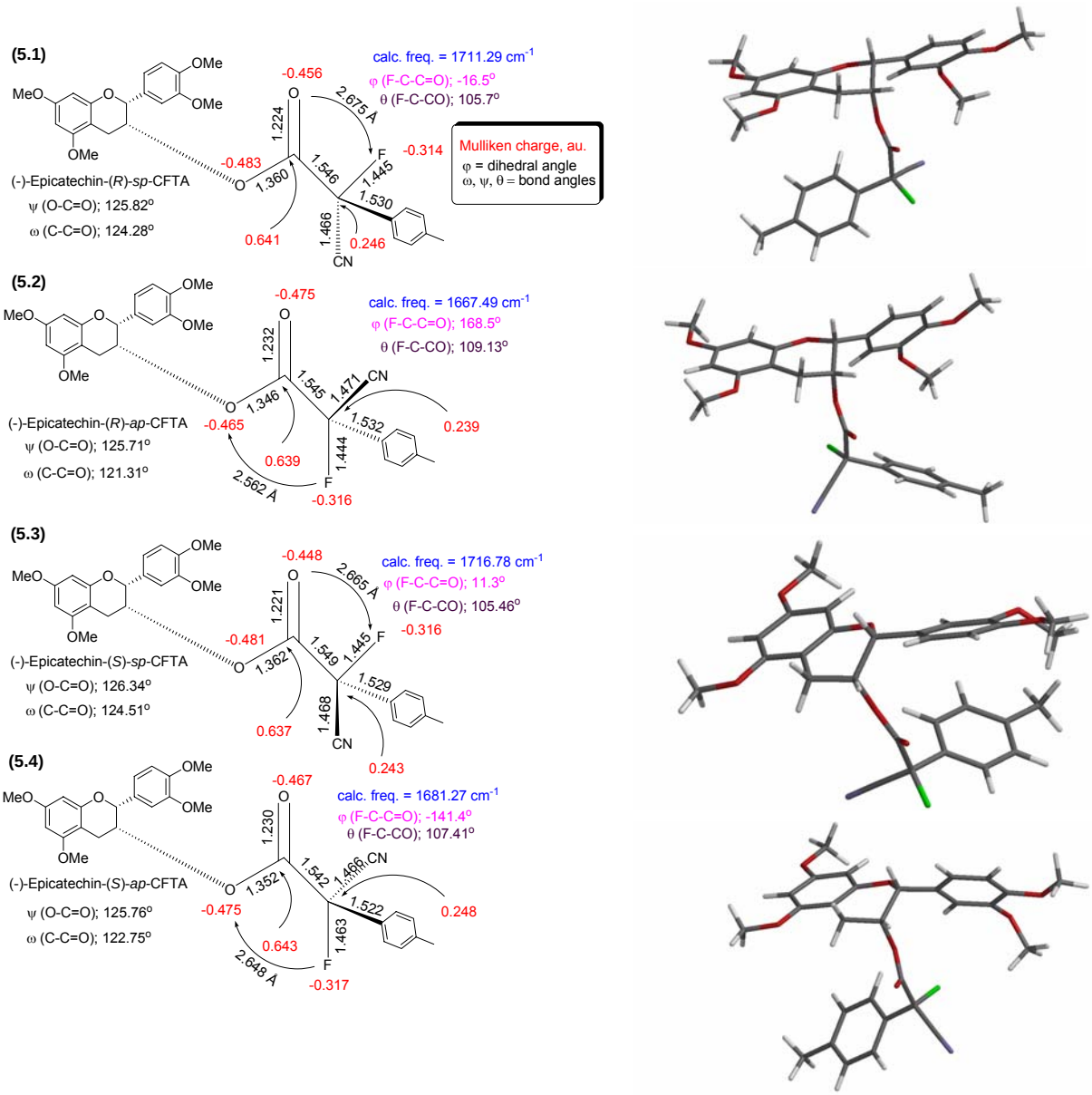

Scheme 5.3 (RB3LYP/6.311G optimized geometries of (-)-epicatechin-(*R*, *S*)-*ap*, *sp*-CFTA esters displaying selected bond lengths, bond angles, dihedral angles, Mulliken charges, C=O frequencies and interatomic distances)

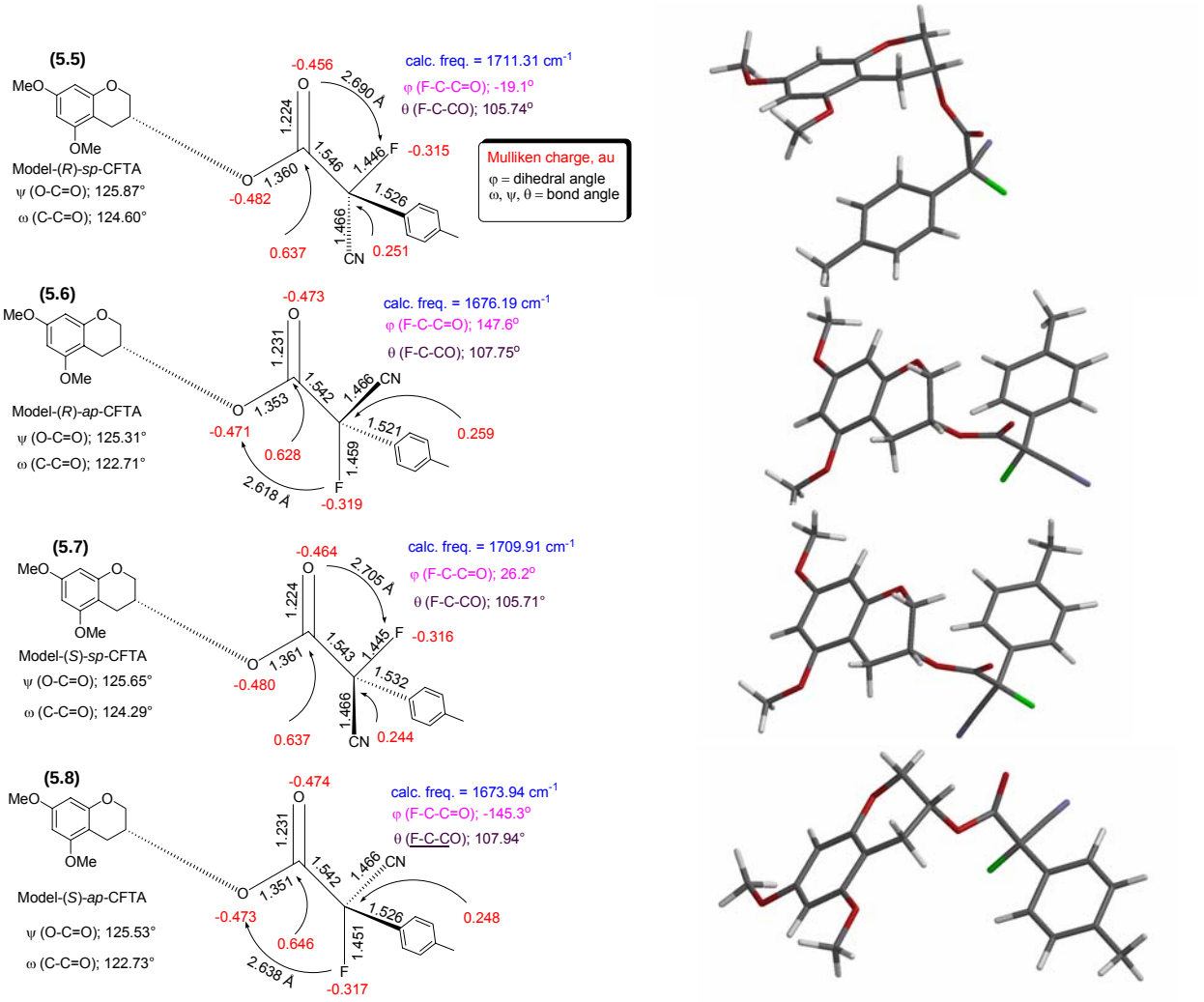

Scheme 5.4 (RB3LYP/6.311G optimized geometries of the model-(*R*, *S*)-*ap*, *sp*-CFTA esters displaying selected bond lengths, bond angles, dihedral angles, Mulliken charges, C=O frequencies and interatomic distances)

As the σ*C-F and σO-CO bond interaction clearly plays an important role in the stabilization of the *sp* conformation, the strongest collective interaction with the σ*C-F bond is in the *ap* conformer. Calculated NBO bond occupancies underscore this, showing a more populated σ*C-F bond in the *ap* conformer (**Table 5.3, 5.6**). This donation originates from the carbonyl $n(O^i)$ LP, and contributes to the lengthening of this bond in the *ap* conformer, although σC=O show little change in NBO population. The calculated interaction energies (E^2) (**Table 5.5**) reveal a significantly large interaction between σ*C-F and the carbonyl oxygen lone pair, $n(O^i)$ in the *ap* isomers.

This lower C=O bond order is then reflected in the lower IR frequency observed experimentally and successfully reproduced by the frequency calculations for the *ap* conformers. It is clear from the IR raw data in **Appendix 5.1** that the dominant *sp* isomer have higher frequency compared to the *ap* isomer. This is reversed from what is observed in the MTPA esters where the *sp* isomers have a lower frequency (**Fig. 4.20**) for the more dominant *sp* isomer.

A consequence of the σ*C-F and σC=O vicinal bond interaction in the CFTA *ap* isomer is observed in the calculated bond length increase for both these interacting bonds in this conformer and also the larger O=C-C-F bonding angle (**Fig 5.9**). The σ*C-F and σC=O vicinal *anti* interaction is responsible for the larger O=C-C-F bonding angle (≈ 2º, **Scheme 5.3, 5.4**) calculated for the *ap* isomer and the slightly shortened central α-C-C bond. The O=C-C bond angle shows a corresponding closing of this angle by about 2° in the *ap* isomer allowing for greater overlap between σ*C-F and σC=O (**Fig. 5.9**).

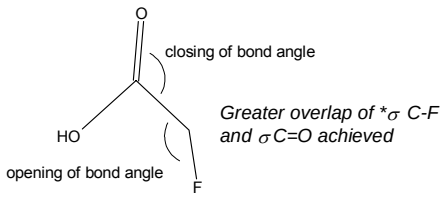

Figure 5.9

These bond length and bond angle differences is in line with vicinal hyperconjugation (Fluorine Negative Hyperconjugation, FNH)[256] between σ*C-F and σC=O (LP), operational in both the *ap* and *sp* isomers. It also explains the lower experimental IR frequency for the *ap* conformer. According to the FNH model[256] a more negative atomic charge on fluorine should be observed. Indeed, the calculated Mulliken charge of fluorine show a more negative value in all the *ap* isomers (**Scheme 5.3, 5.4**) indicative of FNH.

It is only in the past decade that extensive studies, fundamental theoretical calculations of structure and energy, and experimental dynamic NMR and shielding effect calculations have been performed to know the contribution of each conformer to the average NMR shift that is observed. This understanding of the fundamentals of the methods have allowed us to rationally explain not only the way in which the CDA's work but also led to the development of new and more-efficient CDA reagents

and methodologies resulting in improved reliability in the absolute configuration assignment process which is now based on both empirical and theoretical results.

Table 5.1. **Permethylated (-)-epicatechin-CFTA (5.1-5.4)**

	(*R*)-CFTA_*ap* (5.2)	(*R*)-CFTA_*sp* (5.1)	(*S*)-CFTA_*ap* (5.4)	(*S*)-CFTA_*sp* (5.3)
B3LYP/6-311G (hartrees)	-1802.964844	-1802.968869	-1802.968016	-1802.965546
Δ(kcal/mol)	2.525	0		
Δ(kcal/mol)			-1.550	0
Δ(kcal/mol)		-2.085		0
Δ(kcal/mol)	0		-1.99	
Calc. Frequency (C=O, cm^{-1})	1667.4968	1711.2978	1681.2748	1716.7869
Calc. Frequency (intensity)	156.826	201.7523	176.522	206.4641
ΔFrequency (cm^{-1})	-43.801	0	-35.5121	0
Dihedral angle (F-C-C=O,degree)	168.5	-16.5	-141.4	11.3
Obs. Frequency (C=O, cm-1)($CHCl_3$)	1756.83	1772.26	1757.8	1770.33
δ ^{19}F(charge den., B3LYP/6-311G)	-0.324819	-0.327639	-0.310536	-0.32875
Δ(charge)	0.00282	0		
Δ(charge)			0.018214	0
δ ^{19}F(isotropic, B3LYP/6-311G)	317.9017	315.9414	271.9623	318.3422
δ Internal std. ($CFCl_3$)	79.3958	79.3958	79.3958	79.3958
calc. δ^{19}F	-238.5059	-236.5456	-192.5665	-238.9464
Δ(δ, ppm)	-1.9603	0		
Δ(δ, ppm)			46.3799	0
δ ^{19}F(isotropic, HF/6-31+G(d))	370.1444	365.0194	335.6083	365.5618
δ Internal std. ($CFCl_3$)	217.5246	217.5246	217.5246	217.5246
calc. δ^{19}F	-152.6198	-147.4948	-118.0837	-148.0372
Δ(δ, ppm)	-5.125	0		
Δ(δ, ppm)			29.9535	0
avg. calculated. ^{19}F (δ, ppm) Observed. ^{19}F (δ, ppm)	-150.0573 -150.115		-133.06045 -142.665	

Table 5.2. Model CFTA structure (5.5-5.8)

	(*R*)-CFTA_*ap* (5.6)	**(*R*)-CFTA_*sp* (5.5)**	**(*S*)-CFTA_*ap* (5.8)**	**(*S*)-CFTA_*sp* (5.7)**
B3LYP/6-311G (hartree)	-1342.89713	-1342.89784	-1342.89645	-1342.898295
Δ(kcal/mol)	0.445	0		
Δ(kcal/mol)			1.158	0
Δ(kcal/mol)		0.286		0
Δ(kcal/mol)	0		0.427	
Calc. Frequency(C=O, cm^{-1})	1676.1881	1711.3133	1673.9405	1709.9105
Calc. Frequency(intensity)	188.8717	204.4674	183.4333	225.3009
ΔFrequency(cm^{-1})	-35.1252	0	-35.97	0
Dihedral angle (F-C-C=O,degrees)	147.6	-19	-145.3	26.2
F(charge density., B3LYP/6-311G)	-0.313571	-0.324784	-0.320924	-0.329746
Δ(charge)	0.011213	0		
Δ(charge)			0.008822	0
$\delta^{19}F$ (isotropic, B3LYP/6-311G)	268.0535	309.8474	296.2372	318.0775
$\delta^{19}F$ ($CFCl_3$)	79.3958	79.3958	79.3958	79.3958
calc. $\delta^{19}F$	-188.6577	-230.4516	-216.8414	-238.6817
Δ δ (ppm)	41.7939	0		
Δ δ (ppm)			21.8403	0
$\delta^{19}F$ (isotropic, HF/6-31+G(d))	332.8468	359.9092	354.741	366.7583
$\delta^{19}F$ ($CFCl_3$)	217.5246	217.5246	217.5246	217.5246
calc. $\delta^{19}F$	-115.3222	-142.3846	-137.2164	-149.2337
Δ δ (ppm)	27.0624	0		
Δ δ (ppm)			12.0173	0

^{19}F NMR temperature experiments for the (-)-epicatechin-*(R),(S)*-CFTA esters

During the recording of the ^{19}F NMR experiments it was noticed that both the (-)-epicatechin-*(R),(S)*-CFTA esters have a small satellite peak on opposite sides of the main ^{19}F resonance peak. The ratio to the main peak measured 6.7% for the (*S*)-ester (**^{19}F NMR, Plate 5.8, 5.20**) and 9.4% for the (*R*)-ester (**^{19}F NMR, Plate 5.7, 5.19**). This ratio remained identical after numerous purifications with different methods. These methods included medium pressure liquid chromatography (MPLC) and commercial PLC plates in various solvent systems. The fact that the ratio of the satellite peaks always remain the same and occurs on opposite sides, and about the same chemical shift offset, from the main signal for the diastereomeric pair, led to the notion that they could be structurally related. All spectra mentioned here was taken directly after purification and subsequent drying of the sample in order to avoid formation of decomposition products. The carenediol-(*R*), (*S*)-CFTA precursors (**Plate 5.4, 5.16 and ^{19}F NMR, Plate 5.5, 5.17**) utilized in the preparation of the epicatechin esters also show no impurities or similar satellite peaks in their ^{19}F NMR spectra, thus it could not originate from the substrate.

Temperature ^{19}F NMR experiments (**Scheme 5.5, 5.6**) was conducted to investigate the possibility of slow rotational isomerism on the NMR time scale, alluding to another stable isomer in solution for both diastereomers.

Incremental heating from 300K-360K did produce small incremental convergence of the signals for both diastereomers, as is expected from heating of slow rotational isomers.

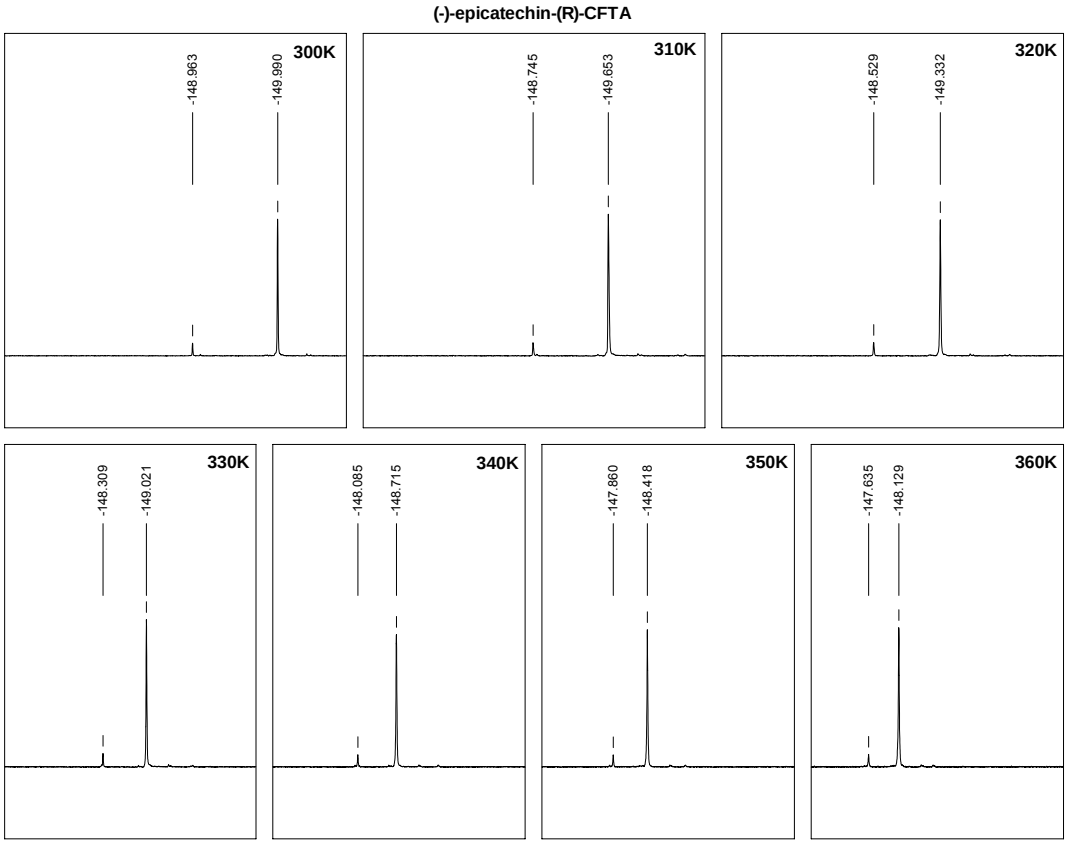

Scheme 5.5

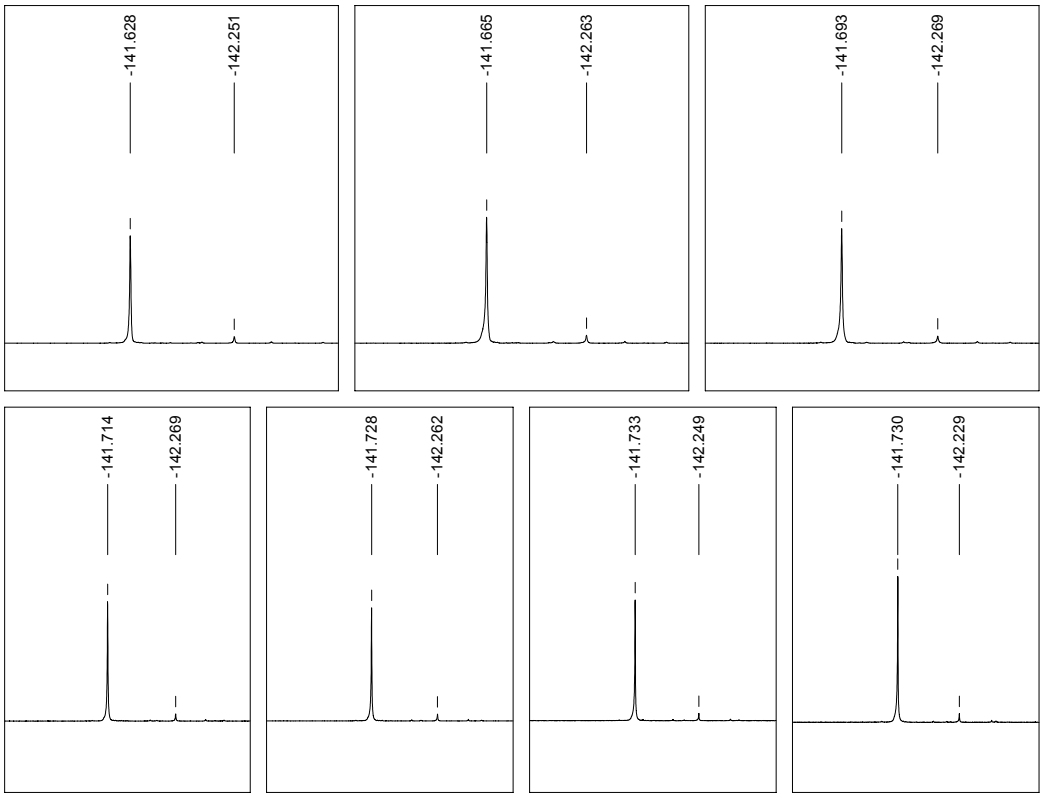

Scheme 5.6

However, the incremental convergence is very small with each 10K increase and at 360K the signal was far from converging. The smaller satellite peak should also converge at a much faster rate towards the major signal which is not observed. It was concluded that the energy barrier is simply to high for these satellite peaks to arise due to slow rotational isomerism on the NMR timescale.

The (-)-epicatechin (90%, Sigma-Aldrich) can not produce this impurity because a small amount of (+)-epicatechin-(*R*)-CFTA in the (-)-epicatechin-(*R*)-CFTA mixture will result in a satellite signal with the same ^{19}F chemical shift as (-)-epicatechin-(*S*)-CFTA, which is not observed. Thus, the origin of this satellite peak could not be resolved.

Experimental

Preparation of optically pure CFTA and their respective diastereomeric (-)-epicatechin esters

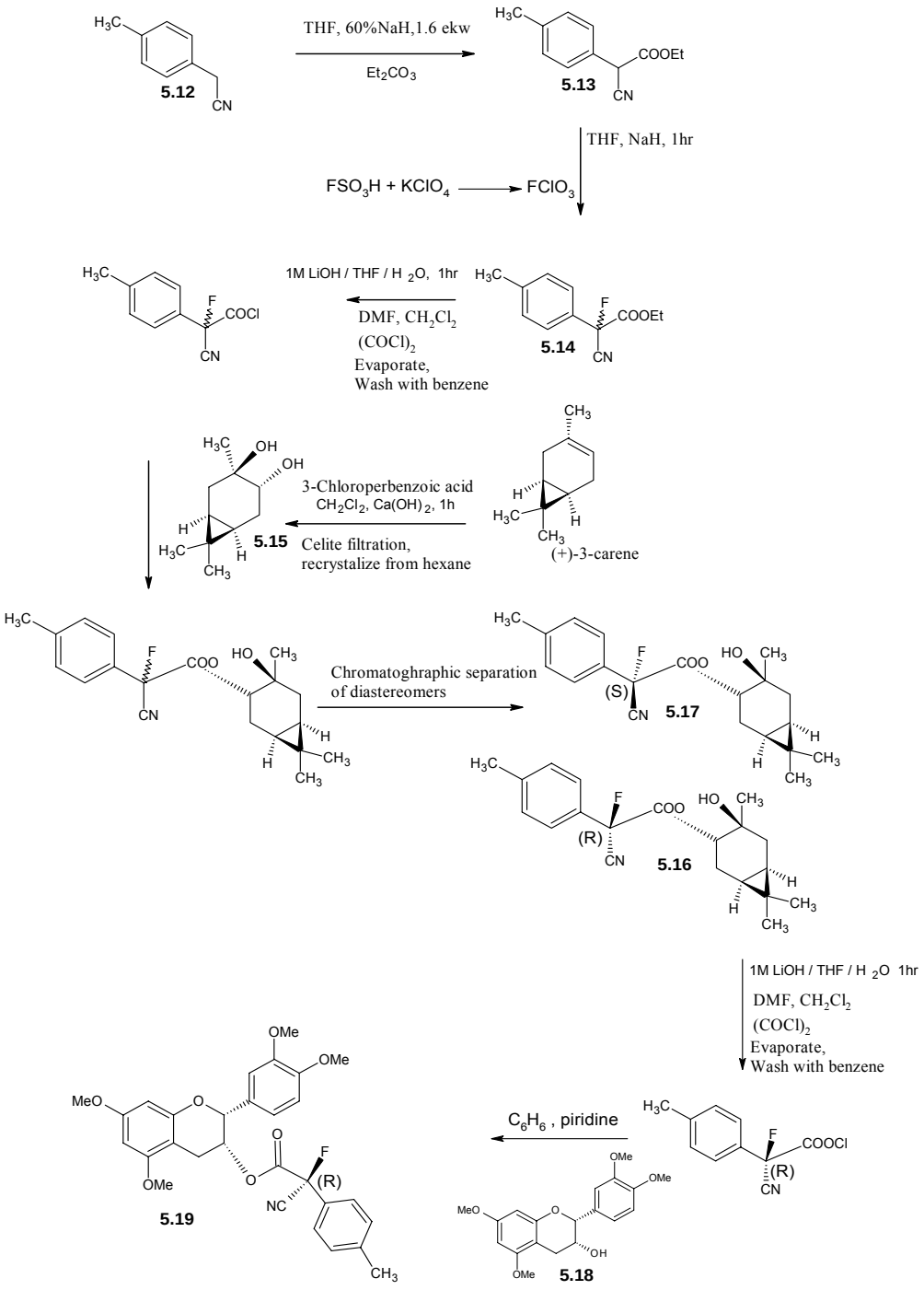

5.20, (-)-EC-(*S*)-CFTA ester

Preparation of ethyl cyano(4-methylphenyl)acetate

60%NaH (0.488g, 1.6eq.) are slowly added to *p*-Tolylacetonitrile **5.12** (1g, 7.62 mmol in 160ml dry THF, 0°C) and stirred for 10 min. under argon atmosphere. Et_2CO_3 (1.47ml, 1.6eq.) are slowly injected to this cooled solution over 3 min. The whole mixture was heated at reflux for 2h. Water (50 ml) was added to the mixture, cooled in a ice bath, and the THF evaporated. The mixture was acidified to pH 1 with conc. HCl in a ice bath and extracted with EtOAc. The combined organic layer was washed with brine, dried over $MgSO_4$ and concentrated *in vacu*. Acetonitrile was added and the mineral oil extracted with hexane. The acetonitrile was evaporated and the residual oil purified by silica gel column chromatography (hexane : EtOAc, 10:1) which yielded 1.17g (76%) ethyl cyano(4-methylphenyl)acetate **5.13**. ^{1}H-NMR (270 MHz) [**Plate 5.1** ($CDCl_3$) 293K]: $CH_2\underline{CH_3}$ (δ1.28, t, J = 7.1 Hz), Ar-CH_3 (δ2.37, s), CH_2 (δ4.24, dd, J = 1.1, 7.1 Hz), CH (δ4.68, s), 2 x ArH (δ7.22, d, J = 8.2 Hz), Ar x ArH (δ7.35, d, J = 8.2 Hz).

Preparation of ethyl (±)-α-cyano-α-fluoro-α-tolylacetate

60%NaH (279.6mg, 3.3eq) were slowly added to ethyl cyano(4-methylphenyl)acetate **5.13** (1.17g, 5.76mmol) dissolved in dry THF (0°C) (30ml.) and stirred for 1hr. at room temperature.

Potassium perchlorate (3.99g, 5eq.) was added to fluorosulphonic acid (11.53ml, 35eq.) and heated incrementally to 78°C. The $FClO_{3(g)}$ produced was carried (N_2) over a 5% $Na_2S_2O_3$, 10% NaOH solution and passed through two columns filled with $CaCl_2$ and NaF granules respectively. This gas mixture was bubbled slowly through the stirred brown THF suspension above.

Fluorination was complete after about 1.5 hr. or the suspension turning light yellow indicating completion of the reaction.

The THF was removed under vacuum; water slowly added, acidified to pH 1 and extracted with ethyl acetate, dried over $MgSO_4$ and evaporated to yield a yellow oil. The mineral oil was removed by hexane extraction from acetonitrile followed by evaporation of the acetonitrile. The oily product was

purified by column chromatography on silica gel (eluent hexane:AcOEt 9:1) to give ethyl (±)-α-cyano-α-fluoro-α-tolylacetate (**5.14**) as a colorless oil (1.16g, 95%). ^{1}H-NMR (270 MHz) [**Plate 5.2** ($CDCl_3$) 293K]: $CH_2C\underline{H}_3$ (δ1.30, t, J= 7.3 Hz), Ar-$C\underline{H}_3$ (δ 2.40, s) $C\underline{H}_2$ (δ 4.25-4.43, m), 2 x ArH (δ7.29, d, J = 8.2 Hz), 2 x ArH (δ7.52 d, J= 7.8 Hz); ^{19}F NMR 254 MHz [$CDCl_3$, 293K] F (δ-144.6, s)

Prepararation of Carene diol

Meta-chloroperbenzioic acid (>70%, 25g, 0.101 mol) and (+)-3-carene (12.4g, 0.072 mol) is added to CH_2Cl_2 (300ml) and stirred for 1.5hr. $Ca(OH)_2$ (32g, 0.432 mol) is added and the reaction stirred for another 1hr.

The reaction suspension is filtered through a celite bed and washed with dichloromethane. After evaporation of the solvent the carene diol (**5.15**) (8.56g, 0.043 mol) is purified by recrystalization from hexane with a 60% yield. ^{1}H NMR (270 MHz) [**Plate 5.3** ($CDCl_3$) 293K]: 2 x >CH- (δ0.67-0.75, m), $C\underline{H}_3(CH_3)C<$ (δ0.97, s), $CH3(C\underline{H}3)C<$ (δ1.03, s), $CH_3(OH)CC\underline{H}HCH<$ (δ1.17-1.28, m), $CH_3(OH)C<$ (δ1.21, s) $HOCHC\underline{H}HCH<$ (δ1.65, ddd, J = 7.7, 10.2, 14.3 Hz), $CH_3(OH)CCH\underline{H}CH<$ (δ1.98, dd, J = 9.6, 14.6 Hz), $HOCHCH\underline{H}CH<$ (δ2.11, dd, J = 7.4, 14.6 Hz), $HOC\underline{H}CH_2$ (δ3.36, dd, J = 7.4, 10.2 Hz).

Preparation of carene diol-CFTA esters

Racemic ethyl-2-cyano-2-fluoro-2-tolylacetate (CFTA ethyl ester) (1.43g, 6.47 mmol) was dissolved in 20ml of THF/H_2O (1:1). To this solution was added 1M lithium hydroxide aqueous solution (6.5ml, 6.47 mmol) and the mixture was stirred at room temperature for 30 min. After evaporation of THF under reduced pressure, unreacted ester (**5.14**) was removed by ether extraction. The aqueous layer was acidified (pH 1) with 10% aqueous HCl at 0°C. The solution was saturated with NaCl and extracted with AcOEt. The organic layer was washed with brine and dried over $MgSO_4$. After removal of the solvent, any residual water was removed as azeotrope with benzene to give crude racemic CFTA as a colorless oil. It was subsequently dissolved in dried CH_2Cl_2 (50 ml) containing a catalytic amount of DMF (65mg) under an argon atmosphere. To the solution was added oxalyl chloride (1.1 ml, 12.94 mmol, 2eq.) at 0°C and the mixture was stirred at room temperature for 3 h. After removal of the

solvent, benzene was added to the residue and the insoluble precipitate was filtered off. The filtrate was concentrated to give crude racemic CFTA-Cl as yellow oil. Subsequently the crude CFTA-Cl was dissolved in 9.4mL of dried CH_2Cl_2 under an argon atmosphere. To the solution were added dry pyridine (1.18ml, 14.5 mmol) and carene diol (1.21 g, 7.3 mmol) at 0°C and the mixture was stirred at room temperature for 15 h. Solvent was evaporated and the residue was dissolved in AcOEt. The solution was washed with water and brine. The organic layer was dried over $MgSO_4$ and evaporated. Several flash column chromatography cycles (eluent: $CHCl_3$/AcOEt 98:2) yields the *R* and *S* diastereomeric carene diol CFTA esters (**5.16**), (**5.17**) as a yellow oil (112mg and 248mg respectively 0.324mmol; 5% yield, 0.718mmol; 11.1% yield, 99% de by ^{19}F NMR).

More polar isomer **[(R)-CFTA ester]**; ^1H NMR 270 MHz (**Plate 5.4**, $CDCl_3$, 293K), >CH- (δ0.64-0.79, m), C<u>H</u>$_3$(CH$_3$)C< (δ0.97, s), CH$_3$(C<u>H</u>$_3$)C< (δ0.99, s), C<u>H</u>$_3$(HO)C< (δ1.30, s), CH$_3$(HO)CC<u>H</u>HCH< (δ1.35, dd, J = 4.5, 5.7 Hz), -OCHC<u>H</u>HCH< (δ1.55-1.67, m), CH$_3$(HO)CCH<u>H</u>CH< (δ1.99-2.1, m), -OCHCH<u>H</u>CH< (δ2.23, dd, J = 7.6, 14.2 Hz), Ar-CH$_3$ (δ2.40, s), COOCH (δ4.71, dd, J = 7.7, 9.6 Hz), 2 x ArH (δ7.28, d, J = 8.2 Hz), 2 x ArH (δ7.52, d, J = 8.0 Hz); ^{19}F NMR (254 MHz, $CDCl_3$); F (δ-144.34, s).

Less polar isomer **[(S)-CFTA ester]**; ^1H NMR 270 MHz (**Plate 5.5**, $CDCl_3$, 293K), >CH- (δ0.73-0.79, m), C<u>H</u>$_3$(CH$_3$)C< (δ0.99, s), CH$_3$(C<u>H</u>$_3$)C< (δ1.00, s), C<u>H</u>$_3$(HO)C< (δ1.14 s), CH$_3$(HO)CC<u>H</u>HCH< (δ1.24-1.32, m), CH$_3$(HO)CCH<u>H</u>CH< (δ1.29, dd, J = 3.6, 14.3 Hz), -OCHC<u>H</u>HCH< (δ1.79-1.89, m), -OCHCH<u>H</u>CH< (δ2.23, dd, J = 7.6, 14.2 Hz), Ar-CH$_3$ (δ2.39, s), COOCH (δ4.66, dd, J = 7.8, 9.8 Hz), 2 x ArH (δ7.28, d, J = 8.2 Hz), 2 x ArH (δ7.53, d, J = 8.0 Hz); ^{19}F NMR (254 MHz, $CDCl_3$); F (δ-143.31, s)

3',4',6,8-Tetra-*O*-Methyl-(-)-Epicatechin

Title compound is selectively methylated with etheric diazomethane described in general procedures and purified by TLC, Hexane: acetone 7:3, in 87% yield. ^1H NMR 270 MHz (**Plate 5.6**, $CDCl_3$, 293K); H-4 ax (δ2.85 dd, J = 3.2, 16.6 Hz), H-

4 eq (δ2.96, dd, J = 4.6, 16.6 Hz,), OMe (δ3.78, s), OMe (δ3.80, s), OMe (δ3.90, s), OMe (δ3.92, s), H-3 (δ4.28, m), H-2 (δ4.90, s), H-6 (δ6.12, d, J = 2.2 Hz), H-8 (δ6.20, d, J = 2.2 Hz), H-5' (δ6.93, d, J = 8.1 Hz), H-6' (δ7.04, dd, J =1.5, 8.1 Hz), H-2' (δ7.09, d, J = 1.5 Hz).

Preparation of optically pure (-)-epicatechin-CFTA esters

Carene diol-(*R*)-CFTA (**5.16**) (300mg, 1.734 mmol) was dissolved in THF/H_2O (4.5 ml) (1:1). To this solution was added 1M lithium hydroxide aqueous solution (3ml, 3.47 mmol) and the mixture was stirred at room temperature for 30 min. After evaporation of THF under reduced pressure, unreacted ester (**5.16**) was removed by ether extraction. The aqueous layer was acidified (pH 1) with 10% aqueous HCl at 0°C. The solution was saturated with NaCl and extracted with AcOEt. The organic layer was washed with brine and dried over $MgSO_4$. After removal of the solvent, the residual water was removed as azeotrope with benzene to give crude racemic CFTA as a colorless oil. It was subsequently dissolved in dried CH_2Cl_2 (10 ml) containing a catalytic amount of dry DMF (0.015ml) under an argon atmosphere. To the solution was added oxalyl chloride (0.225 ml, 3.47mmol, 2eq.) at 0°C and the mixture was stirred at room temperature for 3 h. After removal of the solvent, benzene was added to the residue and the insoluble precipitate was filtered off. The filtrate was concentrated to give crude racemic CFTA-Cl as yellow oil. Subsequently the crude CFTA-Cl was dissolved in 15ml of dried CH_2Cl_2 under an argon atmosphere. To the solution were added dry pyridine (0.15ml, mmol) and permethylated (-)-epicatechin (50mg, 0.144 mmol) at 0°C and the mixture was stirred at room temperature for 15 h. Solvent was evaporated and the residue was dissolved in AcOEt. The solution was washed with water and brine. The organic layer was dried over $MgSO_4$ and evaporated. Flash column chromatography (eluent: $CHCl_3$/AcOEt 98:2, Rf 0.8) gave the diastereomeric (*R*)-CFTA ester (**5.19**) as a yellow oil (75mg , 0.143mmol; 99% yield, 99% de by ^{19}F NMR).

^1H NMR 270 MHz (**Plate 5.7**, $CDCl_3$, 293K); Ph-C$\underline{H}_3$ (δ2.32. s), H-4 ax (δ2.85 dd, J = 1.5, 17.6 Hz), H-4 eq (δ2.96, dd, J = 4.3, 17.6 Hz,), OMe (δ3.68, s), OMe (δ3.82, s), OMe (δ3.91, s), OMe (δ3.93, s), H-3 (δ5.44, m), H-2 (δ5.06, s), H-6 (δ6.05, d, J = 2.1

Hz), H-8 (δ6.20, d, J = 2.1 Hz), H-5’ (δ6.87, d, J = 8.1 Hz), H-6’ (δ7.01, dd, J =1.9, 8.1 Hz), H-2’ (δ7.06, d, J = 1.9 Hz), H-2”,3” (δ6.98, d, J = 8.1 Hz), H-5”,6” (δ7.15, d, J = 8.1 Hz). ^{19}F NMR (254 MHz, $CDCl_3$); F (δ-150.1, s)

The (*S*)-CFTA ester (**5.20**) was synthesized by the same procedure.
^{1}H NMR 270 MHz (**Plate 5.8**, $CDCl_3$, 293K); Ph-C$\underline{H}_3$ (δ2.36. s), H-4 ax (δ2.95 dd, J = 1.5, 17.6 Hz), H-4 eq (δ3.00, dd, J = 4.3, 17.6 Hz,), OMe (δ3.76, s), OMe (δ3.80, s), OMe (δ3.82, s), OMe (δ3.88, s), H-3 (δ5.48, m), H-2 (δ5.05, s), H-6 (δ6.11, d, J = 2.1 Hz), H-8 (δ6.21, d, J = 2.1 Hz), H-5’ (δ6.72, d, J = 8.1 Hz), H-6’ (δ6.80, dd, J =1.9, 8.1 Hz), H-2’ (δ6.93, d, J = 1.9 Hz), H-2”,3” (δ7.05, d, J = 8.1 Hz), H-5”,6” (δ7.17, d, J = 8.1 Hz). ^{19}F NMR (254 MHz, $CDCl_3$); F (δ-143.47, s).

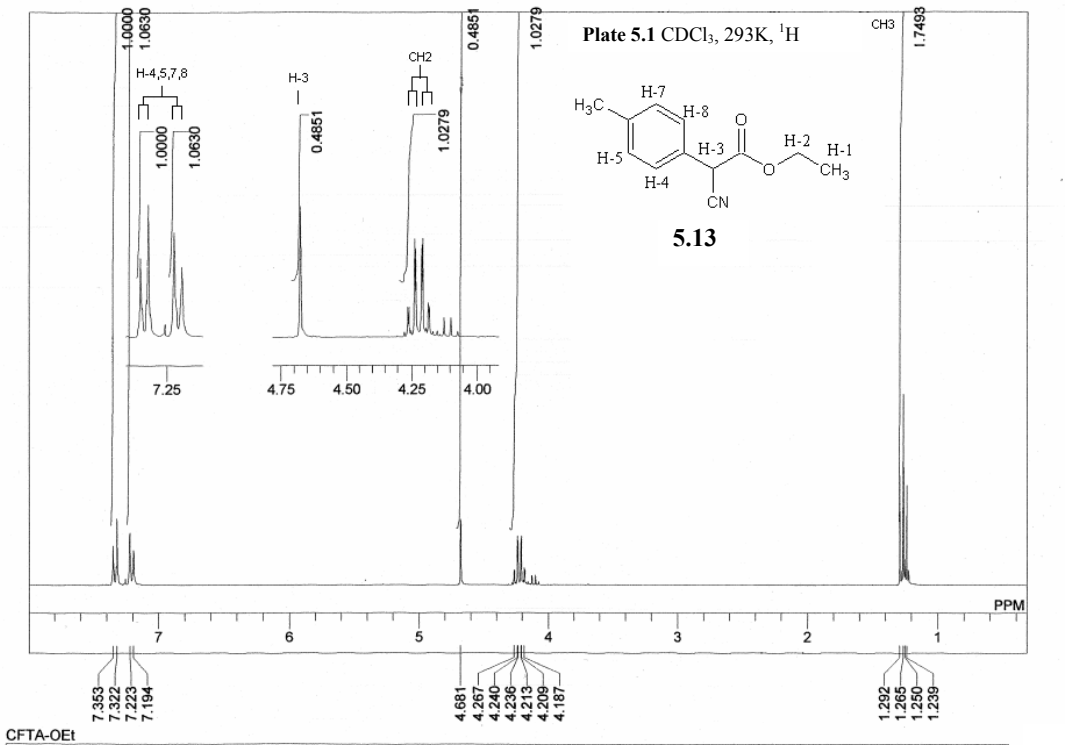
Plate 5.1 CDCl3, 293K, 1H
5.13
H-4,5,7,8
H-3
CH2
CH3
1.0000
1.0630
0.4851
1.0279
1.7493
7.25
4.75
4.50
4.25
4.00
PPM
7.353
7.322
7.223
7.194
4.681
4.267
4.240
4.236
4.213
4.209
4.187
1.292
1.265
1.250
1.239

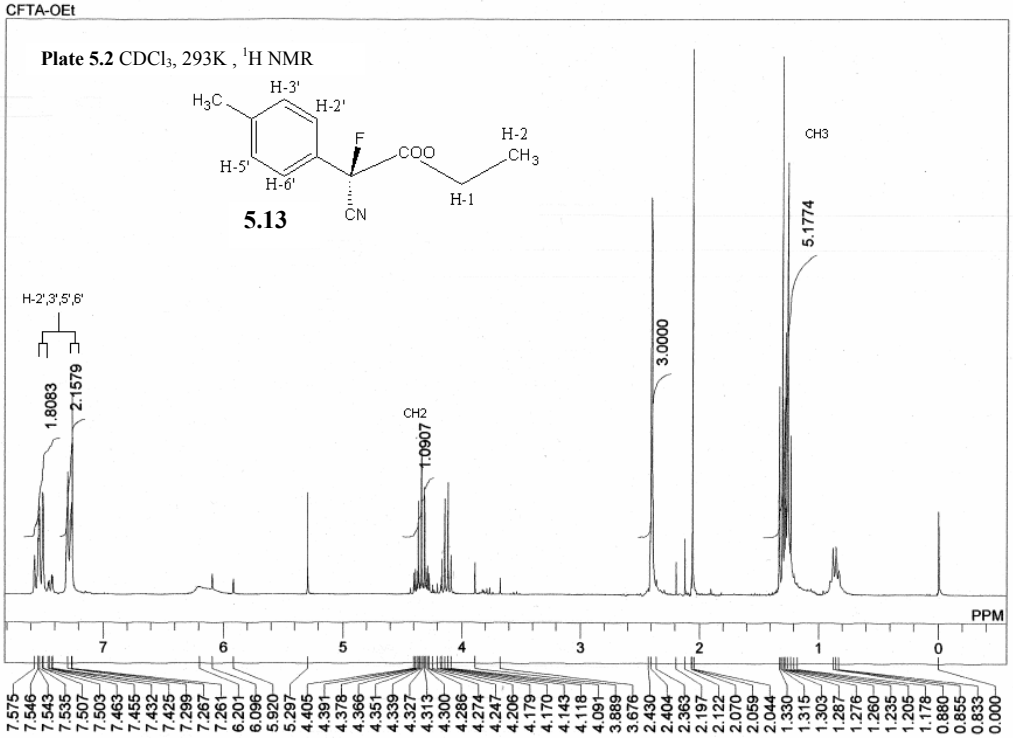
CFTA-OEt
Plate 5.2 CDCl3, 293K , 1H NMR
5.13
H-2',3',5',6'
1.8083
2.1579
CH2
1.0907
3.0000
CH3
5.1774
PPM

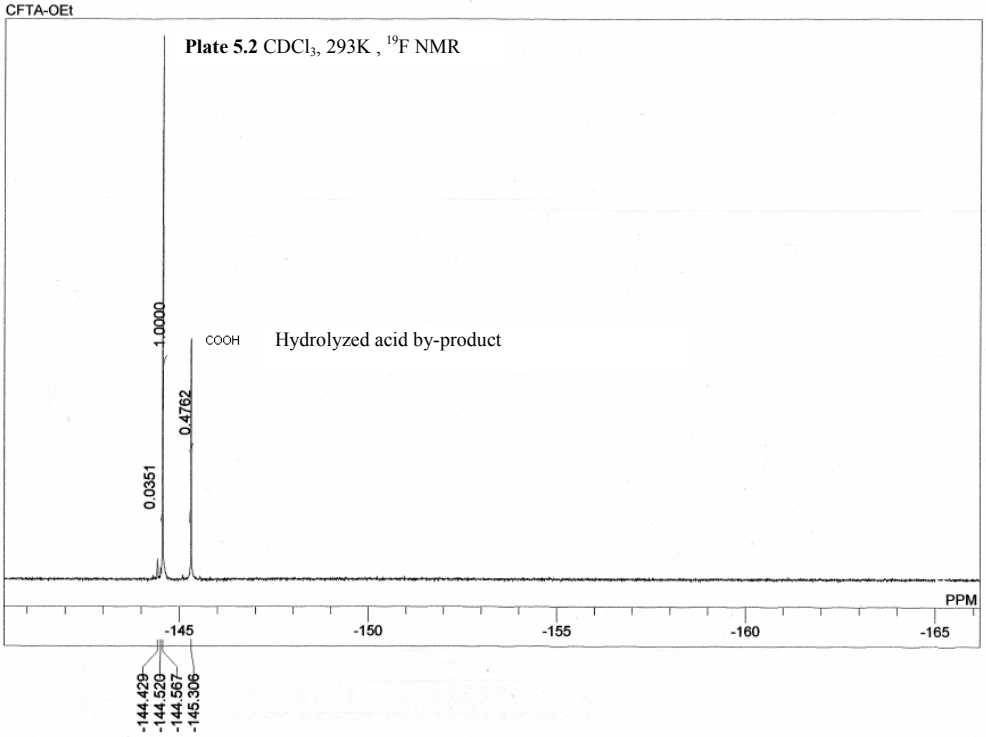
CFTA-OEt
Plate 5.2 CDCl3, 293K , 19F NMR
COOH
Hydrolyzed acid by-product
1.0000
0.4762
0.0351
PPM
-145
-150
-155
-160
-165
-144.429
-144.520
-144.567
-145.306

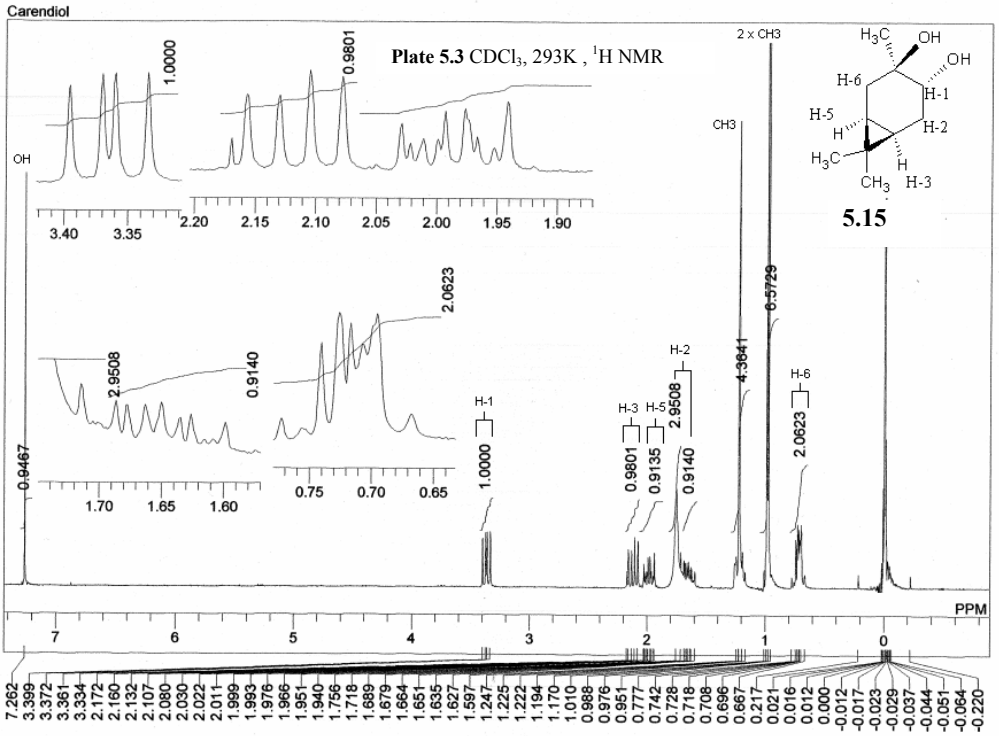
Carendiol
Plate 5.3 CDCl3, 293K , 1H NMR
2 x CH3
CH3
OH
H-1
H-2
H-3
H-5
H-6
5.15
PPM

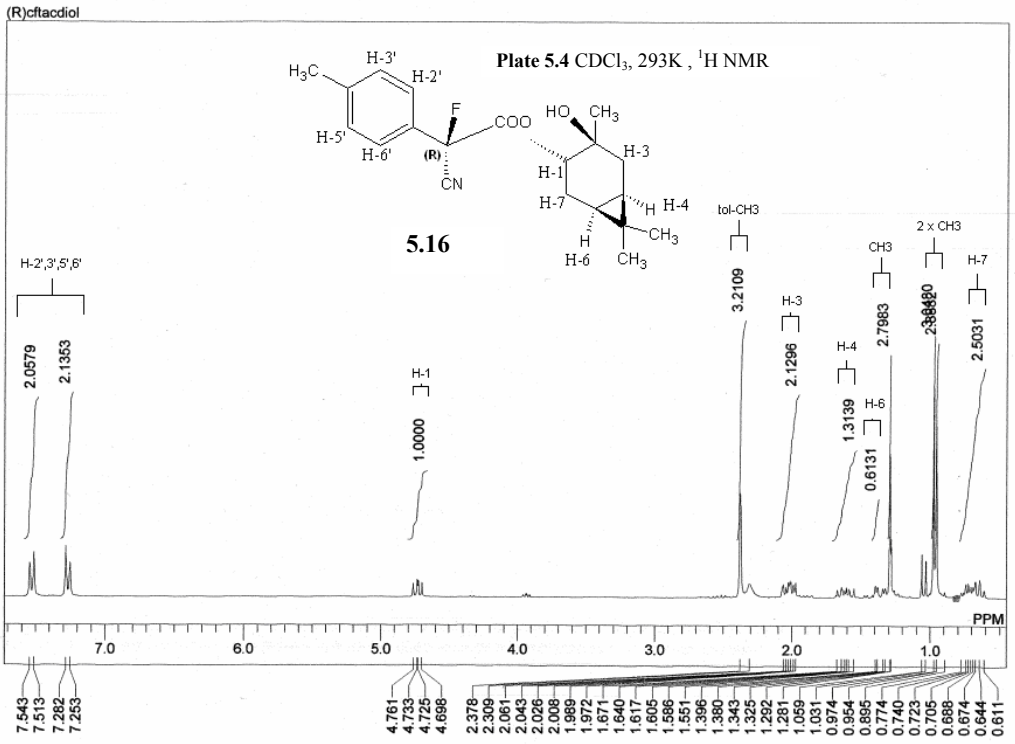

Plate 5.4 $CDCl_3$, 293K , ^{1}H NMR

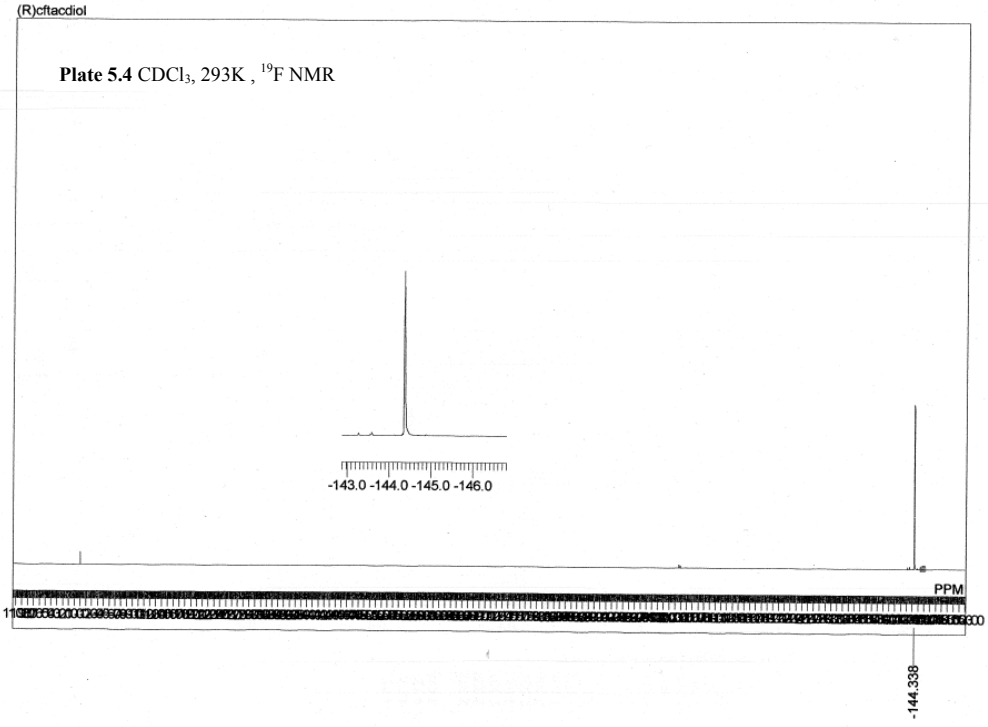

Plate 5.4 $CDCl_3$, 293K , ^{19}F NMR

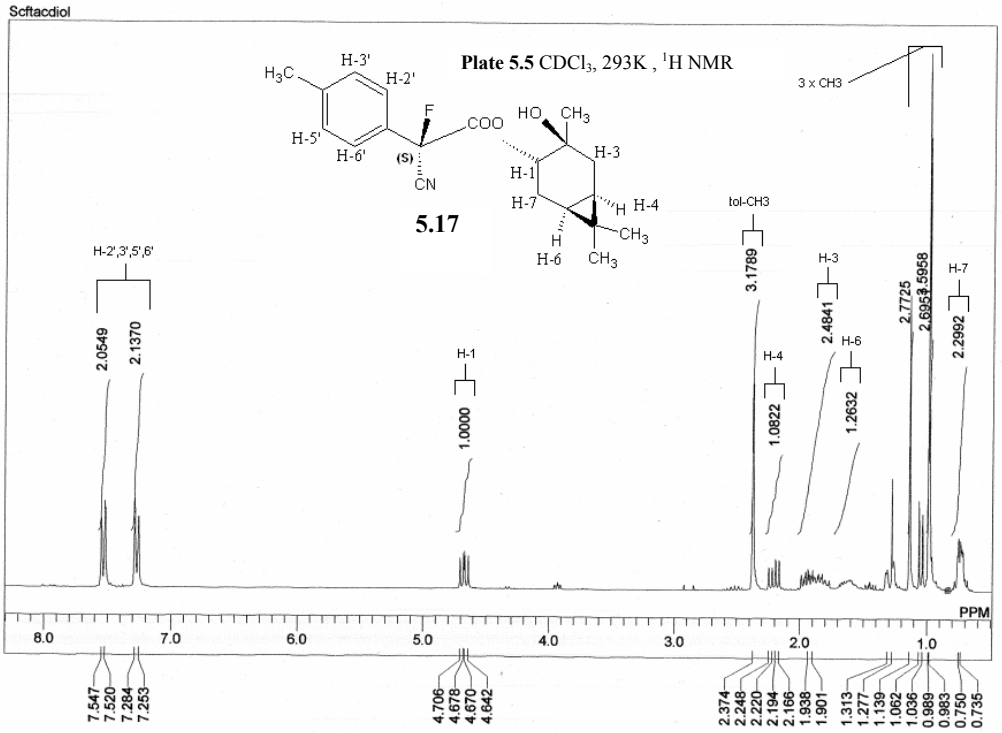
Scftacdiol
Plate 5.5 CDCl3, 293K , 1H NMR
5.17
3 x CH3
H-2',3',5',6'
2.0549
2.1370
H-1
1.0000
tol-CH3
3.1789
H-4
1.0822
H-3
2.4841
H-6
1.2632
2.7725
2.6953
2.5958
H-7
2.2992
PPM
8.0
7.0
6.0
5.0
4.0
3.0
2.0
1.0
7.547
7.520
7.284
7.253
4.706
4.678
4.670
4.642
2.374
2.248
2.220
2.194
2.166
1.938
1.901
1.313
1.277
1.139
1.062
1.036
0.989
0.983
0.750
0.735

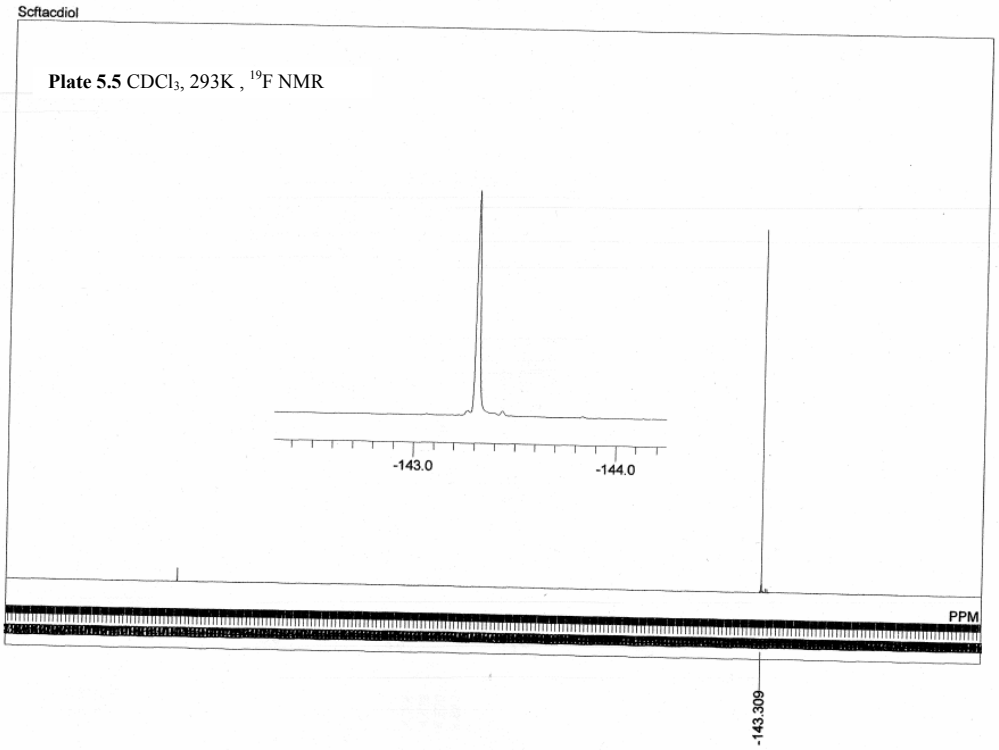
Scftacdiol
Plate 5.5 CDCl3, 293K , 19F NMR
-143.0
-144.0
PPM
-143.309

permethylated epicatechin

Plate 5.6 $CDCl_3$, 293K , ^1H NMR

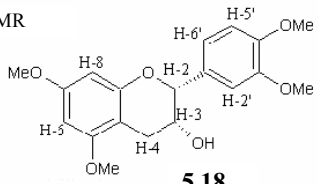

5.18

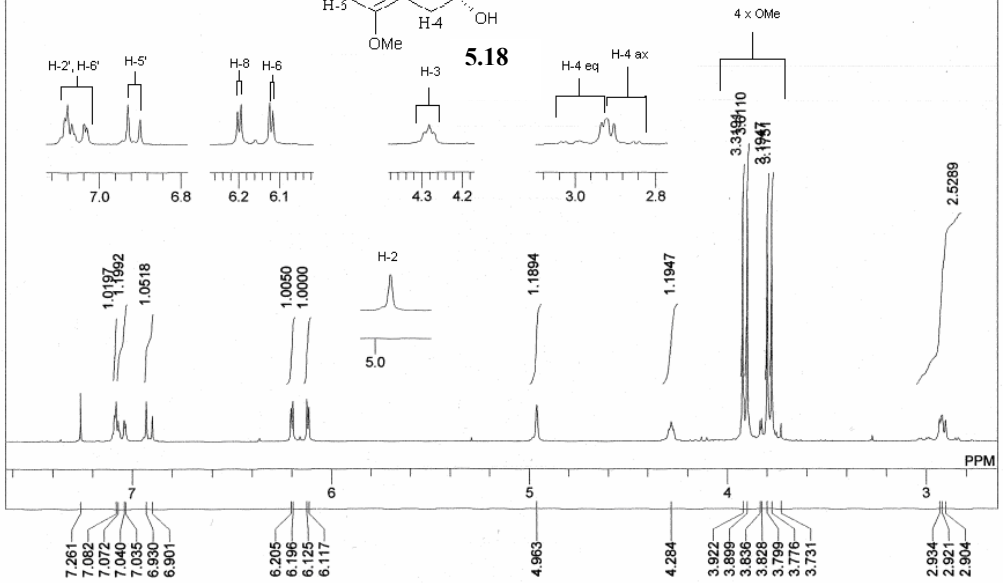

Epicat-(R)-CFTA,0.05M

Plate 5.7 $CDCl_3$, 293K , ^1H NMR

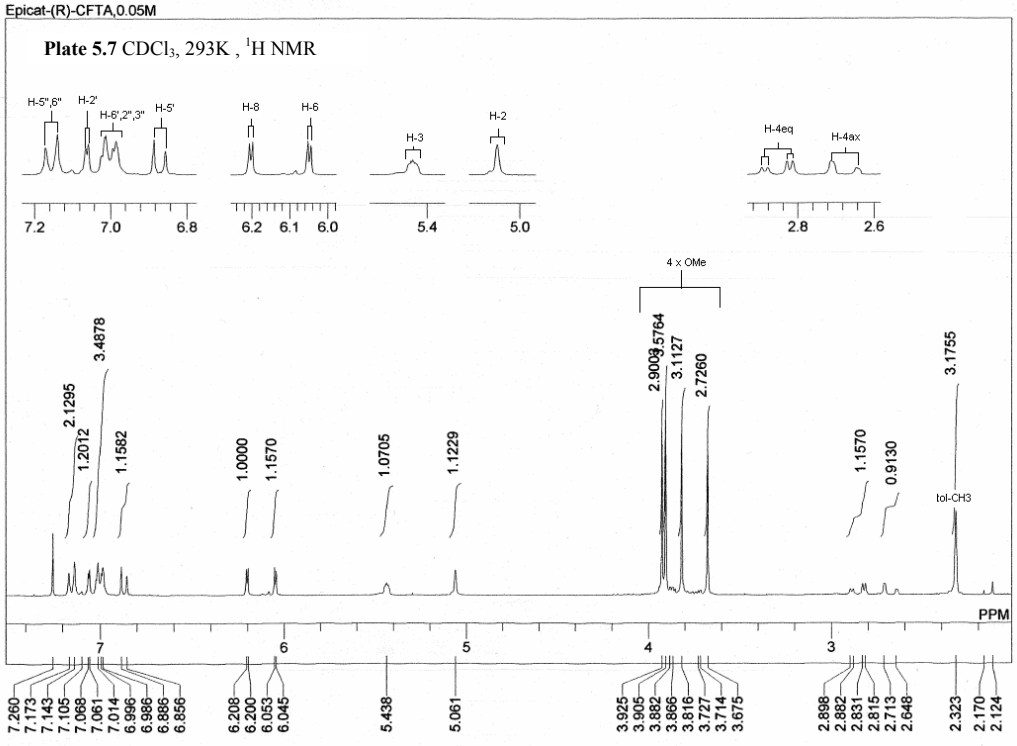

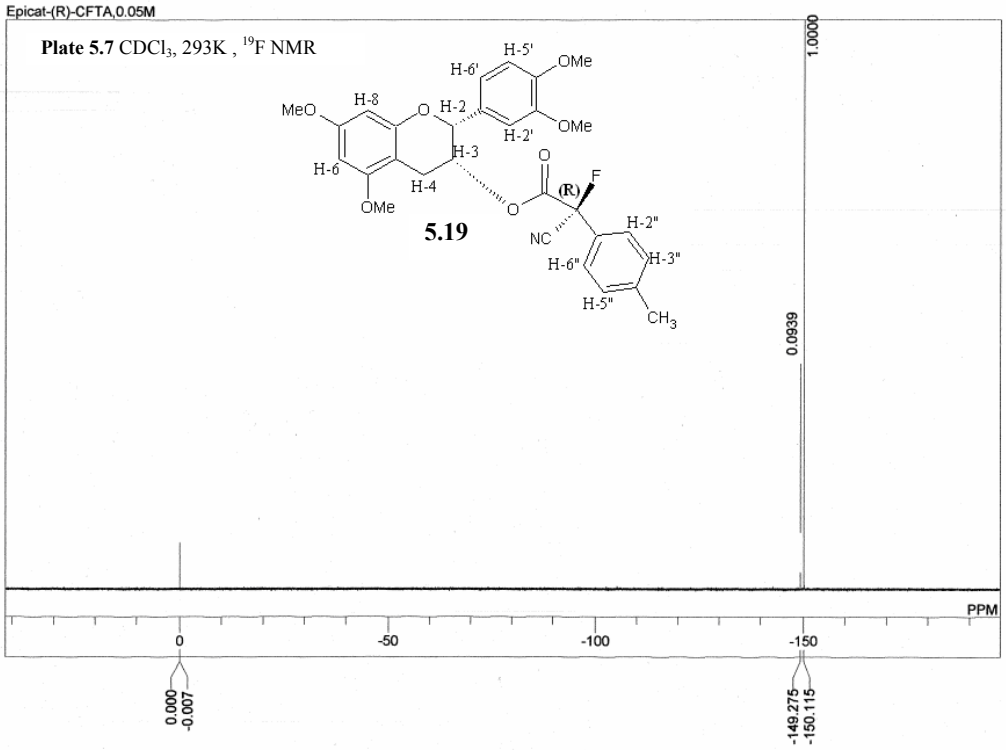
Epicat-(R)-CFTA,0.05M
Plate 5.7 CDCl3, 293K , 19F NMR
5.19
1.0000
0.0939
PPM
0
-50
-100
-150
0.000
-0.007
-149.275
-150.115

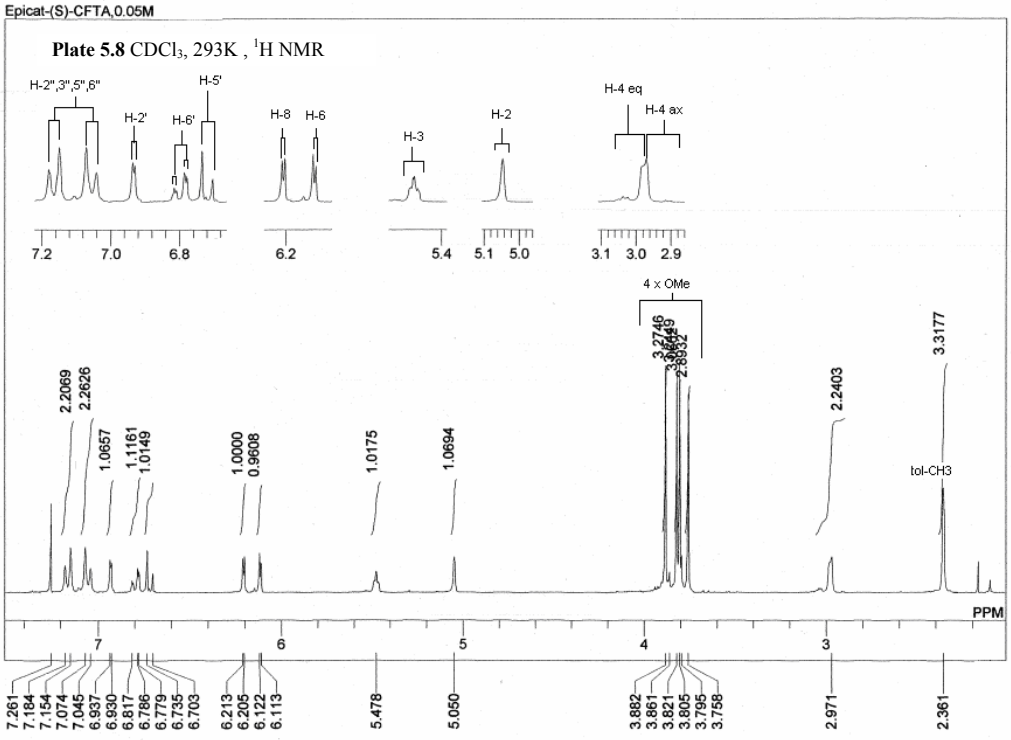
Epicat-(S)-CFTA,0.05M
Plate 5.8 CDCl3, 293K , 1H NMR
H-2",3",5",6"
H-5'
H-2'
H-6'
H-8
H-6
H-3
H-2
H-4 eq
H-4 ax
4 x OMe
2.2069
2.2626
1.0657
1.1161
1.0149
1.0000
0.9608
1.0175
1.0694
2.2403
3.3177
tol-CH3
PPM
7.261
7.184
7.154
7.074
7.045
6.937
6.930
6.817
6.786
6.779
6.735
6.703
6.213
6.205
6.122
6.113
5.478
5.050
3.882
3.861
3.821
3.805
3.795
3.758
2.971
2.361

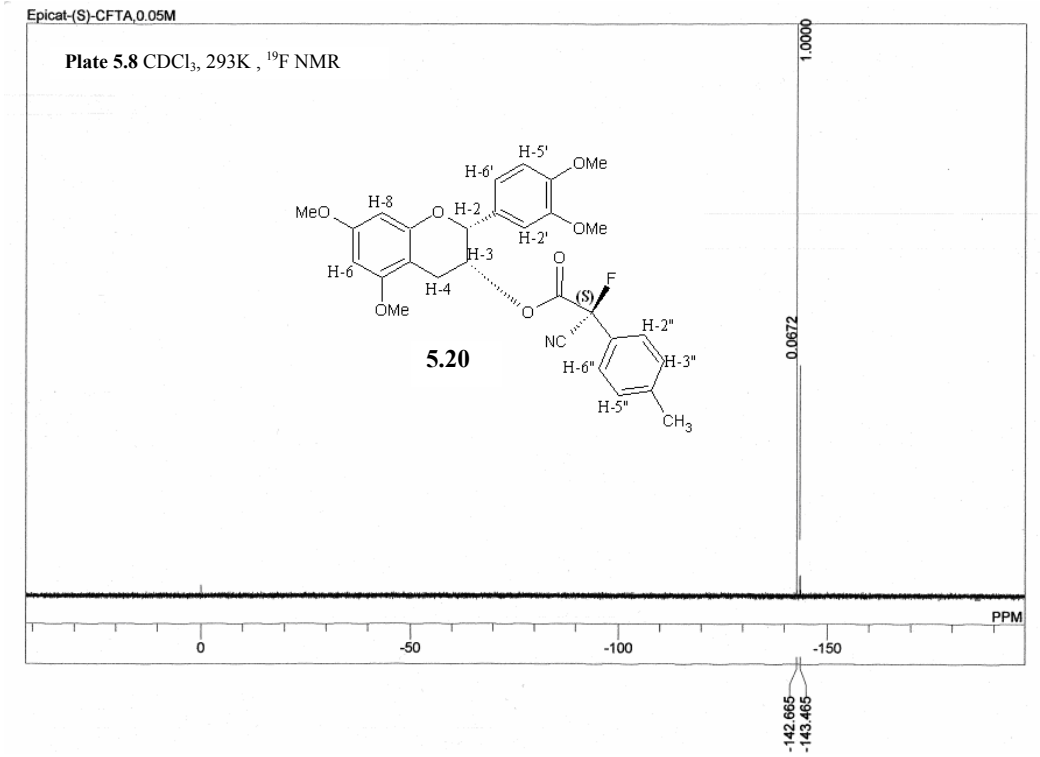
Epicat-(S)-CFTA,0.05M
Plate 5.8 CDCl3, 293K , 19F NMR
H-5'
H-6'
OMe
H-8
MeO
O
H-2
H-2'
OMe
H-3
H-6
O
F
(S)
H-4
OMe
NC
H-2"
H-6"
H-3"
H-5"
CH3
5.20
1.0000
0.0672
PPM
0
-50
-100
-150
-142.665
-143.465

Appendix 5.1

Recording of IR spectra of optically pure (-)-epicatechin-*(R)*,*(S)*-CFTA esters

In order to investigate the rotational behavior of the (-)-epicatechin-(*R*)-CFTA and (-)-epicatechin-(*S*)-CFTA esters (abbreviated EC-(*S*)-CFTA) the IR spectra were taken over a 12hr period at a constant room temperature. The spectra were taken in $CHCl_3$ and CCl_4 and at low concentrations of 0.05M and 0.01M. The deconvoluted carbonyl peak in the spectra is displayed below and the frequency of the individual numbered peaks indicated on each spectra. The name of the compound, concentration and solvent is also indicated.

Spectra of the *(R)* and *(S)* diastereomers in CCl_4 at 0.05M concentration

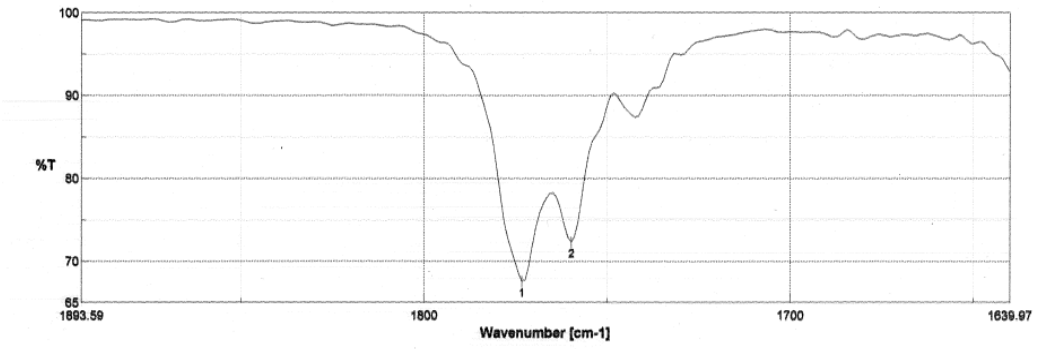

jaco (S)-0.05M-dec CCl4
EC-(S)-CFTA-0.05M CCl4

No.	cm-1	%T	No.	cm-1	%T
1	1773.23	67.577	2	1759.73	72.34

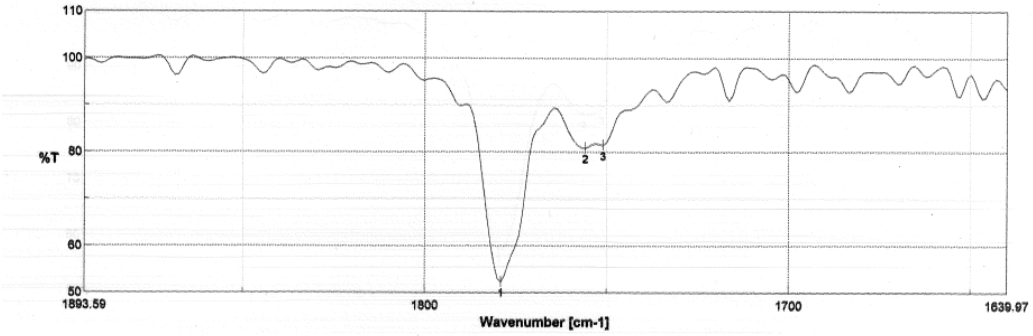

jaco (R)-0.05M-dec CCl4
EC-(R)-CFTA-0.05M CCl4

No.	cm-1	%T	No.	cm-1	%T	No.	cm-1	%T
1	1779.01	52.3147	2	1755.87	80.8753	3	1751.05	81.47

Spectra of the *(R)* and *(S)* diastereomers in CCl_4 at 0.01M concentration

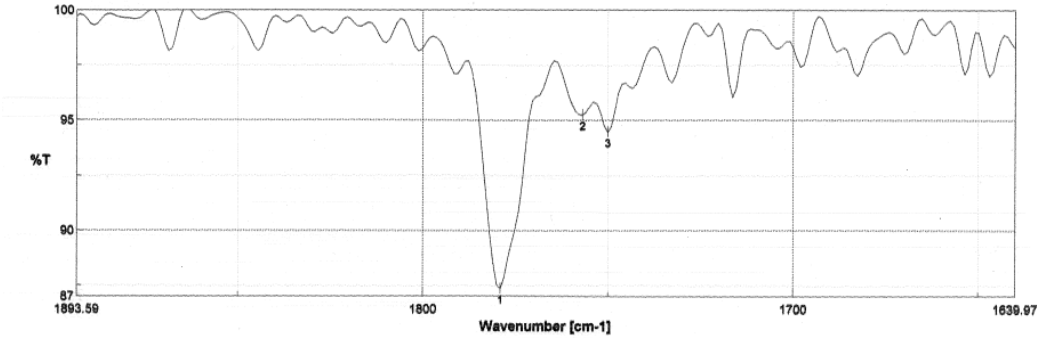

jaco (R)-0.01M-dec CCl4
EC-(R)-CFTA-0.01M CCl4

No.	cm-1	%T	No.	cm-1	%T	No.	cm-1	%T
1	1779.01	87.3508	2	1756.83	95.2402	3	1750.08	94.4535

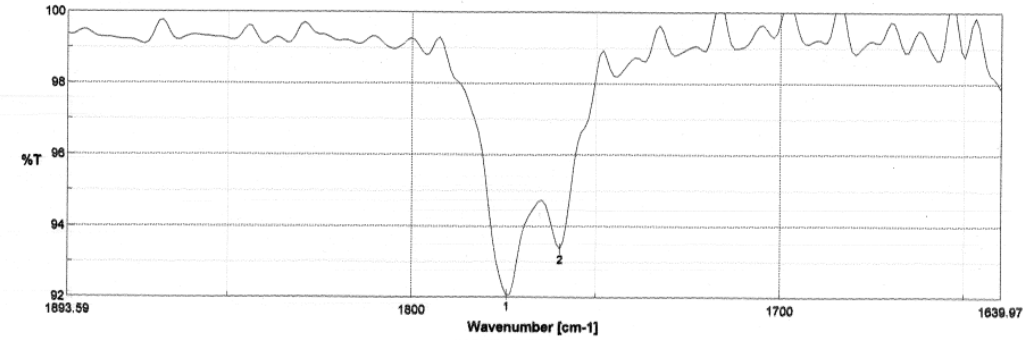

jaco (S)-0.01M-dec CCl4
EC-(S)-CFTA-0.01M CCl4

No.	cm-1	%T	No.	cm-1	%T
1	1774.19	92.0653	2	1759.73	93.3753

Spectra of the *(R)* and *(S)* diastereomers in $CHCl_3$ at 0.05M concentration

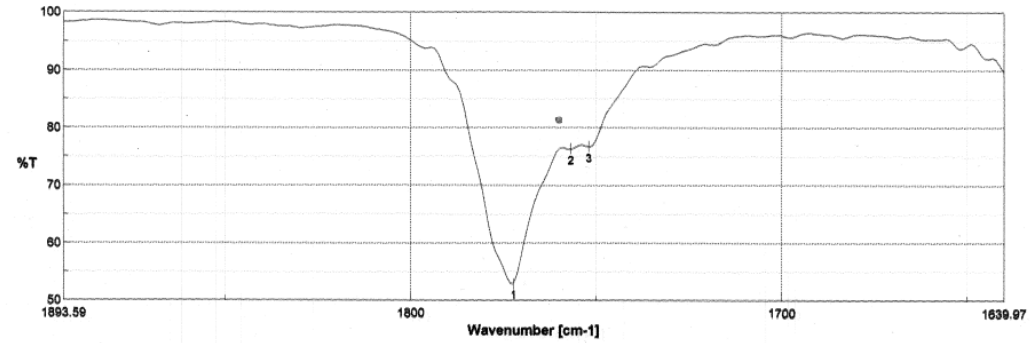

jaco (R)-0.05M-dec CHCl3
EC-(R)-CFTA-0.05M CHCl3

No.	cm-1	%T	No.	cm-1	%T	No.	cm-1	%T
1	1772.26	52.944	2	1756.83	76.2716	3	1752.01	76.6633

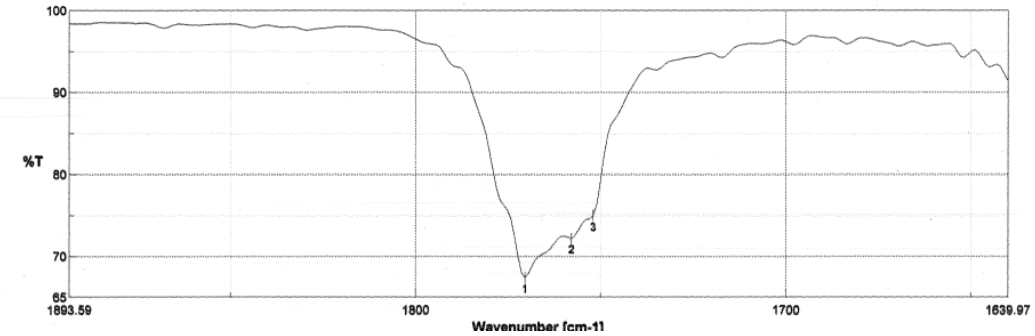

jaco (S)-0.05M-dec CHCl3
EC-(S)-CFTA-0.05M CHCl3

No.	cm-1	%T	No.	cm-1	%T	No.	cm-1	%T
1	1770.33	67.4316	2	1757.8	72.2405	3	1752.01	74.9503

Spectra of the *(R)* and *(S)* diastereomers in $CHCl_3$ at 0.01M concentration

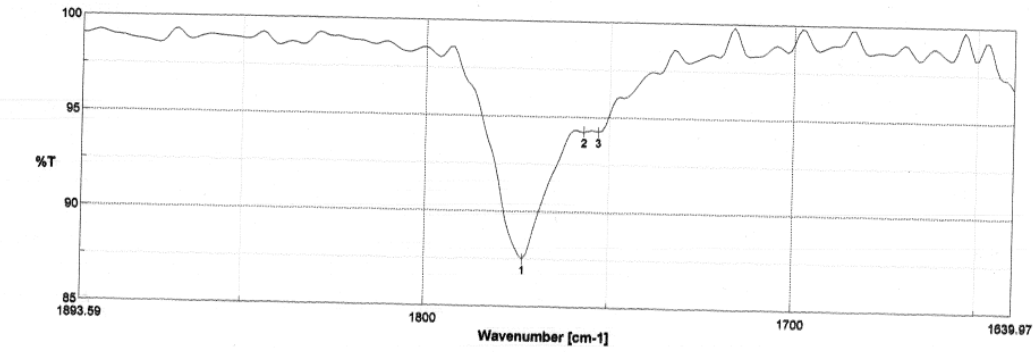

jaco (R)-0.01M-dec CHCl3
EC-(R)-CFTA-0.01M CHCl3

No.	cm-1	%T	No.	cm-1	%T	No.	cm-1	%T
1	1773.23	87.5281	2	1756.83	94.2159	3	1752.98	94.2366

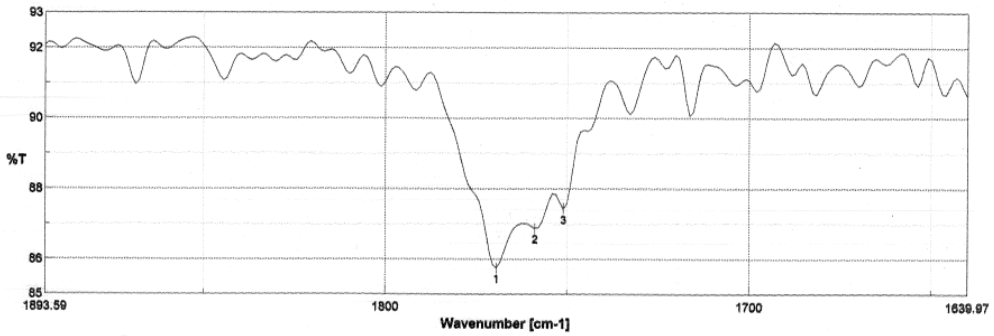

jaco (S)-0.01M-dec CHCl3
pori

No.	cm-1	%T	No.	cm-1	%T	No.	cm-1	%T
1	1769.37	85.7528	2	1758.76	86.8746	3	1751.05	87.4304

Appendix 5.2

NBO Calculation Example for Methylamine

Running an NBO Calculation

This appendix provides an introductory textbook example on running an NBO calculation and interpreting the output. The example chosen is that of methylamine (CH_3NH_2) in Pople-Gordon idealized geometry, treated at the *ab initio* RHF/3-21G level. This simple split-valence basis set consists of 28 AO's (nine each on C and N, two on each H), extended by 13 AO's beyond the minimal basis level.

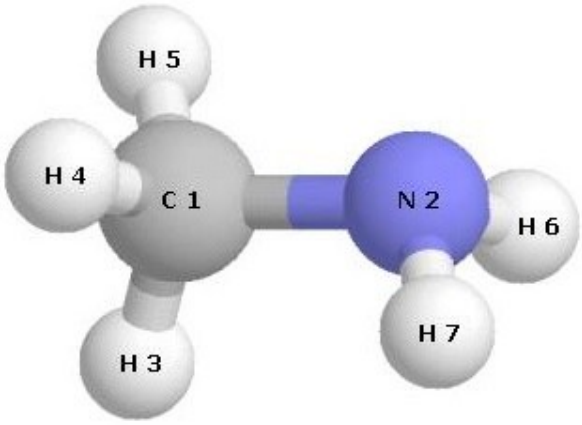

Input files to perform this calculation are given here for Gaussian and GAMESS. The pop=nbo option of the Gaussian program requests default NBO analysis. NBO analysis is requested in the GAMESS calculation by simply including the line

$NBO $END in the GAMESS input file. This "empty" NBO keylist specifies that NBO analysis should be carried out at the *default* level.

The default NBO output produced by this example is shown below, just as it appears in your output file. The start of the NBO section is marked by a standard header, citation, job title, and storage info:

```
********************************** NBO 5.0
**********************************
           N A T U R A L   A T O M I C   O R B I T A L   A N D
         N A T U R A L   B O N D   O R B I T A L   A N A L Y S I S
*******************************************************************
**********
 (c) Copyright 1996-2001 Board of Regents of the University of
Wisconsin System
     on behalf of the Theoretical Chemistry Institute.  All Rights
Reserved.

         Cite this program as:
```

```
         NBO 5.0.  E. D. Glendening, J. K. Badenhoop, A. E. Reed,
         J. E. Carpenter, J. A. Bohmann, C. M. Morales, and F.
Weinhold
         (Theoretical Chemistry Institute, University of Wisconsin,
         Madison, WI, 2001)

Job title: Methylamine...RHF/3-21G//Pople-Gordon standard geometry

Storage needed:        2562 in NPA,        3278 in NBO (     2000000
available)
```

Note that all NBO output is formatted to a maximum 80-character width for convenient display. The NBO heading echoes any requested keywords (none for the present default case).

Natural Population Analysis

The next four NBO output segments summarize the results of natural population analysis (NPA). The first segment is the main table of natural atomic orbitals (NAO's) as shown below: NATURAL POPULATIONS: Natural atomic orbital occupancies

```
 NAO Atom #  lang   Type(AO)    Occupancy      Energy
---------------------------------------------------------
  1    C  1  s      Cor( 1s)     1.99900     -11.04184
  2    C  1  s      Val( 2s)     1.09038      -0.28186
  3    C  1  s      Ryd( 3s)     0.00068       1.95506
  4    C  1  px     Val( 2p)     0.89085      -0.01645
  5    C  1  px     Ryd( 3p)     0.00137       0.93125
  6    C  1  py     Val( 2p)     1.21211      -0.07191
  7    C  1  py     Ryd( 3p)     0.00068       1.03027
  8    C  1  pz     Val( 2p)     1.24514      -0.08862
  9    C  1  pz     Ryd( 3p)     0.00057       1.01801

 10    N  2  s      Cor( 1s)     1.99953     -15.25950
 11    N  2  s      Val( 2s)     1.42608      -0.71700
 12    N  2  s      Ryd( 3s)     0.00016       2.75771
 13    N  2  px     Val( 2p)     1.28262      -0.18042
 14    N  2  px     Ryd( 3p)     0.00109       1.57018
 15    N  2  py     Val( 2p)     1.83295      -0.33858
 16    N  2  py     Ryd( 3p)     0.00190       1.48447
 17    N  2  pz     Val( 2p)     1.35214      -0.19175
 18    N  2  pz     Ryd( 3p)     0.00069       1.59492

 19    H  3  s      Val( 1s)     0.81453       0.13283
 20    H  3  s      Ryd( 2s)     0.00177       0.95067

 21    H  4  s      Val( 1s)     0.78192       0.15354
 22    H  4  s      Ryd( 2s)     0.00096       0.94521

 23    H  5  s      Val( 1s)     0.78192       0.15354
 24    H  5  s      Ryd( 2s)     0.00096       0.94521
```

```
25    H  6  s      Val( 1s)     0.63879       0.20572
26    H  6  s      Ryd( 2s)     0.00122       0.99883

27    H  7  s      Val( 1s)     0.63879       0.20572
28    H  7  s      Ryd( 2s)     0.00122       0.99883
```

For each of the 28 NAO functions, this table lists the atom to which the NAO is attached, the angular momentum type (*s*, p_x, etc.), the orbital type (whether core, valence, or Rydberg, with a conventional hydrogenic-type label), the orbital occupancy (number of electrons, or "natural population" of the orbital), and the orbital energy (in atomic units: 1 a.u. = 627.5 kcal/mol). Note that the occupancies of the Rydberg (Ryd) NAO's are typically much lower than those of the core (Cor) and valence (Val) NAO's of the natural minimum basis (NMB) set, reflecting the dominant role of the NMB orbitals in describing molecular properties.

The NAO's have the expected shapes and nodal structures of hydrogen-like orbitals. For example, some *s*-type and *p*-type NAO's of carbon atom C(1) are displayed below in 3-D (surface), 2-D (contour) and 1-D (profile) orbital images:

Naxos of C(1)

3-D Surface	2-D Contour	1-D Profile
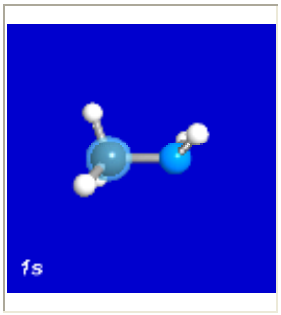	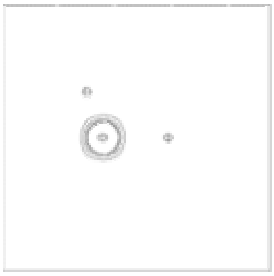	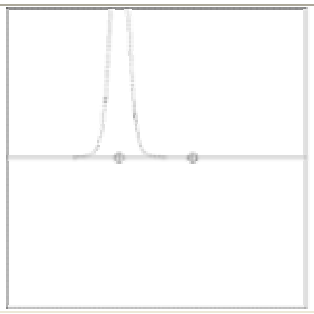
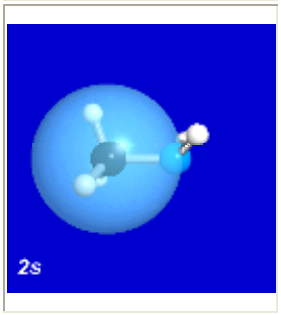	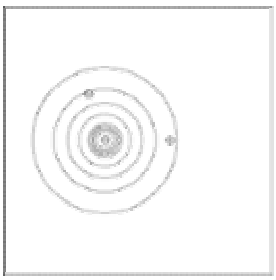	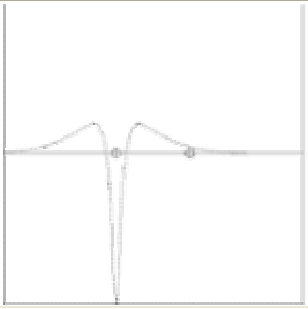

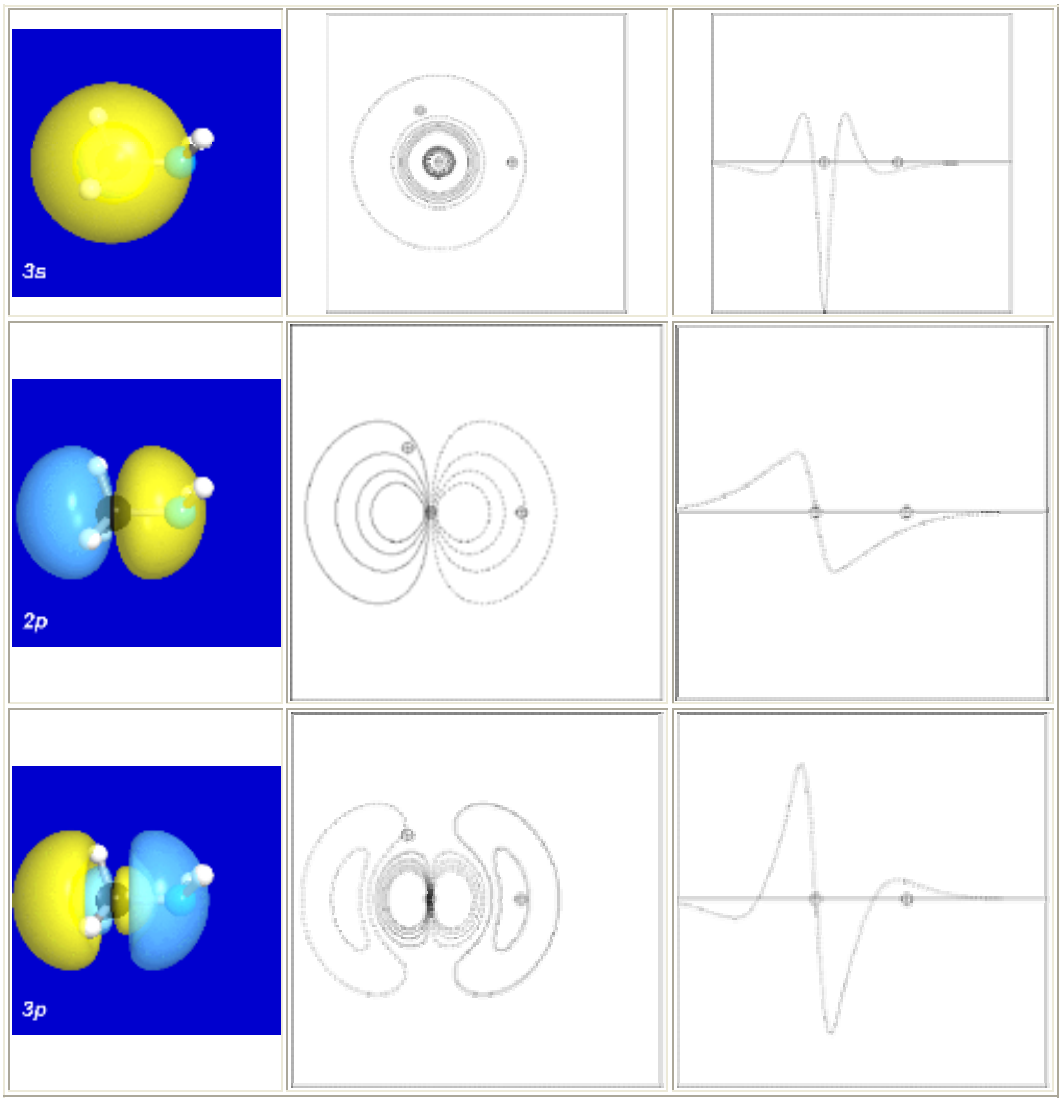

The principal quantum numbers for the NAO labels (1*s*, 2*s*, 3*s*, etc.) are assigned on the basis of the energy if a Fock or Kohn-Sham matrix is available, or on the basis of occupancy otherwise. A message warning of a "population inversion" is printed if the occupancy and energy ordering do not coincide (of interest, but rarely of concern).

The next segment is an atomic summary showing the natural atomic charges (nuclear charge minus summed natural populations of NAO's on the atom) and total core, valence, and Rydberg populations on each atom: Summary of Natural Population Analysis:

		Natural	Natural Population			
Atom	#	Charge	Core	Valence	Rydberg	Total
C	1	-0.44079	1.99900	4.43848	0.00331	6.44079
N	2	-0.89715	1.99953	5.89378	0.00384	7.89715
H	3	0.18370	0.00000	0.81453	0.00177	0.81630
H	4	0.21713	0.00000	0.78192	0.00096	0.78287
H	5	0.21713	0.00000	0.78192	0.00096	0.78287
H	6	0.35999	0.00000	0.63879	0.00122	0.64001
H	7	0.35999	0.00000	0.63879	0.00122	0.64001
* Total *		0.00000	3.99853	13.98820	0.01328	18.00000

This table succinctly describes the molecular charge distribution in terms of NPA charges, as shown in the diagram:

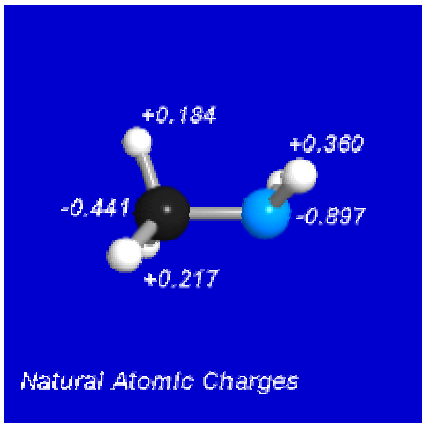

Next follows a summary of the natural minimal basis (NMB) and natural Rydberg basis (NRB) populations for the composite system, summed over atoms:

	Natural Population	
Core	3.99853	(99.9632% of 4)
Valence	13.98820	(99.9157% of 14)
Natural Minimal Basis	17.98672	(99.9262% of 18)
Natural Rydberg Basis	0.01328	(0.0738% of 18)

This reveals the high percentage contribution (typically, > 99%) of the NMB set to the molecular charge distribution.

Finally, the natural populations are summarized as an effective valence electron configuration ("natural electron configuration") for each atom:

```
   Atom #          Natural Electron Configuration
-----------------------------------------------------------------------
-------
     C  1      [core]2s( 1.09)2p( 3.35)
     N  2      [core]2s( 1.43)2p( 4.47)
     H  3           1s( 0.81)
     H  4           1s( 0.78)
     H  5           1s( 0.78)
     H  6           1s( 0.64)
     H  7           1s( 0.64)
```

Although the occupancies of the atomic orbitals are non-integer in the molecular environment, the effective atomic configurations can be related to idealized atomic states in "promoted" configurations. For example, the carbon atom is seen to have valence configuration $(2s)^{1.09}(2p)^{3.35}$, approximating the idealized promoted configuration for sp^3 hybridization.

Natural Bond Orbital Analysis

The next segments of the output summarize the results of NBO analysis. The first segment reports on details of the search for an NBO natural Lewis structure:

```
NATURAL BOND ORBITAL ANALYSIS:

                     Occupancies       Lewis Structure    Low   High
          Occ.    -------------------  -----------------   occ   occ
 Cycle   Thresh.    Lewis   Non-Lewis     CR  BD  3C  LP    (L)   (NL)
Dev
=======================================================================
========
  1(1)    1.90    17.95048   0.04952      2   6   0   1     0      0
0.02
-----------------------------------------------------------------------
--------

Structure accepted: No low occupancy Lewis orbitals
```

Normally, there is but one cycle of the NBO search. The table summarizes a variety of information for each cycle: the occupancy threshold for a "good" pair in the NBO search; the total populations of Lewis and non-Lewis NBO's; the number of core (CR), 2-center bond (BD), 3-center bond (3C), and lone pair (LP) NBO's in the natural Lewis structure; the number of low-occupancy Lewis (L) and high-occupancy (> 0.1e) non-Lewis (NL) orbitals; and the maximum deviation (Dev) of any formal

bond order for the structure from a nominal estimate (NAO Wiberg bond index). The Lewis structure is accepted if all orbitals of the formal Lewis structure exceed the occupancy threshold (default = 1.90 electrons).

Next follows a more detailed breakdown of the Lewis and non-Lewis occupancies into core, valence, and Rydberg shell contributions:

```
WARNING:  1 low occupancy (<1.9990e) core orbital  found on  C 1

------------------------------------------------------------
  Core                      3.99853 ( 99.963% of   4)
  Valence Lewis            13.95195 ( 99.657% of  14)
 ==================       ============================
  Total Lewis              17.95048 ( 99.725% of  18)
 ------------------------------------------------------------
  Valence non-Lewis         0.03977 (  0.221% of  18)
  Rydberg non-Lewis         0.00975 (  0.054% of  18)
 ==================       ============================
  Total non-Lewis           0.04952 (  0.275% of  18)
------------------------------------------------------------
```

This shows the general quality of the natural Lewis structure description in terms of the percentage of the total electron density (e.g., in the above case, about 99.7%). The table also exhibits the relatively important role of the valence non-Lewis orbitals (i.e., the six valence antibonds, NBO's 23-28, listed below) relative to the extra-valence orbitals (the 13 Rydberg NBO's 10-22) in the slight departures from a localized Lewis structure model. The table also includes a warning about a carbon core orbital with slightly less than double occupancy.

Next follows the main listing of NBO's, displaying the form and occupancy of the complete set of orbitals that span the input AO space:

```
    (Occupancy)   Bond orbital/ Coefficients/ Hybrids
--------------------------------------------------------------------------------
  1. (1.99858) BD ( 1) C 1- N 2
               ( 40.07%)   0.6330* C 1 s( 21.71%)p 3.61( 78.29%)
                                    -0.0003 -0.4653 -0.0238 -0.8808 -0.0291
                                    -0.0786 -0.0110  0.0000  0.0000
               ( 59.93%)   0.7742* N 2 s( 30.88%)p 2.24( 69.12%)
                                    -0.0001 -0.5557  0.0011  0.8302  0.0004
                                     0.0443 -0.0098  0.0000  0.0000
  2. (1.99860) BD ( 1) C 1- H 3
               ( 59.71%)   0.7727* C 1 s( 25.78%)p 2.88( 74.22%)
                                    -0.0002 -0.5077  0.0069  0.1928  0.0098
                                     0.8396 -0.0046  0.0000  0.0000
               ( 40.29%)   0.6347* H 3 s(100.00%)
                                    -1.0000 -0.0030
  3. (1.99399) BD ( 1) C 1- H 4
               ( 61.02%)   0.7812* C 1 s( 26.28%)p 2.80( 73.72%)
                                     0.0001  0.5127 -0.0038 -0.3046 -0.0015
                                     0.3800 -0.0017  0.7070 -0.0103
               ( 38.98%)   0.6243* H 4 s(100.00%)
                                     1.0000  0.0008
```

```
 4. (1.99399) BD ( 1) C 1- H 5
              ( 61.02%)   0.7812* C 1 s( 26.28%)p 2.80( 73.72%)
                                       0.0001  0.5127 -0.0038 -0.3046 -0.0015
                                       0.3800 -0.0017 -0.7070  0.0103
              ( 38.98%)   0.6243* H 5 s(100.00%)
                                       1.0000  0.0008
 5. (1.99442) BD ( 1) N 2- H 6
              ( 68.12%)   0.8253* N 2 s( 25.62%)p 2.90( 74.38%)
                                       0.0000  0.5062  0.0005  0.3571  0.0171
                                      -0.3405  0.0069 -0.7070 -0.0093
              ( 31.88%)   0.5646* H 6 s(100.00%)
                                       1.0000  0.0020
 6. (1.99442) BD ( 1) N 2- H 7
              ( 68.12%)   0.8253* N 2 s( 25.62%)p 2.90( 74.38%)
                                       0.0000  0.5062  0.0005  0.3571  0.0171
                                      -0.3405  0.0069  0.7070  0.0093
              ( 31.88%)   0.5646* H 7 s(100.00%)
                                       1.0000  0.0020
 7. (1.99900) CR ( 1) C 1             s(100.00%)p 0.00(  0.00%)
                                       1.0000 -0.0003  0.0000 -0.0002  0.0000
                                       0.0001  0.0000  0.0000  0.0000
 8. (1.99953) CR ( 1) N 2             s(100.00%)p 0.00(  0.00%)
                                       1.0000 -0.0001  0.0000  0.0001  0.0000
                                       0.0000  0.0000  0.0000  0.0000
 9. (1.97795) LP ( 1) N 2             s( 17.85%)p 4.60( 82.15%)
                                       0.0000  0.4225  0.0002  0.2360 -0.0027
                                       0.8749 -0.0162  0.0000  0.0000
10. (0.00105) RY*( 1) C 1             s(  1.57%)p62.84( 98.43%)
                                       0.0000 -0.0095  0.1248 -0.0305  0.7302
                                      -0.0046  0.6710  0.0000  0.0000
11. (0.00034) RY*( 2) C 1             s(  0.00%)p 1.00(100.00%)
                                       0.0000  0.0000  0.0000  0.0000  0.0000
                                       0.0000  0.0000  0.0146  0.9999
12. (0.00022) RY*( 3) C 1             s( 56.51%)p 0.77( 43.49%)
                                       0.0000 -0.0023  0.7517 -0.0237  0.3710
                                      -0.0094 -0.5447  0.0000  0.0000
13. (0.00002) RY*( 4) C 1             s( 41.87%)p 1.39( 58.13%)
14. (0.00116) RY*( 1) N 2             s(  1.50%)p65.53( 98.50%)
                                       0.0000 -0.0062  0.1224  0.0063  0.0371
                                       0.0197  0.9915  0.0000  0.0000
15. (0.00044) RY*( 2) N 2             s(  0.00%)p 1.00(100.00%)
                                       0.0000  0.0000  0.0000  0.0000  0.0000
                                       0.0000  0.0000 -0.0132  0.9999
16. (0.00038) RY*( 3) N 2             s( 33.38%)p 2.00( 66.62%)
                                       0.0000  0.0133  0.5776  0.0087 -0.8150
                                      -0.0121 -0.0405  0.0000  0.0000
17. (0.00002) RY*( 4) N 2             s( 65.14%)p 0.54( 34.86%)
18. (0.00178) RY*( 1) H 3             s(100.00%)
                                      -0.0030  1.0000
19. (0.00096) RY*( 1) H 4             s(100.00%)
                                      -0.0008  1.0000
20. (0.00096) RY*( 1) H 5             s(100.00%)
                                      -0.0008  1.0000
21. (0.00122) RY*( 1) H 6             s(100.00%)
                                      -0.0020  1.0000
22. (0.00122) RY*( 1) H 7             s(100.00%)
                                      -0.0020  1.0000
23. (0.00016) BD*( 1) C 1- N 2
              ( 59.93%)   0.7742* C 1 s( 21.71%)p 3.61( 78.29%)
                                      -0.0003 -0.4653 -0.0238 -0.8808 -0.0291
                                      -0.0786 -0.0110  0.0000  0.0000
              ( 40.07%)  -0.6330* N 2 s( 30.88%)p 2.24( 69.12%)
                                      -0.0001 -0.5557  0.0011  0.8302  0.0004
                                       0.0443 -0.0098  0.0000  0.0000
24. (0.01569) BD*( 1) C 1- H 3
              ( 40.29%)   0.6347* C 1 s( 25.78%)p 2.88( 74.22%)
                                       0.0002  0.5077 -0.0069 -0.1928 -0.0098
                                      -0.8396  0.0046  0.0000  0.0000
              ( 59.71%)  -0.7727* H 3 s(100.00%)
                                       1.0000  0.0030
25. (0.00769) BD*( 1) C 1- H 4
              ( 38.98%)   0.6243* C 1 s( 26.28%)p 2.80( 73.72%)
                                      -0.0001 -0.5127  0.0038  0.3046  0.0015
                                      -0.3800  0.0017 -0.7070  0.0103
              ( 61.02%)  -0.7812* H 4 s(100.00%)
                                      -1.0000 -0.0008
```

```
26. (0.00769) BD*( 1) C 1- H 5
              ( 38.98%)   0.6243* C 1 s( 26.28%)p 2.80( 73.72%)
                                     -0.0001 -0.5127  0.0038  0.3046  0.0015
                                     -0.3800  0.0017  0.7070 -0.0103
              ( 61.02%)  -0.7812* H 5 s(100.00%)
                                     -1.0000 -0.0008
27. (0.00426) BD*( 1) N 2- H 6
              ( 31.88%)   0.5646* N 2 s( 25.62%)p 2.90( 74.38%)
                                      0.0000 -0.5062 -0.0005 -0.3571 -0.0171
                                      0.3405 -0.0069  0.7070  0.0093
              ( 68.12%)  -0.8253* H 6 s(100.00%)
                                     -1.0000 -0.0020
28. (0.00426) BD*( 1) N 2- H 7
              ( 31.88%)   0.5646* N 2 s( 25.62%)p 2.90( 74.38%)
                                      0.0000 -0.5062 -0.0005 -0.3571 -0.0171
                                      0.3405 -0.0069 -0.7070 -0.0093
              ( 68.12%)  -0.8253* H 7 s(100.00%)
                                     -1.0000 -0.0020
```

For each NBO (1-28), the first line of printout shows the occupancy (between 0 and 2 electrons) and unique label of the NBO. This label gives the type (BD for 2-center bond, CR for 1-center core pair, LP for 1-center valence lone pair, RY* for 1-center Rydberg, and BD* for 2-center antibond, the unstarred and starred labels corresponding to Lewis and non-Lewis NBO's, respectively), a serial number (1, 2,... if there is a single, double,... bond between the pair of atoms), and the atom(s) to which the NBO is affixed. The next lines summarize the natural atomic hybrids h_A of which the NBO is composed, giving the percentage (c_A-squared) of the NBO on each hybrid (in parentheses), the polarization coefficient c_A, the atom label, and a hybrid label showing the *sp*-hybridization (percentage *s*-character, *p*-character, etc.) of each h_A. For example, the C-N bond (NBO 1; lower panel) and antibond (NBO 23; upper panel)

$$\sigma_{CN} = 0.663(sp^{3.61})_C + 0.774(sp^{2.24})_N$$
$$\sigma_{CN}^* = 0.774(sp^{3.61})_C - 0.633(sp^{2.24})_N$$

are displayed below, together with the C($sp^{3.61}$) and N($sp^{2.24}$) bonding NHO's (middle panels) of which they are both composed (but with opposing polarizations and phases):

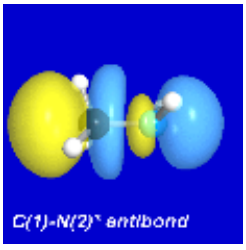

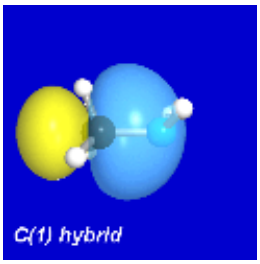

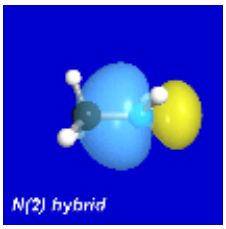

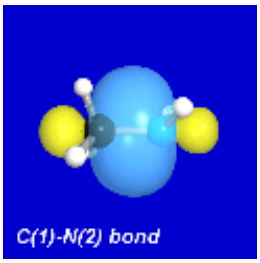

Below each NHO label is the set of coefficients that specify how the NHO is written explicitly as a linear combination of NAO's on the atom. The order of NAO coefficients follows the numbering of the NAO tables.

In the CH_3NH_2 example, the NBO search finds the C-N bond (NBO 1), three C-H bonds (NBO's 2, 3, 4), two N-H bonds (NBO's 5, 6), N lone pair (NBO 9), and C and N core pairs (NBO's 7, 8) of the expected Lewis structure. NBO's 10-28 represent the residual non-Lewis NBO's of low occupancy. In this example, it is also interesting to note the slight asymmetry of the three σ_{CH} NBO's, and the slightly higher occupancy (0.016 *vs.* 0.008 electrons) in the σ_{CH3} antibond (NBO 24) lying *trans* to the nitrogen lone pair.

NHO Directional Analysis

The next segment of output summarizes the angular properties of the natural hybrid orbitals (NHO's):

```
NHO Directionality and "Bond Bending" (deviations from line of nuclear
centers)

        [Thresholds for printing:  angular deviation  >  1.0 degree]
                                   hybrid p-character > 25.0%
                                   orbital occupancy  >  0.10e

                      Line of Centers        Hybrid 1              Hybrid 2
                      ---------------  -------------------   ---------------
---
          NBO           Theta   Phi    Theta   Phi    Dev    Theta   Phi
Dev
================================================================================
===
  1. BD ( 1) C 1- N 2    90.0    5.4     --     --    --      90.0  182.4
3.0
  3. BD ( 1) C 1- H 4    35.3  130.7    34.9  129.0   1.0      --     --
--
  4. BD ( 1) C 1- H 5   144.7  130.7   145.1  129.0   1.0      --     --
--
  5. BD ( 1) N 2- H 6   144.7  310.7   145.0  318.3   4.4      --     --
--
  6. BD ( 1) N 2- H 7    35.3  310.7    35.0  318.3   4.4      --     --
--
  9. LP ( 1) N 2          --     --     90.0   74.8   --       --     --
--
```

The "direction" of a hybrid is specified in terms of the polar (θ) and azimuthal (ϕ) angles (in the coordinate system of the calling program) of the vector describing its *p*-component. For more general $sp^{\lambda}d^{\mu}$ hybrids the hybrid direction is determined numerically to correspond to the maximum angular amplitude. The hybrid direction is then compared with the direction of the line of centers between the two nuclei to determine the bending of the bond, expressed as the deviation angle (Dev, in degrees) between these two directions. For example, in the CH_3NH_2 case shown above, the nitrogen NHO of the σ_{CN} bond (NBO 1) is bent away from the line of C-N centers by 3.0°, whereas the carbon NHO is approximately aligned with the C-N axis (within the 1.0° threshold for printing). The N-H bonds (NBO's 5, 6) are bent even further (by 4.4°). The information in this table is often useful in anticipating the direction of geometry changes resulting from geometry optimization (viz., likely reduced pyramidalization of the -NH_2 group to relieve the ~4° nitrogen bond bending found in the tetrahedral Pople-Gordon geometry).

Perturbation Theory Energy Analysis

The next segment summarizes the second-order perturbative estimates of donor-acceptor (bond-antibond) interactions in the NBO basis:

```
Second Order Perturbation Theory Analysis of Fock Matrix in NBO Basis

    Threshold for printing:   0.50 kcal/mol
                                                                 E(2)  E(j)-E(i) F(i,j)
     Donor NBO (i)              Acceptor NBO (j)               kcal/mol   a.u.    a.u.
===========================================================================================

within unit  1
  2. BD ( 1) C 1- H 3     / 14. RY*( 1) N 2                    0.84    2.18    0.038
  3. BD ( 1) C 1- H 4     / 26. BD*( 1) C 1- H 5               0.52    1.39    0.024
  3. BD ( 1) C 1- H 4     / 27. BD*( 1) N 2- H 6               3.03    1.37    0.057
  4. BD ( 1) C 1- H 5     / 25. BD*( 1) C 1- H 4               0.52    1.39    0.024
  4. BD ( 1) C 1- H 5     / 28. BD*( 1) N 2- H 7               3.03    1.37    0.057
  5. BD ( 1) N 2- H 6     / 10. RY*( 1) C 1                    0.56    1.78    0.028
  5. BD ( 1) N 2- H 6     / 25. BD*( 1) C 1- H 4               2.85    1.51    0.059
  6. BD ( 1) N 2- H 7     / 10. RY*( 1) C 1                    0.56    1.78    0.028
  6. BD ( 1) N 2- H 7     / 26. BD*( 1) C 1- H 5               2.85    1.51    0.059
  7. CR ( 1) C 1          / 16. RY*( 3) N 2                    0.61   13.11    0.080
  7. CR ( 1) C 1          / 18. RY*( 1) H 3                    1.40   11.99    0.116
  7. CR ( 1) C 1          / 19. RY*( 1) H 4                    1.55   11.99    0.122
  7. CR ( 1) C 1          / 20. RY*( 1) H 5                    1.55   11.99    0.122
  8. CR ( 1) N 2          / 10. RY*( 1) C 1                    1.51   16.23    0.140
  8. CR ( 1) N 2          / 12. RY*( 3) C 1                    0.84   16.77    0.106
  8. CR ( 1) N 2          / 21. RY*( 1) H 6                    0.61   16.26    0.089
  8. CR ( 1) N 2          / 22. RY*( 1) H 7                    0.61   16.26    0.089
  9. LP ( 1) N 2          / 24. BD*( 1) C 1- H 3               8.13    1.13    0.086
  9. LP ( 1) N 2          / 25. BD*( 1) C 1- H 4               1.46    1.14    0.037
  9. LP ( 1) N 2          / 26. BD*( 1) C 1- H 5               1.46    1.14    0.037
```

This analysis is carried out by examining all possible interactions between "filled" (donor) Lewis-type NBO's and "empty" (acceptor) non-Lewis NBO's, and estimating their energetic importance by 2nd-order perturbation theory. Since these interactions lead to donation of occupancy from the localized NBO's of the idealized Lewis structure into the empty non-Lewis orbitals (and thus, to departures from the idealized Lewis structure description), they are referred to as "delocalization" corrections to the zeroth-order natural Lewis structure. For each donor NBO (i) and acceptor NBO (j), the stabilization energy $E(2)$ associated with delocalization ("2e-stabilization") $i \rightarrow j$ is estimated as

$$E(2) = \Delta E_{ij} = q_i \frac{F(i,j)^2}{\varepsilon_j - \varepsilon_i}$$

where q_i is the donor orbital occupancy, ε_i, ε_j are diagonal elements (orbital energies) and $F(i,j)$ is the off-diagonal NBO Fock matrix element. [In the example above, the n_N

$\rightarrow \sigma_{CH}^*$ interaction between the nitrogen lone pair (NBO 9) and the antiperiplanar C_1-H_3 antibond (NBO 24) is seen to give the strongest stabilization, 8.13 kcal/mol. As the heading indicates, entries are included in this table only when the interaction energy exceeds a default threshold of 0.5 kcal/mol.

NBO Summary

Next appears a condensed summary of the principal NBO's, showing the occupancy, orbital energy, and the qualitative pattern of delocalization interactions associated with each:

```
Natural Bond Orbitals (Summary):

                                                           Principal
Delocalizations
           NBO              Occupancy    Energy
(geminal,vicinal,remote)
================================================================================
==========
Molecular unit  1  (CH5N)
  1. BD ( 1) C 1- N 2       1.99858    -0.89908
  2. BD ( 1) C 1- H 3       1.99860    -0.69181    14(v)
  3. BD ( 1) C 1- H 4       1.99399    -0.68892    27(v),26(g)
  4. BD ( 1) C 1- H 5       1.99399    -0.68892    28(v),25(g)
  5. BD ( 1) N 2- H 6       1.99442    -0.80951    25(v),10(v)
  6. BD ( 1) N 2- H 7       1.99442    -0.80951    26(v),10(v)
  7. CR ( 1) C 1            1.99900   -11.04131
19(v),20(v),18(v),16(v)
  8. CR ( 1) N 2            1.99953   -15.25927
10(v),12(v),21(v),22(v)
  9. LP ( 1) N 2            1.97795    -0.44592    24(v),25(v),26(v)
 10. RY*( 1) C 1            0.00105     0.97105
 11. RY*( 2) C 1            0.00034     1.02120
 12. RY*( 3) C 1            0.00022     1.51414
 13. RY*( 4) C 1            0.00002     1.42223
 14. RY*( 1) N 2            0.00116     1.48790
 15. RY*( 2) N 2            0.00044     1.59323
 16. RY*( 3) N 2            0.00038     2.06475
 17. RY*( 4) N 2            0.00002     2.25932
 18. RY*( 1) H 3            0.00178     0.94860
 19. RY*( 1) H 4            0.00096     0.94464
 20. RY*( 1) H 5            0.00096     0.94464
 21. RY*( 1) H 6            0.00122     0.99735
 22. RY*( 1) H 7            0.00122     0.99735
 23. BD*( 1) C 1- N 2       0.00016     0.57000
 24. BD*( 1) C 1- H 3       0.01569     0.68735
 25. BD*( 1) C 1- H 4       0.00769     0.69640
 26. BD*( 1) C 1- H 5       0.00769     0.69640
 27. BD*( 1) N 2- H 6       0.00426     0.68086
 28. BD*( 1) N 2- H 7       0.00426     0.68086
     -------------------------------
           Total Lewis    17.95048  ( 99.7249%)
      Valence non-Lewis     0.03977  (  0.2209%)
      Rydberg non-Lewis     0.00975  (  0.0542%)
```

```
      -------------------------------
           Total unit  1   18.00000  (100.0000%)
          Charge unit  1    0.00000
```

This table allows one to quickly identify the principal delocalizing acceptor orbitals associated with each donor NBO, and their topological relationship to this NBO, i.e., whether attached to the same atom (geminal, "g"), to an adjacent bonded atom (vicinal, "v"), or to a more remote ("r") site. These acceptor NBO's will generally correspond to the principal "delocalization tails" of the natural localized molecular orbital (NLMO) associated with the parent donor NBO. [For example, in the table above, the nitrogen lone pair (NBO 9) is seen to be the lowest-occupancy (1.978 electrons) and highest-energy (-0.446 a.u.) Lewis NBO, and to be primarily delocalized into antibonds 24, 25, 26 (the vicinal σ_{CH} NBO's). The summary at the bottom of the table shows that the Lewis NBO's 1-9 describe about 99.7% of the total electron density, with the remaining non-Lewis density found primarily in the valence-shell antibonds (particularly, NBO 24).]

A Textbook example on Energetic Analysis with NBO Deletions ($DEL Keylist)

Introduction to the $DEL Keylist and NBO Energetic Analysis

In G9X and GAMESS implementations, the NBO program makes it possible to determine the energetic effect of *deleting* certain NBO's, groups of NBO's, or specific NBO donor-acceptor interactions. This is done by including (following the main $NBO keylist) a special "deletions" $DEL keylist of the form

$DEL *keyword(s)* $END

(For a G9X host program, the POP=NBODEL keyword must also be included in the route card.)

As described in the NBO 5.0 Manual, a total of nine deletion types (each with specific keyword syntax) can be used to select specific classes of intra- or intermolecular Fock matrix elements for deletion. When combined with geometry optimization, the $DEL keylist also makes it possible to determine the structural consequences of specific NBO donor-acceptor interactions as the difference between the original fully-optimized geometry and the $DEL-optimized geometry.

In this Tutorial we employ $DEL keyword options to illustrate how simple chemical questions may be addressed in the case of a configurational energy difference.

Cis vs. *Trans* Configuration of Difluoroethene

1,2-difluoroethene exists in *cis* and *trans* isomers

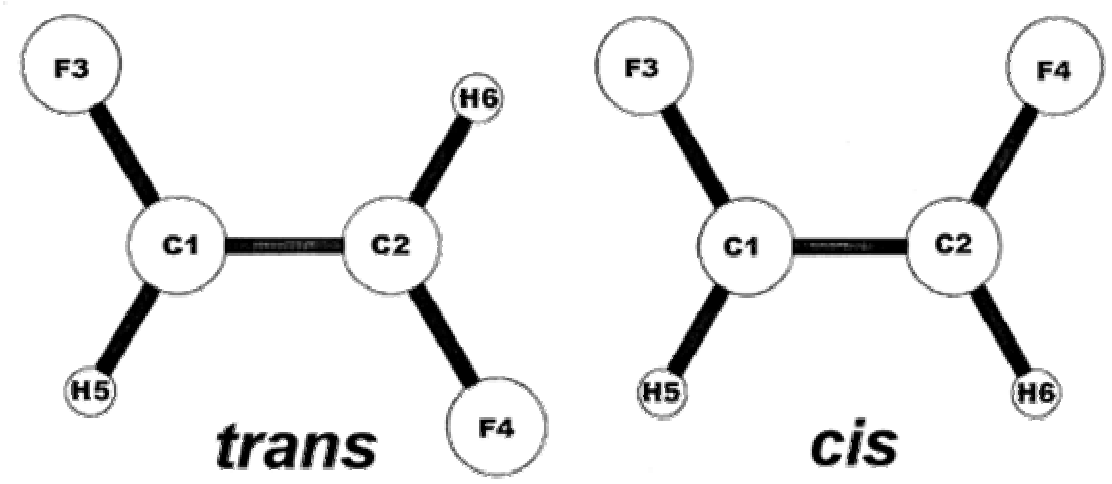

On the basis of steric and electrostatic factors the *trans* isomer is expected to be significantly more stable, because the two bulky F atoms and the repelling negative charges of the two CF bond dipoles are maximally separated in this configuration. However, the *cis* isomer is actually found to be very similar in energy. For example, in a simple RHF/6-31G* model with idealized trigonal geometry (R_{CF} = 1.33 A, R_{CC} = 1.34 A, R_{CH} = 1.08 A) the calculated energies are

$$E_{cis} = -275.71726 \text{ a.u.},$$
$$E_{trans} = -275.71761 \text{ a.u.}$$

corresponding to only a slight energy difference favouring the *trans* isomer.

$$E_{cis} - E_{trans} = 0.22 \text{ kcal/mol}$$

The model RHF calculation exhibits the near-equivalence of *cis* and *trans* configurational energies but does not help us to understand *why* the *cis* configuration is so competitive. In this Tutorial we show how to address such questions by using \$DEL keylists to investigate the effect of specific NBO donor-acceptor interactions on the isomeric energy difference.

Can the Surprising Stability of the *Cis* Isomer be Attributed to Electronic Delocalization?

The role of electronic delocalization can be quantitatively assessed by deleting *all* non-Lewis (starred) NBO's from the basis set with the NOSTAR keyword

$DEL NOSTAR $END

The resulting "natural Lewis structure" wavefunction is perfectly localized, with all Lewis-type NBO's doubly occupied. By the variational principle, the Lewis-type wavefunction has an energy E(L) that is higher than the original energy E(full). The net energy difference E(NL)

$$E(NL) = E(full) - E(L)$$

gives the stabilizing effect of the delocalizing (non-Lewis) contributions.

For the *cis* isomer, the sample G9X input file

```
%mem=2000000
#N HF/6-31G*  NOSYMM POP=NBODel

CHF::CHF (cis)

  0  1
 C
 C   1   1.34
 F   1   1.33   2  120.0
 F   2   1.33   1  120.0  3    0.0
 H   1   1.08   2  120.0  3  180.0
 H   2   1.08   1  120.0  4  180.0

$NBO file=dfe_c $END
$DEL
   nostar
$END
```

leads to the $DEL output shown below. The first output segment identifies the type of deletion ("NOSTAR: Delete all Rydberg/antibond NBO's") and lists the 48 Rydberg and antibond NBO's (17-64) that were deleted:

```
 NOSTAR: Delete all Rydberg/antibond NBO's
 Deletion of the following orbitals from the NBO Fock matrix:
   17  18  19  20  21  22  23  24  25  26  27  28  29  30  31  32  33
34  35  36

   37  38  39  40  41  42  43  44  45  46  47  48  49  50  51  52  53
54  55  56

   57  58  59  60  61  62  63  64
```

The next segment lists the NBO's with their original occupancies ("No deletions") and current occupancies ("This deletion"), together with the net change in each:

```
 Orbital occupancies:

      Orbital                    No deletions   This deletion
Change
 ------------------------------------------------------------------------
----------
  1. BD ( 1) C 1- C 2               1.99763        2.00000    0.00237
  2. BD ( 2) C 1- C 2               1.99676        2.00000    0.00324
  3. BD ( 1) C 1- F 3               1.99702        2.00000    0.00298
  4. BD ( 1) C 1- H 5               1.98669        2.00000    0.01331
  5. BD ( 1) C 2- F 4               1.99702        2.00000    0.00298
  6. BD ( 1) C 2- H 6               1.98669        2.00000    0.01331
  7. CR ( 1) C 1                    1.99873        2.00000    0.00127
  8. CR ( 1) C 2                    1.99873        2.00000    0.00127
  9. CR ( 1) F 3                    1.99994        2.00000    0.00006
 10. CR ( 1) F 4                    1.99994        2.00000    0.00006
 11. LP ( 1) F 3                    1.99224        2.00000    0.00776
 12. LP ( 2) F 3                    1.97331        2.00000    0.02669
 13. LP ( 3) F 3                    1.94914        2.00000    0.05086
 14. LP ( 1) F 4                    1.99224        2.00000    0.00776
 15. LP ( 2) F 4                    1.97331        2.00000    0.02669
 16. LP ( 3) F 4                    1.94914        2.00000    0.05086
 17. RY*( 1) C 1                    0.00613        0.00000   -0.00613
 18. RY*( 2) C 1                    0.00453        0.00000   -0.00453
 19. RY*( 3) C 1                    0.00197        0.00000   -0.00197
 20. RY*( 4) C 1                    0.00131        0.00000   -0.00131
 21. RY*( 5) C 1                    0.00026        0.00000   -0.00026
 22. RY*( 6) C 1                    0.00017        0.00000   -0.00017
 23. RY*( 7) C 1                    0.00008        0.00000   -0.00008
 24. RY*( 8) C 1                    0.00000        0.00000    0.00000
 25. RY*( 9) C 1                    0.00001        0.00000   -0.00001
 26. RY*(10) C 1                    0.00001        0.00000   -0.00001
 27. RY*( 1) C 2                    0.00613        0.00000   -0.00613
 28. RY*( 2) C 2                    0.00453        0.00000   -0.00453
 29. RY*( 3) C 2                    0.00197        0.00000   -0.00197
 30. RY*( 4) C 2                    0.00131        0.00000   -0.00131
 31. RY*( 5) C 2                    0.00026        0.00000   -0.00026
 32. RY*( 6) C 2                    0.00017        0.00000   -0.00017
 33. RY*( 7) C 2                    0.00008        0.00000   -0.00008
 34. RY*( 8) C 2                    0.00000        0.00000    0.00000
 35. RY*( 9) C 2                    0.00001        0.00000   -0.00001
 36. RY*(10) C 2                    0.00001        0.00000   -0.00001
 37. RY*( 1) F 3                    0.00171        0.00000   -0.00171
 38. RY*( 2) F 3                    0.00159        0.00000   -0.00159
 39. RY*( 3) F 3                    0.00007        0.00000   -0.00007
 40. RY*( 4) F 3                    0.00004        0.00000   -0.00004
 41. RY*( 5) F 3                    0.00001        0.00000   -0.00001
 42. RY*( 6) F 3                    0.00001        0.00000   -0.00001
 43. RY*( 7) F 3                    0.00000        0.00000    0.00000
 44. RY*( 8) F 3                    0.00000        0.00000    0.00000
 45. RY*( 9) F 3                    0.00000        0.00000    0.00000
 46. RY*(10) F 3                    0.00001        0.00000   -0.00001
 47. RY*( 1) F 4                    0.00171        0.00000   -0.00171
 48. RY*( 2) F 4                    0.00159        0.00000   -0.00159
 49. RY*( 3) F 4                    0.00007        0.00000   -0.00007
 50. RY*( 4) F 4                    0.00004        0.00000   -0.00004
 51. RY*( 5) F 4                    0.00001        0.00000   -0.00001
 52. RY*( 6) F 4                    0.00001        0.00000   -0.00001
 53. RY*( 7) F 4                    0.00000        0.00000    0.00000
 54. RY*( 8) F 4                    0.00000        0.00000    0.00000
 55. RY*( 9) F 4                    0.00000        0.00000    0.00000
```

```
 56. RY*(10) F 4                    0.00001        0.00000   -0.00001
 57. RY*( 1) H 5                    0.00061        0.00000   -0.00061
 58. RY*( 1) H 6                    0.00061        0.00000   -0.00061
 59. BD*( 1) C 1- C 2               0.02181        0.00000   -0.02181
 60. BD*( 2) C 1- C 2               0.09725        0.00000   -0.09725
 61. BD*( 1) C 1- F 3               0.01035        0.00000   -0.01035
 62. BD*( 1) C 1- H 5               0.01735        0.00000   -0.01735
 63. BD*( 1) C 2- F 4               0.01035        0.00000   -0.01035
 64. BD*( 1) C 2- H 6               0.01735        0.00000   -0.01735
```

Note that this deletion has resulted in all Lewis-type NBO's 1-16 becoming doubly occupied and all remaining non-Lewis-type NBO's becoming empty, the idealized Lewis structure limit.

The next output segment displays the calculated energy of the deletion and the energy change (in atomic units and kcal/mol):

```
 NEXT STEP:  Evaluate the energy of the new density matrix
             that has been constructed from the deleted NBO
             Fock matrix by doing one SCF cycle.

 ------------------------------------------------------------------------
----------
 Warning!  Cut-offs for single-point calculations used.
 Requested convergence on RMS density matrix=1.00D-04 within   1
cycles.
 Requested convergence on MAX density matrix=1.00D-02.
 Requested convergence on             energy=5.00D-05.
 >>>>>>>>>> Convergence criterion not met.
 SCF Done:  E(RHF) =  -275.459598747     A.U. after    2 cycles
             Convg  =    0.9196D-02             -V/T =  2.0040
             S**2   =   0.0000

 ------------------------------------------------------------------------
----------
   Energy of deletion :       -275.459598747
     Total SCF energy :       -275.717261115
                         --------------------
        Energy change :          0.257662 a.u.,         161.690
kcal/mol
 ------------------------------------------------------------------------
----------
```

[Note that the G9X program always prints a "Convergence criterion not met" warning message, because the deleted density does not exactly match the starting density in the one-pass SCF evaluator method used by $DEL. This message can be safely ignored. For the NOSTAR case, the energy of deletion is a strict variational expectation value of the natural Lewis structure wavefunction, but for other deletions a slight variational inconsistency is incurred due to the slight difference between the deleted density

distribution and the final density from which the converged Fock operator was constructed.]

From the above output, we can recognize that

$$E_{cis}(\text{full}) = -275.71726 \text{ a.u.}$$
$$E_{cis}(\text{L}) = -275.45960 \text{ a.u.}$$
$$E_{cis}(\text{NL}) = -0.25762 \text{ a.u.}$$

From the $DEL output for the *trans* isomer we obtain similarly

$$E_{trans}(\text{full}) = -275.71761 \text{ a.u.}$$
$$E_{trans}(\text{L}) = -275.46494 \text{ a.u.}$$
$$E_{trans}(\text{NL}) = -0.25268 \text{ a.u.}$$

From these values we find

$$E_{cis}(\text{L}) - E_{trans}(\text{L}) = +0.00534 \text{ a.u.} = +3.34 \text{ kcal/mol}$$
$$E_{cis}(\text{NL}) - E_{trans}(\text{NL}) = -0.00494 \text{ a.u.} = -3.11 \text{ kcal/mol}$$

Thus, the localized E(L) contribution favours the *trans* configuration by >3 kcal/mol, in accordance with the expected steric and electrostatic differences. However, the small delocalization contribution is seen to strongly favour the *cis* isomer by a similar amount, leading to nearly equal total energies for the two isomers. The surprising stability of the *cis* isomer can therefore be attributed to the electronic delocalization energy E(NL).

What Specific NBO Donor-Acceptor Interactions are Responsible for this Preference?

To further dissect E(NL) into specific donor-acceptor interactions, we can consider more selective $DEL keylists of the form

```
$DEL
delete n elements
 d1 a1
 d2 a2
  . . .
 dn an
```

$END

where each *di* is the number of a Lewis-type donor NBO and *ai* is the number of a non-Lewis-type acceptor NBO. For example, the possible vicinal hyperconjugative delocalizations between the CF bond (NBO 3) and CH bond (NBO 4) on C(1) with the CF antibond (NBO 63) and CH antibond (NBO 64) on C(2) could be specified with

$DEL
delete 4 elements
 3 63
 3 64
 4 63
 4 64
$END

By such exploratory deletions, one can verify that donor-acceptor interactions involving the Rydberg-type (RY*) NBO's 17-58 have negligible effect on the *cis/trans* energy difference. Similarly, interactions involving the acceptor antibond (BD*) NBO's 59-64 are only significant when paired with vicinal donor bond (BD) NBO's on the opposite carbon atom.

The most important contributions to the *cis-trans* energy difference are found to be the two equivalent vicinal interactions involving CH bonds as donors (NBO's 4,6) and CF* antibonds as acceptors (NBO's 61,63). The 4-63 interaction, e.g., can be deleted with the $DEL keylist

```
$DEL
delete 1 element
  4  63
$END
```

The deletion energy for each such CH-CF* interaction is found to be 6.02 kcal/mol in the *cis* isomer but only 1.22 kcal/mol in the *trans* isomer, thus contributing strongly to stabilizing the *cis* isomer. (The calculated deletion energies agree sensibly with the corresponding 2nd-order perturbation estimates of 6.92 and 1.44 kcal/mol.)

Why do vicinal CH-CF* interactions favour the *cis* isomer? Each such CH-CF* interaction is *antiperiplanar* in the *cis* isomer, but *synperiplanar* in the *trans* isomer.

As simple NBO overlap diagrams make clear, this delocalizing interaction is considerably stronger in the *anti* arrangement than in the *syn* arrangement.

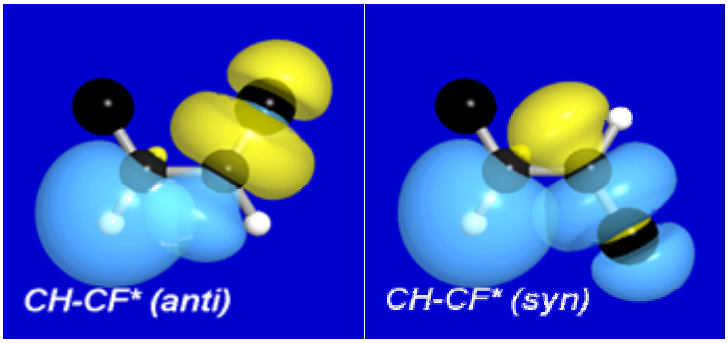

Thus, the *cis* isomer benefits from two strong *antiperiplanar* CH-CF* delocalizations, whereas the *trans* isomer has none. [There is evidently a similar *syn/anti* difference between CH-CH* interactions that favours the *trans* isomer, but the CH-CF* interactions are the more important due to the greater acceptor strength of the CF* antibond.] We can therefore conclude that vicinal CH-CF* donor-acceptor interactions are most responsible for stabilizing the *cis* isomer.

What Influences Do Hyperconjugative Delocalizations Exert on Other Geometrical Variables?

From the NBO overlap diagrams shown above, we can visualize how slight distortions of geometry might further strengthen the donor-acceptor interactions. In the *cis* isomer, for example, opening up the C-C-F angle or closing down the C-C-H angle will both increase the favourable overlap between the backside lobe of the CF* antibond and the shoulder of the CH bond to allow stronger delocalization and stabilization, as will shortening the central C-C bond. Such distortions would naturally be opposed by the skeletal bonding framework, as the bonding hybrids strive to maintain optimal orientations and separations for strong covalent bonding. Given the weakness of hyperconjugative donor-acceptor delocalizations compared to covalent bonding interactions, we expect that the hyperconjugative effects on molecular geometry are small but detectable (perhaps a few degrees or a few hundredths of an Angstrom). How can we quantitate these hyperconjugative distortions?

A $DEL keylist combined with geometry optimization allows one to determine what the optimal geometry would be in the *absence* of a particular hyperconjugative interaction. As a simple example, let us consider how the geometry of difluoroethene would be altered if the two CF* antibonds were not present, so that no hyperconjugative delocalizations involving these orbitals were possible. We can address this question by re-optimizing the geometry with the two CF* antibonds (NBO's 63, 64) deleted. The input file to perform such a $DEL-optimization for the *cis* isomer is shown below.

```
%mem=2000000
#N HF/6-31G*  NOSYMM POP=NBODel OPT

CHF::CHF (cis)

  0  1
 C
 C   1   1.34
 F   1   1.33   2  120.0
 F   2   1.33   1  120.0  3    0.0
 H   1   1.08   2  120.0  3  180.0
 H   2   1.08   1  120.0  4  180.0

$NBO file=dfe_c $END
$DEL
delete 2 orbitals
  63 64
$END
```

In this job, the G9X geometry optimizer searches for an equilibrium structure on the *E*($DEL) surface, which differs from the *E*(full) surface by deletion of contributions from NBO's 63, 64. Removing the "POP=NBODel" keyword and repeating the optimization yields the usual full-basis optimized structure for comparison. Some bond angles and distances for the *E*(full) and *E*($DEL) optimized geometries are shown in the table below:

Optimized Geometry of *Cis* Isomer

Geometry Parameter		Full	$DEL	diff
bond length (Å)	C-C	1.307	1.333	-0.026
	C-F	1.324	1.326	-0.002
	C-H	1.070	1.068	+0.002
bond angle (°)	C-C-F	122.6	120.6	+2.0
	C-C-H	123.0	127.1	-4.1

From these comparisons one can see that inclusion of *C-F delocalizations has three primary effects on the molecular geometry: (i) significant shortening (by 0.026 A) of the central C-C bond; (ii) significant opening (by 2.0 degrees) of the C-C-F bond angle; (iii) significant closing (by 4.1 degrees) of the C-C-H bond angle. As noted above, all three of these changes are expected from the general form of the CH-CF* orbital overlap diagram.

Standard experimental techniques

Chromatography and Derivatization.

Qualitative thin layer chromatography (TLC) was performed on 3 x 7 cm Kieselgel $60F_{254}$, 0.25 mm, aluminium plates (Merck). Development of the TLC plates in the appropriate solvent was followed by spraying with formaldehyde (40%)-sulfuric acid (2:98) or with anisaldehyde–sulfuric acid–ethanol (5:5:90) and heated to 120 ^{o}C. The peracetate derivatives were purified by preparative thin layer chromatography (PLC) carried out on 20 x 20 cm glass plates coated with 1.0 mm Kieselgel PF_{254} (Merck) which were air-dried and used without prior activation. An application of 10-25 mg per plate was used. Small-scale preparative separations were on 20 x 20 cm pre-coated silica gel PF_{254}, 0.25 mm glass plates (Merck). Compounds were located by UV light (254 nm) and eluted from the adsorbent with acetone. Two-dimensional paper chromatography (PC) was done on 28.5 x 46 cm Whatman No. 1 paper in water-saturated *sec*-butanol and acetic acid-water (2:98), respectively, and the chromatograms were sprayed with bis-diazotized benzidine. Column chromatography (CC) was performed on Sephadex LH-20 and compounds were eluted at 0.5 mL/min, collecting fractions of 12 mL. Solvents were evaporated under reduced pressure at 40 ^{o}C in a rotary evaporator or by freeze-drying of aqueous solutions on a Virtis 12 SL freezemobile. Acetylations were performed with acetic anhydride/pyridine at 40 ^{o}C for 12 h.

Unless specified otherwise the following techniques were applied throughout the course of this study.

Chromatographic Techniques

Qualitative thin layer chromatography

(TLC) was performed on Merck TLC-plastic sheets (3 x 8cm): Silica Gel F_{254} (0.2 mm layer). After development, the plates were sprayed with H_2SO_4-HCHO (40:1, v/v) and R_f values reported are those observed in these qualitative TLC assessments.

Preparative scale thin layer chromatography

(PLC) was conducted on glass plates (20 x 20 cm) coated with a layer (1.0 mm) of Merck Kieselgel 60 PF_{254} and air-dried overnight at room temperature. 10 - 15 mg of crude mixture was applied on each plate. Small-scale separations were conducted on Merck Pre-coated (0.25 mm) TLC Plates (20 x 20) Silica Gel 60 F_{254} and each plate charged with 3-5 mg of the crude product. After development in the appropriate eluent the plates were dried in a stream of air and the bands distinguished by either UV-light (254 nm) or appropriate spraying reagent. The bands were scraped off, eluted with acetone and removed under reduced pressure on a water bath at *ca.* 40°C.

Column chromatography

Separations on Sephadex LH-20 were performed on various column sizes and differing flow rates as specified. The Sephadex LH-20 was prepared by soaking it in the eluent (ethanol or ethanol/water solution) for 24 hours. The glass column was filled with this suspension of Sephadex LH-20 and the crude extract, dissolved in a minimum of the eluent, was slowly applied to the column. Columns were run at a flow rate of approximately 0.5 ml/min. and fractions of 15 ml were collected with an ISCO (model 273) automatic fraction collector.

Flash column chromatography

(FCC) was performed on a glass column (5 cm diameter) charged with 100 g of Merck Kieselgel 60 (230-400 mesh) for every 1 g of crude mixture. Air was expelled by elution with the appropriate solvent under N_2-pressure (*ca.* 50 kPa). The crude mixture was dissolved in a minimum amount of the appropriate solvent and slowly applied to the column. The column was developed under N_2-pressure with the appropriate solvent system and 10 ml fractions were collected.

Spray reagents

Formaldehyde-sulphuric acid

Thin layer chromatograms were gently sprayed with a 2% v/v solution of formaldehyde (37 wt. % solution in water) and concentrated sulfuric acid and gently heated to *ca.* 120^{o}C to effect maximum development of color.

Spectroscopic methods

Nuclear magnetic resonance spectroscopy (NMR)

NMR spectra were recorded at 300 MHz (^{1}H), 282 MHz (^{19}F) on a Bruker AVANCE DPX_{300} spectrometer with tetramethylsilane (TMS) used as internal standard. The NMR spectra in Japan (**Chapter 5**) was recorded on a JEOL JNM-GX270 set at 270 MHz for ^{1}H (TMS) and 254 MHz for ^{19}F recordings with $CFCl_3$ as internal standard. The solvents used were deuteriochloroform ($CDCl_3$, δ7.28), deuteriodimetylsulfoxide (C_2D_6OS), deuteriobenzene (C_6D_6, δ7.15) and deuterioacetone [$(CD_3)_2CO$/acetone-d_6, δ2.04]. Chemical shifts are reported in parts per million (ppm) on the δ-scale and coupling constants (J) were measured in Hz.

The following abbreviations are used:

s	singlet
ds	duplicated singlet
d	doublet
dd	doublet-of-doublets
m	multiplet
t	triplet

Circular dichroism (CD)

CD spectra were recorded on a Jasco J-710 spectropolarimeter in spectrophotometric grade methanol (~ 1 mg/10 ml methanol). The formula used to calculate the molecular ellipticity [θ] was:

$$[\theta] = \frac{(L)(\text{scale})(\text{molecular weight})(100)}{\qquad\qquad\qquad\qquad\qquad\qquad}$$

[length of tube (cm)][concentration (g/l)]

where L is the difference (at any given wavelength) between the reading (in cm) of the compound in solution and the reading (in cm) of pure solvent.

Anhydrous solvents and reagents

Acetone was dried over dry K_2CO_3 (oven-dried, 24 hours, 300^oC) for 24 hours. The K_2CO_3 was filtered off and the solvent distilled over 3Å molecular sieves and stored under N_2.

Benzene and THF, were refluxed over sodium/benzophenone under N_2 until a dark blue color persisted with subsequent fresh distillation under N_2 prior to use.

Acetonitrile, dichloromethane and DMF were refluxed over CaH_2 under N_2 for 12 hours with subsequent fresh distillation under N_2 before use.

Chemical methods

Standard work-up procedure

Unless specified to the contrary, the appropriate amount of water was added to the reaction mixture and extracted with diethyl ether, dichloromethane, chloroform or ethyl acetate. The organic extract was washed with water, dried (Na_2SO_4) and the solvent removed on a water bath under reduced pressure at *ca*. 40 °C.

Selective methylation with dimethylsulfate

Phenolic material was dissolved in dry acetone, dry K_2CO_3 (8 *eq*.) was added and dimethylsulfate (3-10 *eq*.) was subsequently added drop wise over a period of 30 min. under N_2. The reaction mixture was refluxed for 8 hours after which the mixture was filtrated and the acetone removed under reduced pressure. The excess dimethylsulfate was destroyed by addition of dilute ammonia and extraction with ethyl acetate afforded the methylated product(s).

Methylation with diazomethane

Methylations were performed with an excess of diazomethane. The latter was generated by the reaction of cold (-10^{o}C) potassium hydroxide [5 g in a 95% (v/v) ethanol solution] (55 ml) with N-methyl-N-nitroso-*p*-toluene sulphonamide (22 g) in cold ether (150ml) and distilled directly into a solution of dry phenolic material (250 mg) in methanol (5-10 ml)] at -10^{o}C. After 48 hours at -15^{o}C the excess diazomethane and solvents were evaporated at room temperature.

Acetylation

Dry phenolic material was dissolved in the minimum volume of pyridine and twice the amount of acetic anhydride was added. After 8-12 hours at ambient temperature the reaction was quenched with crushed ice and the excess pyridine removed by repetitive washing with cold water.

Abbreviations

The following abbreviations are used in the description of the solvent systems used during the development of TLC plates:

A	=	acetone
ACN	=	acetonitrile
B	=	benzene
C	=	chloroform
DCM	=	dichloromethane
DMF	=	*N*,*N*-dimethylformamide
Et_2O	=	diethyl ether
EOAc	=	ethyl acetate
EtOH	=	ethanol
H	=	hexane
M	=	methanol
THF	=	tetrahydrofuran

Summary

Endorsed by results from our initial investigations of the unique South African tea, brewed from *Cyclopia intermedia* (Honeybush), demonstrating the presence of polyphenolic flavonoids and glycosides, the tea is gaining popularity as a health beverage. The presence of these compounds which are claimed to have beneficial pharmacological properties, supported by the fact that the tea contains no caffeine and has low tannin content, as well as its usage as a medicinal plant by the indigenous people of the Western and Eastern Cape, prompted continued investigations also into the metabolic content of *Cyclopia subternata*.

Selected extracts of the unfermented shoots and stems of *C. subternata* were subjected to chromatographic separations that afforded a novel flavan, flavonols, flavanones, flavones, isoflavone and $C_6.C_2$- and $C_6.C_1$-type compounds. The content of the acetone extract has previously been reported as well as the exploration of various synthetic routes in an attempt to confirm the structure of the novel flavan *O*-glucoside isolated from the tea.

A continuation of the investigation of fractions from the methanol extract of the plant yielded a few compounds that were not found in the acetone extract. This work has been summarized in Chapter one and published as the phenolic profile of *Cyclopia subternata*.

The unambiguous confirmation of the structure of the flavan *O*-glucoside and essentially the novel aglycone isolated from the tea, necessitated the use of synthetic, Nuclear Magnetic Resonance spectrometric (^{1}H NMR), mass spectroscopic and circular dichroism methods. Mass spectrometry ('soft' ionization) was utilized to produce signature fragment ions of the synthesized flavan and the aglycone of the natural flavan for direct comparison. Hydroxylation patterns of the synthetic flavan and the natural flavan aglycone, as well as the relative configuration and point of attachment of the sugar moiety was deduced from NMR experiments. The absolute configuration of the aglycone was determined by circular dichroism.

The total synthesis of Aspalathin, a potent antioxidant found in the South African plant, *Aspalathus linearis* (Rooibos Tea), as the free phenol, was demonstrated. The aglycone of aspalathin, phloretin, also a good antioxidant, was synthesized in aqueous

medium without the need for protective groups. This one-step synthesis of phloretin, utilizing a recyclable and environmentally friendly catalyst, has potential commercial applications.

For the past 30 years, Mosher esters have extensively been utilized as chiral derivatizing agents (CDA's) for secondary alcohols and amides with great success. The empirical model employed to deduce the absolute stereochemistry of the resultant ester or amide requires a certain degree of conformational rigidity for the CDA, the origin of which has not yet been determined. The stabilizing atomic orbital hyperconjugative interactions and the location of the prevalent molecular orbitals in such esters were identified with the aid of *ab initio* calculations, ^{1}H, ^{19}F NMR and infrared spectrometry.

Although flavonoid crystal structures are very rare, a novel (-)-epicatechin-Mosher ester crystal was obtained and analyzed by x-ray crystallography with interesting conformational observations.

The theoretical model used to investigate the hyperconjugative effects in the Mosher ester, was published and utilized on a recently developed novel CDA that shows a greater degree of rigidity. This CDA, α-cyano-α-fluoro-*p*-tolyl-acetic acid (CFTA) has greater reactivity and was utilized in cases where the Mosher acid proved inadequate. The investigation regarding the employment of CFTA was carried out with Japanese collaboration and commercial production of the reagent is envisaged. The hyperconjugative molecular model used in the modeling of the Mosher reagent was refined and extended to CFTA. The origin of the very large fluorine chemical shift difference between the epicatechin-CFTA diastereomers was investigated and the results published.

Opsomming

Navorsingsresultate uit die ondersoek op *Cyclopia intermedia* (Heuningbostee), wat die teenwoordigheid van antioksidatiewe polifenoliese flavonïede en hul glikosiede as metaboliete toon, was bydraend tot die steeds toenemende gewildheid van hierdie tee as gesondheidsdrankie. Die teenwoordigheid van hierdie verbindings in die tee, wat belowende farmakologiese eienskappe besit, die afwesigheid van kaffeïen bevat en die medisinale gebruik van die plant deur die inwoners van die Oos en Wes Kaap het verdere navorsing ook van *C. subternata* geregverdig.

Die ekstrakte van die ongefermenteerde blare en takke van *C. subternata* is onderwerp aan verskeie chromatografiese skeidings wat ‘n nuwe flavaan, flavonole, flavanole, isoflavone en verskeie ander $C_6.C_2$- en $C_6.C_1$-tipe verbindings uit die plant gelewer het. Tydens die aanvanklike studie is die asetoon ekstrak ondersoek en verskeie sintetiese roetes verken om die nuwe flavaan aglikoon se struktuur te bevestig. In hierdie voortgesette studie is die methanol ekstrak van die plant volledig ondersoek en hoewel verskeie verbindings oorvleul met die uit die asetoon ekstrak, is addisionele verbindings geïdentifiseer wat bydra tot die polifenoliese profiel van *C. subternata.* Die metaboliete uit die plant is gepubliseer en word in Hoofstuk een kortliks bespreek.

Sintese en spektroskopiese metodes, insluitend Kern Magnetiese Resonans Spektroskopie (^{1}H KMR), Sirkulêre Dichroïsme en Massaspektrometrie is gebruik om die flavaan aglikoon se struktuur te bevestig. ‘Sagte’ ionisasie metodes is tydens massaspektrometrie gebruik om unieke diagnostiese fragmentione te produseer. Sintese van die flavaan het direkte vergelyking met hierdie fragmentione van die geïsoleerde flavaan moontlik gemaak en die struktuur bevestig. Die absolute konfugurasie word deur middel van Sirkulêre Dichroïsme bepaal.

Die totaal sintese van vryfenoliese Aspalatien, ‘n potente antioksidant teenwoordig in die Suid Afrikaanse plant *Aspalathus linearis* (Rooibos tee), is ontwikkel. Die sintese van die aspalatien aglikoon, floretin, in waterige medium sonder die gebruik van beskermende groepe is gedemonstreer. Hierdie een-stap sintese, wat ‘n omgewingsvriendelike herwinbare katalis benut, het kommersieële potensiaal.

Gedurende die afgelope 30 jaar is die Mosher reagens suksesvol gebruik as chirale derivatiserings reagens vir alkohole, amiede en gevolglik ook geselekteerde flavonoïede. Die impiriese model wat gebruik word om die absolute stereochemie van alkohole en amiede af te lei maak staat op ‘n mate van rigiditeit in hierdie ester. Die oorsprong van hierdie rigiditeit kon tot dusver egter nie oortuigend verduidelik word nie. Die stabiliserende hiperkonjugatiewe atoomorbitaal interaksies verantwoordelik vir hierdie rigiditeit en die molekulêre orbitale waar dit gesetel is, is geïdentifiseer deur middel van kwantummeganiese berekenings, ^{1}H, ^{19}F KMR, en infrarooi spektrometrie.

Gegewe dat kristalle van flavonoïede baie raar is, is die kristalle van die epicatechin-Mosher ester wat hier verkry is uniek. X-straal kristallografie toon interressante konformasionele gedrag in hierdie kristal.

Die hiperkonjugatiewe molekulêre modellerings model wat ontwikkel is om die Mosher ester te ondersoek is reeds gepubliseer en ook toegepas op ‘n moderne chirale derivatiserings reagens wat onlangs ontwikkel is. Hierdie chirale derivatiserings reagens, α-cyano-α-fluoro-*p*-tolyl-acetic acid (CFTA), toon ‘n grooter mate van rigiditeit en reaktiwiteit en is suksesvol gebruik in gevalle waar die Mosher ester onsuksesvol was. Ondersoek na die CFTA ester is uitgevoer in samewerking met n Japanese groep wat die CFTA reagens ontwikkel het. Kommersieële vervaardiging van CFTA word in die vooruitsig gestel. Die hiperkonjugatiewe model wat vir die molekulêre modelering van die Mosher ester gebruik is, is verfyn en toegepas op CFTA.

Die oorsprong van die opvallende groot verskil in chemiese verskuiwing van ^{19}F in die KMR spektra van die epicatechin-CFTA diastereoisomere is ook ondersoek en die resultate gepubliseer.